

**New aspects of N-form dependent growth retardation  
as found in physiological and microarray studies  
on seedlings of *Arabidopsis thaliana***

Dissertation

zur Erlangung des Doktorgrades  
der Mathematisch-Naturwissenschaftlichen Fakultät  
der Christian-Albrechts-Universität  
zu Kiel

vorgelegt von

**Anne Hoffmann**

November 2005



Referent/in:

.....

Korreferent/in:

.....

Tag der mündlichen Prüfung:

.....

Zum Druck genehmigt: Kiel,

.....

.....

Der Dekan



## Publications

Parts of this work have been published, are in press or in preparation for publication.

Hoffmann A, Hammes E, Plieth C, Desel C, Sattelmacher B, Hansen UP (2005) Effect of CO<sub>2</sub> supply on ROS formation in *Arabidopsis thaliana*. *Protoplasma in press*

Hammes E, Hoffmann A, Plieth C, Hansen UP (2005) Light-induced decrease in DCF-fluorescence of leaves of wheat in the presence of SHAM. *Protoplasma in press*

Hoffmann A, Milde S, Desel C, Hümpel A, Kaiser H, Hammes E, Piippo M, Soitamo A, Aro EM, Sattelmacher B, Hansen UP. N-form dependent growth retardation of *Arabidopsis thaliana* as revealed from physiological and microarray studies. *In preparation*

Hoffmann A, Desel C, Hammes E, Sattelmacher B, Hansen UP. Dependence of ROS production on developmental state in ammonium-grown and nitrate-grown seedlings of *Arabidopsis thaliana*. *In preparation*

## Posters

Hoffmann A, Milde S, Piippo M, Soitamo A, Hümpel A, Desel C, Sattelmacher B, Aro EM, Hansen UP (2005)

Differential gene expression in *Arabidopsis thaliana* induced by light stress and nutrition. Expert Meeting of the Research Training Programme on "Natural Antioxidants- Effects in Plants, Foods, Animals and Humans" (GRK 820) Salzau (March 9-13, 2005)

Hoffmann A, Desel C, Hammes E, Plieth C, Milde S, Sattelmacher B, Hansen,UP (2004)  
ROS Production in leaves of *A.thaliana* as affected by different nitrogen sources  
Botaniker Tagung, Braunschweig 05.–10.09.2004 Abstract No P 25-04

Hammes E, Hoffmann A, Desel C, Plieth C, Schnieder F, Verreet J, Hansen UP (2004)  
Interference of fungal infection with photosynthesis  
Botaniker Tagung, Braunschweig 05.–10.09.2004 Abstract No P 15-19

Milde S, Hoffmann A, Sprick K, Piippo M, Battchikova N, Soitamo A, Aro EM, Bilger W, Hansen UP (2004)

Gene expression studies of *Arabidopsis thaliana* plants exposed to different kinds of stress. COST 926 Workshop and MC Meeting 30<sup>th</sup> September – 2<sup>nd</sup> October 2004

Milde S, Hoffmann A, Sprick K, Hansen UP (2003)

Genexpression studies on proteins involved in oxidative and antioxidative reactions in plants. Free Radical Research 2003, V37 Supplement 2, p. 28



# Table of Contents

<b>List of Figures</b>	<b>vii</b>
<b>List of Tables</b>	<b>viii</b>
<b>Abbreviations</b>	<b>ix</b>
<b>1 Introduction</b>	<b>1</b>
<b>2 State of Research</b>	<b>3</b>
<b>2.1 Nitrate or ammonium as nitrogen source - Implications on metabolism and signalling</b>	<b>3</b>
<b>2.2 Ammonium-induced sensitivity to light stress in <i>Phaseolus vulgaris</i></b>	<b>7</b>
<b>2.3 <i>Arabidopsis thaliana</i></b>	<b>10</b>
<b>2.4 Gene expression studies</b>	<b>11</b>
2.4.1 Microarray technology	11
2.4.2 Application to the effects of N-nutrition and light	12
<b>2.5 Aims and scope of the project</b>	<b>13</b>
<b>3 Material and Methods</b>	<b>15</b>
<b>3.1 Plant material</b>	<b>15</b>
<b>3.2 Preparation of plant agar</b>	<b>15</b>
<b>3.3 Surface sterilisation of seeds</b>	<b>16</b>
<b>3.4 Growth conditions</b>	<b>16</b>
3.4.1 Growth conditions for physiological measurements	16
3.4.2 Growth conditions for gene expression studies	16
<b>3.5 Verification of constant pH around the roots</b>	<b>17</b>
<b>3.6 Analysis of nutritional status of the plants</b>	<b>18</b>
3.6.1 Measurements of C and N by Elemental Analyzer	18
3.6.2 Measurements of anions by ion chromatography	18
3.6.3 Measurements of amino acids by ion exchange chromatography	19
<b>3.7 Physiological measurements</b>	<b>19</b>
3.7.1 Measurements of processes related to photosynthesis	19
3.7.1.1 Illustration of cell morphology using transmission electron microscope	19
3.7.1.2 Determination of photosynthesis rate	20
3.7.1.3 Determination of chlorophyll content	20
3.7.1.4 Measurement of chlorophyll fluorescence	21
3.7.2 Determination of ROS	22
3.7.2.1 Monitoring O <sub>2</sub> <sup>-</sup> radicals in the leaves by nitroblue tetrazolium	22
3.7.2.2 Monitoring oxidative stress in the leaves by 5-(and-6)-carboxy-2',7'-dichlorodihydrofluorescein diacetate	23

---

3.7.2.3 Confocal laser scanning microscopy	24
3.7.2.4 Determination of source of ROS using inhibitors of metabolic pathways	24
3.7.2.5 Determination of CO <sub>2</sub> dependence of ROS formation	25
3.7.3 Investigations of scavenging systems	25
3.7.3.1 Determination of zeaxanthin using HPLC	25
3.7.3.2 Determination of transport to the vacuole using 2,7-bis-(2-carboxyethyl)-5-(and-6)-carboxyfluorescein acetoxymethyl ester	26
3.7.3.3 Catalase assay	27
3.7.3.3.1 Procedure for extraction	29
<b>3.8 Gene expression studies</b>	<b>29</b>
3.8.1 RNA preparation	29
3.8.2 Preparation of an agarose gel	30
3.8.3 Fluorescence labelling of cDNA	30
3.8.4 Purification of labelled cDNA	32
3.8.5 BSA blocking for cDNA microarrays	32
3.8.6 Preparing of the cover slips	33
3.8.7 Hybridisation	33
3.8.8 Scanning	34
3.8.9 ScanArray and GeneSpring	34
3.8.9.1 GeneSpring experiment format	34
3.8.10 Survey of probe quality using agarose gels	35
<b>3.9 Validation of cDNA microarray results</b>	<b>36</b>
3.9.1 Sequencing of clones	36
3.9.1.1 PCR to amplify products sent from Turku	36
3.9.1.2 Sequencing reaction and clean up	37
3.9.1.3 Sequencing protocol MegaBACE	38
3.9.1.4 Sequence analysis using the internet	38
3.9.2 Northern blot analysis	38
3.9.2.1 Preparation of the hybridisation probes	38
3.9.2.2 Denaturing RNA agarose gel electrophoresis	40
3.9.2.3 Transfer to nylon membrane	40
3.9.2.4 Hybridisation	41
3.9.2.5 Washing and visualisation	41
<b>3.10 Databases for analysis</b>	<b>42</b>
<b>4 Results</b>	<b>43</b>
<b>4.1 Cultivation of plants</b>	<b>43</b>
4.1.1 Selection of growth conditions	43
4.1.2 Retardation of growth	43
4.1.3 Excluding pH effect on growth	44
<b>4.2 Nutritional status of the plants</b>	<b>47</b>
4.2.1 C and N analysis	47
4.2.2 Anion analysis	47
4.2.3 Amino acid analysis	48



<b>4.3 N-form dependent differences related to photosynthesis</b>	<b>50</b>
4.3.1 Differences in starch deposition in the chloroplasts	50
4.3.2 Photosynthetic activity	50
<b>4.4 Determination of ROS</b>	<b>52</b>
4.4.1 Use of dyes to localise sites of ROS formation - assets and drawbacks	52
4.4.2 Testing the method of DCF-DA measurement <i>in vitro</i>	53
4.4.3 Testing the method of DCF-DA measurements <i>in vivo</i>	55
4.4.3.1 Testing of the influence of solvent	55
4.4.3.2 Suitability of reference fluorescence for drift elimination	55
4.4.4 Testing the suitability of the light intensities	57
4.4.4.1 Test for actinic influence of measuring light	57
4.4.4.2 Test of leaf absorption of actinic laser light at 632 nm	58
4.4.4.3 Test of temperature changes induced by the actinic light	58
4.4.5 Testing the infiltration method	58
4.4.6 Measurement of ROS production with DCF in intact leaves as illustrated for NO <sub>3</sub> <sup>-</sup> -grown seedlings	59
4.4.6.1 Attempt to find the locus of ROS production	59
4.4.6.2 Temporal behaviour of ROS production	61
4.4.6.3 Effect of CO <sub>2</sub> supply on ROS formation	62
4.4.7 Comparison of ROS formation in NH <sub>4</sub> <sup>+</sup> - and NO <sub>3</sub> <sup>-</sup> -grown <i>A. thaliana</i>	65
4.4.7.1 Light-induced ROS production at high CO <sub>2</sub>	65
4.4.7.2 Wide scatter of responses in NH <sub>4</sub> <sup>+</sup> -grown leaves	66
4.4.7.3 Systemic ROS production in NH <sub>4</sub> <sup>+</sup> -grown leaves	67
4.4.7.4 The influence of CO <sub>2</sub> and buffer capacity	68
4.4.7.5 Effect of pH on ROS production	70
4.4.8 Investigations of scavenging systems	71
4.4.8.1 Determination of zeaxanthin using HPLC	71
4.4.8.2 Testing for uptake of dye into the vacuole	72
4.4.8.3 Determination of catalase activity	72
<b>4.5 Gene expression studies</b>	<b>73</b>
4.5.1 Experimental strategies	73
4.5.1.1 Experimental design	73
4.5.1.2 Technical and biological replicates	75
4.5.1.3 Normalisation strategies	75
4.5.1.4 Data analysis	76
4.5.2 Evaluation of the microarray experiment	77
4.5.2.1 Control of RNA quality	77
4.5.2.2 Assessment of labelling reactions	78
4.5.2.3 Controlling the annotation of genes to the spots on the microarray	79
4.5.2.4 Verification of differentially expressed genes by Northern blot analysis	81
4.5.2.5 Pitfalls - Genes with different results in microarray and Northern blot	83
4.5.3 Differentially expressed genes	85
4.5.3.1 Overview of microarray results	85

4.5.3.2 Processing, analysis and problems of the evaluation of microarray data as illustrated for nitrate reductase	89
4.5.3.3 Analysis of technical and biological replicates - illustrated by Nia1 and Nia2	91
4.5.3.4 Differentially expressed genes related to growth retardation	94
4.5.3.4.1 Genes of $\beta$ -oxidation-related sucrose metabolism	96
4.5.3.4.2 Genes of photosynthesis-related sucrose metabolism	97
4.5.3.5 Other differentially expressed genes - Detoxification enzymes	99
<b>5 Discussion</b>	<b>103</b>
<b>5.1 Traditional N-form dependent differences</b>	<b>103</b>
5.1.1 Analysis of anion content	103
5.1.2 Primary N-assimilation	104
5.1.3 Survey of stores for nitrogen	106
5.1.4 Analysis of genes encoding for enzymes involved in amino acid synthesis	108
<b>5.2 A new aspect of growth retardation under <math>\text{NH}_4^+</math>-nutrition</b>	<b>110</b>
5.2.1 New experimental results from seedlings of <i>A. thaliana</i>	110
5.2.1.1. ROS production	110
5.2.1.2 Expression of genes encoding for the energy supply of sucrose synthesis	111
5.2.2 The new hypothesis	113
<b>5.3 Explaining previous findings in the light of the scheme in Figure 5.3</b>	<b>113</b>
5.3.1 Influence of N-form on growth	113
5.3.2 Different ROS sources under $\text{NH}_4^+$ -nutrition compared to $\text{NO}_3^-$ -nutrition	114
5.3.3 Influence of $\text{CO}_2$ on ROS formation in $\text{NO}_3^-$ -grown seedlings	116
5.3.4 ROS detoxification and scavenging systems	119
5.3.5 GDP-Epimerase	120
<b>5.4 Excluding possible sources of error</b>	<b>122</b>
5.4.1 Effect of pH in external medium on growth	122
5.4.2 Use of dyes to localise sites of ROS formation - assets and drawbacks	123
5.4.3 Gene expression studies	124
<b>6 General conclusion and Outlook</b>	<b>127</b>
<b>Summary</b>	<b>133</b>
<b>Zusammenfassung</b>	<b>135</b>
<b>Appendix</b>	<b>139</b>
<b>A.1 Solutions</b>	<b>139</b>
A.1.1 General solutions	139
A.1.2 Solutions for Northern blot experiments	140
<b>A.2 Primer sequences</b>	<b>142</b>
<b>A.3 List of differentially expressed genes encoding for enzymes</b>	<b>144</b>
<b>A.4 List of differentially expressed genes encoding for other proteins</b>	<b>148</b>

<b>A.5 Kits, chemicals and enzymes</b>	<b>156</b>
A.5.1 Kits	156
A.5.2 Chemicals	156
A.5.3 Enzymes	157
<b>References</b>	<b>159</b>



## List of Figures

<b>Figure 2.1</b> Scheme of nitrogen uptake from the soil and assimilation in roots and shoots.	4
<b>Figure 2.2</b> Illustration of the pathways of interaction between photosynthesis, photorespiration and respiration with special regards to different N-forms.	9
<b>Figure 2.3</b> <i>Arabidopsis thaliana</i> (mouse ear cress).	10
<b>Figure 3.1</b> Experimental arrangement for applying high-light conditions.	17
<b>Figure 3.2</b> Structure of nitroblue tetrazolium.	22
<b>Figure 3.3</b> Reaction scheme of DCF-DA.	23
<b>Figure 3.4</b> Excitation and emission spectra of BCECF.	27
<b>Figure 4.1</b> Effect of N-form on growth in 15-days old plants of <i>A. thaliana</i> .	44
<b>Figure 4.2</b> Effect of growth on the pH of the medium surrounding roots of <i>A. thaliana</i> .	45
<b>Figure 4.3</b> Effect of growth on the pH of the medium surrounding roots of <i>A. thaliana</i> in unbuffered $\text{NH}_4^+$ -plates.	46
<b>Figure 4.4</b> Testing the function of the pH indicator.	46
<b>Figure 4.5</b> $C_{\text{total}}$ and $N_{\text{total}}$ and C/N ration determined by elemental analyser.	47
<b>Figure 4.6</b> Concentration of anions [in $\text{NO}_3^-$ - and $\text{NH}_4^+$ -grown seedlings.	48
<b>Figure 4.7</b> Concentration of free amino acids in $\text{NO}_3^-$ -grown and $\text{NH}_4^+$ -grown seedlings of <i>A. thaliana</i> .	49
<b>Figure 4.8</b> Ratio of amides to their acids in $\text{NO}_3^-$ - and $\text{NH}_4^+$ -grown seedlings.	49
<b>Figure 4.9</b> N-form dependent starch deposition in chloroplasts.	50
<b>Figure 4.10</b> Photosynthetic activity as measured by $\text{CO}_2$ uptake per chlorophyll	51
<b>Figure 4.11</b> Determination of photosynthetic performance by means of a PAM fluorometer.	52
<b>Figure 4.12</b> pH dependence of the emission spectrum of DCF fluorescence.	54
<b>Figure 4.13</b> Time course of DCF fluorescence of DCF-DA in a petri dish.	54
<b>Figure 4.14</b> Time course of fluorescence without DCF.	55
<b>Figure 4.15</b> Three typical results for the development of DCF-fluorescence without light.	56
<b>Figure 4.16</b> Mean values of DCF-fluorescence without light induction obtained from leaves in different buffers.	57
<b>Figure 4.17</b> PAM measurements of leaves infiltrated with SM and leaves infiltrated with 10 $\mu\text{M}$ DCMU.	59
<b>Figure 4.18</b> Demonstration of light-induced ROS generation by means of two indicator dyes in 2-weeks-old leaves of <i>A. thaliana</i> .	60
<b>Figure 4.19</b> Light-induced ROS production as measured by DCF-fluorescence.	61
<b>Figure 4.20</b> Normalised responses showing the influence of $\text{CO}_2$ -supply on the light-induced generation of ROS.	62
<b>Figure 4.21</b> Determination of photosynthetic performance by means of a PAM fluorometer.	63
<b>Figure 4.22</b> Effect of 10 $\mu\text{M}$ DCMU and 2 mM SHAM in SM medium on ROS generation as measured with DCF fluorescence.	64
<b>Figure 4.23</b> ROS production in (A) $\text{NH}_4^+$ - and (B) $\text{NO}_3^-$ -grown leaves.	65
<b>Figure 4.24</b> Relationship between time courses of DCF fluorescence measured directly under the light guide.	66
<b>Figure 4.25</b> Histogram of values of $F_{\text{max}}$ .	67
<b>Figure 4.26</b> Overall ROS production determined in the area under the light guide and in the wider surrounding field.	68
<b>Figure 4.27</b> Averaged time courses of ROS production in $\text{NH}_4^+$ - and $\text{NO}_3^-$ -grown leaves submerged in high and low $\text{CO}_2$ medium.	69
<b>Figure 4.28</b> ROS production in SM medium at pH 6.1.	71
<b>Figure 4.29</b> Epoxylation status of leaves at low light and after 20 min high light.	72

<b>Figure 4.30</b> Experimental designs for microarray studies.	74
<b>Figure 4.31</b> (A) PCR with actin 2/8 primers on RNA before and after DNase I digestion, (B) RNA on denaturing agarose gel.	78
<b>Figure 4.32</b> Scanned image of 1 % agarose gel for assessing labelling quality	79
<b>Figure 4.33</b> Northern blot analysis of genes not corresponding to microarray results.	84
<b>Figure 4.34</b> Sequence alignment of Nia1.	89
<b>Figure 4.35</b> Northern blot results of Nia1 and Nia2.	90
<b>Figure 4.36</b> Scheme of lipid mobilisation from seed storage reserves.	96
<b>Figure 4.37</b> Northern blots of genes encoding for the enzymes of $\beta$ -oxidation, of PEPCK, fructose biphosphate aldolase and carbonic anhydrase.	97
<b>Figure 4.38</b> Scheme of Calvin cycle and photorespiration.	98
<b>Figure 4.39</b> Northern blot analysis of genes of the Calvin cycle and photorespiration.	98
<b>Figure 4.40</b> Northern blot analysis for AATP.	99
<b>Figure 4.41</b> Scheme of the Halliwell-Assada-Cycle for ascorbate regeneration.	99
<b>Figure 4.42</b> Examples for cellular function of GST.	100
<b>Figure 4.43</b> Proposed <i>de novo</i> pathway for the synthesis of L-ascorbic acid from D-Man in plants.	100
<b>Figure 4.44</b> Northern blot results of DHAR, one GST and Epimerase.	101
<b>Figure 5.1</b> Scheme of GS / GOGAT cycle.	105
<b>Figure 5.2</b> Scheme of the GABA ( $\gamma$ -aminobutyrate) shunt.	109
<b>Figure 5.3</b> Scheme of the putative different pathways of sucrose synthesis in $\text{NO}_3^-$ - and $\text{NH}_4^+$ -grown seedlings of <i>A. thaliana</i> .	112
<b>Figure 5.4</b> Scheme of photosynthetic electron transport chain (ETC).	117
<b>Figure 5.5</b> Pathways of L-ascorbic acid biosynthesis.	121

## List of Tables

<b>Table 3.1</b> Composition of the $\text{NO}_3^-$ - and $\text{NH}_4^+$ -medium.	15
<b>Table 4.1</b> Differential development of leaves in $\text{NO}_3^-$ - and $\text{NH}_4^+$ -grown seedlings.	44
<b>Table 4.2</b> Intensities of 488 nm excitation light.	57
<b>Table 4.3</b> Average values of the light-induced maximum DCF fluorescence of $\text{NH}_4^+$ - and $\text{NO}_3^-$ -grown leaves submerged in high and low $\text{CO}_2$ medium.	69
<b>Table 4.4</b> List of genes sequenced by MegaBACE 1000.	80
<b>Table 4.5</b> Overview: Comparison of Northern blot and microarray results.	82
<b>Table 4.6</b> Microarray results of the genes not corresponding to Northern blot analysis.	84
<b>Table 4.7</b> Differential expression values of enzymes of nitrate assimilation, Calvin cycle, photorespiration, sucrose synthesis, detoxification and amino acid synthesis.	86
<b>Table 4.8</b> Percentage of "loop amplification" in the range from 0.02 to 0.3.	88
<b>Table 4.9</b> Microarray results of Nia1 and Nia2.	90
<b>Table 4.10</b> Normalised, control and raw data of Nia2 from all individual replicates.	92
<b>Table 4.11</b> Normalised data of Nia2 from individual replicates, average value plus SEM and loop amplification.	93
<b>Table 4.12</b> Normalised data of Nia1 from individual replicates, average value plus SEM and loop amplification.	94
<b>Table 4.13</b> Differential expression values of genes encoding for enzymes of sucrose synthesis, Calvin cycle and photorespiration in $\text{NH}_4^+$ - and $\text{NO}_3^-$ -grown seedlings.	95
<b>Table 4.14</b> Microarray results of DHAR, GST and Epimerase.	101

## Abbreviations

AATP	adenine nucleotide translocase
ACX4	gene encoding for acyl-CoA oxidase 4
AGT1	gene encoding for alanine-glyoxylate aminotransferase
AOX	alternative oxidase
APX	ascorbate peroxidase
Arg	arginine
AS	asparagine synthetase
ASN	gene encoding for asparagine synthetase
Asn	asparagine
Asp	aspartate
a.u.	arbitrary units
BCECF	2,7-bis-(2-carboxyethyl)-5-(and-6)-carboxyfluorescein
BSA	bovine serum albumin
CA	carbonic anhydrase
CAT	catalase
cDNA	complementary deoxyribonucleic acid
Chl	chlorophyll
DCF	5-(and-6)-carboxy-2',7'-dichlorodihydrofluorescein
DCMU	3-(3,4-dichlorophenyl)-1,1-dimethylurea
DNA	deoxyribonucleic acid
DHAR	dehydroascorbate reductase
DM	dry mass
DTT	dithiothreitol
ETC	electron transport chain
FBA cyt	fructose biphosphate aldolase cytosolic
FBA plast	fructose biphosphate aldolase plastidic
Fd	ferredoxin
GABA	gamma-aminobutyric acid
GAD	glutamate decarboxylase
Gal	galactose
GapA	glyceraldehyde 3-phosphate dehydrogenase
GDH	glutamate dehydrogenase
GDP	guanosine diphosphate
Gln	glutamine
Glu	glutamate
GOGAT	glutamine oxoglutarate aminotransferase
GOX	glycolate oxidase
GR	glutathione reductase
GS	glutamine synthetase
HL	high light (800 $\mu\text{mol m}^{-2} \text{s}^{-1}$ )
LL	low light (40 $\mu\text{mol m}^{-2} \text{s}^{-1}$ )
Man	mannose
MFP2	multifunctional protein 2
NAD(P)	nicotinamide adenine dinucleotide(phosphate)
NBT	nitroblue tetrazolium
n	number
N	nitrogen

NiR	nitrite reductase
NR	nitrate reductase
PEPc	phosphoenolpyruvate carboxylase
PEPCK	phosphoenolpyruvate carboxykinase
PS I	photosystem I
PS II	photosystem II
Q <sub>A</sub>	permanently bound plastoquinone in the D2-protein of PS II
Q <sub>B</sub>	mobile plastoquinone in the D2-protein of PS II
q <sub>N</sub>	non-photochemical quenching
q <sub>p</sub>	photochemical quenching
Rcf	relative centrifugal force
RNA	ribonucleic acid
ROI	region of interest
ROS	reactive oxygen species
SBPase	sedoheptulose biphosphatase
SD	standard deviation
SEM	standard error of the mean
SF	scatter factor
SHAM	salicyl hydroxamate
SM	standard medium
ZBM	Zentrum für Biochemie und Molekularbiologie Centre of Biochemistry and Molecular Biology



# 1 Introduction

Inorganic nitrogen is one of the major macronutrients for plants besides sulphur, phosphorus, potassium, calcium and magnesium. It can be supplied as nitrate ( $\text{NO}_3^-$ ) or as ammonium ( $\text{NH}_4^+$ ) salt. The form of nitrogen supply has great influence on plant development, e.g. growth, morphology and dry matter (Errebhi and Wilcox 1990, Gerendás and Sattelmacher 1995, Gerendás et al. 1997). Even though there are some plants that prefer ammonium over nitrate (e.g. rice, Marschner 1995) the majority reacts to ammonium as the sole nitrogen source with growth retardation and higher sensitivity to stress (Gerendás et al. 1997, Zhu et al. 2000, Bendixen et al. 2001). Many investigations have been done on nitrate versus ammonia as the sole nitrogen source to unravel the underlying mechanism of the observed "toxicity" syndromes. However, there is still a controversial debate and the reasons for the effects like growth retardation are still not fully resolved.

The negative effect of  $\text{NH}_4^+$ -nutrition has mainly been found under high-light conditions, whereas in many studies, under low-light conditions, no difference has been observed between  $\text{NO}_3^-$ - and  $\text{NH}_4^+$ -grown plants (Zhu et al. 2000, Bendixen et al. 2001). This has led to hypotheses, which assign an important role to photosynthesis in  $\text{NH}_4^+$ -mediated toxicity. The hypothesis of uncoupling of the photosynthetic thylakoid membrane by  $\text{NH}_4^+$  (Magalhaes and Huber 1989) is considered to be unlikely, firstly because the putative high amounts of  $\text{NH}_4^+$  can only be observed in the leaves at very high external ammonium concentrations (Gerendás et al. 1997), and secondly because energy quenching (which would be eliminated by uncoupling) is not smaller in  $\text{NH}_4^+$ - than in  $\text{NO}_3^-$ -grown plants (Bendixen et al. 2001).

The hypothesis developed in the ZBM in cooperation with the Institute of Plant Nutrition, Kiel (Guo 2002, Schinner 2001) deals with export of superfluous redox equivalents from the chloroplasts as a putative cause of  $\text{NH}_4^+$ -induced damage. Higher load of reactive oxygen species in  $\text{NH}_4^+$ -grown plants under high-light conditions was indicated by the activation of scavenging enzymes (Zhu et al. 2000) or depletion of ascorbate (Bendixen et al. 2001). Guo et al. (2005) found different apparent compensation points of  $\text{CO}_2$  uptake in  $\text{NO}_3^-$ - and  $\text{NH}_4^+$ -grown *Phaseolus vulgaris*. Extending the traditional gasflux/ $\text{CO}_2$  equations (von Caemmerer and Farquhar 1981) by a term accounting for light-induced non-photorespiratory  $\text{CO}_2$  evolution has led to the hypothesis that  $\text{NO}_3^-$ -grown plants can use superfluous redox equivalents for N-assimilation, whereas  $\text{NH}_4^+$ -grown plants have to burn them in the

mitochondria. Under these conditions, mitochondria may become a strong source of reactive oxygen species (ROS).

Nevertheless, this model of Guo et al. (2005) is based on many indirect conclusions. The putative ROS evolution has not directly been measured, but concluded from the behaviour of scavenging enzymes (Zhu et al. 2000) and ascorbate depletion (Bendixen et al. 2001). The export of redox equivalents to the mitochondria in  $\text{NH}_4^+$ -grown plants has been concluded from the action of SHAM, an inhibitor of the alternative oxidase, on photosynthetic electron flow (Schinner 2001, Schinner et al. 2001, Guo 2002, Guo et al. 2005).

In order to monitor ROS production, the suitability of the ROS indicating dyes DCF and NBT is tested in the studies presented here. Considering the crucial role of redox fluxes between cellular compartments in the hypothesis of Guo et al. (2005) the study of these putative interactions should be intensified. As mentioned above, evidence has come only from investigations on a physiological level such as measuring photosynthetic activity under the influence of inhibitors. Unfortunately, there are nearly no biophysical signals available which would enable a direct on-line monitoring of fluxes and signals exchanged between different compartments. Thus, physiological experiments come to a limit when the underlying regulatory mechanisms of nitrogen metabolism, especially of ammonium, are to be investigated in detail.

Making use of the "omics" era, transcriptomic or proteomic approaches may enlighten the underlying mechanisms. Gene expression studies using microarray technology are already widely used to address different questions. Some of those deal also with the response to  $\text{NO}_3^-$ -nutrition. However, these studies focus on the action of nitrate readdition on gene expression level after nitrogen deprivation or starvation (Scheible et al. 2004, Wang et al. 2000, 2003, 2004). In order to understand N-form specific reactions, microarray studies comparing gene expression in nitrate- and ammonium-grown plants have to be done.

Even more fundamental is the question of whether photosynthesis is the only mediator of damage induced by  $\text{NH}_4^+$ -nutrition. Because of this, seedlings of *Arabidopsis thaliana* are investigated here. They are in the age, where the transition from supply from the oleosomes to supply from photosynthesis occurs. These plants offer the chance to investigate the question of whether there is already a perception for a signal related to different N-forms before photosynthesis is fully switched on. Seeds germinating on medium containing ammonium as the sole nitrogen source probably have already installed mechanisms to use ammonium at an early stage of development. In these plants, ammonium-dependent mechanisms leading to growth retardation and higher sensitivity to light stress would be already visible.

## 2 State of Research

### 2.1 Nitrate or ammonium as nitrogen source - Implications on metabolism and signalling

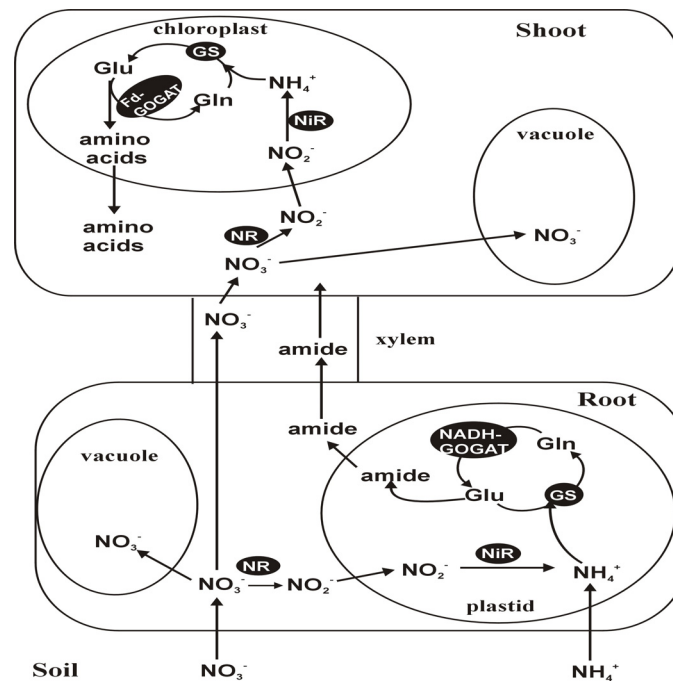
Nitrogen is an indispensable inorganic nutrient for plants. It is a basic constituent of nucleic acids, amino acids, secondary metabolites and many cofactors (Marschner 1995). Nucleic acids provide the letters of the library of life. Amino acids are the bricks of proteins, and proteins are the machines that do the work in metabolism, defence, signalling, proliferation, transport etc. Secondary metabolites are important in defence against herbivores and pathogens as well as in signalling whereas cofactors support multiple enzymatic reactions. Thus, nitrogen is part of a complex network of branching and merging pathways interacting at many sites with carbon flow, pH regulation, ion and assimilate flow at the cellular and whole plant level (Stitt et al. 2002).

The assimilation of nitrogen is one of the most complex and energy consuming biochemical reaction known in living organisms even though it involves just a few steps (Heldt 1999, Crawford and Forde 2002). For example, almost 25 % of the photosynthetic energy is needed to assimilate nitrate but the end products contribute only about 2 % to the dry weight of the plants (Guerrero et al. 1981, Taiz and Zeiger 2000).

In principle, nitrogen is taken up from the soil as nitrate- ( $\text{NO}_3^-$ ) or ammonium-ion ( $\text{NH}_4^+$ ). The assimilation of nitrate involves reduction to nitrite and further to ammonium. Ammonium is then incorporated into amino acids. These reactions can take place either in the roots or in the shoots. If ammonium is taken up from the soil it is, in most cases, assimilated and incorporated into amino acids directly in the roots (Fig. 2.1).

Comparing the energy needed for the assimilation of  $\text{NO}_3^-$  or  $\text{NH}_4^+$  in the roots reveals a better energy balance for  $\text{NH}_4^+$ -supply. For nitrate assimilation 23 % (Marschner 1995) of photosynthetic energy is used whereas only 14 % are needed for  $\text{NH}_4^+$ -assimilation (Bloom et al. 1992). As stated above, the better energy balance of  $\text{NH}_4^+$ -supply results from the absence of the conversion of  $\text{NO}_3^-$  to  $\text{NH}_4^+$  before nitrogen can be incorporated into amino acids. However, this difference in energy balance vanishes if all secondary reactions like detoxification and N-storage are taken into account (Gerendás et al. 1997). Whatsoever, most plant species are sensitive to ammonium as the sole nitrogen source and live better on nitrate. The question of why is still an important field of research.

Because of its broad involvement in the processes of the living cell, the assimilation of nitrogen and its incorporation into amino acids is one of the most important processes in a plant. Thus, nitrogen nutrition plays an important role in agriculture. Nitrogen fertilization had a significant contribution to the remarkable increase of crop yield. Nitrogen fertilization can be done by supplying nitrate- or ammonium-salts. However, the diverse N-forms are of different benefit for the plants. The form of N-supply influences growth, morphology and dry matter of the plants (Errebhi and Wilcox 1990, Gerendás and Sattelmacher 1995, Gerendás et al. 1997, Kuiper 1988, Raab and Terry 1994, Walch-Liu et al. 2000).



**Figure 2.1** Scheme of nitrogen uptake from the soil and assimilation in roots and shoots.  $\text{NO}_3^-$  is assimilated either in the roots or in the shoots or is stored in the vacuole.  $\text{NH}_4^+$  is assimilated in the roots and amides are transported via the xylem to the shoots. Enzymes involved in the assimilation are nitrate reductase (NR), nitrite reductase (NiR), glutamine synthetase (GS) and glutamine-oxo-glutarate-aminotransferase (GOGAT) either using ferredoxin (Fd, in the shoots) or nicotinamide adenine dinucleotide (NADH, in the roots) as reducing agent. Amides are mainly glutamine and asparagine. (Heldt 1999, modified).

Nitrate can be stored in great amounts in the vacuole and can be assimilated in the roots as well as in the shoots. The higher the nitrate content in the soil the more assimilation takes place in the shoots (Andrews 1986, Heldt 1999, Taiz and Zeiger 2000). In contrast, ammonium as the sole nitrogen source causes problems in many plants. Free  $\text{NH}_4^+$  is toxic at quite low concentrations (Marschner 1995). The main pathway of detoxification, i.e. binding of N in non-toxic compounds, is the incorporation of ammonium ions into amino acids, mainly glutamine and asparagine. This incorporation comes along with simultaneous release of protons for charge compensation. Since shoots have a rather limited capacity for disposal of protons, nearly all ammonium taken up is metabolized in the roots (Raven 1986). The amino acids are then transported to the shoot via the xylem exudates (Marschner 1995, Heldt 1999, Taiz and Zeiger 2000). All other amino acids are converted from these amino acids by transamination (Leleu and Vuylsteker 2004).

A major consequence of ammonium as the sole nitrogen source seems to be growth inhibition (Gerendás et al. 1997, Walch-Liu et al. 2000) or higher sensitivity to stress (Zhu et al. 2000). Diverse phenomena have been observed and contradictory hypotheses explaining ammonium toxicity have been suggested (for review see Britto and Kronzucker 2002).

It was suggested that  $\text{NH}_4^+$  mediated uncoupling of electron transport from photophosphorylation in the thylakoid membrane (Krause et al. 1982) is a possible origin of  $\text{NH}_4^+$ -induced damage (Magalhaes and Huber 1989). This was disproved by findings of Bendixen et al. (2001) that even in solutions of high  $\text{NH}_4^+$  concentrations plants of *Phaseolus vulgaris* show high energy quenching of chlorophyll fluorescence. This could not occur if the thylakoid membrane was uncoupled. Also, Gerendás et al. (1995) have found that only under extreme growth conditions (20 mM  $\text{NH}_4^+$ , 0.1 mM  $\text{K}^+$ ) there are reasonable amounts of free  $\text{NH}_4^+$  in the leaves, which may be sufficient to cause uncoupling.

Another cause of toxicity may be enrichment of free  $\text{NH}_4^+$  in the cytosol (Givan 1979, Magalhaes and Huber 1989). This was refuted since feeding both N-forms ( $\text{NH}_4^+$  and  $\text{NO}_3^-$ ) together supports optimal plant growth (Crawford and Glass 1998). In addition, Noctor and Foyer (1998) found that free  $\text{NH}_4^+$  in the cytosol is unlikely, because plants with both kinds of nutrition have installed mechanisms, which can cope with the high fluxes of  $\text{NH}_4^+$  released from the mitochondria during photorespiration.

A third putative mechanism for toxicity is disturbance of cytosolic pH by  $\text{NH}_4^+$  uptake (Kosegarten et al. 1997, Marschner 1995, McQueen and Bailey 1991). However, many scientists found that in most cases intracellular pH was unaffected by the form of N-supply

(Bligny et al. 1997, Gerendás et al. 1990, 1993, Gerendás and Ratcliffe 2000, Wilson et al. 1998).

Another mechanism suggested by Givan (1979) was a high carbon demand for  $\text{NH}_4^+$ -assimilation in the roots, which was assumed to be such a strong load for  $\text{NH}_4^+$ -grown plants that it causes growth reduction. This argument is refuted by the results of the investigation of the present thesis, namely, that growth retardation in  $\text{NH}_4^+$ -grown plants occurs before photosynthesis has reached its full power and when energy consumption seems to be lower than in  $\text{NO}_3^-$ -grown plants (sections 4.3 and 4.5.3.4).

Other reasons for growth retardation may be more likely such as impaired water uptake efficiency, lower contents of cations and organic acids resulting in a higher osmotic potential (Gerendás et al. 1997), or high cost of repair of damage caused by higher production of toxic radicals (Zhu et al. 2000).

N-form may interfere with hormonal signalling, since ammonium inhibition of growth in tomato and tobacco grown on  $\text{NH}_4^+$  as the sole nitrogen source was correlated with a sharp decline in cytokinin concentrations (reversible) (Rahayu et al. 2005, Walch-Liu et al. 2000). Cytokinins are involved in regulation of cell division and cell expansion (Ivanova and Rost 1998, Francis and Sorrell 2001). In contrast to  $\text{NH}_4^+$ ,  $\text{NO}_3^-$  seems to increase the concentration of cytokinins (Rahayu et al. 2005). Because of this, cytokinins may be responsible for  $\text{NO}_3^-$ -induced stimulation of leaf growth. Thus, growth retardation in  $\text{NH}_4^+$ -grown plants might be rather an effect of absence of  $\text{NO}_3^-$  than of toxicity of  $\text{NH}_4^+$  (Walch-Liu et al. 2000, Rahayu et al. 2005)

In addition, direct effects of  $\text{NO}_3^-$  on metabolism have been reported.  $\text{NO}_3^-$  influences the metabolism of nitrogen and carbon, resource allocation and root development (Wang et al. 2000, Zhang et al. 1999). These responses involve rapid and marked changes in gene expression, especially of various genes involved in uptake and utilization of  $\text{NO}_3^-$  (Crawford 1995, Forde and Clarkson 1999, Stitt 1999, Wang et al. 2000). Genes induced by nitrate are for example nitrate and nitrite reductases, nitrate transporters, genes involved in ammonium assimilation as well as genes for starch and organic acid metabolism (Crawford and Glass 1998, Stitt 1999, Wang et al. 2000).

Considering the above two paragraphs, there remains the question of whether nitrate acts as a signal directly or rather indirectly via interaction with cytokinins or other phytohormones (Takei et al. 2002, Rahayu et al. 2005). Takei et al. (2002) and Rahayu et al. (2005) suggest a major role for cytokinins as long-distance signals for  $\text{NO}_3^-$ -induced stimulation of leaf growth.

Ammonium or its metabolites (mainly glutamine and asparagine) exert inhibitory effects on the nitrate assimilatory pathway e.g. expression of nitrate reductase (Faure et al. 1991) and nitrate transporter (Zhuo et al. 1999). The network of nitrogen metabolism is complex and still not fully analyzed and understood. The work presented here aims on the influence of ammonium compared to nitrate in seedlings in order to gain more information on the effect of growth retardation.

### **2.2 Ammonium-induced sensitivity to light stress in *Phaseolus vulgaris***

*P. vulgaris* has been used successfully as a model plant to investigate N-form dependent differences. Investigations on *P. vulgaris* have shown that N-form dependent growth retardation depends on light intensity. It was found that under low-light conditions ( $150 \mu\text{mol m}^{-2}\text{s}^{-1}$ ) growth retardation cannot be observed but under highlight conditions ( $550 \mu\text{mol m}^{-2}\text{s}^{-1}$ ) this phenomenon becomes quite obvious (Zhu et al. 2000). To get an insight into the mechanisms leading to this effect physiological investigations have been done.

Chlorophyll fluorescence as measured by the PAM fluorometer (Schreiber et al. 1986) is widely employed as a means of detecting damage of the photosynthetic apparatus (Schreiber and Bilger 1993). Especially the ratio  $F_v/F_M$  is used to determine the degree of photoinhibition (Demmig and Winter 1988), i.e., the damage of PS II. Bendixen et al. (2001) found that there was no N-form dependent difference in photoinhibition. This indicated that damage of PS II was not a major cause of the observed growth retardation. However, as mentioned above, growth retardation was related to light-intensity. Thus, it was concluded that the sources for harmful production of reactive oxygen species (ROS) are located in processes downstream of PS I (Zhu et al. 2000).

Nevertheless, there was a difference in functioning of PS II between  $\text{NO}_3^-$ - and  $\text{NH}_4^+$ -grown plants, as became obvious from the measurement of zeaxanthin. Zeaxanthin is an antenna carotenoid of PS II, which accelerates thermal deactivation of surplus excitation energy in photosynthetic antennae (Horton et al. 1991). Zeaxanthin formation during light was reduced in  $\text{NH}_4^+$ -grown plants. However, the normally expected higher photoinhibition was not observed (Bendixen et al. 2001). The reason became obvious from experiments with dithiothreitol (DTT), a reducing agent that is used to prevent the conversion of the inactive

form violaxanthin to the active form zeaxanthin (Bilger and Björkman 1990, Jakob et al. 1999). Photoinhibition in  $\text{NO}_3^-$ -grown plants was increased by DTT but it was not affected in  $\text{NH}_4^+$ -grown plants. This indicated that  $\text{NH}_4^+$ -grown plants have an alternative mechanism to protect their photosystems.

The zeaxanthin experiments provided a hint to one of the putative causes of growth retardation in  $\text{NH}_4^+$ -grown plants. Feeding ascorbate via the petiole led to an increased formation of zeaxanthin indicating that ascorbate deficiency was the origin of lower zeaxanthin levels in  $\text{NH}_4^+$ -grown plants (Bendixen et al. 2001). The depletion of ascorbate in  $\text{NH}_4^+$ -grown plants seems to be a hint that there might be a higher need for detoxification of radicals. This interpretation is in line with findings of Zhu et al. (2000) that the scavenging enzymes ascorbate peroxidase and glutathione reductase showed higher activities in  $\text{NH}_4^+$ -grown plants. Interestingly, the activity of superoxide dismutase (SOD) was not dependent on N-form. This again was an indication that damage of photosystems was not a serious problem per se.

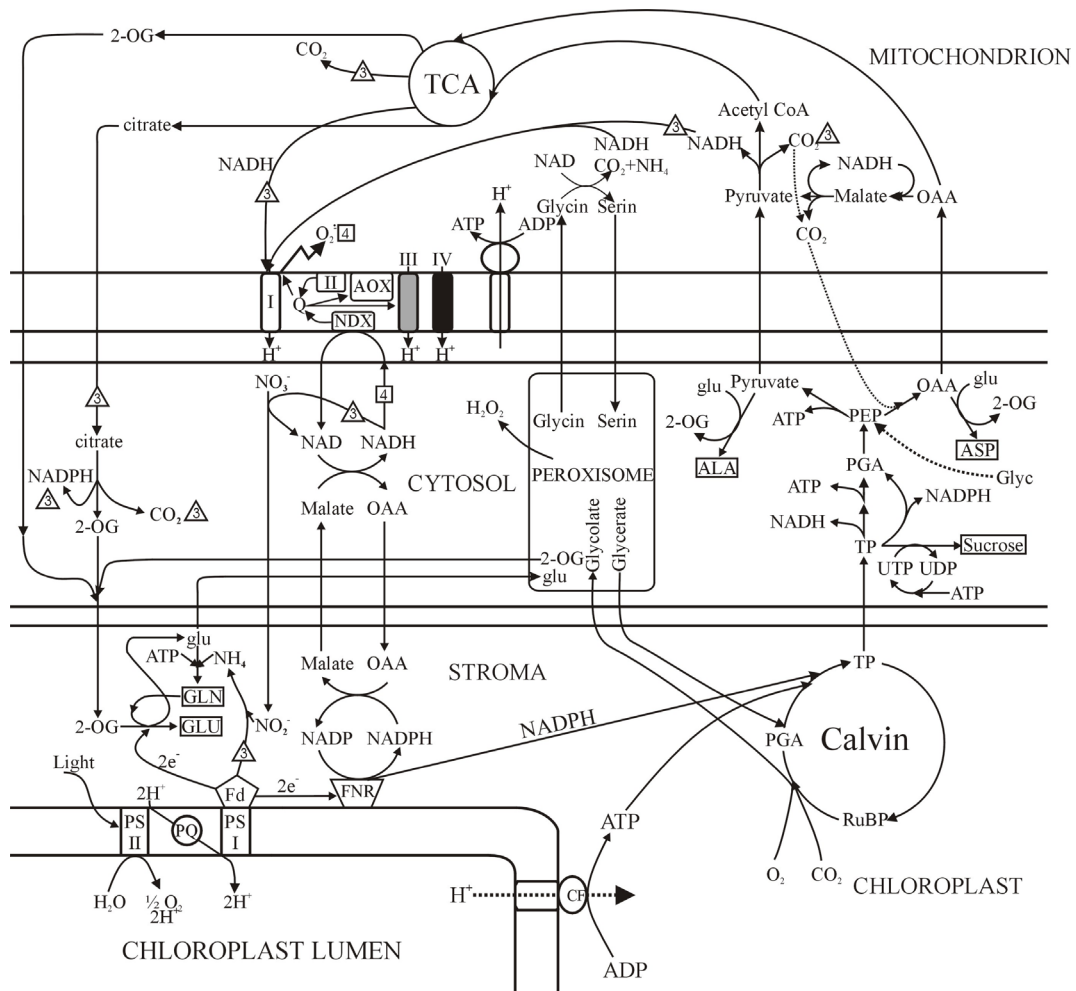
At this point it became more and more evident that there might be an N-form dependent branching in metabolic pathways in the shoots (Vanselow 1993, Guo et al. 2005).  $\text{NO}_3^-$ -grown plants have the facility of exporting superfluous electrons to acceptors involved in N-assimilation, such as nitrate reductase (NR), nitrite reductase (NiR), and the glutamine-2-oxoglutarate-amino transferase (GOGAT) system. For these reactions, they need C-skeletons (Fig. 2.2 below) as indicated by a change in the apparent  $\text{CO}_2$  compensation point of photosynthesis (Guo 2002, Guo et al. 2005, Schinner 2001, Schinner et al. 2001). The absence of this security valve in  $\text{NH}_4^+$ -grown plants leads to employment of more risky reactions in the shoots, e.g. delivery of redox equivalents to the mitochondrial electron transport chain (ETC) downstream of Complex I (Guo et al. 2005). The higher load of ROS in  $\text{NH}_4^+$ -grown plants was indicated by higher lipid peroxidation as measured by malondialdehyde (MDA) content (Zhu et al. 2000).

Additional support came from the reaction of  $\text{NO}_3^-$ - and  $\text{NH}_4^+$ -grown plants to inhibitors of the mitochondrial ETC.  $\text{NH}_4^+$ -grown plants are sensitive to SHAM acting on alternative oxidase in the mitochondria whereas  $\text{NO}_3^-$ -grown ones are sensitive to antimycin A acting on complex 3. This indicated that there are different metabolic pathways involved in the processing of superfluous electrons (Guo et al. 2005, Hammes 2005, Schinner et al. 2001).

Support for the scheme in Fig. 2.2 comes from a mathematical analysis of differences in  $\text{CO}_2$  compensation point. The finding of a higher compensation point in  $\text{NO}_3^-$ -grown plants led to the assumption of a light-induced non-photorespiratory increase in  $\text{CO}_2$  evolution. In



the scheme of Fig. 2.2, the source of this CO<sub>2</sub> evolution is in the pathway for supplying C-skeletons to N-assimilation, i.e., the conversion of citrate to 2-oxo-glutarate (2-OG) on the left-hand side of the scheme. This process occurs only in NO<sub>3</sub><sup>-</sup>-grown plants because N-assimilation of NH<sub>4</sub><sup>+</sup> is done in the roots.



**Figure 2.2** Illustration of the pathways of interaction between photosynthesis, photorespiration and respiration with special regards to different N-forms. Important pathway considered to be related to NO<sub>3</sub><sup>-</sup>-grown plants: conversion of citrate to 2-oxo-glutarate (2-OG) on the left hand side for the supply of C-skeletons for N-assimilation. Important pathway related to NH<sub>4</sub><sup>+</sup>-supply: using of mitochondrial external dehydrogenase (NDX) as sink for superfluous electron via malat-oxalate (OAA)-shuttle probably leading to superoxide production at complex I in the mitochondrial electron transport chain (Guo et al. 2005).

In summary, it was found that  $\text{NH}_4^+$ -grown plants suffer more from light stress than  $\text{NO}_3^-$ -grown plants do. In  $\text{NO}_3^-$ -grown plants, the branching of redox flow downstream of PS I caused light-dependent non-photorespiratory  $\text{CO}_2$  evolution, which resulted from the supply of C-skeletons for N-assimilation. This was most likely the reason why the N-assimilation in  $\text{NO}_3^-$ -grown plants provided a less dangerous electron sink. It was assumed that excess ROS production in  $\text{NH}_4^+$ -grown plants probably resulted from mitochondrial complex I which became idle because NADH exported from the chloroplasts blocked the discharge of electrons from complex I (Casolo et al. 2000). All of these findings led to the general conclusion that chloroplast-mitochondria coupling can no longer be ignored in photosynthesis research.

Since the physiological experiments cannot explain all phenomena associated with N-metabolism other kinds of experiments are required to further unravel the regulatory mechanisms behind the observations. Such new approaches may include gene expression or protein studies.

### 2.3 *Arabidopsis thaliana*

In this project, changing from *P. vulgaris* to *A. thaliana* became necessary in order to study the dependence of gene expression on N-form and light by means of microarrays. *A. thaliana* serves as the model organism for plant molecular biology. No microarrays exist for *P. vulgaris* up to now because its genome is not fully sequenced yet. Furthermore, using *A. thaliana* facilitated cooperation with other groups working on this model organism.



**Figure 2.3** *Arabidopsis thaliana* (mouse ear cress) member of the Brassicaceae family.

*A. thaliana* (mouse ear cress) is of no major agronomic importance. But it is a member of the Brassicaceae family and closely related to radish and cabbage. Scientists all over the world

use *A. thaliana* to study plant development, reproduction and responses to stress and disease since it behaves similar to crop plants but is much simpler to study ([www.mpimp-golm.mpg.de/arabidopsis](http://www.mpimp-golm.mpg.de/arabidopsis)). *A. thaliana* offers important advantages for basic research in genetics and molecular biology because of its rapid life cycle (6 weeks under climate control), its small diploid genome ( $1 \times 10^8$  nucleotide pairs) and little repetitive non-coding DNA (10 %) (Heldt 1999, [www.arabidopsis.org](http://www.arabidopsis.org)). Since 2000 the genome is fully sequenced (The Arabidopsis Genome Initiative 2000). The whole genome of *A. thaliana* consists of about 25000 genes located on five chromosomes. Cultivation is easy, inexpensive and needs only minimal space. The plant is producing thousands of seeds making it very attractive for research. 1943 Friedrich Leibach cultivated the first pure culture and had the first collection of induced mutants. Today, a large number of mutant lines and genomic resources is available ([www.mpimp-golm.mpg.de/arabidopsis](http://www.mpimp-golm.mpg.de/arabidopsis)).

## **2.4 Gene expression studies**

### **2.4.1 Microarray technology**

In recent years, microarray technology has become a key experimental tool, enabling the analysis of expression patterns of thousands of genes or even whole genomes simultaneously. Microarrays are little more than a microscope glass slide on which single stranded DNA or oligonucleotides are spotted. As probes for hybridization on the microarray, fluorochrome or biotin labelled complementary DNA (cDNA) is used. The cDNA of transcripts isolated from the plant material of interest is obtained by reverse transcription in the presence of fluorochrome (e.g. cy3 or cy5) labelled or biotinylated nucleotides.

The microarray technique makes use of the natural mechanism: Adenine specifically binds to thymine and cytosine to guanine. The genes consist of specific sequences (base order) that are complementary to the fragment spotted on the array.

The occurrence of hybridization is made visible by illumination of the array with an appropriate source of light, thus providing an image of the array spots. The intensity of the signal is related to the expression level of the gene presented by the spot. Image processing leads to a large number of expression values (Dràghici 2003, Brewster et al. 2004).

### 2.4.2 Application to the effects of N-nutrition and light

There is a great number of investigations on gene expression related to nitrate and light. Nitrate induces one of the major nutrient responses leading to induction or repression of gene expressions. Additionally it serves as a signal in metabolism including induction of synthesis of nitrate assimilatory enzymes and shifting from starch deposition to production of organic acids (Stitt 1999, Wang et al. 2000, 2003). After nitrogen deprivation or starvation, plants response to nitrate very rapidly. Known nitrate-responsive genes are for example, nitrate and nitrite reductase (NR, NiR), nitrate transporter, fd reductase, glutamine synthetase (GS) and glutamine-2-oxoglutarate-amino transferase (GOGAT) as well as phosphoenolpyruvate carboxylase (PEPc) and ADP-glucose phosphorylase (Koch 1997, Crawford and Glass 1998, Forde and Clarkson 1999, Stitt 1999, Wang 2000).

Investigations on gene expression using microarray-technology usually cover the response to readdition of nitrate after nitrogen deprivation or nitrogen starvation (Wang et al. 2000, 2003, Scheible et al. 2004). These studies involving whole seedlings (Wang et al. 2000) or shoots and roots separately (Wang et al. 2003) revealed that the most responsive genes to low nitrate were genes encoding for enzymes devoted to nitrite reduction and to glycolysis, trehalose-6P metabolism, iron transport and sulphate reduction/uptake. Additionally, Scheible et al. (2004) observed rapid coordinated induction of genes involved in providing of reducing equivalents and in synthesis of organic acids and proteins. They also found coordinated repression of the shikimate pathway, phenylpropanoid and flavonoid metabolism as well as large changes in expression of genes determining redox status. Comparing the response of nitrate re-addition in NR deficient mutants with wild-type plants indicates that mainly genes of energy conversion, metabolism, glycolysis and gluconeogenesis were induced by nitrate. The induction was found to be stimulated directly by nitrate rather than by its down stream metabolites (Wang et al. 2004).

Other gene expression studies focus on the impact of highlight stress on gene expression. High light intensities have the potential to damage the photosynthetic apparatus. The damage is caused by superfluous electrons generating reactive oxygen species. Identification of factors and signalling pathways for diminishing oxidative damage are in the focus of gene expression studies. In addition to those of scavenging enzymes, genes involved in biosynthesis of lignin and flavonoids as well as chaperones and other stress related proteins have been found to be induced (Kimura et al. 2003, Rossel et al. 2002).

Recent research deals with the gene expression during development. Ma and coworkers (2005) investigated the organ-specific gene expression during development and generated a genome expression atlas of 18 organ or tissue types. The analysis of global gene expression during development revealed, that expression levels of transcription factors and signal transduction genes are similar to those of metabolic genes (Schmid et al. 2005). These large sets of data provide a basis for identification of the molecular processes underlying development (Ma et al. 2005).

The investigations mentioned above reflect only a minor amount of research done by means of microarray technology but give an impressive view of the possibilities using this cutting edge technology. Especially interpreting all the generated data is and will be a challenge. For the investigations presented, the published studies dealing with the effects of nitrate and light on metabolism may serve as a guideline for the discussion of the differential effects of nitrate versus ammonium.

### **2.5 Aims and scope of the project**

The physiological data reported for *P. vulgaris* and other crop plants provide important information about the effect of ammonium compared to nitrate as the sole nitrogen source. In the light of the hypothesis for *P. vulgaris* stated in section 2.2 (growth retardation in relation to high-light conditions, Guo et al. 2005) gene expression in the leaf and the role of photosynthesis are of major importance.

Because of this, the investigations reported here are performed on *A. thaliana* in an early state of development grown under low light. This may offer the chance to find out whether an influence of the N-form is exerted also without involvement of photosynthesis.

The studies are focussed on the physiological and metabolic changes in the leaves. The hypothesis of Guo et al. (2005) requires the verification of several predictions that have so far only be concluded from indirect measurements. This holds for development of ROS and for the interaction between cellular compartments. ROS measurements by DCF (or NBT) and gene expression studies are adequate tools for gaining direct access to these processes. Even though the mechanisms in seedlings of *A. thaliana* may be different from those in the plants used by Guo et al. (2005), the application of these techniques here may also provide an estimation of the suitability for the verification of the hypothesis of Guo et al. (2005).

Nevertheless, the focus of the presented investigations lies on the issue mentioned above, i.e., to investigate the fundamental question whether there are N-form-dependent changes in metabolic behaviour, which are not mediated by photosynthesis. This leads to the choice of seedlings and low light intensity.

Thus, the aim of the present work is to characterize different metabolic pathways in  $\text{NO}_3^-$ - or  $\text{NH}_4^+$ -grown seedlings of *A. thaliana* by using physiological, biochemical and gene expression approaches.

## 3 Material and Methods

### 3.1 Plant material

*Arabidopsis thaliana* ecotype Columbia 0 wild type, kindly provided by Dr. C. Plieth, Centre of Biochemistry and Molecular Biology, was used throughout all experiments.

*Spinacia oleracea* L. was provided by Royal Sluis bv, Enkhuizen, Holland.

### 3.2 Preparation of plant agar

The nutrients for  $\text{NH}_4^+$ - or  $\text{NO}_3^-$ -medium (Table 3.1) were solved in distilled water. The pH was adjusted to 6.2 with NaOH. For vertical plates 1.2 % plant agar (Sigma, Steinkirchen, Germany) and for horizontal ones 0.8 % were used. The solution was autoclaved at 1 bar and 121 °C for 20 min.

**Table 3.1** Composition of the  $\text{NO}_3^-$ - and  $\text{NH}_4^+$ -medium. Molarities refer to main nutrient e.g. 4.44mM (N) in  $\text{Ca}(\text{NO}_3)_2$  and 1.2mM (K) in  $\text{K}_2\text{SO}_4$ .

<u><math>\text{NO}_3^-</math>-medium</u>		<u><math>\text{NH}_4^+</math>-medium</u>	
$\text{Ca}(\text{NO}_3)_2$	4.44 mM	$(\text{NH}_4)_2\text{SO}_4$	4.44 mM
$\text{K}_2\text{SO}_4$	1.2 mM	$\text{CaCl}_2$	2.22mM
$\text{MgSO}_4$	0.75mM	$\text{K}_2\text{SO}_4$	1.2 mM
$\text{KH}_2\text{PO}_4$	0.3 mM	$\text{MgSO}_4$	0.75 mM
Fe-Na-EDTA	100 $\mu\text{M}$	$\text{KH}_2\text{PO}_4$	0.3 mM
$\text{MnSO}_4$	1 $\mu\text{M}$	Fe-Na-EDTA	100 $\mu\text{M}$
$\text{ZnSO}_4$	1 $\mu\text{M}$	$\text{MnSO}_4$	1 $\mu\text{M}$
$\text{CuSO}_4$	0.1 $\mu\text{M}$	$\text{ZnSO}_4$	1 $\mu\text{M}$
$\text{H}_3\text{BO}_3$	10 $\mu\text{M}$	$\text{CuSO}_4$	0.1 $\mu\text{M}$
$(\text{NH}_4)_6\text{Mo}_7\text{O}_{24}$	0.01 $\mu\text{M}$	$\text{H}_3\text{BO}_3$	10 $\mu\text{M}$
		$(\text{NH}_4)_6\text{Mo}_7\text{O}_{24}$	0.01 $\mu\text{M}$

### 3.3 Surface sterilisation of seeds

*A. thaliana* ecotype Columbia 0 and *S. oleracea* seeds were placed in glassine paper bags (John Dickinson Stationery limited, Cambridge, UK) in a desiccator jar under a fume hood. A 250 ml beaker containing 100 ml bleach (5%) (sodium hypochlorite, Walter, Kiel, Germany) was put into the jar, and 3 ml concentrated HCl were carefully added to the bleach. The jar was immediately sealed and sterilization by chlorine gas was done for three to 16 hours.

### 3.4 Growth conditions

#### 3.4.1 Growth conditions for physiological measurements

Surface sterilized seeds (see 3.3) of *A. thaliana* ecotype Columbia 0 were grown for 14 to 16 days on vertical agar plates (see 3.2, 1.2 % plant agar, Sigma, Steinkirchen, Germany) at pH 6.2 buffered with 5 mM MES. Light intensity in the temperature-controlled room was  $40 \mu\text{mol m}^{-2}\text{s}^{-1}$ . The temperature was 23 °C at „day time“ (10 h) and 20 °C at „night time“ (14 h).

#### 3.4.2 Growth conditions for gene expression studies

Surface sterilized seeds of *A. thaliana* ecotype Columbia 0 were grown for 15 days on horizontal agar plates (0,8 % plant agar, Sigma, Steinkirchen, Germany) at pH 6.2 buffered with 5 mM MES. Light intensity in the temperature-controlled room was  $40 \mu\text{mol m}^{-2}\text{s}^{-1}$ . The temperature was 23 °C at „day time“ (10 h) and 20 °C at „night time“ (14 h). On the 15<sup>th</sup> day, half of the plates were transferred to a light intensity of  $800 \mu\text{mol m}^{-2}\text{s}^{-1}$  (SON-T Agro 400, Phillips, Hamburg, Germany, Fig. 3.1) for 2 h (these plants are called "stressed"). The control plants remained in the climate chamber. After 2 h, the leaves of control (LL) and stressed plants (HL) were harvested, shock frozen in liquid nitrogen and stored at – 80 °C for further use.





**Figure 3.1** Experimental arrangement for applying high-light conditions of  $800 \mu\text{mol m}^{-2}\text{s}^{-1}$  using SON-T Agro 400 lamp (Phillips, Hamburg, Germany).

Figure 3.1 shows the experimental set-up for light-stress. On top, there is the SON-T Agro 400 lamp. 20 cm below the lamp, there is a water filter with a permanent water flow to filter the infrared and far red light producing heat. The temperature below the filter is about 12 K cooler than above. The agar plate is positioned in a water bath (water temperature is constantly 20 °C, air temperature 23 °C) to keep the temperature in the plate as constant as possible. This was done to ensure that the plants did not suffer from heat stress. No significant temperature increase was determined in the agar plate during light stress (1 K / h).

### 3.5 Verification of constant pH around the roots

$\text{NH}_4^+$  ions are transported into the plants in exchange for  $\text{H}^+$ . For one  $\text{NH}_4^+$  ion, there is one  $\text{H}^+$  ion leaving the plant. This effect leads to an acidification around the root zone as described in Marschner (1995). Acidification causes an altered nutrient uptake. In order to check for this phenomenon the pH indicator bromocresol purple (pH range 6.8-5.2) was added at a concentration of 1.11 mM to the plates.

The agar plates were produced as usual (see 3.2), one half with 5 mM MES as buffer the other half without any buffer. Bromocresol was dissolved in EtOH abs. (0.2 % of final volume). Millipore water was added up to appropriate volume. For sterile filtration, a 0.2  $\mu\text{m}$  filter was used. The sterile pH indicator was added to the autoclaved medium.

*A. thaliana* and *S. oleracea* seeds were plated on buffered and unbuffered plates. *S. oleracea* seeds were used to have a positive control indicating that acidification is dependent on root size and growth rate. The plates were checked every day for changes in pH which was indicated by a colour change from lilac to yellow.

### 3.6 Analysis of nutritional status of the plants

Analysis of C, N, anions and amino acid contents were done in cooperation with AG Prof. Sattelmacher, Institute of Plant Nutrition and Soil science.

#### 3.6.1 Measurements of C and N by Elemental Analyzer

Elemental analyzing is a sensitive method to determine total C, O, H, N and S present in a wide range of organic and inorganic samples. The analytical method is based on the complete and instantaneous oxidation of a sample by "flash combustion" which converts all organic and inorganic substances into combustions products. The resulting combustion gases pass through a reduction furnace and are swept into the chromatographic column by the carrier gas (helium) where they are separated and detected by a thermal conductivity detector. This detector gives an output signal proportional to the concentration of the individual components of the mixture (Manual EA element analyzer). In this case total C and N in *A. thaliana* leaves have been analyzed using the EA 1108 Elemental Analyzer (Carlo Erba instruments, Milan, Italy).

One milligram of dried *A. thaliana* leaves was weighed into a tin container and placed into the autosample drum of the analyzer. The chromatographic column used was a porapak PQS column (Carlo Erba instruments, Milan, Italy).

#### 3.6.2 Measurements of anions by ion chromatography

Ion chromatography is used to separate and quantitate anions and cations. This analytical technique is based on the separation of the components of a mixture in solution by selective adsorption. Here the anions Cl, SO<sub>4</sub>-S, PO<sub>4</sub>-P, NO<sub>3</sub>- N as well as the organic acids malate, oxalate and citrate have been analyzed using the ICS 2500 system (Dionex GmbH, Idstein, Germany) with the following equipment AS50 autosampler, AS50 chromatography compartment, ED50 Electrochemical Detector and GP50 Gradient Pump. For gradient elution 50 mM NaOH has been used. The flow rate was 1.5 ml min<sup>-1</sup>.

Twenty milligrams dried leaf material has been grinded and dissolved in 1 ml of distilled water. This solution was subject to a hot-water extraction. For the extraction the reaction tube was placed in boiling water for 5 min. After 2.5 min the solution had been vortexed once. After another 2.5 min the solution was vortexed again and left on ice for at least 30 min. This step was followed by centrifugation at 4 °C for 30 min at 3800 rpm (Heraeus Biofuge, Thermo Electron, Langensfeld, Germany). The supernatant was filtered

through a RP18 cartridge to clean the extract from phenolic compounds that interfere with the measurement. The samples were diluted in distilled water 1:15.

### **3.6.3 Measurements of amino acids by ion exchange chromatography**

Ion exchange chromatography is also applied to separate substances into their individual compounds. Here the method of Moore, Spackman and Stein (1958, modified) was applied to separate a mixture of amino acids using the automated system Biochrom 30 analyzer (Biochrom AG, Berlin, Germany). The basic system behind is a cation exchanger and gradient-elution (pH 2.85-10.3, 5 steps) with lithium-acetate buffer. The chromatographic column was PEEK HP (Biochrom AG, Berlin, Germany) and the reaction coil had a temperature of 138 °C. Two different wavelength for detection have been used, 440 nm for proline and 570 nm for the other amino acids. For determination of the concentrations an amino acid standard (Sigma, Steinkirchen, Germany) had been analyzed as well.

The material for analysis was the supernatant of the hot water extract described above (see 3.6.2) diluted 1:2 with probe dilution buffer (Biochrom AG, Berlin, Germany). The extract was not filtered before use.

## **3.7 Physiological measurements**

### **3.7.1 Measurements of processes related to photosynthesis**

Measurements in this section were done in cooperation with Dr. Hartmut Kaiser, AG Prof. Bilger, and Dr. Christine Desel, AG Prof. Krupinska, Institute of Botany and Central Microscopy Unit at the University of Kiel, respectively, and with Enno Hammes, ZBM.

#### **3.7.1.1 Illustration of cell morphology using transmission electron microscope**

Transmission electron microscope (TEM) micrographs enable the resolution on the level of cellular compartments. In order to analyze morphological differences in nitrate- and ammonium-grown *A. thaliana* leaves micrographs of leaves from both types were made. For this procedure, leaves (size: 1-2 mm) of *A. thaliana* grown at low light and short day (growth conditions see 3.4.1), were harvested from the agar plate and infiltrated with phosphate buffer saline (see A.1) for 5 min at a sub pressure of 500 mbar (trivac, Leybold-Heraeus, Köln, Germany). After infiltration, the plants stayed for 5 min in the dark. Then, the buffer solution was exchanged with fixation solution and infiltrated for 5min at a sub pressure of 500 mbar.

The plants were fixed in 2 % (w/v) paraformaldehyde / 2.5 % (v/v) glutaraldehyde in 0.1 M cacodylate buffer pH 7.2 overnight at 4 °C. At the next day, the plants were washed 3x for 10-15 min in 0.1 M cacodylate buffer and dehydrated in an ethanol series (2x 50 %, 2x 70 % for 10 min each, 2x 90 % for 5 min and 4x 100 % for 20 min each). The dehydration followed two times incubation in propylene oxide for 5 min, and the dehydrated samples were progressively embedded in Epon (Epoxy embedding medium kit, Fluka, Buchs, Switzerland) at propylene oxide / Epon 3:1 for 2 h, propylene oxide / Epon 1:3 for 2 h and Epon overnight in reaction tubes on a rotating shaker. The next day, fresh Epon was added, and plants were shaken for 2 h. Embedded samples were transferred to fresh Epon and polymerized at 60 °C overnight. The samples were stored at room temperature until further use (Bestwick et al. 1995, Dörr 1997).

Ultra thin sections (60-80 nm) were cut on an Ultramikrotom UCT (Leica, Wetzlar, Germany) using a diamond knife and mounted on uncoated copper grids (300 mesh). Pictures were taken with TEM Philips EM 208S (Phillips, Kassel, Germany) in the Central Microscopy Unit of the University of Kiel. Analysis was done with the software: analySIS Doku.2.11.007 (Soft Imaging System, Münster, Germany). For documentation, the camera KODAK MEGAPLUS Camera, Model 1.6i was used.

### **3.7.1.2 Determination of photosynthesis rate**

CO<sub>2</sub> consumption of the plants is a measure of photosynthetic activity. For this reason, the net-photosynthetic rate of the plants was measured at atmospheric CO<sub>2</sub> with a CMS4P minicuvette system (Walz GmbH, Effeltrich, Germany) equipped with an infrared gas analyzer (Binos 100, Rosemount Analytical, Emerson GmbH, Haan, Germany). The plant material was enclosed in a sealed chamber, and the change in CO<sub>2</sub> concentration of the air passing the cuvette was determined by differential measurement using reference gas stream (Schroeter et al. 1994). The system measured  $\Delta\text{CO}_2$  with an accuracy of 0.1 ppm. During the measurement plants were illuminated with light of 260  $\mu\text{mol m}^{-2} \text{s}^{-1}$  which was found to saturate CO<sub>2</sub> uptake.

### **3.7.1.3 Determination of chlorophyll content**

The net photosynthetic rate was normalised to the chlorophyll content of the plants in order to reveal the CO<sub>2</sub> consumption per chlorophyll. This data reveal the efficiency of chlorophyll in photosynthesis.

For chlorophyll extraction, the plants were harvested, shock frozen in liquid nitrogen and stored in 1.5 ml reaction tubes at  $-80\text{ }^{\circ}\text{C}$  until further use. The extraction had to be done in a darkened room. All material e.g. racks and pistils (Einmal-Mikropistill, Eydam, Kiel, Germany) were pre-cooled with liquid nitrogen. The grinding was done in 1.5 ml reaction tubes. During the grinding process, the powder should not thaw at all. For buffering reasons, one spatula tip of  $\text{MgHCO}_3$  was added. 100  $\mu\text{l}$  of 85 % acetone (in Tris-HCl (see A.1) pH 7.8) were added to the cap, and the material was grinded again. Then 900  $\mu\text{l}$  of 85 % acetone were added, and the pistil was cleaned with the liquid. The powder and acetone were mixed by vortexing and were centrifuged for 5 min at 6000 rpm at  $4\text{ }^{\circ}\text{C}$  using a Heraeus Biofuge (Thermo Electron, Langenselbold, Germany). The supernatant was saved in another cap. The pellet was mixed again with 500  $\mu\text{l}$  85 % acetone and centrifuged for 5 min at 6000 rpm at  $4\text{ }^{\circ}\text{C}$ . The process was repeated until no green colour was visible in the supernatant. Supernatants from all steps were combined, and the final volume had to be determined for the calculation of chlorophyll concentration.

The chlorophyll content was measured in a spectrofluorometer (Uvikon 922, Kontron Instruments, Neufahrn, Germany) at wavelength of 750 nm, 663.6 nm and 646.6 nm and was calculated according to Porra et al. (1989).

Calculation:

$$\begin{aligned} Chla &= 12.25A_{663.6} - 2.55A_{646.6} \\ Chlb &= 20.31A_{646.6} - 4.91A_{663.6} \\ Chla + b &= 17.76A_{646.6} + 7.34A_{663.6} \end{aligned} \tag{3.1}$$

The photosynthetic rate in  $\mu\text{mol CO}_2/(\mu\text{g Chl *s})$  was determined using the following equation:

$$\text{Photosynthetic rate} = \text{molar flow} * \Delta\text{ppm CO}_2 / \mu\text{g Chl} * (-1)$$

The molar flow of  $\text{CO}_2$  was  $0.44615\text{ mmol s}^{-1}$  resulting from flow = 0.6 l/min and molar norm volume = 22.414 l/mol.

#### 3.7.1.4 Measurement of chlorophyll fluorescence

Chlorophyll fluorescence is used to determine the activity of the photosynthetic apparatus and is a well established means of monitoring the influence of stress (Schreiber and Bilger 1993).

Measurements of chlorophyll fluorescence were done with a PAM fluorometer (Walz GmbH, Effeltrich, Germany) according to the protocol of Schreiber et al. (1986).

Photochemical quenching  $q_p$ , non-photochemical quenching  $q_N$  and Genty parameter  $\Phi_e$  (Genty et al. 1989) were obtained from the PAM protocol of chlorophyll fluorescence induced by saturating flashes before ( $F_M$ ) and during actinic light ( $F_M'$ )

$$q_p = \frac{F_M' - F}{F_M' - F_0'}, \quad q_N = \frac{F_M' - F_0'}{F_M - F_0}, \quad \Phi_e = \frac{F_M' - F_0'}{F_M'} \quad (3.2 \text{ a, b, c})$$

with  $F$  being the actual fluorescence induced by the actinic light,  $F_0$  and  $F_0'$  the fluorescence of open reaction centres before and during exposure to actinic light, respectively.

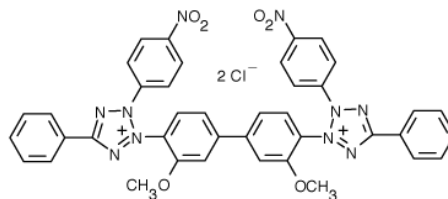
Energy quenching ceases with a time constant of 5 to 20 s (Vanselow et al. 1989, Hansen et al. 1993) resulting in the return of  $F_M'$  to the  $F_M$  level within some minutes after switching off the actinic light. The difference between  $F_M'$  and  $F_M$  which persists longer indicates photo-inhibition of PS II or movement of PS II antennae (Hansen et al. 1993).

### 3.7.2 Determination of ROS

#### 3.7.2.1 Monitoring $O_2^-$ radicals in the leaves by nitroblue tetrazolium

Nitroblue tetrazolium (NBT) is used to monitor  $O_2^-$  radicals. The dye is reduced by superoxide and accumulates as blue precipitate in the cells (Flohe and Otting 1984, Beyer and Fridovich 1987).

The dye was applied after the following protocol. Plants were harvested from the agar plate and infiltrated with 6 mM NBT (Biomol, Hamburg, Germany, Hückelhoven et al. 2000, Freyer et al. 2002) in phosphate buffer saline (see A.1) for 5 min at a sub pressure of 400-500 mbar (trivac, Leybold-Heraeus, Köln, Germany). Then, they were illuminated with 800  $\mu\text{mol m}^{-2}\text{s}^{-1}$  for 25 min (halogen lamp, HLX64653, 24 V, 250 W, Osram, Munich, Germany). Control plants were kept in the dark. In order to make NBT visible, chlorophyll was extracted with ethanol/chloroform (4:1) supplemented with 0.15 % (w/v) trichloroacetic acid.



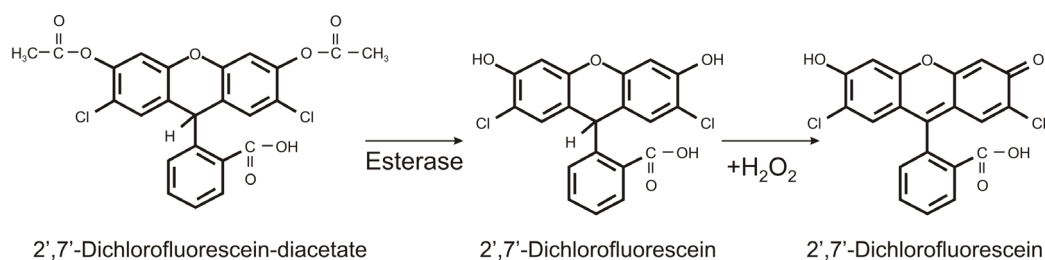
**Figure 3.2** Structure of nitroblue tetrazolium (Molecular Probes, <http://probes.invitrogen.com>)

The bleached plants were submerged in a glycerin:water (1:1) solution und mounted on the stage of a macromicroscope (WILD Heerbrugg Makroskop M 420, Leica, Wetzlar, Germany), at 16x magnification. Pictures of plants were taken by a Sony 3CCD camera. For image storage and proccession, the software Imagic Image Access 3.10 was employed.

#### 3.7.2.2 Monitoring oxidative stress in the leaves by 5-(and-6)-carboxy-2',7'-dichlorodihydrofluorescein diacetate

DCF-DA is a widely used dye for monitoring oxidative stress mainly that caused by peroxides e.g.  $H_2O_2$  (Bass et al. 1983, Myhre et al. 2003, Trayner et al. 1995; Deng et al. 2002, Maxwell et al. 1999, Tarpey et al. 2004).

Plants from the agar plates were vacuum infiltrated with 30  $\mu$ M DCF-DA (Sigma-Aldrich, Munich, Germany, Deng et al. 2002, Maxwell et al. 1999, Tarpey et al. 2004) in SM (see A.1) in a closed 10 ml syringe for 10 to 20 s by moving the piston backwards. DCF-DA was used because only the diacetate form is taken up into the cells. Inside the cell it is cleaved by esterases into the cell-impermeable form (Fig 3.3). The patchiness of the dye distribution caused by this procedure has been reported by Hideg et al. (2002). However, in our set-up only a minor spot with a diameter of 0.5 mm is investigated. Regions greater than 0.5 mm showing evenly distributed fluorescence were selected under the microscope for the actual measurement.



**Figure 3.3** Reaction scheme of DCF-DA. DCF-DA is cell permeable. After cleavage by esterases inside the cell it becomes cell impermeable. Reaction with hydrogen peroxide (or other peroxides) by means of peroxidases is crucial for the formation of the fluorescent form of DCF. Scheme according to Bass et al. (1983).

A single infiltrated leaf of *A. thaliana* was fixed with a steel needle on the bottom of a petri dish (Plieth and Hansen 1996). The dish was mounted on the stage of an inverse microscope (Diaphot, Nikon, Düsseldorf, Germany) and kept under a thin layer of SM. The microscope was equipped with a 10x objective (Fluor Ph2DL, Nikon), and an excitation-ratio imaging

device (TILL Photonics; Gräfelfing, Germany). On the abaxial side of the leaf, DCF fluorescence was excited with light of 488 nm (monochromator, TILL Photonics) and emission was recorded at 535 nm (emission filter: HQ535/50 dichroic mirror: 500 dcxr; AHF, Tübingen, Germany). A light conductor (diameter 250  $\mu\text{m}$ ) was positioned on the adaxial surface of the leaf providing actinic light from a He-Ne-laser. The intensity had to be high ( $9000 \mu\text{mol m}^{-2}\text{s}^{-1}$ ,  $\lambda=632\text{nm}$ ) because it had to penetrate the leaf in order to reach the region of interest on the abaxial side. Five minutes after infiltration, the light protocol (10 min dark adaptation, 20 min actinic light on, 20 min actinic light off) was started. Fluorescent images were taken every 12 seconds. Macro programming of experiments, image acquisition, data collection, and evaluation were carried out using the software TillVision version 3.31 (TILL Photonics) extended by custom-tailored software for the control of the laser.

### 3.7.2.3 Confocal laser scanning microscopy

Confocal optical sections of leaf segments from *A. thaliana* loaded with DCF-DA were made with a Leica TCS SP confocal laser scanning system (Leica, Wetzlar, Germany) using the Argon excitation beam lines at 488 nm. Emission of DCF fluorescence was detected at 508-551 nm (PMT: 540 V, Pinhole: Airy, Frame average:2) and of chlorophyll fluorescence at 618-715 nm (PMT: 728 V, Pinhole: Airy, Frame average:2). A 10x objective (HC PL Apo 20x/0.70) and a zoom-factor of 3.08 were used for monitoring fluorescence. The data was processed by Leica Confocal Software LCS.

### 3.7.2.4 Determination of source of ROS using inhibitors of metabolic pathways

Inhibitors of metabolic pathways were used to examine pathways in living organisms. They act on specific points of the pathways and inhibit the reactions there. The resulting effects were monitored by chlorophyll fluorescence using a PAM (Walz GmbH, Effeltrich, Germany) or a Fluorescence-Clamp set-up (Schinner et al. 1998, Schinner 2001).

Here, 2 mM SHAM (see A.1), an inhibitor of the mitochondrial alternative oxidase, and 10  $\mu\text{M}$  DCMU (see A.1), an inhibitor of PSII electron acceptors, have been used. To monitor the effect of the inhibitors, they were infiltrated together with DCF-DA, and the ROS production under light was determined using the inverse fluorescence microscope as described above.

In order to check whether the inhibitors show their predicted effects a control experiment was done with plants infiltrated with DCMU and PAM measurements. Since



DCMU is an inhibitor of PS II, the photosynthetic activity measured in the PAM should be almost zero (see section 4.4.5).

#### 3.7.2.5 Determination of CO<sub>2</sub> dependence of ROS formation

The infiltration method leads to a loss of gas in the leaves which in turn causes suffering of the plants from CO<sub>2</sub> and O<sub>2</sub> deficiency. In order to compensate this loss and to monitor the effect of CO<sub>2</sub> NaHCO<sub>3</sub> was added to the SM medium (see A.1) embedding the leaf in the petri dish. HCO<sub>3</sub><sup>-</sup> can be converted to HO<sup>-</sup> and CO<sub>2</sub> which can be taken up through the membranes of the cell. "Low" and "high" CO<sub>2</sub> concentrations were achieved with 0.1 mM NaHCO<sub>3</sub> in 10 mM HEPES pH 7.5 and 10 mM NaHCO<sub>3</sub> in 50 mM HEPES pH 7.6. Their effects were compared with those of SM and, in the case of the PAM measurements, of air.

The effect of CO<sub>2</sub> concentration on ROS formation was determined with means of DCF-DA using the inverse fluorescence microscope as described above section 3.7.2.2. Their effect on photosynthetic activity was examined using PAM. In the case of NaHCO<sub>3</sub> and SM the plants were immersed in the liquid during PAM measurements. In the case of air, the plant plates were used without any special treatment.

### 3.7.3 Investigations of scavenging systems

HPLC measurements were done in cooperation with AG Prof. Bilger, Institute of Botany, University of Kiel.

#### 3.7.3.1 Determination of zeaxanthin using HPLC

Zeaxanthin (Z), antheraxanthin (A) and violaxanthin (V) are carotenoids of the xanthophyll-cycle in the chloroplast. Zeaxanthin accumulates under high-light conditions in order to protect the photosynthetic pigments against oxidation. It is built from violaxanthin in a reaction catalysed by deepoxidases (Pfündel and Bilger 1994). Antheraxanthin is the intermediate of this reaction. Violaxanthin has two epoxy groups, antheraxanthin one and zeaxanthin zero. Thus, the epoxylation status (EPS) as determined by

$$EPS = \frac{2 * V + A}{2(V + A + Z)} \quad (3.3)$$

can be used as an indirect measure of the amount of zeaxanthin. An epoxylation status of 1 indicates 100 % violaxanthin in the leaves.

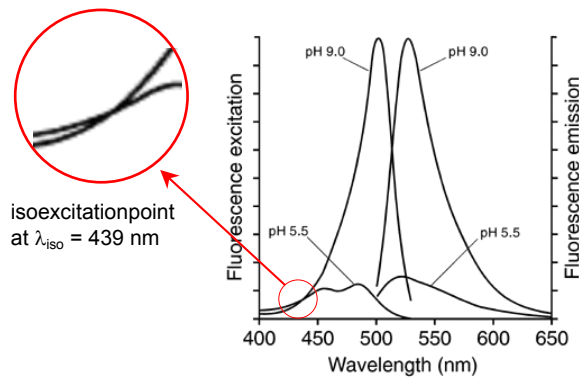
In order to determine the concentrations of the three xanthophylls high performance liquid chromatography (HPLC) measurements were done. HPLC serves as a method to dissociate mixtures of substances. For HPLC analysis the Agilent series 1100 (Agilent, Waghäusel-Wiesental, Germany) with a "Hypersil ODS (5 $\mu$ m) 4,6x250 mm" chromatography column (Agilent) was used. The calibration factors for the pigments have been determined spectrophotometrically by Edith Grubmüller using the extinction-coefficients by Davis (1976).

For HPLC experiments, the plants were harvested, shock frozen in liquid nitrogen and stored in 1.5 ml reaction tubes at  $-80^{\circ}\text{C}$  until further use. For extraction of xanthophylls mortar and pestle were pre-cooled with liquid nitrogen. The sample material was grinded in the pre-cooled mortar. For buffering reasons, one spatula tip of  $\text{MgHCO}_3$  was added. The grinded material was dissolved in 500  $\mu\text{l}$  85 % acetone (in Tris-HCl pH 7.8) and the solution was collected in a 2-ml tube. Another 500  $\mu\text{l}$  5 % acetone were added to the mortar to be sure to have solubilized all pigments and mixed with the other 500  $\mu\text{l}$  in the 2 ml tube. Then the mortar was rinsed with 100 % acetone to dissolve the  $\beta$ -carotenoids. The 100 % acetone was also added to the 2-ml tube. The solution was centrifuged for 5 min at 6000 rpm at  $4^{\circ}\text{C}$  and the supernatant was filtered (0.45  $\mu\text{m}$  PTFE filter, Alltech, Unterhaching, Germany) before use.

### **3.7.3.2 Determination of transport to the vacuole using 2,7-bis-(2-carboxyethyl)-5-(and-6)-carboxyfluorescein acetoxymethyl ester**

Transport of the DCF across the vacuolar membrane (e.g., by an ABC transporter employed for detoxification, Theodoulou 2000) would cause a decrease of fluorescence because the acid pH of the vacuole quenches DCF fluorescence and may mimic a decay of ROS production. The pH in the cytosol is 6.8 to 7.4 and in the vacuole pH is often far below 6.0. In order to check for such a putative mechanism, transfer of the pH-indicating dye BCECF was studied. BCECF is a fluorescent dual-excitation dye widely used for intracellular pH measurements. Typical excitation wavelengths are 490 nm and 439 nm (isosbestic point).

The non-fluorescent acetoxymethyl (AM) derivative of BCECF is cell-permeable allowing non-invasive bulk loading of the cell. It is converted inside the cells by means of intracellular esterases (Molecular Probes product information, <http://probes.invitrogen.com>). BCECF was taken from a 2 mM stock solution (dissolved in DMSO) to give an end concentration in the leaves of 13.4  $\mu\text{M}$  (in 1 mM SM pH 6.1 buffered with 5 mM MES, see A.1).



**Figure 3.4** Excitation and emission spectra of BCECF showing the dependence on pH. (Molecular Probes, <http://probes.invitrogen.com> modified)

Loading the dye into the leaves and ratio imaging was performed as described above (see 3.7.2.2) for DCF-DA. Ratio imaging of BCECF was mainly performed as described in Plieth et al. (1997). Briefly: The excitation wavelengths employed were 439 nm and 475 nm (filter DM 510, Nikon, Düsseldorf, Germany). Emission was recorded at 535 nm (filter BA 520-560 plus, Nikon plus BG18, d = 2 mm, Schott, Mainz, Germany). For measurements the 20x objective (Fluor20 Ph3DL, Nikon) was used. The exposure times for 475 nm and 439 nm were 50 ms and 300 ms, respectively. The emission was detected sequentially. For further description of the measuring method see section 3.7.2. 2 (DCF-DA).

For determination of the transport rate, the ratio  $F(475 \text{ nm})/F(439 \text{ nm})$  was used. The software MicroCal Origin version 2.8 (MicroCal software Inc., Northampton, USA) was employed for data fitting. From the exponential decay of fluorescence

$$f = f_0 \exp\left(-\frac{t}{\tau}\right) \quad (3.4)$$

with  $f$  being the actual value and  $f_0$  the initial value of fluorescence at  $t=0$  the time constant  $\tau$  was determined.

### 3.7.3.3 Catalase assay

Catalase catalyses the conversion of  $\text{H}_2\text{O}_2$  to  $\text{H}_2\text{O}$  and  $\text{O}_2$ . It is found mainly in peroxisomes where  $\text{H}_2\text{O}_2$  is produced during photorespiration. It acts as a scavenging enzyme since  $\text{H}_2\text{O}_2$  is not only a signalling molecule but belongs to the reactive oxygen species which are harmful to the cells in high concentrations.

Here, catalase activity was measured in order to find out whether it depends on the N-form. The catalase assay using an O<sub>2</sub>-Rank-electrode (Rank oxygen electrode, Rank Brothers Ltd, Cambridge, UK) was established to determine the catalase activity in NH<sub>4</sub><sup>+</sup>- and NO<sub>3</sub><sup>-</sup>-grown plants by measuring the O<sub>2</sub> production dependent on a given H<sub>2</sub>O<sub>2</sub> concentration.

Catalase EC1.11.1.6 (Sigma, Steinkirchen, Germany) from bovine liver (30mg protein/ml, 47000 U / mg protein, 1.41 kU μl<sup>-1</sup>) was used to create a standard curve. The catalase concentrations used were 7.05 U ml<sup>-1</sup> down to 0.22 U ml<sup>-1</sup> in the measurement chamber. The H<sub>2</sub>O<sub>2</sub> concentration was 0.003 % of total volume. H<sub>2</sub>O<sub>2</sub> and catalase were diluted in 0.1 M phosphate buffer (see A.1).

A two-point calibration of the electrode (Rank oxygen electrode, Rank Brothers Ltd, Cambridge, UK) was performed. Gassing with ambient air at 20 °C revealed a O<sub>2</sub>-saturation current I<sub>max</sub> corresponding to 280 μM O<sub>2</sub> (Table 2.8.1, Hütter 1994) and gassing with N<sub>2</sub> revealed the background current I<sub>min</sub> corresponding to 0 μM O<sub>2</sub>. I<sub>max</sub> and I<sub>min</sub> were used to convert the current signal I of each experiment into oxygen concentration ([O<sub>2</sub>]) by the following equation:

$$[O_2] = \frac{I - I_{\min}}{I_{\max} - I_{\min}} \cdot 280 \mu M \quad (3.5)$$

The experiment procedure was as follows. First 1 ml of 0.1 M phosphate buffer (see A.1) was added to the electrode chamber and aerated with nitrogen to eliminate all O<sub>2</sub> left in the buffer. Then the chamber was sealed and 10 μl 0.3 % H<sub>2</sub>O<sub>2</sub> were added to the buffer. After the electrode showed a constant current signal 10 μl catalase (or plant extract) was added and the current increase was monitored. The more O<sub>2</sub>/s, the higher is the catalase activity in the extract.

By means of the inverse Boltzmann equation

$$x = dx * \ln\left(\frac{Y - A_1}{A_2 - Y}\right) + x_0 \quad (3.6)$$

with dx = 0.39, A<sub>1</sub> = 4.99 (initial Y), A<sub>2</sub> = -0.07 (Y final), x<sub>0</sub> = -0.65 and Y = [O<sub>2</sub>]/s the catalase concentration in the plant extract is calculated.

### 3.7.3.3.1 Procedure for extraction

15-day old leaf material stored at  $-80\text{ }^{\circ}\text{C}$  was grinded with a pistil in reaction tubes on ice. The grinded material was dissolved in 0.1M phosphate buffer pH 7.4 (100 mg fresh weight per ml buffer). 10  $\mu\text{l}$  of the extract were used as described above.

## 3.8 Gene expression studies

Gene expression studies were done in cooperation with the Group of Eva-Mari Aro, Plant Physiology and Molecular Biology, Department of Biology, University of Turku, Finland. Their 8k cDNA microarray is based on GEM1 clone set from InCyte Genomics (Palo, USA) manufactured by Eva-Mari Aro's group and Centre of Biotechnology (Biocity, Turku, Finland). The 7942 clones represent genes from all major *A. thaliana* tissue categories (roots, rosettes and inflorescence). The clones came from sequence-verified libraries of InCyteGenomics and the Ohio State University. Purified PCR products of the cDNA clones were spotted in triplicate and divided to two slides. For further details see [www.ebi.ac.uk/arrayexpress/entry/query](http://www.ebi.ac.uk/arrayexpress/entry/query) (A-MEXP-38, A-MEXP-39).

### 3.8.1 RNA preparation

Total RNA from leaves was extracted using an RNeasy Plant Mini Kit (Qiagen, Hilden Germany) according to manufacturer's instruction. The leaf material was grinded in 1.5 ml reaction tubes containing 3-5 glass pearls ( $\phi$  2.8-3.2 mm, Roth, Karlsruhe, Germany) using a retsch shaker MM2 (Retsch GmbH, Haan, Germany) with pre-cooled racks for 5 min at 90 % speed. For RNA elution two times 50  $\mu\text{l}$  RNase-free water has been applied to the column. After the extraction, a digestion with DNaseI (2 Kunitz units, Qiagen, Hilden, Germany) has been carried out to remove remaining genomic DNA. The digestion was followed by an ethanol precipitation using 4 M NaCl. The precipitate was centrifuged at  $4\text{ }^{\circ}\text{C}$  for 20 min at maximum speed in a Heraeus Biofuge (Thermo Electron, Langenselbold, Germany). The supernatant was discarded and the pellet was carefully washed with 1 ml of precooled 70 % EtOH. The EtOH was removed and the pellet was dried. The RNA was dissolved in 20-40  $\mu\text{l}$  RNase-free water depending on the RNA concentration.

Quantification was done spectrophotometrically using NanoDrop ND-1000 (NanoDrop technology's, Wilmington, USA).

#### DNase digestion

up to 45 µg RNA in 100 µl H<sub>2</sub>O

2 µl DNase

45 min at 37 °C

#### EtOH precipitation

1/10 (v/v) 4 M NaCl

3x Volume EtOH abs.

-20 °C overnight (-80 °C 30-60 min)

The quality of the RNA was checked on an agarose gel (see 3.8.2).

### **3.8.2 Preparation of an agarose gel**

Agarose gels are used to visualize the quality of e.g. PCR products, RNA or plasmid-DNA. For agarose gels agarose was melted in 0.5x TBE buffer in the microwave, cooled down to 40-50 °C and mixed with 0.1 % (w/v) ethidiumbromide. For control of run distance and raising of the probe density a 10x loading buffer (see A.1) is added to 5 µl of the PCR reaction. For molecular weight determination a 1kb ladder was used. Usually the electrophoresis was carried out at 100 V (PowerPac 300, BIO-RAD, Munich, Germany) until the expected separation had been reached. The separation was visualized using the UV-illuminator (GelDoc2000™, BIO-RAD, Munich, Germany) due to the ethidiumbromide fluorescence.

### **3.8.3 Fluorescence labelling of cDNA**

50 µg total RNA was labelled with direct incorporation of cy5 or cy3 dUTP (GE Healthcare, Freiburg, Germany) using Superscript II reverse transcriptase and oligo-dT primer (Invitrogen, Karlsruhe, Germany).

First, the annealing reactions had to be prepared by mixing total RNA with oligo-d(T)<sub>12-18</sub> primer. If the volume of total RNA exceeded 15 µl Microcon® YM 30 columns (Millipore, Eschborn, Germany) were used to concentrate the solution. The RNA was added to the column and centrifuged at 4 °C for 5-7 min depending on the volume at maximum speed using a Heraeus Biofuge (Thermo Electron, Langenselbold, Germany). For recovery the

### 3 Material and Methods

---

columns were turned upside down into a new reaction tube and were centrifuged for 2min at maximum speed.

The preparation of annealing reactions was as follows:

2.0  $\mu$ l oligo d(T)<sub>12-18</sub> primer (1 mg/ml)  
1.0  $\mu$ l total RNA (50  $\mu$ g)  
-----  
H<sub>2</sub>O up to 17.0  $\mu$ l

This mixture was denatured at 70 °C for 10 min, transferred onto ice and spun down quickly (if this step is prolonged, RNA forms secondary structures and the cDNA synthesis is prohibited). While the RNA was denaturing the labelling mix was prepared. After all substrates were added the following mix was spun down and left on ice protected from light

#### Labelling mix (cy3/cy5)

8  $\mu$ l 5x First Strand Reaction Buffer

4  $\mu$ l 0.1 M DTT

4  $\mu$ l unlabelled dNTP mix

3  $\mu$ l cy3/cy5-dUTP(1 mM)

2  $\mu$ l Superscript II (200 U/ $\mu$ l)

1  $\mu$ l RNase inhibitor (30 U/ $\mu$ l)

with unlabelled dNTP mix: 5 mM dATP, dCTP, dGTP and 2 mM dTTP

After denaturing the RNA was combined with the labelling mix and incubated at 42 °C for at least 40 min (step can be prolonged). Then, another 2  $\mu$ l of superscript was added and the reaction was prolonged for another 40 min at 42 °C (step can be prolonged). The reaction was stopped by adding 4  $\mu$ l of 0.5 M EDTA pH 8.0. Then, the RNA was denatured by adding 10 ml 1 M NaOH and incubating at 65 °C for 15 min. (This step should **not** be prolonged). After the incubation 25  $\mu$ l of 1 M Tris-HCl (see A.1) pH 7.5 was added to neutralize the solution.

### 3.8.4 Purification of labelled cDNA

The following procedure was done to remove salts and unbound cy dyes from the labelling reaction mix.

The labelled cDNAs were purified using Microcon<sup>®</sup> YM 30 columns (Millipore, Eschborn, Germany). 400 µl of TE buffer (see A.1) were added to the labelling mix, and the solution was given onto the Microcon<sup>®</sup> YM 30 columns. The columns were centrifuged for 12 min at 14000 rcf. The supernatant was removed and 400 µl of TE buffer was added to the column. Again, it was centrifuged for 11min at 14000 rcf, and the supernatant was removed. Another 400 µl TE buffer was added together with 2 ml of Poly-A (10 mg ml<sup>-1</sup>) and 4.2 µl of yeast t-RNA (10 mg ml<sup>-1</sup>). The solution was centrifuged for 10 min at 14000 rcf or longer until the volume was lower than 10 µl. For recovery the columns were placed upside down into a new tube and centrifuged for 2 min with full speed. The total volume of cDNA should be around 20 µl. The quantity of labelled cDNA was determined using NanoDrop ND-1000 spectrophotometer (NanoDrop Technologies, Wilmington, USA). Around 10 pmol of each labelled cDNA were used and cy3 and cy5 labelled products were combined as follows:

NH<sub>4</sub><sup>+</sup> LL / NO<sub>3</sub><sup>-</sup> LL, NO<sub>3</sub><sup>-</sup> HL / NO<sub>3</sub><sup>-</sup> LL, NH<sub>4</sub><sup>+</sup> HL / NH<sub>4</sub><sup>+</sup> LL, NH<sub>4</sub><sup>+</sup> HL / NO<sub>3</sub><sup>-</sup> HL.

The probe before the slash was cy5 labelled and the one after cy3.

### 3.8.5 BSA blocking for cDNA microarrays

Unspecific binding produces in the end a high background fluorescence. That is why fragments for unspecific binding should be blocked in advance using BSA.

The blocking solution was prepared fresh each time before use.

#### Blocking solution (100 ml for one staining jar)

1 % (w/v) BSA, fraction V

5x SSC

0.1 % SDS

add H<sub>2</sub>O to 100 ml

The solution had to be dissolved at 50 °C for 30 min (step can be prolonged) and filtered through a sterile filter (0,45 µm Schleicher and Schuell, Whatman, Dassel, Germany). The slides were immersed in a staining jar containing the BSA solution and incubated for 30 min at 50 °C. After the incubation they were washed 3 min with 2x SSC (see A.1) at room



temperature (RT) followed by a 3 min wash with 0.2x SSC at RT. Then the slides were centrifuged (Eppendorf 5810R, Hamburg, Germany) for 10 s until they were dry. The slides had to be used for hybridisation the same day.

#### **3.8.6 Preparing of the cover slips**

Just before hybridisation the cover slips (Lifter slips; 24\*60 mm, Erie Scientific Company, Portsmouth, USA) were prepared using the following solutions in Falcon tube:

First the cover slip was dipped into 0,2 % SDS, then in H<sub>2</sub>O and in the end into EtOH (95 %). They were dried on filterpaper and should be used shortly afterwards.

#### **3.8.7 Hybridisation**

The hybridisation mixture was as below. The hybridisation mix was heated for 2 min at 95-98 °C and cooled down at RT. 80 µl of the hybridisation mix was pipetted onto the slide. Any possible air bubbles were removed with one corner of the cover slip. The array was slowly and carefully covered. The covering of the arrays was started on one side of the array and the hybridisation mix was let suck along the cover slip before the cover slip was laid down completely. One piece of Whatman microfiber filters (Whatman, Dassel, Germany) was moistened in 3x SSC and laid in the hybridisation chamber (Corning, Kaiserslautern, Germany). Hybridisation was done overnight at 65 °C.

Before scanning the cover slips had to be removed by carefully shaking of the array in 0.5x SSC/0.1 % SDS. Then the slides were washed at room temperature for 15 min with 0.5 % SSC / 0.1 % SDS followed twice (5 and 1 min) by 0.5 % SSC / 0.01 % SDS. In the end they were washed twice for 1 min with 0.06 % SSC and spun dry for 10 s.

##### Hybridisation mixture for one set of slides with lifter slips 22x60:

50x Denhardt`s	2.1 µl
20x SSC	25 µl
10 % SDS	5 µl
labelled cDNA	20 pmol/dye (use equal amount of each dye)
H <sub>2</sub> O	to 160 µl

### 3.8.8 Scanning

Slides were scanned using ScanArray Express 5000 device (GSI Lumonics, USA). Two lasers were needed to excite both fluorophores, one at 633 nm for cy5 and the other one at 543 nm for cy3. For sensitivity calibration the settings "Laser fixed" and "photomultiplier tube (PMT) variable", 10  $\mu$ m scanning rate were used. First a prescan of the first blocks was performed with initial settings of 90 % laser power and 80 % PMT gain. Then a line scan was performed and the laser power settings were adjusted to get as equal cy3 and cy5 channel intensity as possible. Scanning took 10 min per fluorophore. The images were saved as .tif files.

The spot intensities were quantified using ScanArray ExpressMicroarray analysis System 2.0 (Perkin-Elmer, Boston, USA). For further data analysis GeneSpring 7.2 (Agilent, Böblingen, Germany) software was used. The normalisation strategy was intensity dependent (LOWESS, per spot and per chip).

### 3.8.9 ScanArray and GeneSpring

The software ScanArray ExpressMicroarray analysis System 2.0 (Perkin-Elmer, Boston, USA) was used to assign the spots to rows and columns. This step is called gridding. After the gridding their intensity values were calculated. A list of all spots and their intensity values were saved as .csv file. These .csv files were transformed to a .txt (tab delimited) file to import in the data analysis software. In the .txt files the spots were assigned to clone numbers (saved in another .xls file) which were used later for annotation of the gene.

For further data analysis, GeneSpring 7.2 (Agilent, Böblingen, Germany) software was used. From the three technical replicates of each array, the mean value, averaged on a log scale, was taken for further calculation of intensity-dependent normalisation (Lowess, Per spot and Per microarray). Expression values were created of Lowess normalised data having at least 1.5-fold change in the up or down regulation of the gene in all three biological replicates. Next, the normalised values of up or down regulated genes were tested for statistical significance using t-test P values less than 0.05. In addition, a standard error of the mean (SEM, n = 3) was calculated for each normalised value.

#### 3.8.9.1 GeneSpring experiment format

Experiment file

Name : Turku

ControlInSeparateFile : false

Gene Column : Name  
Headlines : 0  
Signal Column : Ch2 Median  
Reference Column : Ch1 Median  
Signal Background Column : Ch2 B Median  
Reference Background Column : Ch1 B Median  
Experiment Worked Column : Flags  
Experiment Worked Designation : 3  
Experiment Absent Designation : 1  
Experiment Marginal Designation : M  
Treat no signal as invalid : no  
Hard Normalization Number : 1.0  
ColumnHeaderLine : 1  
Locale : de\_DE

In GeneSpring the subsets of slides were combined. The normalisation strategy used was intensity dependent (lowess) per chip and per spot.

#### **3.8.10 Survey of probe quality using agarose gels**

Agarose gels were used to assess the quality of the labelling process with cy3 and cy5. The size of labelled products and the amount of incorporated dye can be compared. The size and the amount of dyes have to be the same to ensure high quality hybridisation results.

A vertical protein gel rig was set up. The gel plates were wiped with water followed by EtOH to remove residues. A 1 % agarose gel was prepared in 1x TAE buffer (see A.1). With a syringe with a 20 gauge needle melted agarose was sucked up and loaded into the gel bed. This had to be done very quickly since the gel cooled down very fast when running between the glass plates. To slow down the cooling the glass plates were preheated. Air bubbles and holes had to be avoided, otherwise the gel would have been run crooked.

The comb was placed not all the way down in the gel. The gel was cooled at 4 °C with some wrap over top for at least one hour. Afterwards the gel was placed onto the electrical lead plate and secured tightly. The inner buffer chamber was filled until the level of buffer came up into the wells but not over the glass. Then the gel comb was removed and the entire

assembly was placed in the buffer chamber. The chamber was filled with buffer until electrodes were covered (about 1/3 the way up).

The probes were prepared as follows: 1  $\mu$ l of each cy3 and cy5 labelled cDNA was mixed with 3  $\mu$ l 30 % glycerine. The same cy3 and cy5 probes as used for hybridisation were combined in one well.

The gel was run at 100 V for 30 min. Afterwards the gel was cut into pieces which fitted on a glass slide. The gel was dried on a glass slide at 70 °C on a heating block for 15 min or until nothing was seen anymore. Then the glass slides were scanned using ScanArray Express 5000 device (GSI Lumonics, Munich, Germany)

## 3.9 Validation of cDNA microarray results

### 3.9.1 Sequencing of clones

The spotted PCR products need to be sequenced for validation purposes. It had to be verified if the annotation of genes (PCR products) to spots is correct. The sequencing was done using the capillary sequencer MegaBACE 1000 (GE Healthcare, Freiburg, Germany).

#### 3.9.1.1 PCR to amplify products sent from Turku

The PCR products used for spotting were prepared from cloned cDNA fragments using T7 and SP6 primer. Samples of these PCR products were sent to our lab for validation purposes. First more DNA material was amplified with SP6 and T7. The template DNA was diluted 1:100 in water and 2  $\mu$ l of the dilution were used in the reaction.

<u>PCR reaction</u>		<u>PCR-protocol</u>	
4 $\mu$ l	H <sub>2</sub> O	Step1	95 °C 5 min
10 $\mu$ l	MasterMix	Step2	95 °C 30 s
2 $\mu$ l	T7 (5 $\mu$ M)	Step3	48 °C 1 min
2 $\mu$ l	SP6 (5 $\mu$ M)	Step4	72 °C 1 min
2 $\mu$ l	Template-DNA (1:100)	<b>Step2-4 35 times</b>	
-----		Step5	72°C 10min
20 $\mu$ l		Step6	4°C $\infty$

For quality assessment of the PCR a 1 % agarose gel was used (see 3.8.2).

#### 3.9.1.2 Sequencing reaction and clean up

Before the sequencing reaction was mixed together the PCR product had to be cleaned up. The QIAquick PCR Purification Kit (Qiagen, Hilden, Germany) was used corresponding to the manufacturer's protocol. The DNA was eluted in 30  $\mu$ l H<sub>2</sub>O.

The sequencing reaction was carried out using the DYEnamic ET Dye Terminator Cyclor sequencing kit from Amersham (GE Healthcare, Freiburg, Germany). In the reaction 20-50 ng PCR product were used. That meant the PCR product had to have a concentration of 4-10 ng/ $\mu$ l. Quantification was done spectrophotometrically using the NanoDrop ND-1000.

<u>sequencing reaction mix</u>		<u>sequencing reaction protocol</u>	
5 $\mu$ l	PCR product (20-50ng)	Step1	95 °C 20 s
1 $\mu$ l	Primer <i>forward</i> or <i>reverse</i> (20 $\mu$ M)	Step2	x °C 15 s
1 $\mu$ l	Premix (4x diluted)	Step3	60 °C 1 min
3 $\mu$ l	Dilution buffer	<b>Step1-3 25 times</b>	
-----		Step4	4 °C $\infty$
10 $\mu$ l			

After the sequencing reaction is done the reaction mix has to be cleaned up using 1.5 M sodium acetate in an ethanol precipitation. The precipitate was centrifuged for 20 min at 4 °C at 13000 rpm using a Biofuge fresco (Heraeus, Thermo Electron, Langensfeld, Germany). The supernatant was carefully discarded by pipetting. The pellet was dried for 3-4 min at 70 °C in a heating block and was resolved in 10  $\mu$ l loading buffer contained in the DYEnamic sequencing kit.

#### Ethanol precipitation

10  $\mu$ l of sequencing reaction mix

1  $\mu$ l 1.5 M sodium acetate (pH > 8.0)

30  $\mu$ l EtOH abs.

mix well

### 3.9.1.3 Sequencing protocol MegaBACE

The sequencing protocol was applied according to manufacturer's instruction using the following parameters:

- Sample Injection Volt	=>	2
- Sample Injection Time	=>	30
- Run Voltage	=>	8
- Run Time	=>	120 (variable)
- Chemistry Parameters	=>	ET Terminator

The filter set used was also according to manufacturer's instruction (520DF20, 595DRLP, 540DRLP, 585DF20, 610LP, 555DF20).

After sequencing base-calling was done using the MegaBACE software "Sequence Analyzer".

### 3.9.1.4 Sequence analysis using the internet

The base called data were evaluated via internet using the Blast algorithm at <http://www.ncbi.nlm.nih.gov/BLAST/>. The blast algorithm compares the entered sequences with other sequences in the databases and gives out an expected value (e-value). The smaller the e-value the higher the reliability of the degree of identity. NCBI database covers genome sequences of almost all sequenced organisms. The same can be done using TAIR ([www.arabidopsis.org](http://www.arabidopsis.org)), a database using only the *Arabidopsis* genome sequence.

## 3.9.2 Northern blot analysis

Northern blot analyses were performed using total RNA (preparation see 3.8.1) separated on denaturing formaldehyde-agarose gel and blotted onto nylon filters (Hybond-N<sup>+</sup>, Amersham). All hybridisation probes were dig labelled (Roche, Mannheim, Germany). Membranes were hybridised with the labelled probes in high SDS-buffer containing formamide overnight at 50 °C. Blots were visualized by chemiluminescence using CDP-Star<sup>®</sup> (Roche, Mannheim, Germany). The protocols for the solutions are found in the appendix A.1.2.

### 3.9.2.1 Preparation of the hybridisation probes

PCR fragments for the hybridisation (hybridisation probes) were labelled by direct incorporation of DIG labelled dNTPs according to manufacturer's protocol.

### 3 Material and Methods

---

<u>Dig-Labeling mix</u>		<u>PCR-protocol</u>	
21,75 µl	H <sub>2</sub> O	Step1	95 °C 1 min
5 µl	10x PCR-buffer	Step2	95 °C 30 s
3 µl	MgCl <sub>2</sub> (25 mM)	Step3	x °C* 1 min
5 µl	10x DIG-dNTP-Label-Mix	Step4	72 °C 1 min
5 µl	Template-DNA	<b>Step2-4 35 times</b>	
5 µl	Primer <i>forward</i> (5 µM)	Step5	72 °C 10 min
5 µl	Primer <i>reverse</i> (5 µM)	Step6	20 °C ∞
0.25 µl	Taq-Polymerase (5 U/µl)		
-----			( * temperature depends on primer pair )
50 µl			

For quality and quantity assessment of the labelling process 5 µl probe were loaded in an 1 % agarose gel (3.8.2). For quantity determination 0.5 µg and 1 µg *HindIII* digested λ phage DNA was loaded. The mass of the bands could be determined using the manufacturers specifications.

For probe preparation different cDNA and primers were used. Some probes were prepared from cloned cDNA fragments previously used for spotting of the microarrays (Turku PCR products) with SP6 and T7 primers. Others were prepared using the Turku PCR products with specific primers (for primer sequence see A.2) or using RT PCR products from total RNA extracted from *A. thaliana* in our lab with the specific primers.

#### Reverse transcription

1 µg	RNA		
x µl	H <sub>2</sub> O		
2 µl	buffer	1 h	37 °C
2 µl	dNTPs		
2 µl	Primer		
1 µl	Omniscript® (Qiagen, Hilden, Germany)		
-----			
20 µl			

### 3.9.2.2 Denaturing RNA agarose gel electrophoresis

It is important that all steps are carried out in an absolutely RNase free environment and that autoclaved materials are used. Before starting the electrophoresis 2 l H<sub>2</sub>O (Millipore water), 1 Erlenmeyer flask (500 ml) and 2 measuring cylinder (20,100 ml) were autoclaved. The gel chamber, gel casting tray and the comb were incubated in 0.1 M sodium hydroxide solution (300 ml/ gel chamber) for 30 min to eliminate any nucleic acids and RNases in the gel system. After the incubation all equipment was cleaned 2 times with autoclaved water.

For the 1.2 % denaturing agarose gel, agarose (Serva, Heidelberg, Germany) was boiled to solve in sterile water. Evaporated water was refilled. Then 10x MOPS-buffer and formaldehyde (37 % v/v) were added and the solution was poured in the gel casting tray.

The necessary amount of RNA (7.5 µg) had to be provided in a volume of only 3 µl. Therefore a vacuum centrifuge (speedvac DNA 120, Savant, NY, USA) without heating was used to reduce the volume of the probes. For 15 µl it will take 10 min. To 3µl RNA solution 9 µl loading buffer (3x volume of RNA solution, see A.1) was added and the mixture was denatured at 60 °C for 10 min. After denaturing the solution was cooled on ice quickly and spun down in a centrifuge. Then the RNA mixture was loaded onto the gel. In one lane 10 µl 10x blue loading buffer (see A.1) as run control was added. The electrophoresis was conducted for 2 h at 50 V (8 V/cm gel). After the run the gel was photographed by gel documentation system (GelDoc2000, BIO-RAD, Munich, Germany) using a fluorescent ruler.

### 3.9.2.3 Transfer to nylon membrane

After the electrophoresis, the gel was washed twice for 15 min in 20x SSC on shaker (light rocking). Then the RNA was transferred to the nylon membrane by a capillary blot using 20x SSC. The gel was put with the pockets down on a bridge of filterpaper (Gel blotting paper GB002 Schleicher and Schüll, Dassel, Germany) which ends have contact to a 20x SSC reservoir. The blotting “tower” was built as follows: three pieces of filter paper (pre soaked with 20x SSC), then gel with pockets down on top of the gel the membrane and then three pieces pre soaked filter paper. Trapped air bubbles were carefully removed. All papers and membranes were art to fit gel size. On top of the “tower” 10 cm of other dry paper (e.g. paper towels) was positioned and weighted down using a 1 kg weight, e.g. water. The blotting was performed over night at room temperature.

The next day soaked paper and membrane were removed. To mark the blots the left corner of the membrane was cut off and another cut on the side was made. The RNA side is on top when the right corner is cut off. The membrane was only handled with forceps.



Fixation of the RNA on the membrane was done by cross linking with 120 mJ UV-light for 1 min (auto crosslink function) in the UV1800 Stratalinker (Stratagene, Heidelberg, Germany). Until further use it can be stored well in freezer bag.

#### 3.9.2.4 Hybridisation

The nylon membrane loaded with RNA was prehybridised in an rotating oven (GFL, Wunstorf, Germany) with 15-25 ml of prehybridisation buffer for 1 h at 50 °C. The prehybridisation buffer was exchanged with hybridisation buffer (15-25 ml). Prior the first use the hybridisation probes have to be denatured for 10 min at 100 °C. Thereafter prior to hybridisation the hybridisation solution has to be denatured for 10 min in 68 °C. The hybridisation was done for 12 to a maximum of 48 h at 50 °C. Both buffers, prehybridisation and hybridisation buffer, can be reused.

Before the start hybridisation tubes need to be autoclaved. The hybridisation tubes were preheated in the oven. All buffers stored at -20 °C were thawed at 65 °C (68 °C) in the water bath.

#### 3.9.2.5 Washing and visualisation

The next day the membrane was washed to eliminate superfluous probes and to let the antibody against the dig-labelled probes bind on the probes bound to RNA. Buffer P2 with and without antibody need to be thawed in the water bath at max. 25°C.

The washing protocol was as follows:

	<b>Buffer</b>	<b>Time</b>	<b>T</b> <b>[°C]</b>	
<b>Wash</b>	2x SSC + 0,1 % SDS	2x 5 min	RT	rotate hybridisation tubes manually; while oven is heating to 68°C
<b>Wash</b>	0,5x SSC + 0,1 % SDS	2x 15 min	68°C	rotate in oven
<b>Wash</b>	P1-buffer	1 min	RT	shake membranes with
<b>Blocking</b>	P2-buffer without AB	min. 1 h	RT	RNA-side on top in
<b>Hybridisation</b>	P2-buffer with AB	<b>exact</b> 30 min	RT	plastic trays on shaker
<b>Wash</b>	P1 + 0.3 % Tween	3x 15 min	RT	
<b>Wash</b>	P3-buffer	Quick dip	RT	

Buffer P2 is reused for convenience, all others have to be discarded. For washing in tubes 50 ml of solutions were taken, for washing in plastic trays the volume was adjusted to cover membranes.

The prepared membranes were incubated in freezer bags. First 10  $\mu$ l CDP-Star<sup>®</sup> substrate diluted in 1 ml P3-buffer was evenly spread on the blots and let sat for about 5 min. The membrane was then transferred to a freezer bag and sealed tight. The membrane should never be dried out. The freezer bag from the outside and the developing cassette were cleaned with EtOH. Then the membrane with RNA on top was put in the cassette. In the dark room the films were developed with varying exposure time as needed.

#### Film development

5 min	shaking in developer (Roentoroll HC, Tentenal, Norderstedt, Germany)
1 min	shaking in H <sub>2</sub> O
10 min	shaking in fixer (Superfix MRP, Tentenal, Norderstedt, Germany)
15 min	minimum under running H <sub>2</sub> O
	Drying at RT

### **3.10 Databases for analysis**

Databases used for analysis were mainly:

KEGG: <http://www.genome.ad.jp/kegg/kegg2.html>

Swiss-Prot and TrEMBL: Roche biochemical pathways: <http://ca.expasy.org/>

TAIR: <http://www.arabidopsis.org/>

MIPS: <http://mips.gsf.de/proj/plant/jsf/athal/index.jsp>

TIGR: [http://www.tigr.org/tigr-scripts/tgi/T\\_index.cgi?species=arab](http://www.tigr.org/tigr-scripts/tgi/T_index.cgi?species=arab)

## 4 Results

### 4.1 Cultivation of plants

#### 4.1.1 Selection of growth conditions

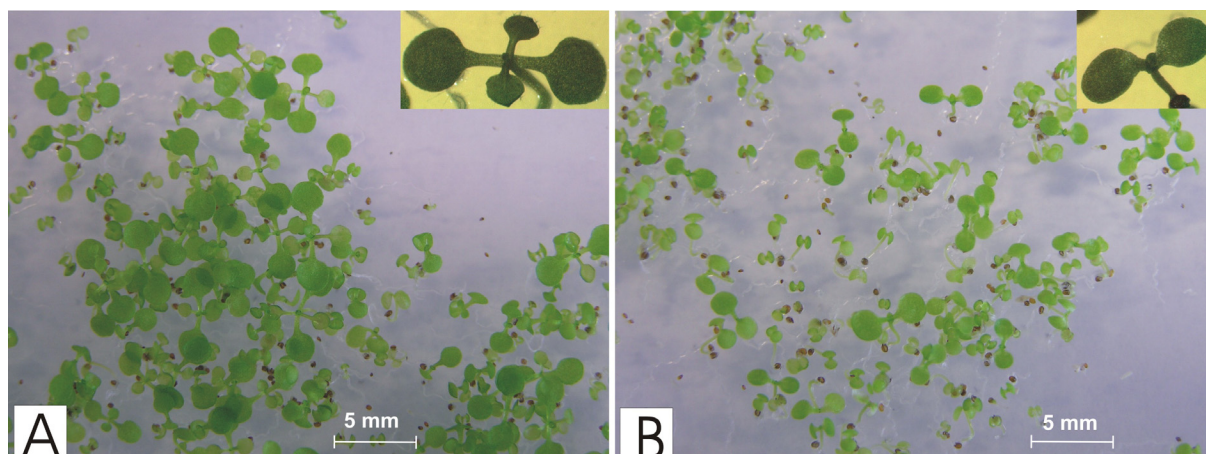
One of the major topics to be considered before starting the experiments is the growth condition. This holds even more for gene expression studies than for physiological studies. The slightest changes in nutrient mixture, light regime and mechanical stress can significantly impair the reproducibility of the experiments. The selection of growth conditions was influenced by the findings of Tocquin et al. (2003): They reported that homogenous growth and a high shoot biomass could be supported by N-supply of 7 mM. For reasons of comparability with results of Guo et al. (2005) a slightly lower N-concentration was used. The data presented below show that a concentration of 4.44 mM resulted in clearly N-form dependent phenomena.

Furthermore, it was found that low light and short-day conditions seem to be favourable for homogeneous growth (Tocquin et al. 2003). Especially, low light delays floral transition. Floral transition has to be avoided since it induces senescence of the leaves. This results in changes of gene expression and induces ROS production (Hinderhofer and Zentgraf 2001, Orendi et al. 2001).

The problem is that *A. thaliana* has a very short vegetative growth period. At light conditions of  $120 \mu\text{mol m}^{-2} \text{s}^{-1}$  the plants show floral transition after six weeks. In order not to mingle to the influence of the reproductive phase and senescence on gene expression and ROS production with the influence of N-form, it was decided to use 15-days old plants. This decision was in line with the choice of growth conditions reported by many other workers (Kimura et al. 2003, Wang et al. 2004).

#### 4.1.2 Retardation of growth

Figure 4.1 shows 15-days old plants of *A. thaliana* grown under  $\text{NO}_3^-$  (Fig. 4.1A) or  $\text{NH}_4^+$ -nutrition (Fig. 4.1B) at a light intensity of  $40 \mu\text{mol m}^{-2} \text{s}^{-1}$ . The development of the  $\text{NH}_4^+$ -grown seedlings was retarded. Under both kinds of nutrition, the cotyledons were well developed. In contrast, the primary leaves were less developed in  $\text{NH}_4^+$ -grown seedlings as compared to  $\text{NO}_3^-$ -grown ones. Table 4.1 gives a comparison of the developmental states of the leaves. It is obvious that growth in  $\text{NH}_4^+$ -grown seedlings was retarded.



**Figure 4.1** Effect of N-form on growth in 15-days old plants of *A. thaliana*. Light of  $40 \mu\text{mol m}^{-2} \text{s}^{-1}$  was given 10 h per day. Solution for (A)  $\text{NO}_3^-$ -grown plants and (B)  $\text{NH}_4^+$ -grown plants was as given in Materials and Methods.

**Table 4.1** Differential development of leaves in  $\text{NO}_3^-$ - and  $\text{NH}_4^+$ -grown seedlings.

	Number of plants with cotyledons and no indication of primary leaves	Number of plants with primary leaves as in the inset of Fig. 1B	Number of plants with primary leaves as in the inset of Fig. 1A	Total number of plants
Nitrate	8	8	17	33
Ammonium	18	2	0	20

### 4.1.3 Excluding pH effect on growth

Usually, a range of pH from 5.5 to 6.5 is recommended for optimal growth of *A. thaliana* (ABRC 2004, Wang et al. 2004). Here, *A. thaliana* was grown on agar plates at a pH of about 6.0 buffered with 5 mM MES.

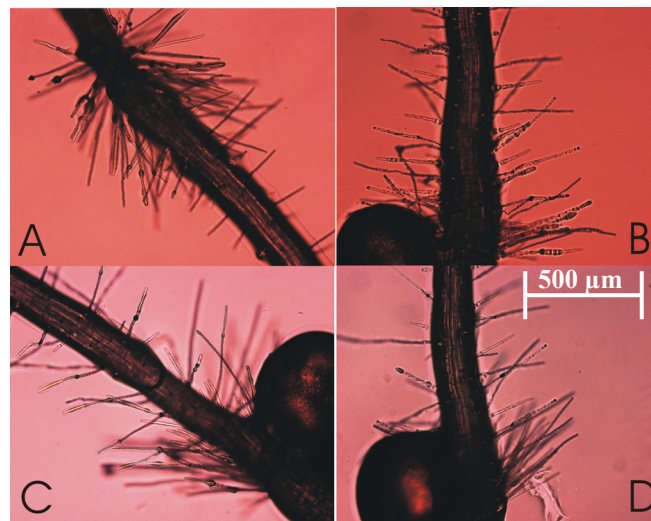
Growth of plants may change the originally adjusted pH of the medium depending on the N-form. This results from the uptake mechanism of the N-nutrient.  $\text{NH}_4^+$  ions are transported into the plants in exchange for one  $\text{H}^+$  each. This effect leads to an acidification around the root zone as described by Marschner (1995). Acidification results in an altered nutrient uptake. In  $\text{NO}_3^-$ -grown plants, alkalization has been observed (Marschner 1995).

In a first series of experiments, the effect of N-form on the bulk medium was investigated by means of a pH electrode inserted in the agar. With plants, the overall pH showed a 0.6 unit difference between the two conditions after 15 days. In  $\text{NH}_4^+$ -plates, the pH was  $5.9 \pm 0.07$  and  $6.5 \pm 0.11$  in  $\text{NO}_3^-$ -plates. This, however, is not of importance for the

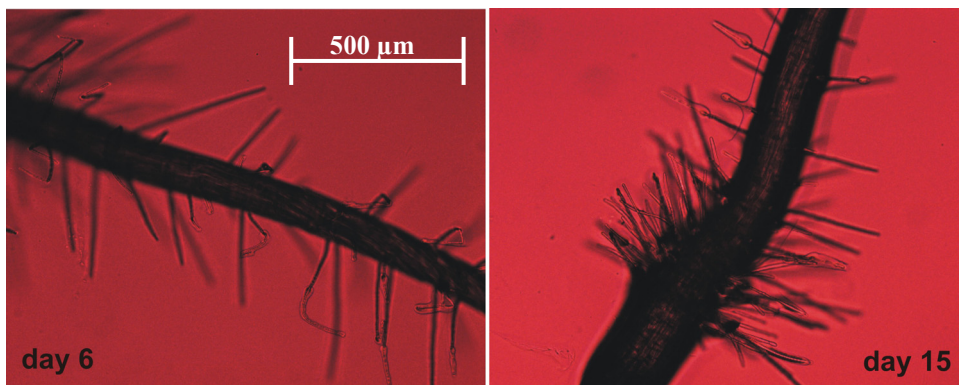
evaluation of our data since fresh weight of  $\text{NO}_3^-$ -grown plants is insensitive to pH at least in the range of 5.5 to 6.5 (Wang et al. 2004).

Measurements using the pH electrode in the bulk medium cannot exclude local pH changes in the vicinity of the roots. In order to check for a possible effect of growth on the pH of the agar surrounding the roots, the sterile pH indicator bromocresol (Römheld et al. 1984, pH range 6.8-5.2; colour change from lilac to yellow) was added to the medium at a final concentration of 1.11 mM for the agar plate after autoclaving. On these agar plates, *A. thaliana* and *S. oleracea* seeds were cultivated.

Figures 4.2 and 4.3 demonstrate that no acidification was observed along the roots of *A. thaliana* seedlings. This was in strong contrast to roots of *S. oleracea*, which caused a strong yellow colour due to a pH decrease already on the fourth day. Incidental fungal infections on the same plates induced the same pH decrease indicated by yellow colouring around the spores (Fig. 4.4). These observations indicate that the transport activity of the roots of young *A. thaliana* plants was so small that the medium was not acidified.

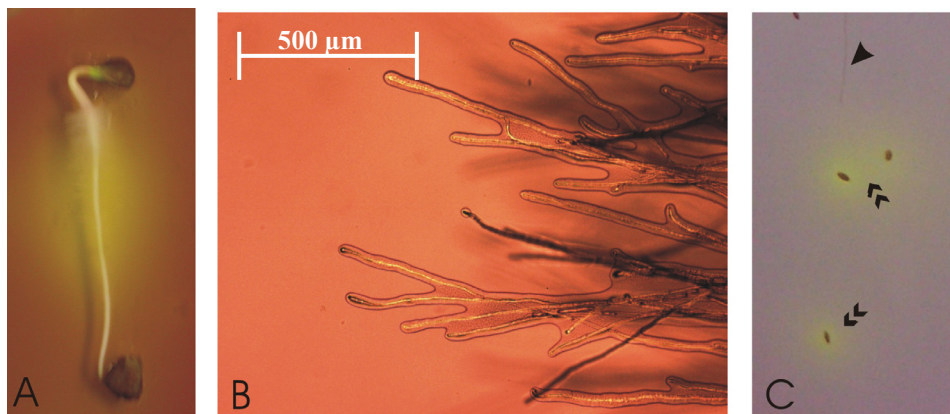


**Figure 4.2** Effect of growth on the pH of the medium surrounding roots of *A. thaliana*. The agar plates contained 1.11 mM bromocresol as pH indicator and were buffered with 5 mM MES at pH 6.1. (A)  $\text{NH}_4^+$  8-days; (B)  $\text{NH}_4^+$  15-days, (C)  $\text{NO}_3^-$  8-days; (D)  $\text{NO}_3^-$  15-days (Leica DMLS micrograph 10x objective). Scale bar represents 500 $\mu\text{m}$  in all panels.



**Figure 4.3** Effect of growth on the pH of the medium surrounding roots of *A. thaliana* in unbuffered  $\text{NH}_4^+$ -plates containing 1.11 mM bromocresol. Plants on the left-hand plate are 6-days old and those on the right-hand side are 15-days old (Leica DMLS micrograph 10x objective). Scale bar represents 500 $\mu\text{m}$  in both panels.

The different background colours of the pictures are due to technical reasons such as thickness of agar. Pictures of Figs. 4.2 and 4.3 were taken by microscope (Leica DMLS) using the 10x objective, light exposure 6 and aperture stop 1.



**Figure 4.4** Testing the function of the pH indicator. The proper indication of the effect of growth on the pH was demonstrated by means of systems that were known to disturb the pH of the medium. The agar plates were unbuffered and contained 1.11 mM bromocresol. (A) 4-days old spinach seedling, (B) root hairs of 4-days old spinach seedling (Leica DMLS micrograph 10x objective) (C) Different effects on pH caused by fungi (double arrow head) or by a root of *A. thaliana* (arrow head). (A, C) pictures taken by digital camera.

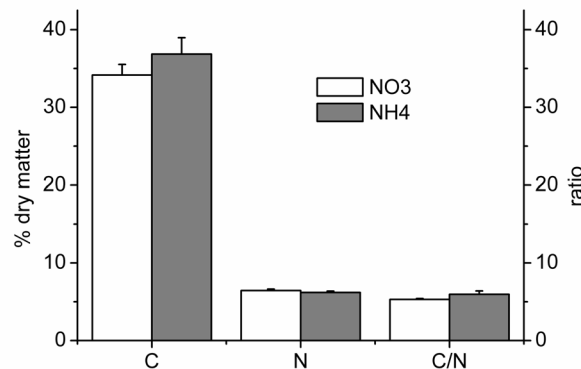


## 4.2 Nutritional status of the plants

Investigations of the spectrum of free amino acids, C/N ratio and concentration of anions were done in order to check whether the seedlings of *A. thaliana* used here show the N-form dependent pattern known from other plant species.

### 4.2.1 C and N analysis

The analysis of total C and N contents in the leaves was done using an elemental analyzer (EA 1108, Carlo Erba, see 3.6.1) in cooperation with B. Biegler, Institute of Plant Nutrition. The analysis revealed a C content of  $37 \pm 2.1$  % dry matter and  $34 \pm 1.4$  % dry matter and a N content of  $6.2 \pm 0.2$  % dry matter and  $6.4 \pm 0.2$  % dry matter in  $\text{NH}_4^+$ - and  $\text{NO}_3^-$ -grown seedlings, respectively. The C/N ratio was  $6 \pm 0.4$  ( $\text{NH}_4^+$ ) and  $5.3 \pm 0.1$  ( $\text{NO}_3^-$ ) (Fig. 4.5). According to the results in Fig. 4.5 there was not a very significant difference in C and N content between  $\text{NO}_3^-$ - and  $\text{NH}_4^+$ -grown seedlings.

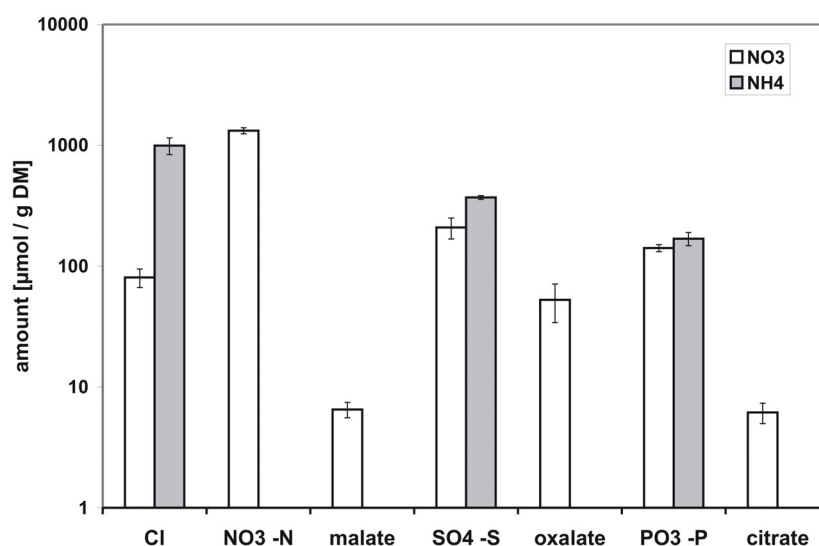


**Figure 4.5**  $C_{\text{total}}$  and  $N_{\text{total}}$  (in percent dry matter, left hand axis) and C/N ratio (right hand axis) determined by elemental analyzer (EA 1108, Carlo Erba). White columns indicate  $\text{NO}_3^-$ , grey columns indicate  $\text{NH}_4^+$ . Error bars present SD with  $n=5$ .

### 4.2.2 Anion analysis

The analysis of anions was done using ion chromatography (3.6.2) in cooperation with S. thor Straten, Institute of Plant Nutrition. The results are shown in Fig. 4.6. As expected they revealed no  $\text{NO}_3^-$ -N in  $\text{NH}_4^+$ -grown seedlings. The high  $\text{Cl}^-$  peak probably accounted for ion balance. The other striking difference was the concentration of the organic acids malate, oxalate and citrate which were totally absent in  $\text{NH}_4^+$ -grown seedlings and accounted for 3 %

of the anions measured in  $\text{NO}_3^-$ -grown ones. Nevertheless, the results verified N-form dependent differences as known from other studies (Gerendás et al. 1997, Marschner 1995).



**Figure 4.6** Concentration of anions [ $\mu\text{mol/g DM}$ ] in  $\text{NO}_3^-$ - and  $\text{NH}_4^+$ -grown seedlings determined by ion exchange chromatography. Error bars present SD with  $n=5$ . y-axis in logarithmic scale for clarity.  $\text{NO}_3\text{-N}$  describes amount of N in  $\text{NO}_3^-$ , the same accounts for S and P.

### 4.2.3 Amino acid analysis

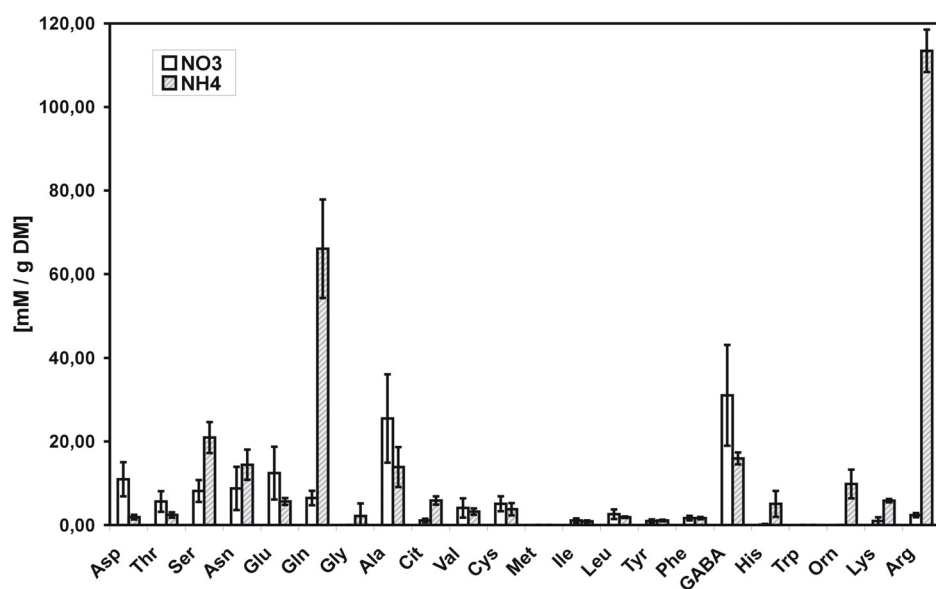
The analysis of amino acids was done using ion exchange chromatography (3.6.3) in cooperation with B. Kawiani and J. Gerendás, Institute of Plant Nutrition.

Investigations of N-form dependent free amino acids revealed differences in the amount and the composition (Fig. 4.7). In  $\text{NH}_4^+$ -grown *A. thaliana* there were 2.3 times more free amino acids compared to  $\text{NO}_3^-$ -grown ones but the amount of total N did not differ significantly (see 4.2.1). The amino acids valin (Val), isoleucin (Ile), leucin (Leu), tyrosine (Tyr) and phenylalanine (Phe) were not different between the N-forms and occurred in only minor concentrations. The concentrations of serine (Ser), glycine (Gly), histidine (His), lysine (Lys), asparagine (Asn), glutamine (Gln) and arginine (Arg) were higher in  $\text{NH}_4^+$ -grown seedlings and of alanine (Ala), threonine (Thr), glutamate (Glu), and aspartate (Asp) were higher in  $\text{NO}_3^-$ -grown ones. Tryptophane (Trp) and methionine (Met) were absent (Fig. 4.7). The most striking differences were seen in the high amounts of Gln and Arg in  $\text{NH}_4^+$ -grown seedlings. Gln is among the amino acids being involved in primary N-assimilation including also Glu, Asp and Asn. Arg has a very effective C/N ratio of 6/4 and can act as a precursor for

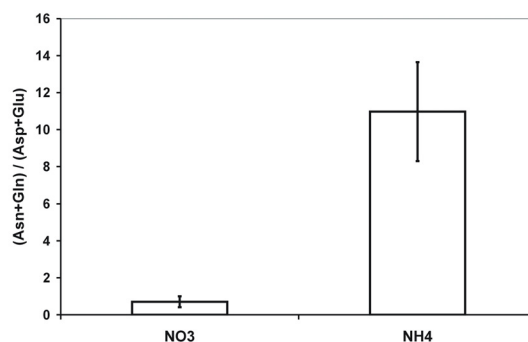


polyamines. Ornithine (Orn) and citrulline (Cit) are precursors for Arg. Thus, it was not surprising that their amounts were also higher in  $\text{NH}_4^+$ - than in  $\text{NO}_3^-$ -grown seedlings.

The high amount of  $\gamma$ -aminobutyrate (GABA) might be an indication of stress during growth or sample preparation. GABA (a non-protein amino acid) is formed by decarboxylation of glutamate (Shelp et al. 1999).



**Figure 4.7** Concentration of free amino acids [mM/g DM] in  $\text{NO}_3^-$ -grown and  $\text{NH}_4^+$ -grown seedlings of *A. thaliana* determined by ion exchange chromatography. Error bars present SD with  $n=5$ .



**Figure 4.8** Ratio of amides (glutamine, asparagine) to their acids (glutamate, aspartate) in  $\text{NO}_3^-$ - and  $\text{NH}_4^+$ -grown seedlings. Error bars present SD with  $n=5$ .

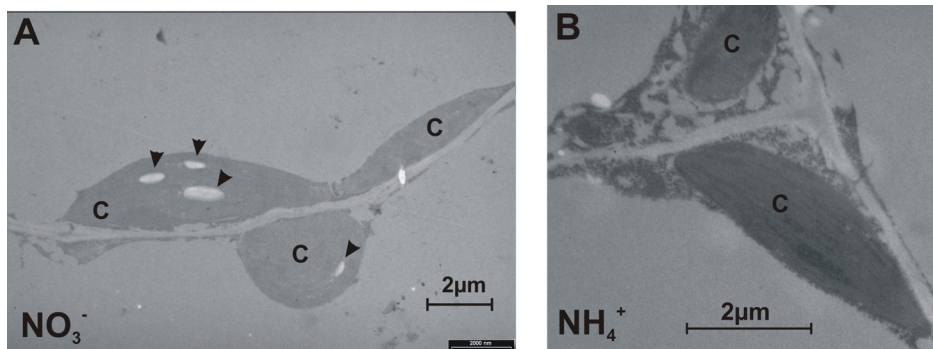
The ratio of the amides Asn and Gln to their acidic forms glutamate and aspartate shown in Fig. 4.8 was higher in  $\text{NH}_4^+$ -grown *A. thaliana* compared to  $\text{NO}_3^-$ -grown ones. Gln and Asn are important in primary N-assimilation for storage and long-distance transport in the plants. They have a better C/N ratio than their acidic forms. This ratio describes the amount of carbons needed to store one N in amino acids. The higher the amount of N per C the better is

the carbon economy (Marschner 1995). The higher ratio of Asn and Gln to Asp and Glu showed that in  $\text{NH}_4^+$ -grown *A. thaliana* more N had to be stored in free amino acids than in  $\text{NO}_3^-$ -grown ones. Especially the relationship between Gln and Glu showed a clear shift towards Gln in  $\text{NH}_4^+$ -grown plants (Fig. 4.7). This makes sense thinking about the toxicity of  $\text{NH}_4^+$  and the detoxification strategy of the plants. Their detoxification strategy is the incorporation of superfluous N, resulting from assimilation of ammonium, in amino acids. To lower their carbon cost N is stored in amino acids with a good C/N value. This is supported taking the very high amount of Arg into account. Arg has a very effective C/N ratio of 6/4. The remaining amino acids were not subject to further research.

### 4.3 N-form dependent differences related to photosynthesis

#### 4.3.1 Differences in starch deposition in the chloroplasts

Electron micrographs of chloroplasts in  $\text{NO}_3^-$ - and  $\text{NH}_4^+$ -grown seedlings are shown in Fig. 4.9. There was one striking difference: Whereas starch deposits can clearly be seen in  $\text{NO}_3^-$ -grown seedlings, they seem to be absent or of negligible magnitude in  $\text{NH}_4^+$ -grown ones. This seemed to indicate that photosynthetic net production is low in  $\text{NH}_4^+$ -grown leaves.



**Figure 4.9** N-form dependent starch deposition in chloroplasts. Transmission electron micrographs of chloroplasts were obtained from seedlings grown (A) on  $\text{NO}_3^-$  and (B) on  $\text{NH}_4^+$ . “C” labels the chloroplast, arrow heads indicate starch deposits. Pictures were taken in cooperation with C. Desel, Institute of Botany.

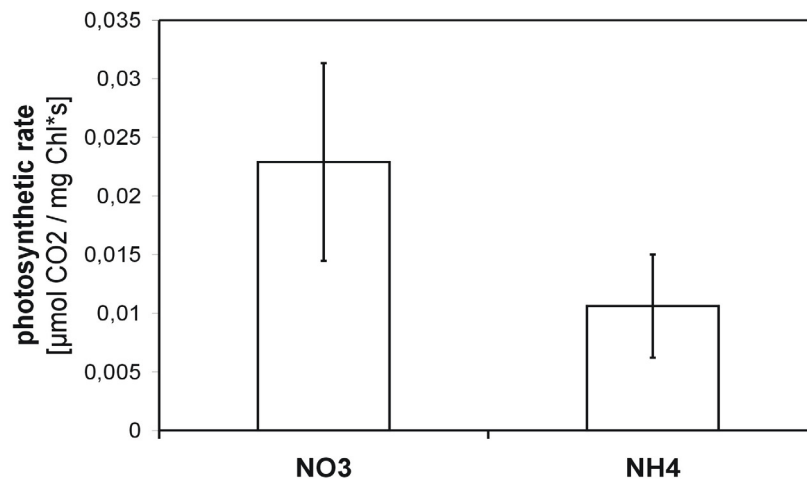
#### 4.3.2 Photosynthetic activity

To test whether there are N-form dependent differences in energy retrieval net photosynthetic rate was measured as  $\text{CO}_2$  uptake per total chlorophyll and by means of the parameters of chlorophyll fluorescence as provided by the PAM. The gas flux measurements were done in

cooperation with H. Kaiser, Institute of Botany. For the measurements of CO<sub>2</sub> uptake, plants were grown on small agar plates (diameter 5 cm) as described above. Test experiments showed that there was no CO<sub>2</sub> evolution or uptake by agar plates without plants.

During the measurement of CO<sub>2</sub> uptake per chlorophyll in the minicuvette system (see 3.7.1.2), seedlings were illuminated with light of 260 μmol m<sup>-2</sup>s<sup>-1</sup>, which was found to saturate CO<sub>2</sub> uptake. Figure 4.10 shows CO<sub>2</sub> uptake per mg chlorophyll. Chlorophyll content was determined by fluoro-spectrometry after extraction.

Averaged values of total chlorophyll content in NO<sub>3</sub><sup>-</sup>- and NH<sub>4</sub><sup>+</sup>-grown seedlings were 13.0 ± 7.4 μg and 6.6 ± 2.1 μg per plate and of the net photosynthetic rate 0.023 ± 0.0084 and 0.011 ± 0.0044 μmol CO<sub>2</sub> mg Chl<sup>-1</sup> s<sup>-1</sup> respectively. Obviously photosynthetic activity was twice as high in NO<sub>3</sub><sup>-</sup>-grown seedlings than in NH<sub>4</sub><sup>+</sup>-grown ones.



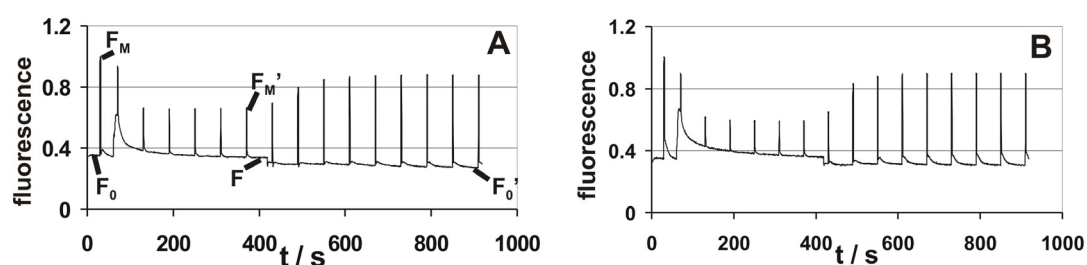
**Figure 4.10** Photosynthetic activity as measured by CO<sub>2</sub> uptake per chlorophyll in NO<sub>3</sub><sup>-</sup>- and NH<sub>4</sub><sup>+</sup>-grown seedlings of *A. thaliana*. Light intensity was 260 μ mol m<sup>-2</sup>s<sup>-1</sup>. Average values from 12 plates, each. p = 0.001.

The results from CO<sub>2</sub> uptake were compared with PAM measurements of chlorophyll fluorescence (Schreiber and Bilger 1993). Figure 4.11 shows the responses of chlorophyll fluorescence to the standard illumination and detection protocol. The spikes caused by saturating flashes ( $F_M' - F$  in Fig. 4.11) were shorter in NH<sub>4</sub><sup>+</sup>-grown seedlings than in NO<sub>3</sub><sup>-</sup>-grown ones, indicating that photochemical quenching (Eq. 3.2a) was smaller and thermal deactivation (Eq. 3.2b) was higher in NH<sub>4</sub><sup>+</sup>-grown seedlings. However, the differences were small as can be seen from the numerical evaluation of three experiments. Genty parameter was calculated by means of Eq. 3.2c at the end of the illumination period: 0.554 ± 0.034 in NO<sub>3</sub><sup>-</sup>-grown seedlings and 0.485 ± 0.05 in NH<sub>4</sub><sup>+</sup>-grown seedlings. The values for

photochemical quenching  $q_p$  were  $0.88 \pm 0.02$  and  $0.73 \pm 0.05$  and for non-photo-chemical quenching  $q_N$   $0.42 \pm 0.02$  and  $0.56 \pm 0.02$  in  $\text{NO}_3^-$ -grown seedlings and in  $\text{NH}_4^+$ -grown seedlings, respectively.

These small differences of about 15 % seemed to be in contradiction to the results from gas flux analysis in Fig. 4.10 as a factor of two was not found in the Genty parameter. Thus it has to be concluded that the electron flux of the electron transport chain (ETC) has to go to other sinks than carboxylation. This was in line with the gene expression studies described below in section 4.5.3.4, which show that photosynthesis has not yet developed its full strength in  $\text{NH}_4^+$ -grown seedlings. Guo et al. (2005) considered that superfluous redox equivalents from the photosynthetic ETC are burnt in the mitochondria of  $\text{NH}_4^+$ -grown plants.

A hint to different sinks of electron flow in  $\text{NH}_4^+$ - and  $\text{NO}_3^-$ -grown seedlings was obtained from the rear slopes of fluorescence induced by saturating flashes in Fig. 4.11 especially in dark adapted plants (first and last flash response). The response to a flash of light initially returned very rapidly to the normal level  $F$  but the decline in a second phase slowed down substantially. This phase describes the discharge of the acceptor pools between PS II and I and downstream of PS I. It became greater if the Calvin cycle had been blocked by glyceraldehyde (Hammes 2005). Such an enhanced slow phase was also observed in  $\text{NH}_4^+$ -grown seedlings indicating that the activity of the Calvin cycle was lower in these plants (compare the traces following the flash-induced peaks in Fig. 4.11A and B after the period of actinic illumination).



**Figure 4.11** Determination of photosynthetic performance by means of a PAM fluorometer. Measurements were done on seedlings grown on (A)  $\text{NO}_3^-$  and on (B)  $\text{NH}_4^+$ . The intensity of the measuring light was  $12.4 \mu\text{mol m}^{-2}\text{s}^{-1}$  and that of the actinic light  $94 \mu\text{mol m}^{-2}\text{s}^{-1}$ . Typical records of three nearly identical measurements.

## 4.4 Determination of ROS

### 4.4.1 Use of dyes to localise sites of ROS formation - assets and drawbacks

The use of dyes, fluorescent or non-fluorescent, is a common method to track different kinds of ROS in the cell and to localize sites of ROS formation. Even though dyes are commonly

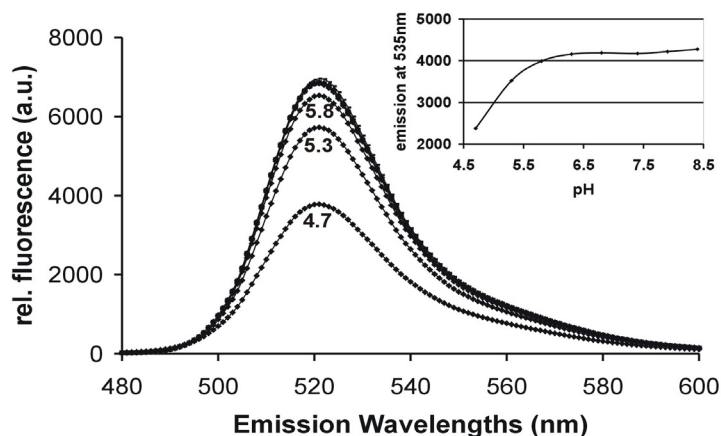
used to investigate ROS formation *in vivo* there are many concerns related to their interactions. Especially DCF is in focus of controversial discussion (Esposti et al. 1998, Ohasi et al. 2002, Rota et al. 1999, Tarpey et al. 2004). DCF is widely used to detect the generation of reactive oxygen intermediates, mainly H<sub>2</sub>O<sub>2</sub> and peroxides. But it also determines all cellular substrates that yield peroxy products and peroxy radicals (Rota et al. 1999). However, it seems quite clear that DCF is not oxidised directly by singlet oxygen (Bilski et al. 2002) or superoxide anion, and it is unlikely to be oxidised by free hydroxyl radical (LeBel et al. 1992). In contrast, Myhre et al. (2003) proposed that the hydroxyl radical contributes to the oxidation of DCF. These conflicting findings reflect the highly complex structures of cells and numbers of biochemical reactions occurring in seconds to minutes. It does not seem to be feasible to determine exactly the reaction between dye and molecule. The reaction *in vitro* is in most cases not transferable one-to-one to the *in vivo* situation since there are various other reaction partners. Thus, the situation is more complex. Despite all contradictory findings the dye remains an attractive probe as an overall index of oxidative stress.

### 4.4.2 Testing the method of DCF-DA measurement *in vitro*

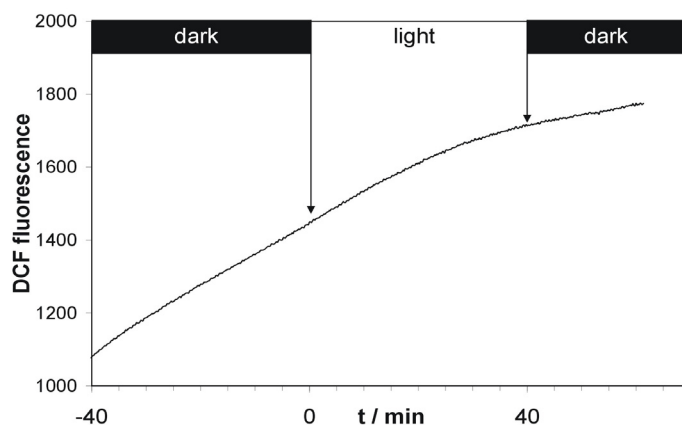
Despite of the problems mentioned above, DCF-DA is a widely used dye for monitoring oxidative stress mainly peroxides e.g. H<sub>2</sub>O<sub>2</sub>. (Bass et al. 1983, Myhre et al. 2003, Trayner et al. 1995, Deng et al. 2002, Maxwell et al. 1999, Tarpey et al. 2004). Before applying DCF-DA in the following investigations, some physical properties of the dye have been tested.

First the pH dependency of the fluorescence has been determined using a fluorospectrometer (F 2500 Hitachi). For this investigation, the unesterified derivative DCF was used. Figure 4.12 shows the emission spectrum from 480 nm to 600 nm. Excitation wavelength was 488 nm. The inset shows the pH dependence at 535 nm. The measurements revealed a strong quenching effect at pH below 5.8. The reaction was reversible.

Second, the light-stimulated photo-oxidation of the dye itself without any external ROS source was determined. For these measurements, the diacetate derivative of DCF (DCF-DA) was used. One drop of DCF-DA was poured in the petri dish on the inverse fluorescence microscope and the fluorescence was recorded at 535 nm. Figure 4.13 shows an increase of fluorescence over a time course of 100 min. At the marked time points (zero and 40) the laser light was turned on, respectively, off. There was no obvious light induced fluorescence. This evidence is important since it becomes clear that increase of fluorescence under light is not due to the dye itself but to reactions with mainly peroxides.



**Figure 4.12** pH dependence of the emission spectrum of DCF fluorescence excited at 488 nm as measured with the fluorospectrometer F 2500 (Hitachi). The inset shows the pH dependence at 535 nm.



**Figure 4.13** Time course of DCF fluorescence of DCF-DA in a petri dish. Measuring light was  $0.8 \mu\text{mol m}^{-2}\text{s}^{-1}$ . “Dark” and “light” indicate switching on and off the actinic light of  $22.300 \mu\text{mol m}^{-2}\text{s}^{-1}$  provided by a red laser (632 nm). Fluorescence was measured in the illuminated spot.

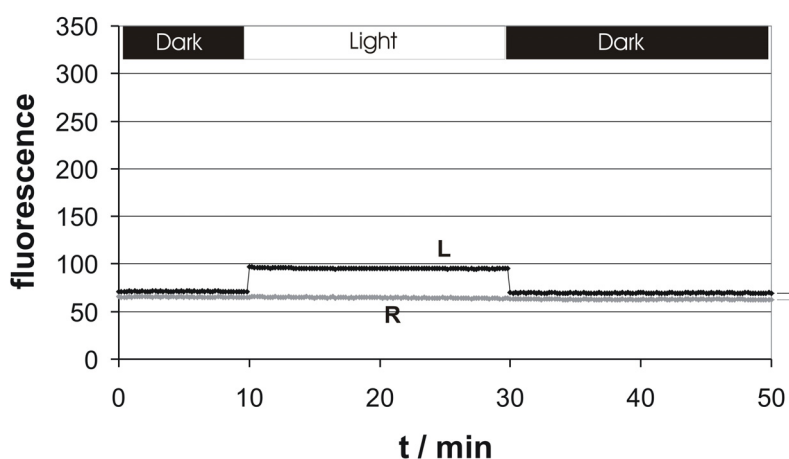
DCF-DA is usually not fluorescent before the diacetate is split off by esterases. However, there was a non-negligible increase of fluorescence (Fig. 4.13). This effect was probably due to esterases occurring in the petri dish. This behaviour should be taken as a caveat that only light-induced changes should be evaluated. Long-term effects should be interpreted with great care. The increase of fluorescence had no adverse effect on the measurements of ROS in the leaves since a background subtraction could be applied which offered the possibility to account for a drift of fluorescence over the time course of the experiment.

### 4.4.3 Testing the method of DCF-DA measurements *in vivo*

For interpretation of light- (ROS-) induced fluorescence of DCF, some control experiments have been done. The effect of the solvent of DCF and the effects of buffer and pH were studied *in vivo*. The source of fluorescence was determined to exclude occurrence of light-dependent auto-fluorescence in the leaf and any effect of buffer or solvent.

#### 4.4.3.1 Testing of the influence of solvent

The influence of ethanol, the solvent of DCF-DA, was investigated using the same light protocol as usual. Testing the effect of infiltration of ethanol without DCF-DA revealed no light-induced fluorescence (Fig. 4.14). The constant intensity level of 70 arbitrary units (a.u.) was probably due to auto-fluorescence of the leaf. The rectangular steps upon switching on/off the actinic light were artefacts caused by the light itself sneaking through the filter in front of the CCD camera. Besides these two effects, the curves R and L look the same, and there was no increase of fluorescence visible at any time point.

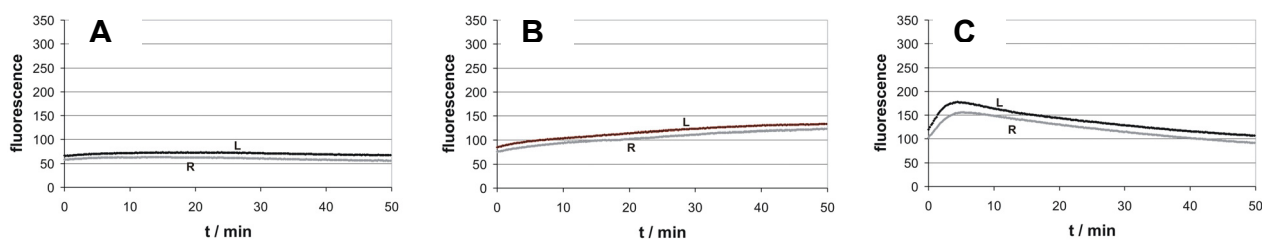


**Figure 4.14** Time course of fluorescence without DCF. Only the solvent ethanol was infiltrated in the leaf. L labels the trace obtained from the spot under the light guide, R indicates the reference spot. “Dark, light, dark” indicates the switching on/off the actinic light. Intensity of measuring light:  $0.8 \text{ mol m}^{-2} \text{ s}^{-1}$ , Intensity of actinic light:  $9000 \text{ } \mu\text{mol m}^{-2} \text{ s}^{-1}$ .

#### 4.4.3.2 Suitability of reference fluorescence for drift elimination

The next set of experiments was done to test the effects of buffer solution respectively pH on fluorescence from intact leaves without light stimulation. Important results are as shown in Fig. 4.15. The curves under the light guide (L) and the reference curve (R) had the same

incline. This proved the spatial homogeneity of the fluorescence signal (background drift). The ratio of L / R should be “1”.

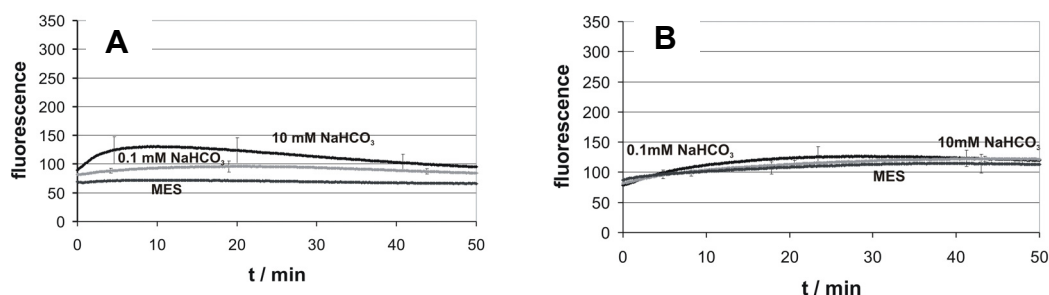


**Figure 4.15** Three typical results for the development of DCF-fluorescence without light. (A) Typical result at pH 6.1 in 5 mM MES in  $\text{NH}_4^+$ , (B) typical result in  $\text{NO}_3^-$  independent of buffering and pH, (C) typical result in  $\text{NH}_4^+$  pH 7.6 in 50 mM HEPES

The ratios of L/R of experiments were close to 1, since region of interest 1 ( $\text{ROI}_1$ ) (L) and  $\text{ROI}_2$  (R) yielded about equal fluorescence signals. There was about 10 % divergence between the curves. This deviation was found to be acceptable because the relevant signals mostly exceeded 100 %. Therefore the reference curve can be used for drift elimination. The divergence might be due to mechanical stress under the light guide and was not taken into account.

In the experiments of Fig. 4.16, the influence of the solution covering the leaves during the measurements is investigated. Interestingly, the reaction of  $\text{NH}_4^+$ -grown seedlings to different pH was totally different from that one of  $\text{NO}_3^-$ -grown seedlings. This dependence of DCF fluorescence on pH (or buffer) in  $\text{NH}_4^+$ -grown seedlings occurred even in the absence of light. At a pH of 6.1, there was almost no increase of fluorescence during the first 50 min. At pH of 7.5 with only minor buffering capacity of 0.1 mM  $\text{NaHCO}_3$  in 10 mM HEPES, the leaves showed a slight increase of fluorescence over the time. The most striking effect was seen using 10 mM  $\text{NaHCO}_3$  in 50 mM HEPES at pH 7.6. In experiments using this buffering system there was a transient burst in the first 5 min before the fluorescence decreases. In  $\text{NO}_3^-$ -grown seedlings, the increase of fluorescence was in all three cases the same indicating that the source of ROS was probably different to that of  $\text{NH}_4^+$ -grown ones.





**Figure 4.16** Mean values of DCF-fluorescence without light induction obtained from leaves in different buffers. The curves labelled MES were obtained in SM solution buffered with MES adjusted to pH 6.1. For the curves labelled 0.1 or 10 mM NaCO<sub>3</sub>, HEPES and bicarbonate in SM were used adjusted to pH 7.6. (A) NH<sub>4</sub><sup>+</sup>, (B) NO<sub>3</sub><sup>-</sup>, n=3-5.

#### 4.4.4 Testing the suitability of the light intensities

##### 4.4.4.1 Test for actinic influence of measuring light

To be sure that there is no actinic effect of the measuring light the intensity of the xenon-laser was determined. For this issue, the light intensity using different objectives (4x, 10x, 20x) was measured with a light sensor (diameter 8mm, Li-250, LiCor, Lincoln, Nebraska, USA). The diameter of the light spot on the surface of the sensor as caused by different objectives is given in Table 4.2. The factor between area of light sensor and area of the actually illuminated spot was calculated and the measured intensity was multiplied by this factor to determine the real intensity.

For the calculation of the average actinic intensity, the time interval between the measurements (12 s) and the time interval of excitation light (5 ms) have to be taken into account. The duty factor of pulses was 2400 in this case. The actinic light intensity of the measuring light of  $0.8 \mu\text{mol m}^{-2} \text{s}^{-1}$  is unlikely to have an actinic effect on the measurements.

**Table 4.2** Intensities of 488 nm excitation light. The ratio between measured intensity and real intensity is determined from the diameter of the light sensor (8 mm) and the diameter of the actually illuminated spot.

Objective	Ø light spot	factor	measured intensity	real intensity	actinic intensity
4x	2 mm	15.21	$41 \mu\text{mol m}^{-2} \text{s}^{-1}$	$623 \mu\text{mol m}^{-2} \text{s}^{-1}$	$0.3 \mu\text{mol m}^{-2} \text{s}^{-1}$
10x	1.2 mm	42.25	$45 \mu\text{mol m}^{-2} \text{s}^{-1}$	$1901 \mu\text{mol m}^{-2} \text{s}^{-1}$	$0.8 \mu\text{mol m}^{-2} \text{s}^{-1}$
20x	0.5 mm	243	$40 \mu\text{mol m}^{-2} \text{s}^{-1}$	$9734 \mu\text{mol m}^{-2} \text{s}^{-1}$	$4 \mu\text{mol m}^{-2} \text{s}^{-1}$

#### 4.4.4.2 Test of leaf absorption of actinic laser light at 632 nm

The intensity of the actinic laser light was  $9000 \mu\text{mol m}^{-2}\text{s}^{-1}$  at the surface of the leaf as determined by Li-250 (LiCor, Lincoln, Nebraska, USA).

Determining leaf absorption was important since the light conductor was positioned on the adaxial surface of the leaf but fluorescence was detected at the abaxial side. Because of this, the intensity of the laser light was measured on the microscope stage with and without a leaf by means of a CCD camera (Till photonics, Gräfelfing, Germany). In order not to overload the camera the laser intensity had to be reduced using a grey filter with 1.2 % transmission. The quotient of the intensities with and without leaf revealed a transmission rate of about 70 % through an infiltrated leaf. This is more than sufficient to be sure that an actinic effect can be observed.

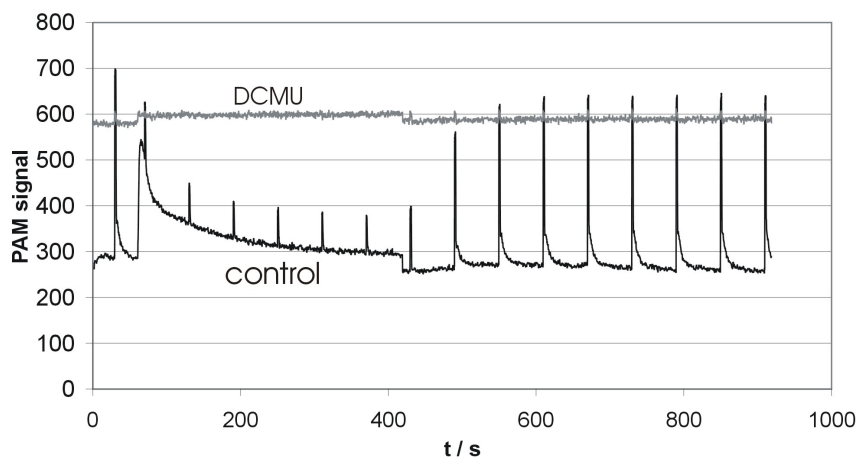
#### 4.4.4.3 Test of temperature changes induced by the actinic light

High temperatures produced by the light guide positioned directly on the surface of the leaf would lead to heat stress. This would induce ROS production falsifying the measurement of light-induced ROS production. The temperature under the light guide was determined using a temperature sensor (RS digital thermometer 206-3750, RS Components GmbH, Mörfelden-Walldorf, Germany). The sensor was fixed on the output window of the light guide, and temperature was checked before and 15 min after the laser was turned on. The temperature was stable at  $21.1 \text{ }^\circ\text{C}$  indicating that there was no heat stress during the measurements.

#### 4.4.5 Testing the infiltration method

In order to analyse the effectiveness of the infiltration procedure by means of a syringe a substance was used which is known to penetrate all membranes and which gives a clear indication when it has reached the locus of its action. Such a substance is DCMU which impedes electron flux on PS II in the chloroplasts and whose successful application can easily be visualised by observing chlorophyll fluorescence. Under DCMU, chlorophyll fluorescence reaches a maximum value, because  $Q_A$  is fully reduced.

Thus, DCMU was infiltrated and chlorophyll fluorescence was measured by means of a PAM with the standard protocol (Schreiber et al. 1986, Schreiber and Bilger 1993). Three independent experiments yielded identical results. One of those is shown in Fig. 4.17. The horizontal line in Fig. 4.17 verified that DCMU had successfully been infiltrated, i.e. it reached the locus of its interference at PS II in the chloroplasts.



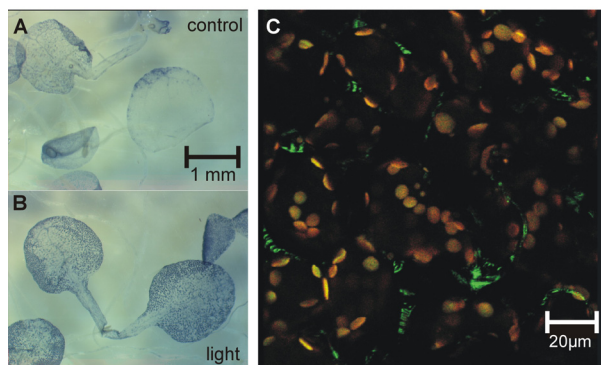
**Figure 4.17** PAM measurements of leaves infiltrated with SM (control) and leaves infiltrated with 10  $\mu\text{M}$  DCMU. Typical result out of three measurements. The difference in maximum fluorescence in the two traces results from the usage of different leaves. The intensity of the measuring light was  $12.4 \mu\text{mol m}^{-2}\text{s}^{-1}$  and that of the actinic light  $94 \mu\text{mol m}^{-2}\text{s}^{-1}$ .

#### 4.4.6 Measurement of ROS production with DCF in intact leaves as illustrated for $\text{NO}_3^-$ -grown seedlings

$\text{NO}_3^-$ -grown seedlings may be considered as "normal" plants, as becomes obvious from the investigations described below. Because of this, they were used to investigate the basics of the usage of DCF for the measurement of ROS production in intact leaves.

##### 4.4.6.1 Attempt to find the locus of ROS production

For the measurement of ROS generation, 2-weeks-old leaves of *A. thaliana* were incubated with NBT as described in Materials and Methods (section 3.7.2.1) and illuminated for 5 min with  $800 \mu\text{mol m}^{-2}\text{s}^{-1}$  prior to fixation. Figure 4.18A,B shows NBT precipitation (A) before and (B) after 5 min of illumination. The comparison of these two graphs indicated that  $\text{O}_2^-$  generation was light-induced. With the available magnification it was difficult to identify the locus of ROS-production.



**Figure 4.18** Demonstration of light-induced ROS generation by means of two indicator dyes in 2-weeks-old leaves of *A. thaliana*. (A, B)  $O_2^{\cdot-}$  generation as indicated by NBT precipitation in the leaves. (A) Plants were held in the dark or (B) illuminated for 5 min with  $800 \mu\text{mol m}^{-2}\text{s}^{-1}$ . (C) Overlay of chlorophyll fluorescence (red) and DCF fluorescence (green) after illumination for 25 min. Yellow colour indicates co-localization of chloroplasts and sources of ROS production.

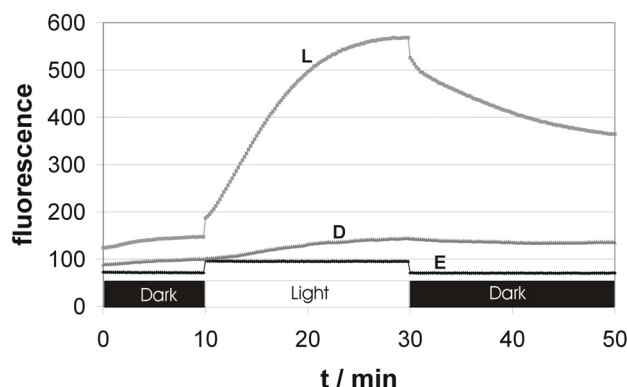
The advantage of DCF over NBT is that measurements can be done in the intact living leaf. This enables a better approach to reveal the locus of ROS production, namely the simultaneous usage of two optical indicators: Chlorophyll fluorescence (680 nm, red pseudo colour in Fig. 4.18C) and DCF fluorescence (535 nm, green pseudo colour in Fig. 4.18C) were measured using emission bands as described in Material and Methods (section 3.7.2.2).

An overlay of these two pictures is given in Fig. 4.18C. The yellow colour indicated that the origin of ROS seemed to be in the chloroplasts as found also by Hideg et al. (2002) using the fluorescent dye DanePy. However, there is one caveat: It has to be considered that peroxisomes or mitochondria may sit directly on the surface of the chloroplasts (Del Rio et al. 1998). DCF fluorescence emitted from these organelles being in touch with chloroplasts cannot spatially be distinguished from the fluorescence coming from the chloroplasts. Nevertheless, we think that we do not have to take this objection too serious. If the ROS would come from peroxisomes and/or mitochondria it would be expected to see more green fluorescence coming from those organelles in the cytosol which have a wider distance from the chloroplasts. Furthermore, there were some green fields, which do not coincide with chloroplasts. They seemed to be related to ROS production in the cell walls, which was not in the focus of the present investigations.

#### 4.4.6.2 Temporal behaviour of ROS production

For the study of the temporal behaviour, pictures of DCF fluorescence were grabbed by a CCD camera as described in Materials and Methods (section 3.7.2.2). The following regions of interest (ROI) were selected by visual inspection: ROI<sub>1</sub> was the position under the light guide, and ROI<sub>2</sub> a location on the leaf outside the area illuminated by the actinic light.

Figure 4.19 shows three original traces. The lower trace labelled E (only ethanol) served as a control. It was obtained from a leaf infiltrated similar to the other ones, but only ethanol and no DCF was added to SM. The trace shows that there was no intrinsic source of light-dependent fluorescence in the leaf. The other two traces were obtained from selected regions of the leaf infiltrated with DCF. The trace labelled L was obtained from ROI<sub>1</sub> exposed to the actinic light, and trace D from ROI<sub>2</sub>, i.e. a spot outside the beam of the light conductor. Two traces (E and L) showed superimposed rectangular response to switching on the actinic light. They were easily identified as artefacts resulting from a minor part of the actinic light, which could still pass the selective filter in front of the camera. These artefacts were eliminated by subtracting the rectangular steps from the L-curve.



**Figure 4.19** Light-induced ROS production as measured by DCF-fluorescence. Trace E = control experiment with SM and ethanol, but without DCF-DA. Trace D = control experiment on a DCF loaded leaf not illuminated with actinic light, trace L = example for a record of light-induced stimulation of ROS production in a leaf loaded with DCF as in trace D. The light protocol of the actinic light was: 10 min dark adaptation, 20 min light on, 20 min light off. Light intensities, measuring light  $0.8 \mu\text{mol m}^{-2} \text{s}^{-1}$ , actinic light  $9000 \mu\text{mol m}^{-2} \text{s}^{-1}$ .

Furthermore, there was a very small light response in the D-curve. This resulted from the fact that the “dark” spot still got some actinic light, because the spatial window of the camera limited the distance from the actinic beam. This effect was ignored if it resulted in a deflection much smaller than that of the L curve.

Before the actinic light was switched on background drift was visible probably resulting from unidentified sources like mitochondrial ROS production or wounding caused by handling the leaves. This may be enhanced due to O<sub>2</sub> depletion during the infiltration procedure.

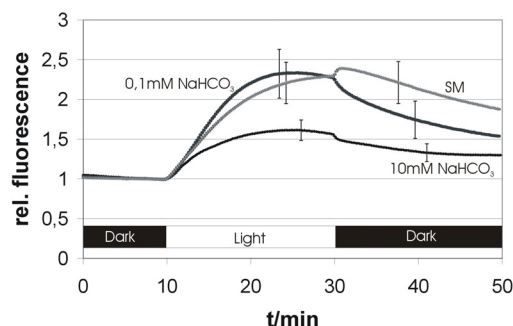
The effect of background drift on the light-induced responses was minimised by calculating the normalised drift-free response of ROS production to light as follows

$$F_r = \frac{F_1 - \frac{F_{1,0}}{F_{2,0}} F_2 + F_{1,0}}{F_{1,0}} \quad (4.1)$$

with  $F_1$ ,  $F_2$  being the DCF fluorescence from ROI<sub>1</sub> and ROI<sub>2</sub>, respectively.  $F_{1,0}$  and  $F_{2,0}$  present the averages of twenty data points of  $F_1$  or  $F_2$  prior to illumination. In the above equation all signals are normalised to start with “1”. For this issue, the increase of the background signal  $F_2$  from ROI<sub>2</sub> had to be adapted to the calibration of the F1 trace before it was subtracted (second term in the numerator).

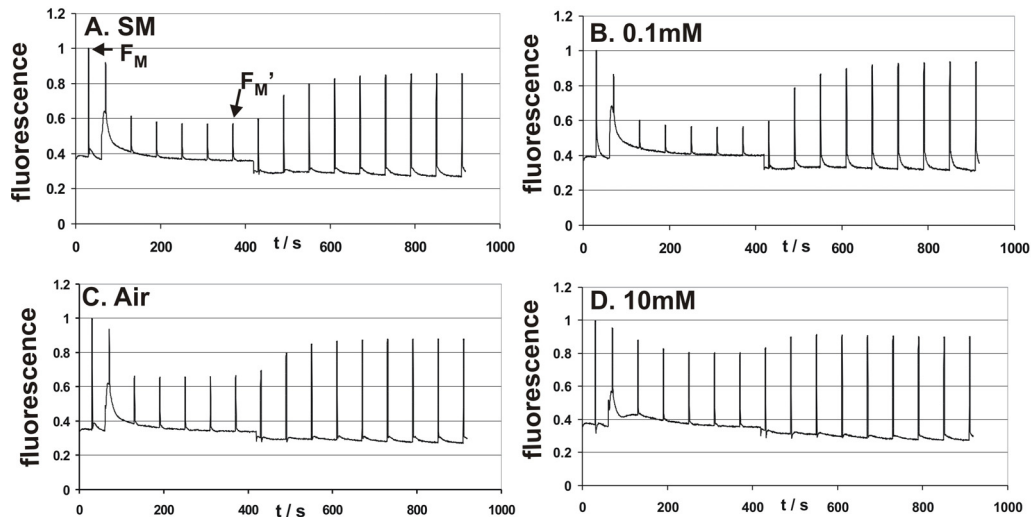
#### 4.4.6.3 Effect of CO<sub>2</sub> supply on ROS formation

Infiltration causes flooding of the air spaces in the leaf, and this may compromise CO<sub>2</sub> supply. Thus, 0.1 mM or 10 mM NaHCO<sub>3</sub> were added to the standard medium (Padmasree and Raghavendra 1999, see 3.7.2.5). Figure 4.20 shows ROS generation in leaves infiltrated with three different media as given in the legend.



**Figure 4.20** Normalised responses (Eq. 4.1) showing the influence of CO<sub>2</sub> supply on the light-induced generation of ROS in leaves of two-weeks-old *A. thaliana*. 6-10 repetitions per curve. Error bars are standard errors of the mean (SEM). Plants were infiltrated with standard medium without bicarbonate, pH = 6.1 (SM) or with standard medium supplemented with 0.1 or 10 mM NaHCO<sub>3</sub>, and 50 mM HEPES, pH = 7.6. Light protocol as described in Fig. 4.19.

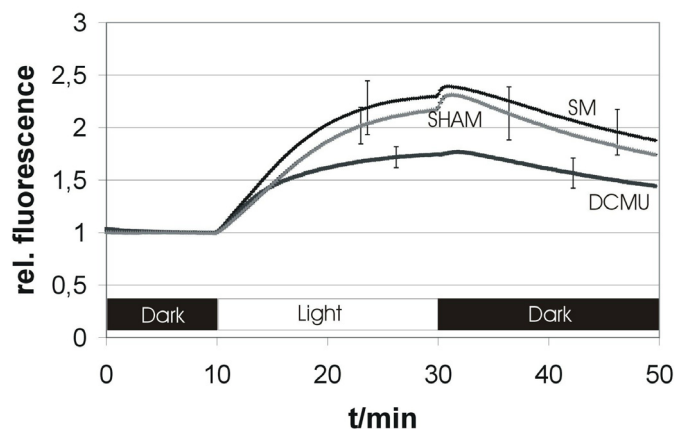
The effects of different CO<sub>2</sub> concentrations on light-induced ROS generation (Fig. 4.20) were compared with the effects on chlorophyll fluorescence. Figure 4.21 shows the influence of the three different infiltration media of Fig. 4.20 and of air on photosynthetic parameters as measured by the PAM.



**Figure 4.21** Determination of photosynthetic performance by means of a PAM fluorometer. Measurements were done on plants infiltrated with (A) SM medium, pH 6.1, or with (B,D) SM medium supplemented (B) by 0.1 mM or (D) 10 mM NaHCO<sub>3</sub>, 50mM HEPES-KOH, pH 7,6 or (C) exposed to air. The intensity of the measuring light was 12.4  $\mu\text{mol m}^{-2}\text{s}^{-1}$  and that of the actinic light 94  $\mu\text{mol m}^{-2}\text{s}^{-1}$ . Typical records of three nearly identical measurements, each.

According to Eq. 3.2, higher energy-quenching is indicated by stronger decrease of the flash-induced peaks ( $F_M - F_M'$  in Fig. 4.21A) during actinic illumination. In SM medium (Fig. 4.21A), energy quenching was higher than in leaves exposed to air (Fig. 4.21C), indicating that the leaves suffer from CO<sub>2</sub> deficiency. This can be shown under more controlled conditions using bicarbonate as a source of CO<sub>2</sub> (Padmasree and Raghavendra 1999). In a medium with 0.1 mM NaHCO<sub>3</sub> (Fig. 4.21B), the behaviour was similar to that in SM medium. In the medium containing 10 mM NaHCO<sub>3</sub> (Fig. 4.21D), energy quenching was even more strongly reduced than in air (Fig. 4.21C). The higher energy quenching as given by  $(F_M - F_M')/F_M$  in SM indicated, that the ability of the Calvin cycle to accept redox equivalents was strongly reduced by CO<sub>2</sub> deficiency (and also by O<sub>2</sub> depletion as may be caused by degassing during the dye-loading procedure). This was the situation when ROS was determined by DCF-DA as in Figs. 4.18 and 4.19.

The question arises as to whether it is merely the decrease in PS I electron acceptors which impedes reoxidation of PS II acceptors and consequently leads to higher ROS production. Thus, the ETC was blocked by DCMU. Figure 4.22 shows that the increase of ROS generation was diminished under the influence of DCMU.



**Figure 4.22** Effect of 10  $\mu$ M DCMU and 2 mM SHAM in SM medium on ROS generation as measured with DCF fluorescence. 7-10 repetitions per curve. Representative error bars are standard errors of the mean. Same light protocol as in Fig. 4.19.

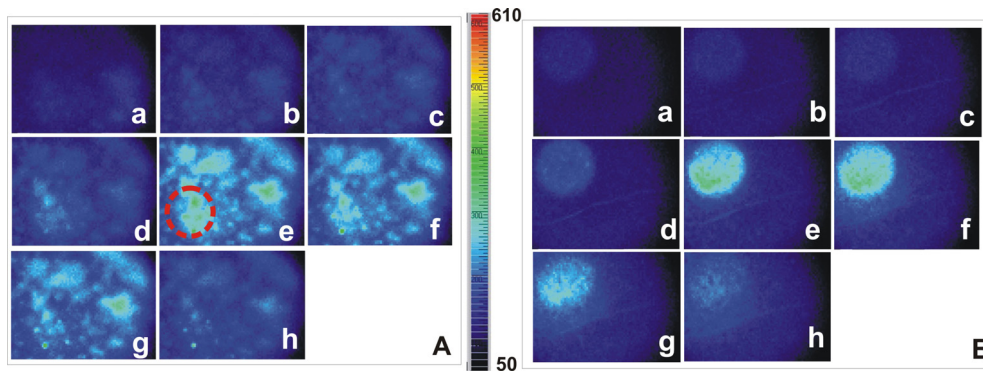
Many workers assume that the Alternative Oxidase (AOX) is employed to reduce ROS production (Maxwell et al. 1999, Affourtit et al. 2001), when mitochondria have to burn superfluous redox equivalents from the chloroplasts. The involvement of the AOX was concluded from a decrease of photosynthetic electron flow with SHAM (Padmasree and Raghavendra 1999, Schinner et al. 2001, Guo et al. 2005). Thus, SHAM was added to the DCF-DA infiltration medium. The small, but probably not significant reduction of ROS production in Fig. 4.22 shows that the AOX did not play a major role in these experiments. This is in line with the findings that electron flux in  $\text{NO}_3^-$ -grown plants (as employed here) is not sensitive to SHAM in contrast to  $\text{NH}_4^+$ -grown plants (Schinner et al. 2001, Guo et al. 2005). This insensitivity to SHAM cannot result from a possible low  $\text{O}_2$  concentration in the degassed medium, because the  $K_m$  of the AOX is somewhere between 1 to 20  $\mu$ mol (Sluse and Jarmuszkiewicz 1998).



#### 4.4.7 Comparison of ROS formation in $\text{NH}_4^+$ - and $\text{NO}_3^-$ -grown *A. thaliana*

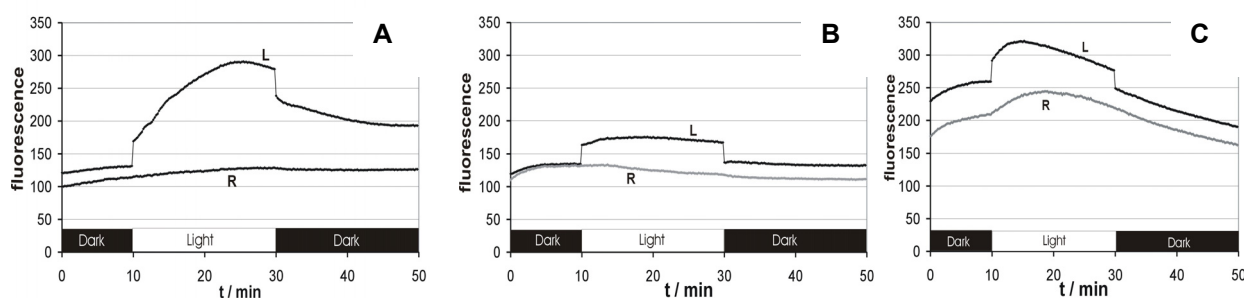
##### 4.4.7.1 Light-induced ROS production at high $\text{CO}_2$

The first set of experiments was done on leaves emerged in SM medium enriched by 10 mM  $\text{NaHCO}_3$ , a means of providing sufficient  $\text{CO}_2$  to leaves covered by water (Padmasree and Raghavendra 1999). The necessity of this procedure is illustrated in Fig. 4.20.



**Figure 4.23** ROS production in (A)  $\text{NH}_4^+$ - and (B)  $\text{NO}_3^-$ -grown leaves of *A. thaliana* emerged in SM supplemented by 10 mM  $\text{NaHCO}_3$  and 50mM HEPES pH 7.6. a) 10 min before light on, b) 5 min before light on, c) immediately before light on, d) directly after light on, e) 10 min after light on, f) 20 min after light on and g) immediately after light off, h) 20 min after light off. The calibration of DCF fluorescence is the same in both panels. The colour coding ranging from 50 to 610 arbitrary units is given by the bar between (A) and (B).

Figure 4.23 shows typical images of ROS production obtained before, during and after switching on the actinic light. In the  $\text{NH}_4^+$ -grown leaf, the effect of illumination was not restricted to the area under the light guide. There was some ROS production already before illumination, probably caused by mechanical stress of dye loading and handling during the transfer to the stage of the microscope (Fig. 4.23A). After light-on, starting with panel d there was an increase in DCF fluorescence, which seemed to be weaker than in the  $\text{NO}_3^-$ -grown leaves shown in Fig. 4.23B. In the  $\text{NO}_3^-$ -grown leaf, there was also some weak increase in DCF fluorescence already before illumination, which was (in contrast to Fig. 4.23A) restricted to the area under the light guide. Here, it was more obvious that this was caused by mechanical stress of the light guide touching the leaf during positioning. The light-induced ROS production vanished after light off.



**Figure 4.24** Relationship between time courses of DCF fluorescence measured directly under the light guide (trace L, obtained from the area indicated by the circle in Fig. 4.23Ae) and in a reference area outside the illuminated part (trace R). (A)  $\text{NO}_3^-$ -grown leaf (B) Type 1  $\text{NH}_4^+$ -grown leaf, (C) Type 2  $\text{NH}_4^+$ -grown leaf. Light protocol as in Fig. 4.19. Leaves were emerged in SM supplemented by 10 mM  $\text{NaHCO}_3$  and 50mM HEPES pH 7.6.

A clear increase of DCF fluorescence was found in the  $\text{NO}_3^-$ -grown leaf of Fig. 4.24A. The rectangular steps upon switching-on and -off the light were artefacts caused by the actinic light itself sneaking through the filter in front of the CCD camera. This could easily be eliminated. However in Fig. 4.24, this correction had not been done in order to provide a means of checking the calibration and the positioning of the light guide. Such a step was seen in the record beneath the light guide, and must not occur in the reference area. The control of the correct selection of the reference area was important in the case of Fig. 4.24A.

In the case of  $\text{NH}_4^+$ -grown leaves, two different types of the responses are shown. Type 1 "baby" with average fluorescence maxima of  $23 \pm 18$  a.u. (Fig. 4.24B) and type 2 "grown-up" with average maximal fluorescence of  $74 \pm 49$  a.u. (Fig. 4.24C).  $\text{NO}_3^-$ -grown leaves showed only one type of response with averaged maximal fluorescence of  $162 \pm 60$  a.u. (Fig. 4.24A).

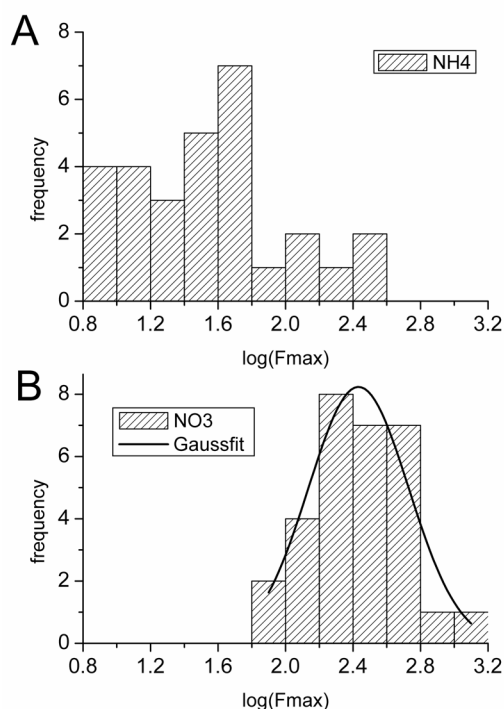
There was nearly no light-induced increase in DCF-fluorescence in Fig. 4.24B, whereas the response in Fig. 4.24C became similar to those found in  $\text{NO}_3^-$ -grown leaves.

The reference traces did not coincide with that one obtained directly under the light guide. In the  $\text{NO}_3^-$ -grown leaves this was caused by ROS production induced by touching the leaf with the guide. In the case of  $\text{NH}_4^+$ -grown leaves, the patchiness visible in the panels of Fig. 4.23A gave an additional contribution to this difference.

#### 4.4.7.2 Wide scatter of responses in $\text{NH}_4^+$ -grown leaves

All measurements of DCF fluorescence showed high scatter. Nevertheless, for  $\text{NO}_3^-$ -grown leaves the histogram of logarithmically binned values of  $F_{\max}$  can roughly be fitted by a gaussian distribution (Fig. 4.25B). The fit was not very smooth resulting from the limited

availability of data, but the approximation to a gaussian distribution was clearly indicated. For  $\text{NH}_4^+$ -grown leaves, the distribution cannot be fitted by a gaussian. The values of  $F_{\text{max}}$  were distributed over a wide range without any prominent peak (Fig. 4.25A). This implies that there was no unique relationship between light stress and ROS production. Instead, different seedlings with quite different responses were included as also presented by the examples in Fig. 4.24 B,C.



**Figure 4.25** Histogram of values of  $F_{\text{max}}$  obtained (A) from  $\text{NH}_4^+$ -grown and (B) from  $\text{NO}_3^-$ -grown leaves. The data in (B) were fitted with a gaussian distribution.

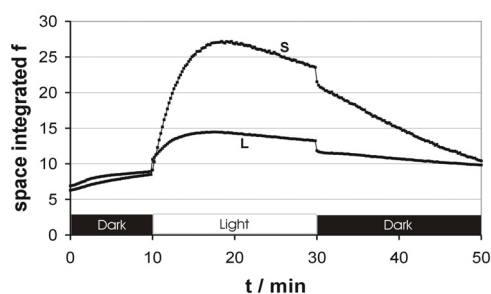
#### 4.4.7.3 Systemic ROS production in $\text{NH}_4^+$ -grown leaves

Figure 4.23A shows that there was no obvious allocation of ROS production to the illuminated part of  $\text{NH}_4^+$ -grown leaves. However, there was a clear light-induced increase in DCF fluorescence in the time courses of DCF fluorescence in Fig. 4.24C. In contrast to  $\text{NO}_3^-$ -grown leaves, there was no constant reference trace in the  $\text{NH}_4^+$ -grown leaf of Fig. 4.24C.

From these findings it had to be concluded that in  $\text{NH}_4^+$ -grown leaves there was a systemic response of ROS production to light. This had been checked by comparing the density of ROS production obtained from averaging over the illuminated spot (area =  $0.058 \text{ mm}^2$ ) and over an area of  $0.23 \text{ mm}^2$  including unilluminated areas. The ratio of the density in the spot divided by the density in the wider area was  $0.99 \pm 0.16$ . Density was

defined as overall fluorescence divided by the evaluated area and was equivalent to average intensity. This strongly supported the observation in Fig. 4.23Ae-g, namely that ROS production was induced by light but was not restricted to the illuminated spot.

As a consequence of this systemic response, overall ROS production in  $\text{NH}_4^+$ -grown leaves was much higher than estimated from Fig. 4.24C. Overall fluorescence was defined by multiplying the average fluorescence density (given as F in the graphs above) by the area of the investigated field. Figure 4.26 shows integral ROS production in the illuminated spot compared with that obtained from the wider area of  $480 \mu\text{m} \times 472 \mu\text{m}$ . The artefact resulting from the laser light (rectangular step) was of equal magnitude in both traces as the response in the illuminated area was part of both traces



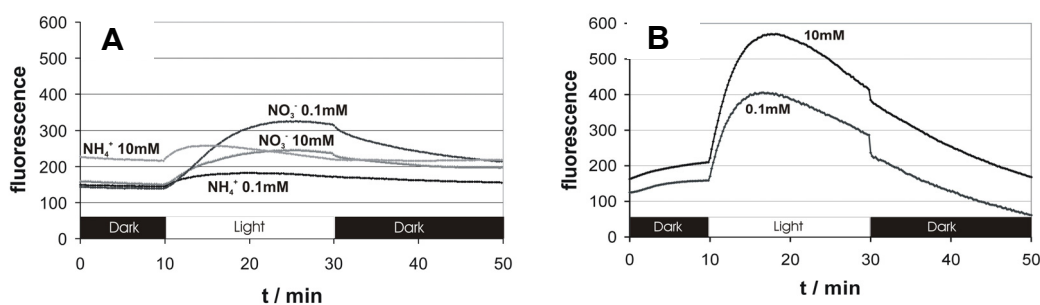
**Figure 4.26** Overall ROS production determined in the area under the light guide (area =  $0.058 \text{ mm}^2$ , trace L) and in the wider surrounding field (area =  $0.23 \text{ mm}^2$ , trace S). Leaf was submerged in SM buffered with 50mM HEPES at pH 7.6. Light protocol as described in Fig. 4.19.

In  $\text{NO}_3^-$ -grown leaves, spreading effects as described above for  $\text{NH}_4^+$ -grown ones have not been observed. Whereas in  $\text{NH}_4^+$ -grown leaves the average ratio, of the integral fluorescence from the surrounding field to that obtained from the area under the light guide (ring in Fig. 4.23), was  $3.85 \pm 0.6$  corresponding to the ratio of the related areas (3.89), it was  $1.2 \pm 0.3$  in the  $\text{NO}_3^-$ -grown leaves. This shows that only 20 % of the overall fluorescence came from the surrounding field. It may be caused by improper determination of the border of the illuminated spot. It clearly showed that there was no spreading in  $\text{NO}_3^-$ -grown leaves.

#### 4.4.7.4 The influence of $\text{CO}_2$ and buffer capacity

The next set of experiments was performed in SM-medium supplemented with 0.1 mM  $\text{NaHCO}_3$  in order to study the effect of  $\text{CO}_2$  deficiency on ROS production (Hoffmann et al. 2005). In section 4.4.6.3 it has been found that photosynthetic efficiency as measured by chlorophyll fluorescence is reduced under these conditions. Figure 4.27 shows records

obtained in  $\text{NH}_4^+$ - and  $\text{NO}_3^-$ -grown leaves emerged in SM medium supplemented either with 0.1 mM or with 10 mM  $\text{NaHCO}_3$ .



**Figure 4.27** Averaged time courses of ROS production in  $\text{NH}_4^+$ - and  $\text{NO}_3^-$ -grown leaves submerged in high and low  $\text{CO}_2$  medium. SM was supplemented with 0.1 mM or with 10 mM  $\text{NaHCO}_3$  and 10 mM or 50 mM HEPES, respectively, pH 7.6. (A) Traces obtained under the light guide in  $\text{NO}_3^-$ - and  $\text{NH}_4^+$ -grown leaves (B) Overall fluorescence as obtained from the full field of the microscope for  $\text{NH}_4^+$ -grown leaves. (0.1 mM = 0.1 mM  $\text{NaHCO}_3$ , 10 mM = 10 mM  $\text{NaHCO}_3$ )

Figure 4.27A shows that the records obtained from  $\text{NO}_3^-$ -grown leaves and from  $\text{NH}_4^+$ -grown ones in 0.1 mM  $\text{NaHCO}_3$  started from the same level before illumination.  $\text{NH}_4^+$ -grown leaves in 10 mM  $\text{NaHCO}_3$  started from a higher level prior to illumination. In  $\text{NO}_3^-$ -grown leaves, reduction of  $\text{CO}_2$  availability (0.1 mM vs. 10 mM  $\text{NaHCO}_3$ ) caused a doubling of ROS production. These data have already been discussed by Hoffmann et al. (2005) and in section 4.4.6.3. The curves for  $\text{NH}_4^+$ -grown leaves in 10 mM  $\text{NaHCO}_3$  are averages obtained from three curves of the insensitive type (Fig. 4.24B) and three of the sensitive type (Fig. 4.24C). The curves show the ROS production under the light guide. As a reference curve was not available in  $\text{NH}_4^+$ -grown leaves (because of the systemic response described in section 4.4.7.3) the reference trace was obtained by extrapolation of the trace before illumination. Averaged values of the maximum of the light-induced DCF fluorescence were as shown in Table 4.3.

**Table 4.3** Average values of the light-induced maximum of DCF fluorescence of  $\text{NH}_4^+$ - and  $\text{NO}_3^-$ -grown leaves submerged in high and low  $\text{CO}_2$  medium (Fig. 4.27A).

sample	$\Delta F_{\max}$
$\text{NH}_4^+$ 0.1 mM $\text{NaHCO}_3$	$71 \pm 58$
$\text{NH}_4^+$ 10 mM $\text{NaHCO}_3$	$48 \pm 43$
$\text{NO}_3^-$ 0.1 mM $\text{NaHCO}_3$	$268 \pm 128$
$\text{NO}_3^-$ 10 mM $\text{NaHCO}_3$	$162 \pm 61$

The higher scatter of the DCF-fluorescence value of  $\text{NH}_4^+$ -grown leaves has a physiological meaning. As discussed above, the  $\text{NH}_4^+$ -grown seedlings were a mixture of plants, which were at the breakpoint of energy supply from the seeds or from photosynthesis. In the case of  $\text{NO}_3^-$ -grown seedlings, most of them have already installed fully functional photosynthesis.

In order to account for the systemic response in  $\text{NH}_4^+$ -grown leaves, Figure 4.27B shows responses obtained from measuring DCF fluorescence in the wider area (i.e. nearly the full field seen by the camera (Fig. 4.23)). However, in contrast to Fig. 4.26 not the space integrated fluorescence is shown. Instead the fluorescence from the wider field is given as average fluorescence density multiplied by the ratio of the wide field to that under the light guide. This ensures compatibility with Fig. 4.27A.

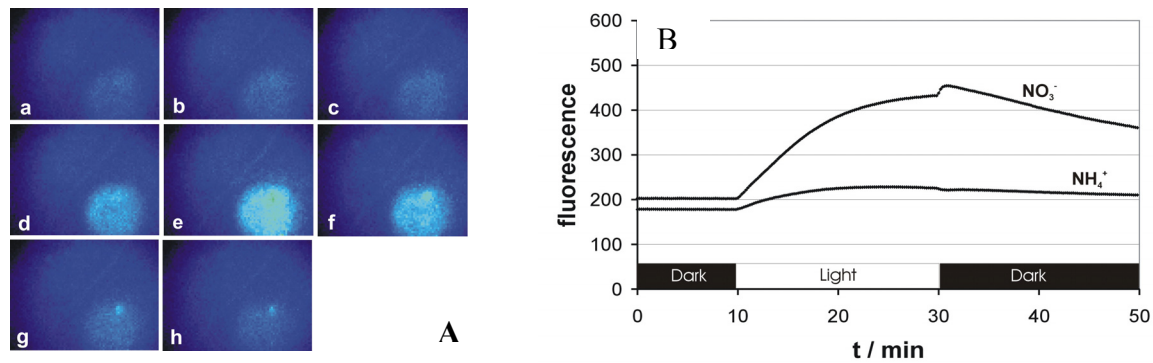
As already shown in Fig. 4.26, ROS production in the full field was much larger. It was even larger than that obtained in  $\text{NO}_3^-$ -grown leaves (Fig. 4.27A). The difference between the ROS production in 0.1 mM and 10 mM  $\text{NaHCO}_3$  in  $\text{NH}_4^+$ -grown leaves was much smaller than in  $\text{NO}_3^-$ -grown ones (no obvious difference in Fig. 4.27A and a difference of about 30 % in Fig. 4.27B).

#### 4.4.7.5 Effect of pH on ROS production

The systemic response in  $\text{NH}_4^+$ -grown seedlings led to the question of how a signal initiated by illumination is propagated through the leaf. A possible candidate for the involved compartment is the apoplast connecting all cells.

In order to get an approach to its possible involvement, the pH was changed by using SM medium with 5 mM MES buffered at pH 6.1 without bicarbonate. Figure 4.28 shows pictures of DCF fluorescence obtained from  $\text{NH}_4^+$ -grown leaves in SM medium at pH 6.1. There was no systemic response. Light-induced DCF fluorescence was restricted to the illuminated part as found for  $\text{NO}_3^-$ -grown leaves in Fig. 4.23B. The picture of DCF fluorescence from  $\text{NO}_3^-$ -grown leaves was similar to that in Fig. 4.23B and thus it is not shown here.

Again, two different types of response were observed in  $\text{NH}_4^+$ -grown leaves. There were eleven records with nearly no response to light as in Fig. 4.24B, and three records similar to those in Fig. 4.24C. Averaged values of  $F_{\text{max}}$  were 19 (SF = 1.8) and 91 (SF = 2.5), respectively. For  $\text{NO}_3^-$ -grown leaves the averaged value of  $F_{\text{max}}$  was 236 (SF = 2). SF means that the scatter was high and thus averaging was done on a logarithmic scale leading to a scatter factor (SF) that replaces linear standard deviation (multiply or divide the mean value by SF).



**Figure 4.28** ROS production in SM medium at pH 6.1. (A) There is no spreading of ROS production from the illuminated circle to the surrounding leaf area in  $\text{NH}_4^+$ -grown leaves. a) 10 min before light on, b) 5 min before light on, c) immediately before light on, d) directly after light on, e) 10 min after light on, f) 20 min after light on and g) immediately after light off, h) 20 min after light off. (B) Comparison of the light-induced responses in  $\text{NH}_4^+$ - and  $\text{NO}_3^-$ -grown leaves.

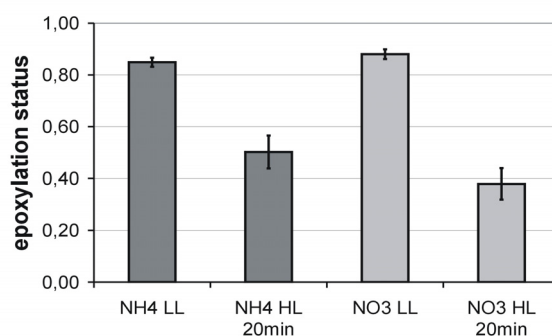
The absence of spreading in Fig. 4.28 may originate from two putative mechanisms: 1. Low pH in the apoplast prevents indication of ROS (quenching of DCF fluorescence) or 2. the mechanism of ROS production in the apoplast is prevented by low pH. Support for the first mechanism was provided by Fig. 4.12. However, the second one cannot be excluded. Nevertheless, the statement remains that ROS was produced in the apoplast and this seemed to be the origin of spreading. The minor remaining fluorescence under the light guide in Fig. 4.28A (but also B) probably was from the same photosynthesis-related mechanism as active in  $\text{NO}_3^-$ -grown seedlings (Fig. 4.18). Due to Fig. 4.10 photosynthesis did occur in  $\text{NH}_4^+$ -grown seedlings, but it was weaker.

#### 4.4.8 Investigations of scavenging systems

##### 4.4.8.1 Determination of zeaxanthin using HPLC

HPLC measurements (see 3.7.3.1) were done in cooperation with E. Grubmüller, Institute of Botany, to determine the xanthophylls violaxanthin, zeaxanthin and antheraxanthin. The xanthophylls cycle is thought to protect the photosynthetic pigments against oxidation. The epoxylation status is a mean to describe the amount of zeaxanthin, the xanthophylls accumulation at high light conditions, in the plants. The closer to 1 the epoxylation status is the less zeaxanthin is present.

Figure 4.29 shows the epoxylation status of  $\text{NH}_4^+$ - and  $\text{NO}_3^-$ -grown seedlings at HL ( $800 \mu\text{mol m}^{-2}\text{s}^{-1}$ ) and LL conditions. It was obvious that under 20min HL the amount of zeaxanthin present in the seedlings increased compared to LL. The important result was that there was less zeaxanthin present in  $\text{NH}_4^+$ -grown plants under HL than in  $\text{NO}_3^-$ -grown ones. This result is in line with investigations of Bendixen et al. (2001) and Zhu et al. (2000).



**Figure 4.29** Epoxylation status of seedlings at low (LL) and after 20 min high light ( $800 \mu\text{mol m}^{-2}\text{s}^{-1}$  light, HL). Dark grey indicates  $\text{NH}_4^+$ -grown seedlings and light grey  $\text{NO}_3^-$ -grown ones. Error bars = SEM,  $n=3$ .

#### 4.4.8.2 Testing for uptake of dye into the vacuole

Measurement of ROS production may be impaired by transport of the fluorescent dye into the vacuole since this may mimic the action of a scavenging system. There, the fluorescence would be quenched due to the acidity of the vacuole. The uptake into the vacuole may be mediated by ABC transporters involved in detoxification (Theodoulou 2000). In order to estimate the relevance of such an effect, the uptake of a pH indicating dye was studied.

Such a dye is BCECF AM which is a fluorescent dual-excitation dye widely used for intracellular pH measurements. It is very suitable for the determination of dye depletion by transport from the cytosol (pH  $\sim 6.8$ - $7.4$ ) to the vacuole (pH  $\sim 4.5$ - $6.0$ ). The velocity of the change of BCECF fluorescence is a measure of velocity of dye transported into the vacuole. More details of the method are given in section 3.7.3.2.

The measurements revealed that in  $\text{NO}_3^-$ -grown seedlings dye depletion by transport had a time constant of  $23 \pm 2.5$  min and in  $\text{NH}_4^+$ -grown ones of  $30 \pm 7$  min. Thus, a significant difference could not be found between the two N-forms.

#### 4.4.8.3 Determination of catalase activity

Catalase is a detoxification enzyme catalyzing the reaction of hydroxyperoxide to water and oxygen. This is important since hydroxyperoxide is toxic for the cell at high concentrations. The catalase concentration was determined to gain information of whether there are any N-form dependent differences in catalase activity thus providing a hint to the origin of the different sources of ROS.



Catalase concentration calculated by the inverse Boltzmann equation (section 3.7.3.3) gave the following results for  $\text{NO}_3^-$ -grown seedlings  $0.35 \pm 0.13 \text{ U ml}^{-1}$  and for  $\text{NH}_4^+$ -grown ones  $0.28 \pm 0.08 \text{ U ml}^{-1}$ . There was no N-form dependent significant difference found.

## 4.5 Gene expression studies

### 4.5.1 Experimental strategies

The gene expression studies have been done in cooperation with Prof. Aro's group at the University of Turku, Finland. Their 8k-cDNA microarray based on the GEM1 clone set from InCyte Genomics (Palo, USA manufactured by Eva-Mari Aro's group and by the Centre of Biotechnology) was used to obtain differential gene expression data. All experiments were done in Turku using the on-site expertise for all practical questions.

Here, gene expression studies have been applied to investigate the N-form dependent transcriptome of *A. thaliana*. Physiological studies can supply information about the *in vivo* situation. However, the absence of biophysical signals, which allow on-line determination of the processes between cellular compartments, impose severe restrictions to a more refined analysis of the underlying mechanisms. Studying the transcriptome together with physiological studies may bring some new insight in N-form dependent regulatory mechanisms and metabolic pathways used.

#### 4.5.1.1 Experimental design

When doing gene expression studies, one of the major questions is the experimental design. There are two different kinds of design, the “reference” design and the “loop” design (Simon et al. 2002). In Fig. 4.30 both possibilities are shown. The coloured dots indicate the labelling dye. Red indicates cy5 and green cy3. HL and LL indicate high light ( $800 \mu\text{mol m}^{-2}\text{s}^{-1}$  for 2 h) and low light ( $40 \mu\text{mol m}^{-2}\text{s}^{-1}$ ) conditions, respectively. The expression values of the cy3 labelled probe are always used as control levels. This means that the values for differential expressed genes in one particular hybridisation are always related to the cy3 value.

In the “reference design”, always the same RNA probe is used as control for each hybridisation ( $\text{NO}_3^-$  LL in Fig. 4.30A). This design has the advantage that all expression values are calculated with reference to the same control condition. However, there is a great disadvantage. A substantial amount of RNA from the reference probe is required to ensure that for all reactions one RNA-pool can be used which is obtained from exactly the same plant

material. This is important for the issue of comparison. Different pools of biological plant material can lead to a high degree of variation. One pool of raw material lowers the risk of variation due to different biological material.

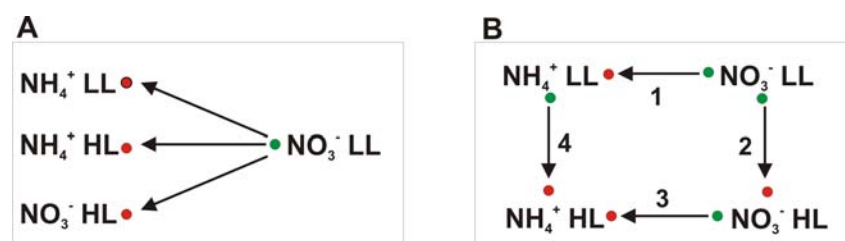
The “loop design”, in contrast, enables the direct comparison of treatments which are the basis for the conclusions drawn, for instance the effect of light under one kind of nutrition or the effect of nutrition under constant light. This decreases contingent experimental errors. If two treatments are related via an intermediate (e.g.  $\text{NH}_4^+$  HL and  $\text{NO}_3^-$  HL via  $\text{NO}_3^-$  LL in Fig. 4.30A) the error value rises. It has to be calculated from the sum of the two squares of the errors of the involved steps (e.g. the error of  $\text{NH}_4^+$  HL -  $\text{NO}_3^-$  LL and the error of  $\text{NO}_3^-$  HL -  $\text{NO}_3^-$  LL in Fig. 4.30A). This is avoided in the loop of Fig. 4.30B because the interesting treatments are neighbours.

Furthermore, the loop yields an intrinsic control of reliability. In a loop (A-B-C-D-A), A is compared with itself if the individual ratios are multiplied as indicated by the following equation

$$\frac{A}{B} \frac{B}{C} \frac{C}{D} \frac{D}{A} = \frac{A}{A} = 1 \quad (4.2)$$

In the scheme of Fig. 4.30B, two of the ratios have a definition which is inverse to the flow around the loop (indicated by a change of the sequence of the red and green dots in Fig. 4.30B). Because of this the inverted ratios have to be used for those two ratios, which have the opposite sequence of red/green than the other two pairs. Thus, the quotient of the products of expression values of 1\*4 and 2\*3 (Fig. 4.30B) has to give "1" according to the following rearrangement of Eq. 4.2

$$\frac{A}{B} \frac{D}{A} \left[ \frac{C}{B} \frac{D}{C} \right]^{-1} = \frac{A}{A} = 1 \quad (4.3)$$



**Figure 4.30** Experimental designs for microarray studies: (A) Reference design, one common control, (B) Loop design, no common control. Arrows connect the two probes hybridised on one microarray. The coloured dots indicate the labelling dye. Red presents cy5 and green cy3. The numbers in (B) indicate the four different hybridisations. HL and LL indicate high light ( $800 \mu\text{mol m}^{-2}\text{s}^{-1}$  for 2 h) and low light ( $40 \mu\text{mol m}^{-2}\text{s}^{-1}$ ) conditions, respectively.

As mentioned above, the “loop design” in Fig. 4.30B is more adequate to address two different questions. One question is the difference between N-form under LL and HL conditions (Fig. 4.30B horizontal arrows). The other one addresses the effect of light for the same N-form (Fig. 4.30B, vertical arrows). It may be argued that there exists no “real “control condition. This, however, is estimated to be less important than the benefits described above.

### **4.5.1.2 Technical and biological replicates**

Another point to consider is the number and nature of replicates needed. It has to be distinguished between technical replicates and biological replicates. Technical replicates take technical variations into account e.g. pipetting problems, inhomogeneous distribution of hybridisation solution on the microarray or variations in labelling of cDNA (Schuchhardt et al. 2000, Simon et al. 2002, Müller and Röder 2004, Drăghici 2003). Biological replicates, in contrast, account for any biological variations mainly heterogeneity between individuals (Müller and Röder 2004, Lee et al. 2000, Simon et al. 2002)

In this case, three technical replicates (chapter 3.8) means that three times the same PCR product is spotted at different locations (in each third of the slide). This accounts for inhomogeneous hybridisation of the probes. From the three signal intensities the geometric mean is calculated, i.e., replicates are averaged on a log scale. This mean value was used for further analysis. The geometric means is more adequate for data with large scatter than the linear mean, because outliers exert less impact on the result.

The biological variability was accounted for in two ways. First, plant material grown on one agar plate was pooled to account for differences of the population on the plate. Second, three independent pools of plant material were grown on different agar plates at different days. Harvesting at the same time of the day was done in order to eliminate diurnal changes of gene expression. Thus, three independent biological replicates were hybridised.

### **4.5.1.3 Normalisation strategies**

An important premise that the analysis yields reliable and comparable data is a good normalisation strategy. Normalisation is applied to account for differences in signal intensities between microarrays and for differences in signal intensities of the dyes on one microarray. These are caused by e.g. instability of cy5 or variations in the labelling process. For normalisation, two procedures were applied, the background correction and the colour normalisation.

The effect of non-specific binding causing the background was eliminated by subtraction of the median value of the background signal for each spot (local background correction). This possibility was chosen because there might be substantial variation in the size and shape of spots and especially inhomogeneity of the distribution of hybridisation solution on the whole array (Simon et al. 2002, Schuchhardt et al. 2000, Dràghici 2003). There are lots of other methods for background corrections amongst others e.g. sub-grid background correction, group background correction or background correction using blank spots (Dràghici 2003).

Subsequent to background correction colour normalisation was applied to each array. The purpose of colour normalisation is to eliminate dye-related data artefacts that cause the cy5/cy3 ratio to deviate from a bisecting line. These artefacts occur due to slightly different biochemical properties of the dyes and to non-linear rates of dye incorporation (Dràghici 2003, GeneSpring manual). The normalised values for two-colour data are determined by the ratio between the signal and the control channel. As in the case of background correction there are different strategies of colour normalisation, e.g. a method called "curve fitting an correction", "LOWESS" (locally weighted polynomial regression) or "piece-wise normalization" (Dràghici 2003).

Here, "LOWESS" was used. The "LOWESS" is a fitting routine that fits a first-order polynomial (straight line) to the data using a narrow (sliding) window. A smooth curve is obtained by moving the window over the data set and combine the individual straight lines to a continuous curve. This curve serves as a model to transform the fitted curve to a bisecting line. The correction factor of this transformation is used for colour-normalisation (Dràghici 2003).

#### **4.5.1.4 Data analysis**

Another source of error can be false positive results due to e.g. non-specific hybridisation. This problem was addressed during the analysis of the expression data. Only genes showing differential expression in all three biological replicates were subject to Northern blot analysis to finally uncover false positives.

After normalisation of the data, gene-lists from all differentially expressed genes can be obtained. There are two ways of filtering the data set: One possibility is to consult the average value of all replicates for the decision of whether the gene is differentially expressed or not. The other possibility is to look at all replicates separately and only genes differentially expressed in all cases are included in the gene list. Using the first possibility leads to inclusion of more genes. Consequently the risk for analyzing outliers is higher than using the second

approach. Here, only genes differentially expressed individually in all three biological replicates were subject to further analysis.

For final data interpretation, there are different approaches. One can, for example, filter for the highest differential expression values and do cluster analysis to obtain expression patterns. Another possibility is to do a hypothesis-driven analysis. That means looking for differentially expressed genes belonging to one particular metabolic pathway. Here, the analysis was hypothesis-driven and the gene lists were divided into pathway related groups. The results are presented in the following sections.

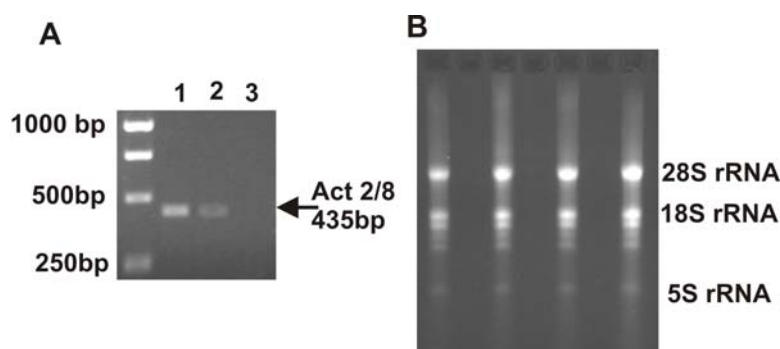
### **4.5.2 Evaluation of the microarray experiment**

There are many steps in the microarray procedure where quality checks are important in order to reveal any systematic faults and to minimize the risk of misjudgement of the results. The following procedures have to be scrutinized: RNA preparation, labelling reaction and annotation of genes (PCR products) to spots. As a final validation of the results the control by independent Northern blot analysis is important. In the following sections the individual evaluation methods are described in detail.

#### **4.5.2.1 Control of RNA quality**

Total RNA was found to be convenient for use in microarray experiments. Thus the higher effort of mRNA isolation could be avoided.

Because of equal nucleic acid characteristics there were traces of genomic DNA found in the extraction of RNA. Since genomic DNA is also complementary to the probes on the microarray it could hybridise as well and lead to false positive results. To eliminate these traces a DNase I hydrolysis of genomic DNA was applied. In order to control that the DNA was totally eliminated, PCR was carried out on the digested RNA using an actin specific primer-set (act2/8, see A.2). Fig. 4.31A shows that an actin amplicon has been obtained by PCR using crude RNA as template. DNase I treated RNA has been found to be almost free of genomic DNA, as no actin PCR product has been found to be amplified (Fig. 4.31A, lane 3). The RNA quality was additionally checked on a denaturing agarose gel and found to be intact (Fig. 4.31.B).



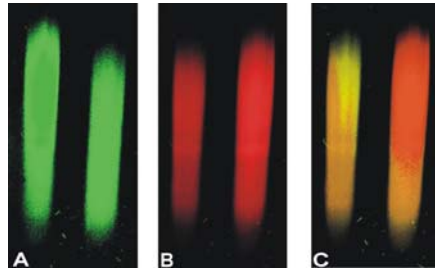
**Figure 4.31** (A) PCR with actin 2/8 primers on RNA before (2) and after DNase I digestion (3) on 1% agarose gel for control of whether there is any genomic DNA left. (1) Positive control, PCR on cDNA, (B) RNA on denaturing agarose gel to check for degradation.

Due to the results above (Fig. 4.31) all extracted total RNA was digested with DNase I prior to the labelling procedure. Before use in the microarray experiments, a quality check of the RNA was done using a denaturing agarose gel. Only non-degraded RNA without any traces of DNA was used.

Three independent RNA samples of light stressed (HL) and low light (LL) plants from both nitrate ( $\text{NO}_3^-$ ) and ammonium ( $\text{NH}_4^+$ ) nutrition were used. They were harvested at the same time of the day to diminish diurnal differences in gene expression.

#### 4.5.2.2 Assessment of labelling reactions

The RNA probes were labelled with the fluorescent cyanine dyes cy3 and cy5. Due to their steric structure the dUTPs labelled with cy3 or cy5 are greater than unlabeled dNTPs. Consequently, their incorporation rate is not as efficient. Thus, the quality of the cDNA synthesis has to be assessed. Important is the length of the labelled cDNA in order to achieve equal intensity of cy3- and cy5-labelled probes when binding to the same spot, i.e., the reverse transcription using either cy3 or cy5 dyes for labelling should produce the same amount of cDNA with the same size for even hybridisation purposes. If the labelling with one dye produces smaller sizes of cDNA products than the other one, the competition for binding on the spot during hybridisation is not equal. The greater the size the higher is the binding under stringent hybridisation conditions. Fig. 4.32 shows the results assessing the probe quality on an agarose gel after scanning (see 3.8.2). Almost no difference was found in size range between cy3 and cy5 labelling as indicated by the orange colour in Fig. 4.32C.



**Figure 4.32** Scanned image of 1 % agarose gel for assessing labelling quality. (A) cy3 channel, (B) cy5 channel, (C) composite image.

There are other processes assessing the reliability of the fluorescence labelling e.g. a process called dye swap. A dye swap is the exchange of cy3 or cy5 in the same experiment. There are two possibilities to carry out a dye swap. In a so-called internal control, the same RNA is labelled with cy3 or cy5 and hybridised on the same microarray. Then, only a uniform orange colour should be seen, because there should not be any differentially expressed genes (the same RNA). The second possibility is that on one microarray RNA 1 is cy3-labeled and RNA 2 cy5-labeled, and on the second array RNA1 is cy5 labelled and RNA 2 is cy3-labeled. Then the corresponding spots of the two microarrays should deliver inverse results. These evaluation steps were not carried out in this project due to experimental design (the loop design yields an intrinsic control of reliability Eq. 4.2), and limited resources in time and RNA.

#### 4.5.2.3 Controlling the annotation of genes to the spots on the microarray

Many routines of cDNA array preparation are error-prone. At almost any step before spotting a mixing up of PCR-samples can occur. Such mistakes have to be uncovered before the results are considered to be true. Therefore, it has to be verified that the annotation of genes (PCR products) to spots is correct by a sequence comparison of the spotted PCR products in the database. Thus, at least PCR products of the most important genes have to be sequenced.

The following genes of interest were sequenced for control reasons by using the MegaBACE 1000 (see 3.9.1) and are listed in Table 4.4. The sequences identities were confirmed using the *Arabidopsis* database [www.arabidopsis.org/blast](http://www.arabidopsis.org/blast).

**Table 4.4** List of genes sequenced by MegaBACE 1000 and results after confirmation in the database

Gene bank accession	Clone ID	Chromosomal location and gene name	Sequencing result compared with database
AI994315	701502677	At1g75270 dehydroascorbate reductase	Correct
AI993165	701495555	At5g18170 glutamate dehydrogenase	Correct
AW004570	701956503	At3g26650 glyceraldehyde 3-phosphate dehydrogenase A	Correct
AW004292	701547625	At2g33040 mitochondrial F1-ATPase, gamma subunit	Not correct (At3g12740 LEM3)
AI993567	701496656	At3g04790 ribose 5-phosphate isomerase	Correct
AI994888	701500329	At1g32060 phosphoribulokinase precursor	Correct
AI996004	701549625	At3g55800 sedoheptulose-bisphosphatase precursor	Correct
AI992702	701493348	At5g38410 (RuBisCO small subunit 3b)	Not sequenced
AW004084	701493687	At5g38420 (RuBisCO small subunit 2b)	Correct
AI997674	701669913	At1g68010 glycerate dehydrogenase	Correct
AI997303	701553173	At2g13360 alanine-glyoxylate aminotransferase	Not sequenced
AI993203	701495687	At4g37930 glycine hydroxymethyltransferase	Not sequenced
AI993750	701497383	At5g53460 glutamate synthase [NADH]	Not sequenced
AI997067	701551870	At5g50950 fumarate hydratase	Correct
AI993855	701515173	At1g80300 adenine nucleotide translocase	Correct
AI994385	701493716	At4g16760 acyl-CoA oxidase like protein	Correct
AI999414	701555793	At3g14420 glycolate oxidase	Correct
AI994219	701500373	At2g02390 glutathione transferase	Correct
AI998742	701546761	At2g29490 glutathione transferase	Not sequenced
AI994473	701498411	At2g44350 citrate synthase	Not correct (At5g58640 selenoprotein)
AI992452	701557821	At3g21720 isocitrate lyase	Not correct (At2g04400 indole-3-glycerol phosphate synthase)
AW004331	701956478	At3g01500 carbonic anhydrase	Correct
AI996316	701664914	At4g37870 phosphoenolpyruvate carboxykinase	Correct
AI996208	701550585	At1g37130 nitrate reductase 2	Correct
AW004371	701956665	At1g77760 nitrate reductase 1	Correct
AI999702	701557102	At2g29450 glutathione transferase (103-1A)	Correct



AI993798	701514666	At1g14150 PsbQ domain protein family extrinsic pII protein	Correct
AI995432	701674073	At4g10120 sucrose-phosphate synthase	Not correct (At5g38420 Rubisco 2b)
AI995244	701503147	At5g28840 NAD-dependent epimerase/dehydratase family	Correct
AI994456	701498361	At4g26530 fructose-bisphosphate aldolase cytosolic	Correct (sequenced in Turku)
AI992920	701495044	At4g38970 fructose-bisphosphate aldolase plastidic	Correct (sequenced in Turku)
AI995830	701548833	At4g35090 catalase 2	Correct (sequenced in Turku)
AI996006	701549636	At4g11600 glutathione peroxidase	Correct (sequenced in Turku)

The results of Table 4.4 reveal that about 10 % of annotations of the genes on the microarray were wrong. Furthermore, another 10 % were not sequenced, because they could not be amplified in our lab neither with standard primer T7 / SP6 nor with a specific primer constructed on EST sequence.

#### 4.5.2.4 Verification of differentially expressed genes by Northern blot analysis

The microarray data need to be verified by a second independent method since variation among the RNA samples and problems during hybridisation (e.g. non-specific hybridisation) can lead to false positive or false negative results. Northern blot analysis is a very sensitive and well-established method. Another possibility would be Real-time PCR. Here, Northern blotting was preferred (see 3.9.2). In this chapter only a quick overview of the results as verification for the microarray results is given. A more detailed description is presented in the subsequent sections.

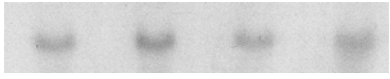

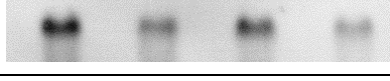
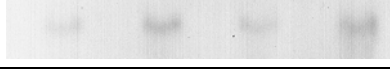





Table 4.5 gives an overview of the results of Northern blots in comparison with the mean values of the microarray results. Only the genes verified by sequencing were subject to further analysis. Table 4.5 is to be read the following way. The Northern blots are shown in the third column. The heading in this column indicates the particular treatment e.g. LL, HL, and N-form. The microarray results (column 4-7) are given as cy5/cy3 fluorescence ratios. The probe before the slash is cy5 labelled the one after is cy3 labelled. A ratio above 1.5 indicates a 1.5 times higher level of transcription (i.e. up-regulation) of the gene detected by the cy5 labelled probe. And *vice versa*: a more than 1.5 times down-regulated transcript is indicated by a ratio below 0.67. The ratios showing differentially expressed genes (at least 1.5 times up- or down-regulated) are highlighted by bold numbers.

For example if the Northern blot shows a light-induced up-regulation in  $\text{NO}_3^-$ -grown plants the ratio  $\text{NO}_3^-$  HL/LL should be above 1.5. In that case the Northern blot supports the microarray result.

**Table 4.5** Overview: Comparison of Northern blot and microarray results. The RNA traces always used as a standard are not displayed here for the sake of a clearer presentation. In most cases expression was in line with the microarray data (indicated in the last column, ok). Details on the results of Northern blot analysis are given in subsequent sections. Values in columns 4-7 show average values of the results of three biological replicates.

Gene	Primer and Template	X-Film				$\text{NH}_4^+ / \text{NO}_3^-$ LL	$\text{NH}_4^+ / \text{NO}_3^-$ HL	$\text{NO}_3^- : \text{HL} / \text{LL}$	$\text{NH}_4^+ : \text{HL} / \text{LL}$	
		$\text{NH}_4^+$ LL	$\text{NH}_4^+$ HL	$\text{NO}_3^-$ LL	$\text{NO}_3^-$ HL					
At3g01500 CH	T7/Sp6 EST clone					0.78	<b>0.54</b>	<b>2.58</b>	<b>1.76</b>	Ok
At2g29450 GST	specific EST clone					1.27	1.18	<b>3.05</b>	<b>3.88</b>	Ok
At1g77760 Nia1	Specific RT-PCR					<b>0.33</b>	0.72	<b>0.47</b>	1.02	Ok
At1g37130 Nia2	specific EST clone					<b>0.24</b>	<b>0.67</b>	1.33	<b>1.71</b>	Ok
At4g37870 PEPCK	specific EST clone					<b>2.20</b>	1.13	0.81	0.71	Ok
At1g14150 PsbQ	specific EST clone					0.75	<b>0.60</b>	<b>1.58</b>	0.74	false
At1g75270 DHAR	specific EST clone					1.45	1.34	<b>2.59</b>	<b>1.87</b>	Ok
At5g18170 GDH1	specific RT-PCR					<b>1.85</b>	1.03	1.01	<b>0.54</b>	false
At3g26650 GapA	specific EST clone					1.22	0.97	<b>1.77</b>	1.26	Ok
At3g04790 Rpi	specific RT-PCR					1.10	1.03	<b>1.68</b>	<b>1.49</b>	false
At1g32060 PRK	specific EST clone					0.88	0.84	<b>1.81</b>	1.42	false
At3g55800 SBPase	specific EST clone					1.04	1.05	<b>2.02</b>	<b>1.69</b>	Ok
At5g38420 RCO2b	specific EST clone					1.08	0.69	<b>1.95</b>	<b>1.57</b>	Ok

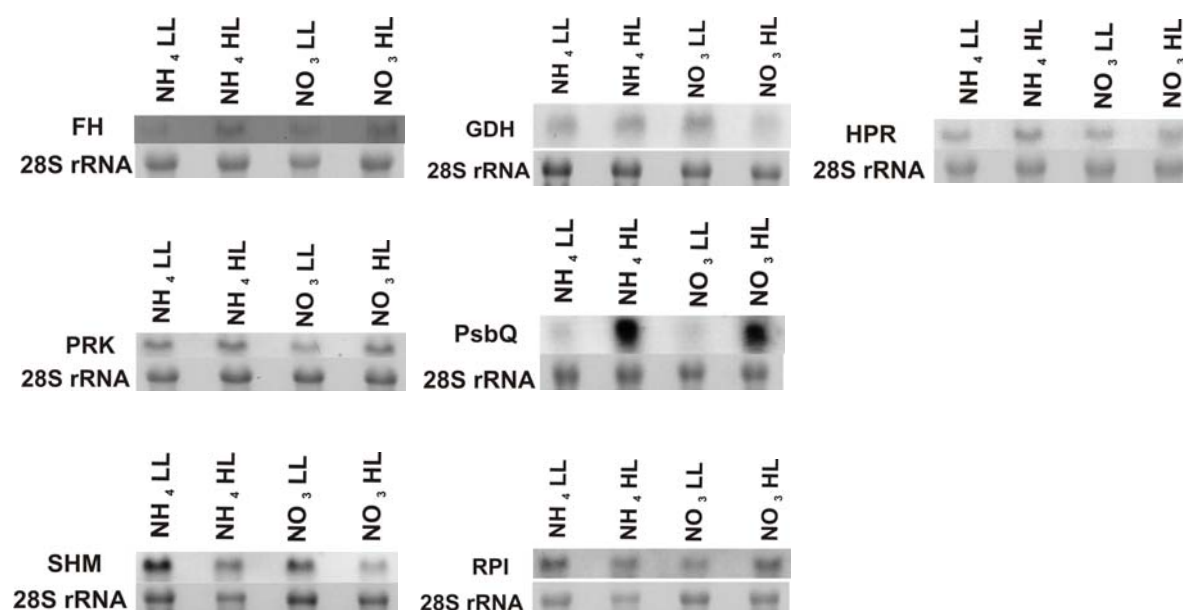
## 4 Results

At1g68010 HPR	specific EST clone		0.85	1.03	<b>1.81</b>	1.43	false
At2g13360 AGT1	specific RT-PCR		1.30	1.33	<b>2.16</b>	<b>1.63</b>	Ok
At4g37930 SHM1	specific RT-PCR		0.92	0.79	<b>1.58</b>	1.24	false
At5g50950 FH	specific RT-PCR		<b>0.46</b>	0.95	<b>0.60</b>	0.76	false
At1g80300 AATP1	specific RT-PCR		0.97	0.95	<b>1.70</b>	1.36	Ok
At3g14420 GOX	specific EST clone		1.14	1.25	<b>1.74</b>	1.46	Ok
At4g26530 FBA cyt	T7/Sp6 EST clone		0.73	0.69	<b>1.76</b>	<b>1.57</b>	Ok
At4g38970 FBA plast	specific EST clone		1.18	1.05	<b>1.78</b>	1.49	Ok
At5g28840 EPI	specific RT-PCR		1.28	0.95	<b>2.02</b>	1.4	Ok

Seven out of 22 (~30 %) of the Northern blot results did not support the microarray results. This is indicated by the right hand column in Table 4.5. In section 4.5.3 the differentially expressed genes are presented in more detail.

### 4.5.2.5 Pitfalls - Genes with different results in microarray and Northern blot

About 30 % of genes, which were found to be differentially expressed by microarray analysis could not be confirmed by Northern blot analysis. Fig. 4.33 shows the seven genes tested on Northern blot which do not show the same trend as they do on the microarray. In addition, for glycine hydroxymethyltransferase (SHM) and ribose-5phosphate isomerase (RPI) a conclusive statement was not possible because the RNA showed differences. Fumarate hydratase (FH), glutamate dehydrogenase (GDH), glycerate dehydrogenase (HPR), extrinsic pII protein (PsbQ) and phosphoribulokinase (PRK) definitely did not reveal the same results as the microarray (Table 4.6).



**Figure 4.33** Northern blot analysis of genes not corresponding to microarray results. RNA was obtained from leaves of 15-days old *A. thaliana* subject to four different treatments:  $\text{NH}_4^+$  LL,  $\text{NH}_4^+$  HL,  $\text{NO}_3^-$  LL,  $\text{NO}_3^-$  HL. 7.5  $\mu\text{g}$  RNA were loaded per lane. 28S-RNA is used for calibration.

**Table 4.6** Microarray results of the genes not corresponding to Northern blot analysis. LL and HL denote low light and high light treatments, respectively. Bold numbers indicate statistically significant differences (t-test,  $p = 0.05$ ). Average values of three biological replicates  $\pm$  SEM are shown. "Loop amplification" is calculated by means Eq. 4.3. Assignment to compartments according to TAIR.

compartment		$\text{NH}_4^+ / \text{NO}_3^-$ LL	$\text{NH}_4^+ / \text{NO}_3^-$ HL	$\text{NO}_3^-$ : HL / LL	$\text{NH}_4^+$ : HL / LL	"loop amplification"
Mitochondrion	At5g50950 fumarate hydratase	<b>0.46 <math>\pm</math> 0.08</b>	0.95 $\pm$ 0.49	<b>0.6 <math>\pm</math> 0.09</b>	0.76 $\pm$ 0.15	<b>0.61</b>
Thylakoid lumen	At1g14150 PsbQ	0.75 $\pm$ 0.1	<b>0.6 <math>\pm</math> 0.11</b>	<b>1.58 <math>\pm</math> 0.2</b>	0.74 $\pm$ 0.71	<b>0.59</b>
Chloroplast	At3g04790 ribose 5-phosphate isomerase	1.1 $\pm$ 0.12	1.03 $\pm$ 0.13	<b>1.68 <math>\pm</math> 0.17</b>	<b>1.49 <math>\pm</math> 0.24</b>	<b>0.95</b>
Chloroplast	At1g32060 phosphoribulokinase precursor	0.88 $\pm$ 0.18	0.84 $\pm$ 0.14	<b>1.81 <math>\pm</math> 0.18</b>	1.42 $\pm$ 0.23	<b>0.82</b>
Mitochondrion	At4g37930 glycine hydroxymethyltransferase	0.92 $\pm$ 0.15	0.79 $\pm$ 0.16	<b>1.58 <math>\pm</math> 0.32</b>	1.24 $\pm$ 0.22	<b>0.91</b>
Peroxisome	At1g68010 glycerate dehydrogenase	0.85 $\pm$ 0.15	1.03 $\pm$ 0.29	<b>1.81 <math>\pm</math> 0.18</b>	<b>1.43 <math>\pm</math> 0.23</b>	<b>0.65</b>
Mitochondrion	At5g18170 glutamate dehydrogenase	<b>1.85 <math>\pm</math> 0.28</b>	1.03 $\pm$ 0.18	1.01 $\pm$ 0.13	<b>0.54 <math>\pm</math> 0.13</b>	<b>0.96</b>

### **4.5.3 Differentially expressed genes**

In the following sections an overview of the results of the microarray experiment is given. The differentially expressed genes encoding for enzymes of N-assimilation, photosynthesis related processes and detoxification are described in more detail.

#### **4.5.3.1 Overview of microarray results**

In total, there were 330 genes differentially expressed. Only genes differentially expressed on each single slide were included in the gene list (containing only the differentially expressed genes). Mean values were calculated after checking that all replicates resulted in a differential expression with a factor of at least 1.5. Six percent of the 330 differential expressed genes were not annotated, so called "no hits found". Around 18 % of the 330 differential expressed genes were annotated merely as "expressed proteins" and not taken into account for further analysis. Thirty-three percent of the 330 differential expressed genes were enzymes, and 42 % of the 330 differential expressed genes were other proteins. The evaluation of the data was focussed on the enzymes since the aim of this project was to analyze metabolic pathways involved in assimilation of nitrate or ammonium as the sole nitrogen source.

Thus, the focus was not on the highest differentially expressed genes. The standard routines of microarrays analysis, i.e., cluster analysis or gene trees, were not applied to this data set. The software GeneSpring 7.2 normally applied for these routines was only used to normalise the raw data and to utilize a user friendly surface for handling the voluminous data set.

Table 4.7 presents a selection of genes encoding for enzymes of nitrate assimilation, Calvin cycle, photorespiration, sucrose synthesis, detoxification and amino acid synthesis. A survey of all differentially expressed genes can be found in the appendix (A.3, A.4) divided into subgroups for the sake of clarity.

**Table 4.7** Differential expression values of enzymes of nitrate assimilation, Calvin cycle, photorespiration, sucrose synthesis, detoxification and amino acid synthesis in  $\text{NH}_4^+$ - and  $\text{NO}_3^-$ -grown *A. thaliana* seedlings. LL and HL denote low light and high light treatments, respectively. Bold numbers indicate statistically significant differences (t-test,  $p = 0.05$ ). Average values plus SEM are shown. "Loop amplification" is calculated by means Eq. 4.3. Assignment to cell compartments according to TAIR.

		$\text{NH}_4^+ / \text{NO}_3^-$ LL	$\text{NH}_4^+ / \text{NO}_3^-$ HL	$\text{NO}_3^-$ : HL / LL	$\text{NH}_4^+$ : HL / LL	"loop" amplification
<b>Nitrate assimilation</b>						
<b>Compartment</b>						
Chloroplast	At5g53460 glutamate synthase [NADH]	<b>0.64 ± 0.11</b>	1.05 ± 0.16	<b>0.54 ± 0.08</b>	0.8 ± 0.1	<b>0.9</b>
Cytosol	At1g66200 glutamine synthetase (GLN1;2)	1.21 ± 0.18	1.06 ± 0.25	<b>2.3 ± 0.26</b>	<b>1.68 ± 0.22</b>	<b>0.83</b>
Not clear	At3g17800 glutamine synthetase (GLN1;3)	-	1.0 ± 0.24	<b>2.33 ± 0.34</b>	1.38 ± 0.59	-
Membrane	At1g37130 nitrate reductase 2 (Nia2)	<b>0.24 ± 0.05</b>	0.67 ± 0.98	1.33 ± 0.27	1.71 ± 0.4	<b>0.46</b>
Cytosol	At1g77760 nitrate reductase 1 (Nia1)	0.33 ± 0.1	0.72 ± 0.06	0.47 ± 0.28	1.02 ± 0.17	<b>0.995</b>
<b>Calvin cycle</b>						
Chloroplast	At5g38420 RuBisCO 2b	1.08 ± 0.39	0.69 ± 0.21	<b>1.95 ± 0.27</b>	<b>1.57 ± 0.24</b>	<b>1.26</b>
Chloroplast	At3g26650 glyceraldehyde 3-phosphate dehydrogenase A subunit	1.22 ± 0.25	0.97 ± 0.21	<b>1.77 ± 0.3</b>	1.26 ± 0.27	<b>0.9</b>
Chloroplast	At4g38970 fructose-bisphosphate aldolase plast	1.18 ± 0.24	1.05 ± 0.19	<b>1.78 ± 0.19</b>	<b>1.49 ± 0.21</b>	<b>0.94</b>
Chloroplast	At3g55800 sedoheptulose-bisphosphatase precursor	1.04 ± 0.19	1.05 ± 0.19	<b>2.02 ± 0.32</b>	<b>1.69 ± 0.14</b>	<b>0.83</b>
Chloroplast	At5g38410 RuBisCO 3b	1.18 ± 0.33	0.81 ± 0.17	<b>2.11 ± 0.36</b>	<b>1.7 ± 0.4</b>	<b>1.17</b>
Chloroplast	At3g04790 ribose 5-phosphate isomerase	1.1 ± 0.12	1.03 ± 0.13	<b>1.68 ± 0.17</b>	<b>1.49 ± 0.24</b>	<b>0.95</b>
Chloroplast	At1g32060 phosphoribulokinase precursor	0.88 ± 0.18	0.84 ± 0.14	<b>1.81 ± 0.18</b>	1.42 ± 0.23	<b>0.82</b>
Chloroplast	At3g01500 Carbonic anhydrase	0.78 ± 0.19	<b>0.54 ± 0.14</b>	<b>2.58 ± 0.37</b>	<b>1.76 ± 0.22</b>	<b>0.98</b>
Chloroplast membrane	At1g80300 Adenine nucleotide translocator	0.97 ± 0.23	0.95 ± 0.16	<b>1.7 ± 0.3</b>	<b>1.36 ± 0.18</b>	<b>0.82</b>

<b>Photorespiration</b>						
Cytosol	At3g14420 glycolate oxidase	1.14 ± 0.14	1.25 ± 0.21	<b>1.74 ± 0.19</b>	1.46 ± 0.23	<i>0.77</i>
Mitochondrion	At2g26080 glycine dehydrogenase	1.16 ± 0.18	<b>0.59 ± 0.11</b>	<b>3.52 ± 0.68</b>	<b>1.76 ± 0.32</b>	<i>0.98</i>
Mitochondrion	At4g37930 glycine hydroxymethyltransferase	0.92 ± 0.15	0.79 ± 0.16	<b>1.58 ± 0.32</b>	1.24 ± 0.22	<i>0.91</i>
Peroxisome	At1g68010 glycerate dehydrogenase	0.85 ± 0.15	1.03 ± 0.29	<b>1.81 ± 0.18</b>	<b>1.43 ± 0.23</b>	<i>0.65</i>
Peroxisome	At4g35090 catalase 2	1.05 ± 0.13	1.08 ± 0.24	<b>4.05 ± 0.49</b>	<b>2.78 ± 0.55</b>	<i>0.67</i>
Peroxisome	At2g13360 alanine-glyoxylate aminotransferase	1.3 ± 0.14	1.33 ± 0.13	<b>2.16 ± 0.37</b>	<b>1.63 ± 0.31</b>	<i>0.73</i>
unknown	At4g13930 hydroxymethyltransferase	1.1 ± 0.19	1.07 ± 0.14	<b>1.60 ± 0.19</b>	1.67 ± 0.28	<i>1.02</i>
<b>Detoxification</b>						
Cytosol	At1g75270 dehydroascorbate reductase	1.45 ± 0.24	1.34 ± 0.18	<b>2.59 ± 0.49</b>	<b>1.87 ± 0.31</b>	<i>0.78</i>
Cytosol	At2g02390 glutathione transferase	<b>1.64 ± 0.24</b>	<b>1.43 ± 0.15</b>	<b>2.18 ± 0.21</b>	<b>1.24 ± 0.15</b>	<i>0.65</i>
Cytosol	At2g29450 glutathione transferase (103-1A)	1.27 ± 0.09	1.18 ± 0.20	<b>3.04 ± 1.14</b>	<b>3.88 ± 0.26</b>	<i>1.37</i>
Cytosol	At2g29490 glutathione transferase	<b>1.54 ± 0.26</b>	<b>1.76 ± 0.23</b>	1.66 ± 0.49	1.48 ± 0.29	<i>0.78</i>
Cytosol	At4g11600 glutathione peroxidase	1.29 ± 0.14	1.2 ± 0.29	<b>1.86 ± 0.35</b>	<b>2.22 ± 0.37</b>	<i>1.28</i>
Mitochondrion	At4g33420 peroxidase	<b>2.11 ± 0.29</b>	1.68 ± 0.54	1.42 ± 0.27	1.17 ± 0.15	<i>1.03</i>
Peroxisome	At4g35090 catalase 2	1.05 ± 0.13	1.08 ± 0.24	<b>4.05 ± 0.49</b>	<b>2.78 ± 0.55</b>	<i>0.67</i>
unknown	At5g28840 NAD-dependent epimerase/dehydratase family	1.28 ± 0.26	0.95 ± 0.14	<b>2.02 ± 0.23</b>	1.4 ± 0.29	<i>0.93</i>
<b>Sucrose synthesis</b>						
Cytosol	At4g26530 fructose biphosphate aldolase cytosolic	0.73 ± 0.13	<b>0.69 ± 0.08</b>	<b>1.76 ± 0.2</b>	<b>1.57 ± 0.2</b>	<i>0.94</i>
unknown	At4g37870 phosphoenolpyruvate carboxykinase (ATP)	<b>2.2 ± 0.28</b>	1.13 ± 0.66	0.81 ± 0.11	0.70 ± 0.15	<i>1.7</i>

<b>Amino acid synthesis</b>						
Chloroplast	At2g16500 arginine decarboxylase	1.38 ± 0.23	1.02 ± 0.2	<b>2.03 ± 0.29</b>	1.37 ± 0.23	<b>0.91</b>
Chloroplast	At4g34740 amidophosphoribosyltransferase 2 precursor	1.02 ± 0.16	1.25 ± 0.13	<b>2.12 ± 0.26</b>	<b>1.53 ± 0.21</b>	<b>0.59</b>
Chloroplast	At4g39980 2-dehydro-3-deoxyphosphoheptonate aldolase (DHS1)	0.91 ± 0.15	0.82 ± 0.12	<b>1.68 ± 0.18</b>	1.19 ± 0.20	<b>0.79</b>
Chloroplast	At5g17330 glutamate decarboxylase 1 (GAD 1)	<b>1.62 ± 0.22</b>	<b>1.84 ± 0.29</b>	<b>1.35 ± 0.16</b>	1.04 ± 0.16	<b>0.68</b>
Cytosol	At1g55920 serine acetyltransferase	1.25 ± 0.17	0.89 ± 0.11	<b>3.39 ± 0.41</b>	<b>2.48 ± 0.4</b>	<b>1.02</b>
Cytosol	At1g75270 dehydroascorbate reductase	1.45 ± 0.24	1.34 ± 0.18	<b>2.59 ± 0.49</b>	<b>1.87 ± 0.31</b>	<b>0.78</b>
Cytosol	At3g47340 glutamine-dependent asparagine synthetase	1.24 ± 0.34	0.77 ± 0.2	<b>1.81 ± 0.43</b>	0.81 ± 0.28	<b>0.72</b>
Mitochondrion	At1g54100 aldehyde dehydrogenase	<b>2.5 ± 0.42</b>	<b>1.72 ± 0.27</b>	<b>1.71 ± 0.18</b>	1.13 ± 0.16	<b>0.96</b>
Mitochondrion	At3g61440 cysteine synthase	1.34 ± 0.18	1.22 ± 0.26	<b>1.74 ± 0.25</b>	1.43 ± 0.28	<b>0.9</b>
Mitochondrion	At3g30775 osmotic stress-induced proline dehydrogenase (pro1)	<b>2.3 ± 0.42</b>	0.84 ± 0.17	<b>2.3 ± 0.62</b>	0.76 ± 0.2	<b>0.9</b>
Mitochondrion	At5g18170 glutamate dehydrogenase	<b>1.85 ± 0.28</b>	1.03 ± 0.18	1.01 ± 0.13	<b>0.54 ± 0.13</b>	<b>0.96</b>
Mitochondrion	At4g08870 arginase	1.06 ± 0.1	1.1 ± 0.12	<b>1.72 ± 0.22</b>	<b>2 ± 0.3</b>	<b>1.12</b>
unknown	At4g13930 hydroxymethyltransferase	1.1 ± 0.19	1.07 ± 0.14	<b>1.60 ± 0.19</b>	1.67 ± 0.28	<b>1.07</b>

**Table 4.8** Percentage of "loop amplification" in the range from 0.02 to 0.3

<b>deviation</b>	0.98-1.03	0.9-1.1	0.8-1.2	0.7-1.3
<b>percentage</b>	<b>15.91</b>	<b>45.45</b>	<b>61.36</b>	<b>79.55</b>

In Table 4.8 it is shown that about 80 % of the data were in the range of ± 30 % variance.

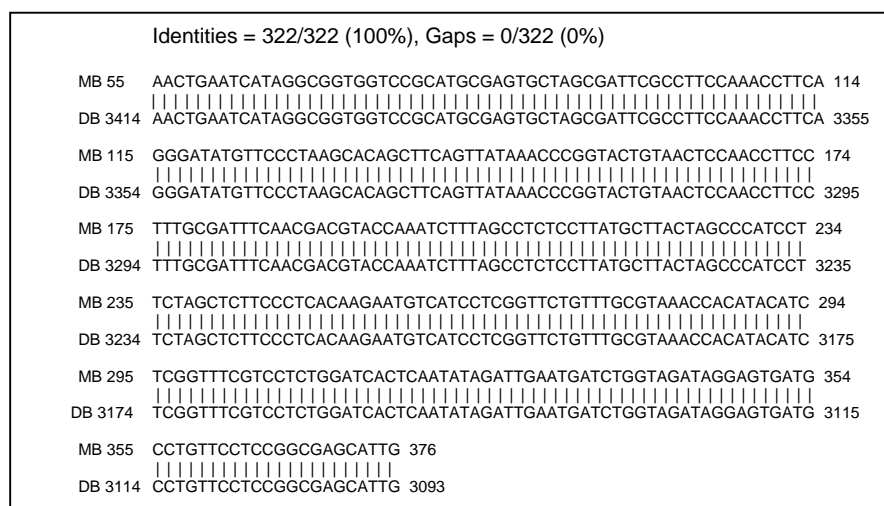


#### 4.5.3.2 Processing, analysis and problems of the evaluation of microarray data as illustrated for nitrate reductase

In this chapter, the process of interpreting the data is demonstrated for the two genes (Nia1, Nia2) encoding for nitrate reductase (NR). NR mainly catalyses the reduction of nitrate to nitrite. There are two isoforms of NR, NR1 (encoded by Nia1) and NR2 (encoded by Nia2). They differ mainly in their location in the cell. NR1 is found in the cytosol, and NR2 is a membrane bound protein.

Nitrate induces the transcription of genes encoding for NR and ammonium-grown plants do not have any nitrate. Therefore it was expected that the transcript level of NR was lower in  $\text{NH}_4^+$ -grown seedlings than in  $\text{NO}_3^-$ -grown ones. Indeed, both genes encoding for NR were stronger expressed in  $\text{NO}_3^-$ -grown seedlings. Their differential expression was the first indication of N-form dependent differences being visible on transcript level.

For verification of the data, the spotted PCR products (provided by Eva-Mari Aro's group) had been sequenced. This was the only way to ensure the reliability of annotation of the actual spot. The sequence of the PCR product generated by sequencing with the MegaBACE was compared with the genome of *A. thaliana* using the blast search algorithm of TAIR database. In Fig. 4.34, the sequence alignment for Nia1 is shown. The alignment revealed 100 % identity of the obtained sequence to Nia1. The same was true for Nia2.



**Figure 4.34** Sequence alignment of Nia1. MB: MegaBACE sequence, DB: database sequence

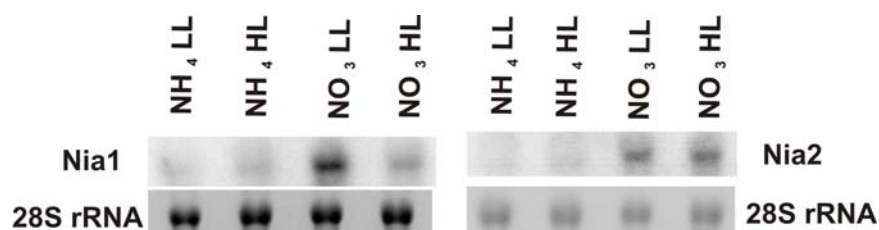
After the approval that Nia1 and Nia2 had the right annotation, verification of the differential expression was done by Northern blot analysis. Fig. 4.35 shows the results of Northern

blotting of *Nia1* and *Nia2*. These results were then compared to the corresponding microarray results (Table 4.9). The Northern blot results for *Nia1* corresponded exactly to the microarray data. For *Nia2* they corresponded quite well, except for the feature that it was up-regulated in ammonium-grown seedlings in the light on the microarray. This slight up-regulation was hardly visible on the Northern blot. However, this was not found to be of major importance for the further interpretation of the data. The crucial finding was a strong up-regulation of the genes encoding for NR in nitrate-grown seedlings as compared to ammonium-grown ones. This up-regulation was important to verify the N-form dependent difference and was found in both types of experiments (see Table 4.9 and Fig. 4.35). This finding is not impaired by the slight light-induced up-regulation of *Nia2* in ammonium-grown seedlings, which may not even be significant because the loop of *Nia2* has a bad "loop amplification" (Eq. 4.3).

A striking fact (still not quite understood in detail) was the down regulation of *Nia1* in the light. One would expect the up-regulation of *Nia1* in the light due to higher demand of assimilation of nutrients. In contrast to *Nia1*, this is true for *Nia2*. The sequence of the *Nia1* hybridisation probe did not have any sequence homologies with the coding sequence of *Nia2*. Therefore, the result of Northern blot analysis for *Nia1* was isoform specific. The sequence of the *Nia2* hybridisation probe did have some homologies with the coding sequence of *Nia1*. Nevertheless, this is of minor importance since the main conclusion, that in both cases the transcript level in  $\text{NH}_4^+$  plant material was much lower than in  $\text{NO}_3^-$  plant material, is not affected by this homology.

**Table 4.9** Microarray results of *Nia1* and *Nia2*. Average value plus SEM.

		$\text{NH}_4^+ / \text{NO}_3^-$ LL	$\text{NH}_4^+ / \text{NO}_3^-$ HL	$\text{NO}_3^-$ : HL / LL	$\text{NH}_4^+$ : HL / LL	"loop amplification"
Membrane	At1g37130 nitrate reductase 2 ( <i>Nia2</i> )	<b>0.24 ± 0.05</b>	0.67 ± 0.98	1.33 ± 0.27	1.71 ± 0.4	<b>0.46</b>
Cytosol	At1g77760 nitrate reductase 1 ( <i>Nia1</i> )	0.33 ± 0.1	0.72 ± 0.06	0.47 ± 0.28	1.02 ± 0.17	<b>0.995</b>



**Figure 4.35** Northern blot results of *Nia1* and *Nia2*. RNA was obtained from leaves of 15-days old *A. thaliana* subject to four different treatments:  $\text{NH}_4^+$  LL,  $\text{NH}_4^+$  HL,  $\text{NO}_3^-$  LL,  $\text{NO}_3^-$  HL. 7.5  $\mu\text{g}$  RNA were loaded per lane. 28S-RNA is used for calibration.

Wilkinson and Crawford (1991) found that NR1 has only 10 % of the overall activity of NR whereas NR2 has 90 % activity.

At this point it becomes clear that literature and database search is essential to gain all information required to interpret the results. Especially the analysis of the isoforms is important since they differ e.g. in regulation, location (cell compartment) and importance for catalyzing reactions. The last point becomes obvious looking at the NR forms. Since NR1 just accounts for only 10 % of overall activity its down regulation under HL conditions is of minor importance.

In the case of NR it was quite easy to get information because NR is a well investigated enzyme. Not only the information about the protein but also about the genes are well documented (e.g. Sherameti et al. 2002, MacKintosh and Meek 2001, Cheng et al. 1991, Crawford et al. 1988). In other cases it is more complicated, sometimes enzymes catalyse two different reactions and have two different EC numbers. Sometimes the annotation in one database is not correct or incomplete since the annotation of genes is still an ongoing work. Another main drawback is definitely that not all isoforms are investigated. Furthermore, often physiological measurements only reveal overall activity of the enzyme and do not tell anything about the individual isoforms. Another problem arises from the fact that one gene sometimes has two or more abbreviations due to different cloning strategies or functional assignments.

The whole procedure of gaining information becomes even more complicated if there is a gene family with more than 10 isoforms such as the GST family. There are 48 isoforms divided in 5 subfamilies (Dixon et al. 2002). In the experimental set here, only three of them were differentially expressed. Unfortunately there was not enough information available to analyse exactly their importance and function.

### **4.5.3.3 Analysis of technical and biological replicates - illustrated by Nia1 and Nia2**

As mentioned above technical and biological replicates are of major importance accounting for technical and biological variations. First, a short definition of the terms used in Table 4.10 is given.

Normalised value: raw data divided by the control value.

Control value: cy3 signal (already processed to account for inhomogeneity of signal intensities between cy3 and cy5)

Raw value: signal intensities of the cy5 signal

The control and raw values are already background corrected (as described in 4.5.1.3). In all cases, the minimum (Min) and maximum (Max) values of the technical replicates are shown. The differences between the replicates and their implications on further analysis are illustrated by Nia2 and Nia1. Table 4.10 shows normalised, control and raw values for each individual replicate whereas in Tables 4.11 and 4.12 the normalised values, the average of them and the loop amplification (Eq. 4.3) are shown.

**Table 4.10** Normalised, control and raw data of Nia2 from all individual replicates. Min and Max show the values of the technical replicates. T-test p-value gives reliability that average value of technical replicates (bold) is different from one. LL and HL denote low light and high light treatments, respectively.

Replicates	Normalised Value	Min	Max	Control Value	Min	Max	Raw value	Min	Max
<b>A: NH<sub>4</sub><sup>+</sup> / NO<sub>3</sub><sup>-</sup> LL</b>									
1	<b>0.21</b>	0.20	0.22	<b>1848</b>	1651	2097	<b>387</b>	375	405
2	<b>0.20</b>	0.16	0.24	<b>2505</b>	2099	3020	<b>499</b>	408	589
3	<b>0.33</b>	0.23	0.44	<b>247</b>	235	269	<b>83</b>	58	108
<b>B: NH<sub>4</sub><sup>+</sup> / NO<sub>3</sub><sup>-</sup> HL</b>									
1	<b>0.28</b>	0.22	0.39	<b>6453</b>	4578	8765	<b>1838</b>	1438	2523
2	<b>0.31</b>	0.30	0.32	<b>559</b>	410	708	<b>174</b>	166	181
3	<b>3.43</b>	2.40	4.93	<b>270</b>	199	357	<b>925</b>	648	1332
<b>C: NO<sub>3</sub><sup>-</sup> : HL / LL</b>									
1	<b>1.54</b>	0.93	2.64	<b>3732</b>	2356	5472	<b>5764</b>	3479	9857
2	<b>1.69</b>	1.29	2.41	<b>295</b>	268	338	<b>497</b>	379	711
3	<b>0.91</b>	0.74	1.05	<b>498</b>	472	527	<b>452</b>	368	525
<b>D: NH<sub>4</sub><sup>+</sup> : HL / LL</b>									
1	<b>2.13</b>	1.19	3.02	<b>630</b>	343	994	<b>1344</b>	750	1902
2	<b>2.16</b>	1.90	2.45	<b>382</b>	354	404	<b>824</b>	727	937
3	<b>1.09</b>	1.00	1.19	<b>574</b>	374	824	<b>625</b>	575	684

For analysis, there are a few issues to be addressed, e.g. the importance of normalisation, the variation of technical replicates and the variation of expression values of replicates. The importance of normalisation becomes obvious in Table 4.10. The signal intensities (displayed in control and raw columns) varied much more between the replicates than the normalised values did. For simplicity, the differences are highlighted by focussing on just one condition for Nia2. In Part A of Table 4.10, the expression values of low-light condition between nitrate and ammonium (NH<sub>4</sub><sup>+</sup> / NO<sub>3</sub><sup>-</sup> LL) are displayed. The signal intensity of the raw values varied

by e.g. a factor of 6 (499 and 83: raw values of replicate 2 and 3, respectively) between the biological replicates. The normalised values, however, were not affected.

The homogeneity between technical replicates can be analyzed looking at the Min and Max values. In Table 4.10 they are quite homogenous. Unfortunately, this did not hold for all technical replicates on the microarray.

The variation of differential expression between biological replicates also needs special attention. In this case (Table 4.10, section B, normalised value, Table 4.11 indicated in red) it was found that the third replicate showed a totally different behaviour than the other two replicates. Replicate one and two showed a down regulation (0.28, 0.31) whereas replicate three showed a strong up-regulation (3.43). This abnormality did only occur in this hybridisation. In all other cases replicate three showed the same behaviour than the other two replicates (Table 4.10, 4.11). This indicated that it was probably an outlier in the particular case. As seen in Table 4.11 this outlier had a great impact on the average value and the "loop amplification". It led to a high error. Without the outlier the "loop amplification" would have been about 0.97 (values indicated in red in Table 4.11). After elimination of this outlier the results for Nia2 were treated with great confidence.

**Table 4.11** Normalised data of Nia2 from individual replicates, average value plus SEM and loop amplification. Red indicates outlier and average value and loop amplification disregarding the outlier.

Replicates	Normalised Value	Average $\pm$ SEM	"loop amplification"
<b>NH<sub>4</sub><sup>+</sup> / NO<sub>3</sub><sup>-</sup> LL</b>			<b>0.46</b> <b>(0.97)</b>
1	<b>0.21</b>	<b>0.24 <math>\pm</math></b> <b>0.05</b>	
2	<b>0.20</b>		
3	<b>0.33</b>		
<b>NH<sub>4</sub><sup>+</sup> / NO<sub>3</sub><sup>-</sup> HL</b>			
1	<b>0.28</b>	<b>0.67 <math>\pm</math></b> <b>0.98</b> <b>(0.29)</b>	
2	<b>0.31</b>		
3	<b>3.43</b>		
<b>NO<sub>3</sub><sup>-</sup> : HL / LL</b>			
1	<b>1.54</b>	<b>1.33 <math>\pm</math></b> <b>0.27</b>	
2	<b>1.69</b>		
3	<b>0.91</b>		
<b>NH<sub>4</sub><sup>+</sup> : HL / LL</b>			
1	<b>2.13</b>	<b>1.71 <math>\pm</math> 0.4</b>	
2	<b>2.16</b>		
3	<b>1.09</b>		

**Table 4.12** Normalised data of Nia1 from individual replicates, average value plus SEM and loop amplification. Min and Max show the values of the technical replicates.

Replicates	Normalised Value	Min	Max	Average $\pm$ SEM	"loop amplification"
<b>NH<sub>4</sub><sup>+</sup> / NO<sub>3</sub><sup>-</sup> LL</b>					<b>0.995</b>
1	<b>0.26</b>	0.13	0.49	$0.33 \pm 0.1$	
2	<b>0.4</b>	0.22	0.73		
3					
<b>NH<sub>4</sub><sup>+</sup> / NO<sub>3</sub><sup>-</sup> HL</b>					
1	<b>0.76</b>	0.64	0.88	$0.72 \pm 0.06$	
2	<b>0.68</b>	0.61	0.79		
3					
<b>NO<sub>3</sub><sup>-</sup> : HL / LL</b>					
1	<b>0.35</b>	0.12	0.57	$0.47 \pm 0.28$	
2	<b>0.79</b>	0.33	1.24		
3	<b>0.26</b>	0.17	0.36		
<b>NH<sub>4</sub><sup>+</sup> : HL / LL</b>					
1	<b>0.9</b>	0.78	1.11	$1.02 \pm 0.17$	
2	<b>1.14</b>	0.93	1.56		
3					

Sometimes, it may happen that the gridding software discards single spots due to bad signal quality. This results in blanks in the read out of Gene Spring. An example is given in Table 4.12. In the case of Table 4.12 the reliability of the averages of the remaining two replicates were very good (0.995) and the results were supported by Northern blot analysis. Because of this, the data were used for further conclusions.

#### 4.5.3.4 Differentially expressed genes related to growth retardation

The physiological experiments (section 4.1 to 4.4) indicate that growth and development of photosynthetic activity was retarded in NH<sub>4</sub><sup>+</sup>-grown plants. Hence the sources of energy supply were investigated, especially the role of photosynthesis and of lipid mobilisation from seed storage reserves. Expression values of genes relevant for storage lipid mobilisation and for photosynthesis as a source of sucrose synthesis are shown in Table 4.13.

## 4 Results

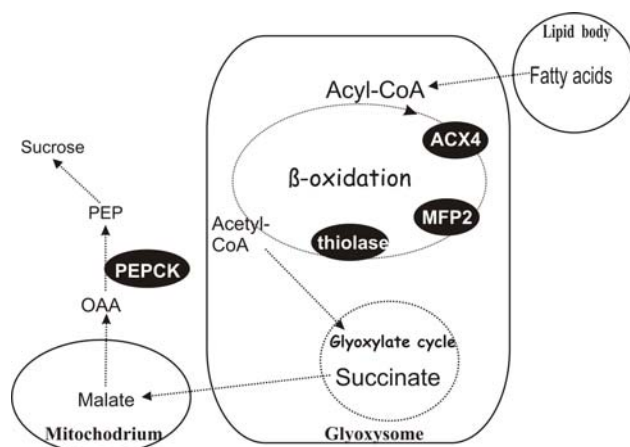
**Table 4.13** Differential expression values of genes encoding for enzymes of sucrose synthesis, Calvin cycle and photorespiration in  $\text{NH}_4^+$ - and  $\text{NO}_3^-$  grown seedlings of *A. thaliana*. LL and HL denote low light and high light treatments, respectively. Bold numbers indicate statistically significant difference (t-test,  $p = 0.05$ ). Average value plus SEM is shown. "Loop amplifications" are found in Table 4.7.

	$\text{NH}_4^+ / \text{NO}_3^-$ LL	$\text{NH}_4^+ / \text{NO}_3^-$ HL	$\text{NO}_3^-$ : HL / LL	$\text{NH}_4^+$ : HL / LL
<b>sucrose metabolism via <math>\beta</math>-oxidation</b>				
PEP carboxykinase (PEPCK) At4g37870	<b>2.2 ± 0.281</b>	1.13 ± 0.66	0.812 ± 0.113	0.707 ± 0.150
<b>sucrose metabolism via photosynthesis</b>				
Carbonic anhydrase (CA) At3g01500	0.782 ± 0.185	<b>0.54 ± 0.14</b>	<b>2.578 ± 0.367</b>	<b>1.755 ± 0.220</b>
Fructose biphosphate aldolase cytosolic (FBA cyt) At4g26530	0.728 ± 0.128	<b>0.686 ± 0.083</b>	<b>1.758 ± 0.196</b>	<b>1.568 ± 0.198</b>
<b>Calvin Cycle</b>				
RuBisCO At5g38420	1.077 ± 0.391	0.686 ± 0.210	<b>1.949 ± 0.269</b>	<b>1.565 ± 0.238</b>
glyceraldehyde 3P dehydrogenase A subunit (GapA) At3g26650	1.221 ± 0.245	0.969 ± 0.212	<b>1.769 ± 0.294</b>	1.261 ± 0.266
Fructose biphosphate aldolase plastidic (FBA plast) At4g38970	1.182 ± 0.24	1.052 ± 0.188	<b>1.782 ± 0.19</b>	<b>1.487 ± 0.207</b>
Sedoheptulose biphosphatase (SBPase) At3g55800	1.041 ± 0.192	1.045 ± 0.193	<b>2.021 ± 0.320</b>	<b>1.692 ± 0.136</b>
<b>Photorespiration</b>				
glycolate oxidase (GOX) At3g14420	1.137 ± 0.139	1.245 ± 0.205	<b>1.737 ± 0.192</b>	1.46 ± 0.227
alanine-glyoxylate aminotransferase (AGT) At2g13360	1.296 ± 0.138	1.331 ± 0.127	<b>2.164 ± 0.366</b>	<b>1.631 ± 0.305</b>
<b>ADP /ATP transport</b>				
adenine-nucleotide translocator (AATP1) At1g80300	0.97±0.23	0.95±0.16	<b>1.7±0.3</b>	<b>1.36±0.18</b>

4.5.3.4.1 Genes of  $\beta$ -oxidation-related sucrose metabolism

In order to assess putative differences in energy supply differential expression of some genes controlling the synthesis of sucrose from these different sources is inspected, starting with the genes of  $\beta$ -oxidation (ACX4, MFP2, thiolase) and of phosphoenolpyruvate carboxykinase (PEPCK). The location of these enzymes is shown in Fig. 4.36.

PEPCK catalyses the final step in the pathway using lipid storage mobilisation for sucrose synthesis (Rylott et al. 2003, Chen et al. 2004) as illustrated in Fig. 4.36. The gene encoding for PEPCK was found to be more strongly expressed in  $\text{NH}_4^+$ -grown seedlings than in  $\text{NO}_3^-$ -grown ones under low light (LL). Northern blot analysis (Fig. 4.37) verified the higher expression in  $\text{NH}_4^+$ -grown seedlings under LL conditions. Northern blot analysis revealed also a higher gene expression of PEPCK under HL in  $\text{NH}_4^+$ -grown seedlings compared to  $\text{NO}_3^-$ -grown ones, which was only indicated but not significant on the microarray.

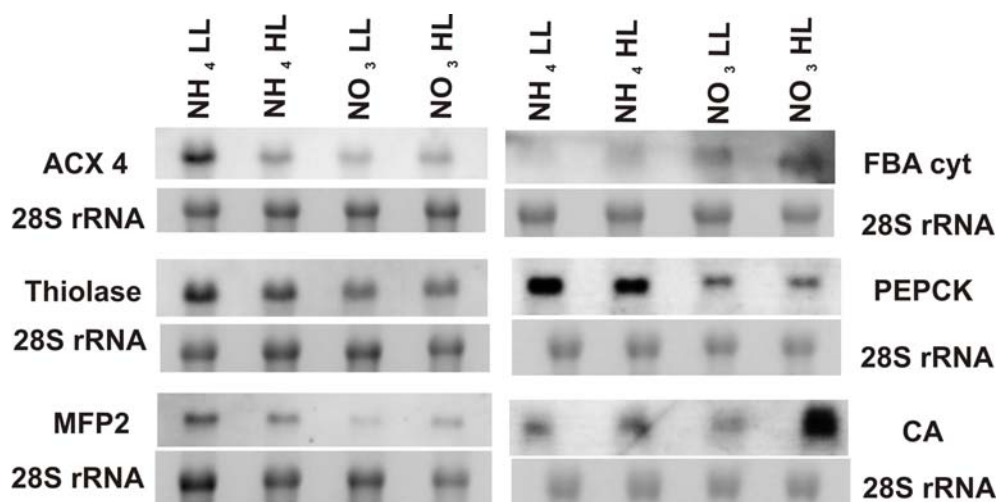


**Figure 4.36** Scheme of lipid mobilisation from seed storage reserves. Enzymes of interest are indicated by black ellipse. All other enzymes involved in lipid mobilisation are not included.

Enzymes of  $\beta$ -oxidation were not represented on the microarray. Because of this, Northern blot analysis (Fig. 4.35) was used for gene expression studies of acyl-CoA oxidase 4 (ACX4), the most active isoform of the acyl-CoA-oxidase family (Eastmond et al. 2000), L-ketoacyl-CoA thiolase (thiolase) the most active isoform and multi functional protein 2 (MFP2, with exhibits activity of 2-trans-enoyl-CoA hydratase, L-3-hydroxyacyl-CoA dehydrogenase, D-3-hydroxyacyl-CoA epimerase and  $\Delta^3, \Delta^2$ -enoyl-CoA isomerase). All three enzymes showed the



strongest expression in  $\text{NH}_4^+$ -grown seedlings under low light (LL). ACX4 of  $\text{NH}_4^+$ -grown seedlings is down regulated in the light. Such a down regulation is less obvious in the case of thiolase and in MFP2. Expression of these enzymes was much lower in  $\text{NO}_3^-$ -grown seedlings.



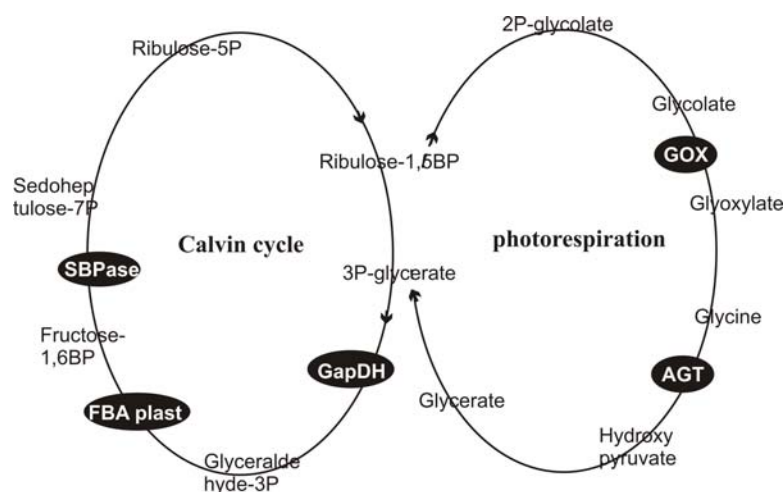
**Figure 4.37** Northern blots of genes encoding for the enzymes of  $\beta$ -oxidation (ACX4, MFP2, thiolase), of PEPCK, fructose biphosphate aldolase and carbonic anhydrase obtained from leaves of 15-days old *A. thaliana* subject to four different treatments:  $\text{NH}_4^+$  LL,  $\text{NH}_4^+$  HL,  $\text{NO}_3^-$  LL,  $\text{NO}_3^-$  HL. 7.5  $\mu\text{g}$  RNA were loaded per lane. 28S-RNA is used for calibration.

In contrast, CA and cytosolic FBA showed a stimulation of expression by  $\text{NO}_3^-$ -nutrition and high light (Fig. 4.37, Table 4.13). These results indicated a different source of sucrose synthesis in  $\text{NO}_3^-$ -grown seedlings.

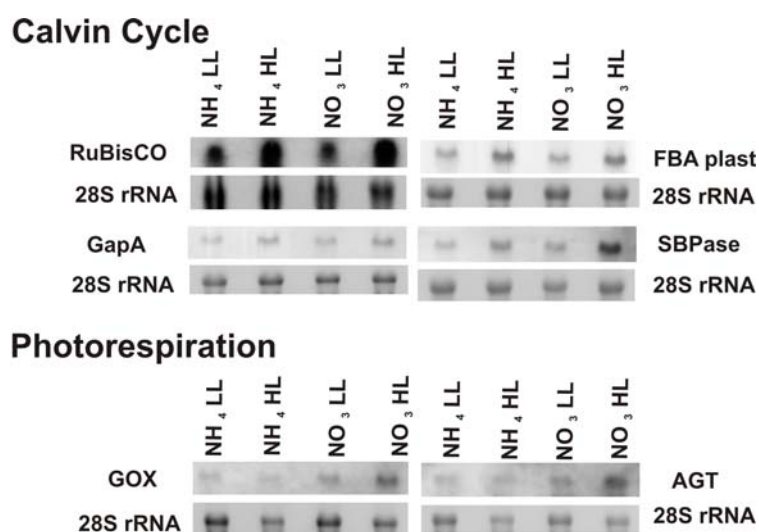
#### 4.5.3.4.2 Genes of photosynthesis-related sucrose metabolism

The other possible source for sucrose synthesis is photosynthesis. The enzymes of the Calvin cycle and of photorespiration investigated here are shown in Fig. 4.38. Expression of genes encoding for several enzymes in these pathways were found to be stimulated by light rather than N-form dependent (indicated on microarray Table 4.13 and Northern blot Fig. 4.39). This accounts especially for the genes of the Calvin cycle. Nevertheless, strong support for a higher activity of the Calvin cycle in  $\text{NO}_3^-$ -grown seedlings came from the light-induced up-regulation of the gene encoding for sedoheptulose biphosphatase (SBPase). The results of microarray and Northern blot analysis showed the same trend.

In the pathway of photorespiration, both microarrays and Northern blot analysis show stronger stimulation of the genes encoding for glycolate oxidase (GOX) and alanine-glyoxylate aminotransferase (AGT) by light in  $\text{NO}_3^-$ -grown seedlings (Fig. 4.39).



**Figure 4.38** Scheme of Calvin cycle and photorespiration. Enzymes of interest are indicated by black ellipse. glycolate oxidase (GOX), alanine-glyoxylate aminotransferase (AGT), glyceraldehyde 3P dehydrogenase (GapDH), fructose biphosphate aldolase plastidic (FBA plast) and sedoheptulose bisphosphatase (SBPase). All other enzymes are not included.



**Figure 4.39** Northern blot analysis of genes of the Calvin cycle and photorespiration. The four different treatments:  $\text{NH}_4^+$  LL,  $\text{NH}_4^+$  HL,  $\text{NO}_3^-$  LL,  $\text{NO}_3^-$  HL are indicated above the lanes. 7.5  $\mu\text{g}$  total RNA were loaded per lane. 28S-rRNA is used for calibration.

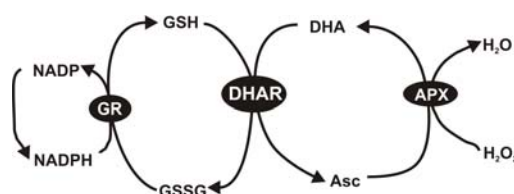
Higher photosynthetic activity seems also to be indicated by the expression of adenine nucleotide translocase (AATP). This Adenine nucleotide translocase is located in the chloroplast membrane and is an important carrier protein for ADP/ATP. Fig. 4.40 shows the results of Northern blot analysis. They revealed an up-regulation in the light in both N-forms but it was stronger in  $\text{NO}_3^-$ . According to Fig. 4.10 photosynthetic  $\text{CO}_2$  fixation was higher by a factor of two in  $\text{NO}_3^-$ -grown seedlings than in  $\text{NH}_4^+$ -grown ones. Thus, it is not unexpected that also transporters for adenine nucleotides are more highly expressed.



**Figure 4.40** Northern blot analysis for AATP. 28S rRNA is used for calibration.

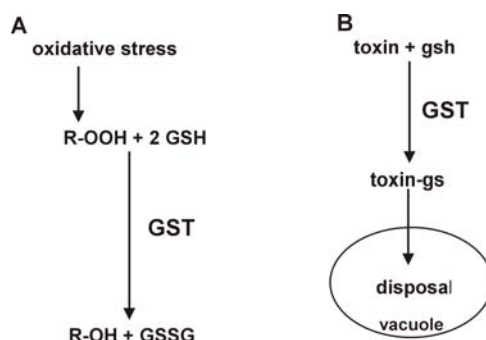
#### 4.5.3.5 Other differentially expressed genes - Detoxification enzymes

There are some detoxification enzymes differentially expressed. Few of them were subject to Northern blot analysis like genes encoding for DHAR, one GST (At2g29450) and GDP-epimerase. DHAR catalyses the reduction of dehydroascorbate to ascorbate. It oxidises glutathione and regenerates ascorbate for the detoxification of hydroxyperoxide (Fig. 4.41).



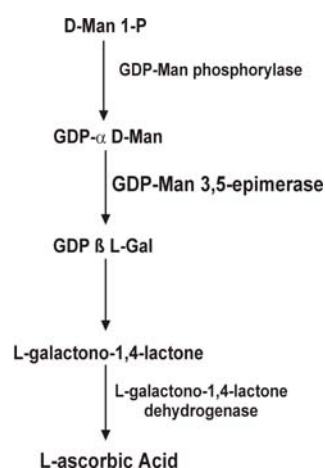
**Figure 4.41** Scheme of the Halliwell-Assada-Cycle for ascorbate regeneration. Glutathione reductase (GR), dehydroascorbate reductase (DHAR) and ascorbate peroxidase (APX).

Glutathione and ascorbate possess antioxidative capacities and decontaminate oxygen radicals. GST catalyses detoxification reactions involving glutathione. Glutathione reacts with toxic substances supported by GSTs and forms glutathione conjugates which can be transported into the vacuole (Fig. 4.42).



**Figure 4.42** Examples for cellular function of GST. (A) Role of GST in stress metabolism acting as peroxidase, (B) Role of GST in detoxifying toxins by conjugation with GSH. The conjugates are then transported into the vacuole for disposal. (Dixon et al. 2002 modified)

GDP-epimerase catalyses one step of the proposed *de novo* pathway for the synthesis of L-Ascorbic acid from D-Mannose in plants (Wheeler et al. 1998, Wolucka et al. 2001, Fig. 4.43).



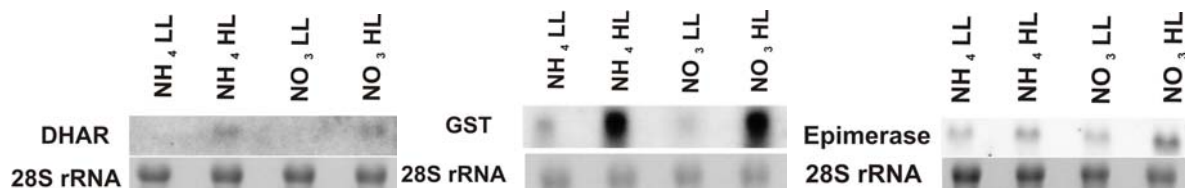
**Figure 4.43** Proposed *de novo* pathway for the synthesis of L-ascorbic acid from D-Man in plants (Wheeler et al. 1998 modified).

In Fig. 4.44 the Northern blot results of DHAR, of one GST and of GDP-epimerase are presented. It is quite clear that there was a light regulation in all three cases. DHAR and the GST did not seem to be differentially expressed between  $\text{NH}_4^+$ - and  $\text{NO}_3^-$ -grown seedlings even though the microarray data (Table 4.14) suggested a stronger increase for DHAR under  $\text{NO}_3^-$  nutrition.

The GDP-epimerase showed a stronger light regulation in  $\text{NO}_3^-$ -grown seedlings. For this gene both methods yielded the same result. There was a slight difference in RNA loading

## 4 Results

seen for both  $\text{NO}_3^-$  RNA. This was an even stronger hint that the light regulation in  $\text{NO}_3^-$ -grown seedlings was much higher than in  $\text{NH}_4^+$ -grown ones. The finding of higher expression of the GDP-epimerase in  $\text{NO}_3^-$ -grown seedlings (resulting probably in higher ascorbate synthesis) may shed some new light on the finding that ascorbate was found to have a higher level in  $\text{NO}_3^-$ -grown plants and in  $\text{NH}_4^+$ -grown plants (Bendixen et al. 2001) as discussed below.



**Figure 4.44** Northern blot results of DHAR, one GST and Epimerase. RNA was obtained from leaves of 15-days old *A. thaliana* subject to four different treatments:  $\text{NH}_4^+$  LL,  $\text{NH}_4^+$  HL,  $\text{NO}_3^-$  LL,  $\text{NO}_3^-$  HL. 7.5  $\mu\text{g}$  RNA were loaded per lane. 28S-RNA is used for calibration.

**Table 4.14** Microarray results of DHAR, GST and Epimerase. Bold numbers indicate that the t-test showed significance with  $p = 0.05$ . Average value plus SEM and loop amplification are shown.

		$\text{NH}_4^+ / \text{NO}_3^-$ LL	$\text{NH}_4^+ / \text{NO}_3^-$ HL	$\text{NO}_3^- : \text{HL} / \text{LL}$	$\text{NH}_4^+ : \text{HL} / \text{LL}$	"loop" amplification
Cytosol	At1g75270 dehydroascorbate reductase	1.45±0.24	1.34±0.18	<b>2.59±0.49</b>	<b>1.87±0.31</b>	<b>0.78</b>
Cytosol	At2g29450 glutathione transferase (103-1A)	1.27±0.09	1.18±0.20	<b>3.04±1.14</b>	<b>3.88±0.26</b>	<b>1.37</b>
unknown	At5g28840 NAD-dependent epimerase/dehydratase family	1.28 ±0.26	0.95±0.14	<b>2.02±0.23</b>	1.4±0.29	<b>0.93</b>



## 5 Discussion

Growth retardation under  $\text{NH}_4^+$ -nutrition is a widely observed phenomenon (Walch-Liu et al. 2000, Zhu et al. 2000, Gerendás et al. 1997). This is also observed for the seedlings of *A. thaliana* used here (Fig. 4.1). In the introduction it was mentioned that it might be a useful approach to investigate the effect of ammonium as the sole nitrogen source at an early stage of development of plants. This idea turned out to be stimulating. It enabled the comparison of plants living already from photosynthesis with those still using olesosomes for energy supply. Evaluating the related effects revealed new aspects explaining the phenomenon of growth retardation observed here. Before setting up a new model, explaining the results described here, similarities and differences to previous results (called traditional) are discussed.

### 5.1 Traditional N-form dependent differences

Before going into detail it had to be verified that ammonium and nitrate grown *A. thaliana* showed N-form dependent differences in phenomenology. The seedlings of *A. thaliana* used in the present studies showed a variety of phenomena that have been already reported as N-form dependent differences e.g. anion content, genes encoding for enzymes of primary N-assimilation and spectrum of free amino acids (e.g. Gerendás et al. 1997, Wang et al. 2003, Bialczyk et al. 2004).

#### 5.1.1 Analysis of anion content

The result of the analysis of anion content of the seedlings was not surprising because the absence of  $\text{NO}_3^-$  in  $\text{NH}_4^+$  media has to be supplemented by other anions available in the medium (e.g.  $\text{Cl}^-$ ), taken up by the plants, in order to achieve electro-neutrality. Thus, in the experiments presented *A. thaliana* exhibited similar behaviour as known from N-form dependencies of other studies: The most prominent feature in Fig. 4.6 is the 11-fold higher concentration of  $\text{Cl}^-$  in  $\text{NH}_4^+$ -grown plants. This corresponds to 3.5 % of the dry weight in contrast to 0.29 % in  $\text{NO}_3^-$ -grown plants. This value is in line with the findings of Vessey et al. (1990) that  $\text{Cl}^-$  is about 5 % of the dry weight in tobacco when supplied with  $\text{NH}_4\text{Cl}$ . The effect is even stronger than in the data given by Marschner (1995, Table 2.24). Chloride in  $\text{NH}_4^+$ -grown plants is only higher by a factor of 2.5 compared to  $\text{NO}_3^-$ -grown shoots of Castor bean. The cause for the difference may be found in the content of the organic acids.

There is nearly no malate, oxalate and citrate found in  $\text{NH}_4^+$ -grown leaves of *A. thaliana* used here. This finding is quite surprising, since Marschner (1995, Table 2.24) gives concentrations of organic acids of 137 and 59 meq per 100 g dry weight for  $\text{NO}_3^-$ - and  $\text{NH}_4^+$ -grown shoots of Caster beans. This reduction of the organic acids is by far not as strong as in our studies (Fig. 4.6). The explanation for this differences might be: The youth of the  $\text{NH}_4^+$ -grown plants used here (Figs. 4.1, 4.9) may lead to lower metabolic activities and thus to lower concentrations of organic acids. Under this condition, the high  $\text{Cl}^-$  concentration in  $\text{NH}_4^+$ -grown leaves of *A. thaliana* alleviates the need to compensate the charge of the cations by organic acids.

### 5.1.2 Primary N-assimilation

The enzymes related to the biosynthesis pathway of primary N-assimilations are nitrate reductase (NR) and nitrite reductase (NiR). As expected the genes encoding for the two isoforms of NR were up-regulated in  $\text{NO}_3^-$ -grown seedlings. In these plants, *Nia1* is down-regulated in the light, in contrast to *Nia2*, which is slightly up-regulated (Fig. 4.35). Since the enzyme NR2 contributes to about 90 % of total NR activity (Wilkinson and Crawford 1991), the behaviour of *Nia1* is not a contradiction to what is expected for  $\text{NO}_3^-$ -grown plants. Thus, the gene expression studies of NR are in line with the well-known induction of these genes by nitrate (e.g. Wang et al. 2003), since  $\text{NO}_3^-$  needs to be reduced to nitrite. The unusual regulation of NR in cotyledons of *Brassica napus* (Leleu and Vuylsteker 2004) could not be confirmed in this studies.

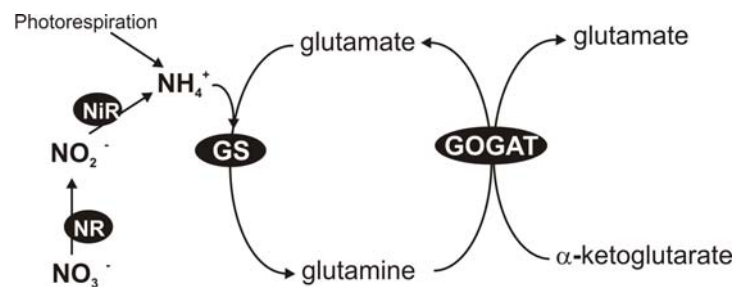
The nitrite reductase did not show differential expression in this microarray study. This may account for the fact that  $\text{NO}_2^-$  is extremely toxic (causing conversion of cytosine to uracile, Heldt 1999 p. 282). Thus, plants do not dare to decrease the efficiency of NiR.

Further downstream, the reactions of the glutamine synthetase - glutamine oxoglutarate aminotransferase cycle (GS/GOGAT) are important (Fig. 5.1). A major difference between  $\text{NO}_3^-$ - and  $\text{NH}_4^+$ -grown leaves might be expected for the expression of the genes of GS/GOGAT cycle, because this is the reaction where  $\text{NO}_3^-$ -assimilation takes place. In contrast, the assimilation of  $\text{NH}_4^+$  from the soil takes place in the roots.

The major enzymes in the GS/GOGAT cycle are Fd-GOGAT and chloroplastic GS. Surprisingly, the genes encoding for these two enzymes did not show any differential expression on the microarray. The explanation may be quite obvious: Photorespiration seems to differ by not more than a factor of two if proportionality to  $\text{CO}_2$  fluxes is assumed (Fig.



4.10). Photorespiration has to be considered because it is connected to a cyclic reaction in which  $\text{NH}_4^+$  is released in the mitochondria and assimilated in the GS/GOGAT cycle. As photorespiratory  $\text{NH}_4^+$ -fluxes are at least 4-fold higher (Noctor and Foyer 1998) than those of N-assimilation in  $\text{NO}_3^-$ -grown plants, the fluxes related to N-assimilation from  $\text{NO}_3^-$  may be hidden by the background  $\text{NH}_4^+$  assimilation related to photorespiration. Thus, differential expression of the genes of the GS/GOGAT cycle should not be a priori expected.



**Figure 5.1** Scheme of GS / GOGAT cycle.  $\text{NH}_4^+$  comes either from nitrogen assimilation or from photorespiratory glycine/serine conversion in the mitochondria in the leaf.

In contrast, the genes encoding for NADH-GOGAT (localised in the chloroplast according to the *Arabidopsis* database TAIR, 3.10) and the cytosolic isoform of GS were differentially expressed. The gene encoding for NADH-GOGAT showed strong down regulation in  $\text{NH}_4^+$ -grown plants whereas the gene encoding GS was slightly up-regulated (Table 4.7). NADH-GOGAT is a single-copy gene (Lancien et al. 2002) and contributes only 5 % to the overall GOGAT activity (Somerville and Ogren 1980). In the leaves, it is expressed in low levels only. In the case of the cytosolic form of GS, there are 5 different isoforms encoding for the enzyme (Ishiyama et al. 2004). Out of these five only three (Gln1;2, Gln1;3 and Gln1;4) were present on the microarray. Gln1;4 did not show any differential expression. Gln1;2 and 3 were up-regulated in the light. Gln1;2 was also slightly up-regulated in  $\text{NH}_4^+$ -grown plants at LL. Unfortunately, the spots for Gln1;3 had an absent call (spot without sufficient signal intensity) in the hybridisation comparing  $\text{NH}_4^+/\text{NO}_3^-$  LL (Table 4.7). The enzymes are found mainly in roots and vasculature (Ishiyama et al. 2004).

However, both enzymes are thought to act in cotyledons (Buchanan et al. 2000). The up-regulation of the gene encoding for the cytosolic GS in  $\text{NH}_4^+$ -grown seedlings supports the dominance of glutamine mentioned below (section 5.1.3).

### 5.1.3 Survey of stores for nitrogen

In  $\text{NH}_4^+$ -grown plants, nitrogen is mainly stored in form of amino acids (Marschner 1995). They also serve as transporters of N from sources to sinks and N stores for nitrogen released during protein degradation (Buchanan et al. 2000). Important in primary N-assimilation are the amino acids glutamate, glutamine, aspartate and asparagine. Glutamine and asparagine are mainly used for N transport and storage. In young plants their role in N storage is of different importance in  $\text{NH}_4^+$ -grown and  $\text{NO}_3^-$ -grown plants.

For young  $\text{NO}_3^-$ -grown plants, the N-storage in amino acids is not of major importance. The plants store most of the excess nitrogen in the vacuole until further use. Only the amount of nitrogen immediately required for metabolism is assimilated. There is no need for N storage in amino acids, because for *de novo* synthesis of amino acids N can be taken from the vacuole. For older plants this has to be stated with more caution but since they are not subject of investigation this is of minor interest and will not be discussed in greater detail.

In contrast,  $\text{NH}_4^+$ -grown plants cannot store  $\text{NO}_3^-$  in the vacuole. As mentioned above, they have to store N in form of amino acids. For this purpose, the C/N ratios of the amino acids are relevant in order to minimize the requirement of carbon skeletons. The higher the amount of N per C the lower is the carbon cost (Buchanan et al. 2000, Marschner 1995). C/N ratios are for glutamate 5/1, glutamine 5/2, aspartate 4/1 and asparagine 4/2. There is another aspect of N storage in amino acids, i.e., detoxification: As stated in chapter 2 ammonium is toxic in quite low concentrations. Thus, nearly all of the ammonium taken up by the roots is assimilated and incorporated into amino acids right there.

In order to minimise the carbon costs for transport from roots to shoots, the assimilation products are nitrogen-rich compounds with  $\text{C/N} < 2.5$  (Streeter 1979, Marschner 1995). The amides glutamine (Gln) and asparagines (Asn) as well as arginine (Arg) are best suited for this carbon economy and feature effective N-storage. The amino acid preferred for N-storage is dependent on the plant species.

Thus, in order to study whether the seedlings investigated here show the typical features related to the applied N form the contribution of free amino acids to the total amount of C and N was determined. This difference becomes obvious in the results of the amino acid analysis (section 4.2.3) of  $\text{NO}_3^-$ - and  $\text{NH}_4^+$ -grown seedlings of *A. thaliana*. There were 2.3 times more free amino acids [mM / g DM] in  $\text{NH}_4^+$ -grown seedlings than in  $\text{NO}_3^-$ -grown ones but the amount of total N did not differ significantly (Figs. 4.7, 4.5). These results underline that the  $\text{NH}_4^+$ -grown seedlings have to store their nitrogen in assimilates. To minimise their carbon

costs  $\text{NH}_4^+$ -grown plants store their N in amides (Gln, Asn) since these forms have a better C/N ratio than the acidic form (Glu, Asp). This is in line with the finding that there are 10.7 times more amides than acids observed in  $\text{NH}_4^+$ -grown plants (Fig. 4.8). Glutamine accounted for 22 % (plus 5 % Asn) of the total free amino acids content in  $\text{NH}_4^+$ -grown leaves. In  $\text{NO}_3^-$ -grown ones, the amides accounted only for 12 % of the total amount of free amino acids and the ratio amides to acids was only 0.65.

Interestingly, arginine accounted for almost 40 % (2 % in  $\text{NO}_3^-$ ) of the total amount of free amino acids. Its precursors ornithine and citrulline are found in minor amounts (Fig. 4.7). There are two explanations for this phenomenon. First, arginine has an effective C/N ratio (6/4) and second it serves as the main precursor for polyamines (Gerendás et al. 1997).

The polyamine concentration and composition was not investigated here, but the gene encoding for the enzyme arginine decarboxylase (catalyzing the first step of polyamine synthesis) appeared to be more strongly induced in  $\text{NH}_4^+$ -grown seedlings under LL conditions than in  $\text{NO}_3^-$ -grown ones (Table 4.7). Together with the high amounts of arginine this might provide evidence that the amount of polyamines is higher in  $\text{NH}_4^+$ -grown seedlings. Further research in this field may be important, because their concentration seems to be increased under  $\text{NH}_4^+$ -nutrition (Gerendás et al. 1997). At high concentrations, they may retard growth as found here in *A. thaliana* (Fig. 4.1) (Gerendás 1992, Bennett et al. 1964, Merkel 1973).

So far, the determination of the amino acids indicates that the seedlings used here show typical  $\text{NH}_4^+$  or  $\text{NO}_3^-$  behaviour. However, these plants differ from those commonly used for N-form studies with respect to age. They were not grown-up, and the  $\text{NH}_4^+$ -grown seedlings seemed to live still to a great part from the oleosomes of their seeds (as discussed in more detail below). The question is whether the same phenomenology is expected with respect to amino acids. Probably it is, because the young  $\text{NH}_4^+$ -grown plants have to face the same problem as the grown-up ones. They cannot use  $\text{NO}_3^-$  as a store for nitrogen, because there is no  $\text{NO}_3^-$  in the nutrient solution or in the oleosomes. Thus, they have to employ similar strategies irrespective of whether they take their nitrogen from the oleosomes or from the uptake of  $\text{NH}_4^+$ . The  $\text{NO}_3^-$ -grown seedlings, in contrast, have already fully developed photosynthesis and N assimilation, including  $\text{NO}_3^-$  uptake from the solution, is active. This is also indicated by the higher expression of the genes encoding for nitrate reductase (Fig. 4.35) in  $\text{NO}_3^-$ -grown seedlings.

#### 5.1.4 Analysis of genes encoding for enzymes involved in amino acid synthesis

Other genes encoding for enzymes involved in the amino acid synthesis are glutamate decarboxylase (GAD, catalyzing the conversion from Glu to GABA), glutamate dehydrogenase (GDH, two way enzyme, catalyzing synthesis and catabolism of Glu) and asparagine synthetase (ASN, catalyzing synthesis of asparagines). All of these enzymes have multiple isoforms making the interpretation of the results quite difficult, especially since not all isoforms have been investigated separately in previous studies.

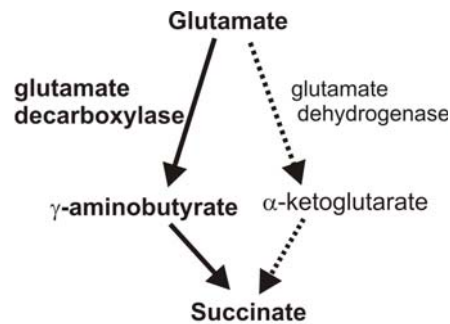
In the case of GAD, searching the *Arabidopsis* database TAIR ([www.arabidopsis.org](http://www.arabidopsis.org)) yields six isoforms. Only one of those, i.e., isoform GAD1, was differentially expressed in the plants as revealed by microarray analysis (Table 4.7). Interestingly, the annotation in the databases (TAIR, MIPS, TIGR, see section 3.10) is controversy to what has been found by Turano and Fang (1998). The databases suggest chloroplast targeting, whereas Turano and Fang (1998) detected the transcript only in the roots. This findings make the interpretation even more difficult.

Nevertheless, GAD1 was up-regulated in  $\text{NH}_4^+$ -grown seedlings (Table 4.7) indicating a higher synthesis of  $\gamma$ -aminobutyric acid (GABA) as compared to  $\text{NO}_3^-$ -grown plants. GABA is a significant component of the free amino acid pool in most pro- and eukaryotic organisms. It is characterized as a four-carbon non-protein amino acid. GABA is synthesized from the decarboxylation of glutamate and is thought to be involved in multiple stress responses as well as pH regulation, nitrogen storage, plant development and defence. It can serve as a compatible osmolyte and as an alternative pathway for glutamate utilization (Shelp et al. 1999, Turano and Fang 1998).

In contrast to the above mentioned up-regulation of GAD1 in  $\text{NH}_4^+$ -grown seedlings, the amount of GABA was higher in  $\text{NO}_3^-$ -grown seedlings. It was about 24 % of the total amount of free amino acids compared to only 5 % in  $\text{NH}_4^+$ -grown ones (Fig. 4.7). This apparent discrepancy is resolved looking at the ratio between Glu and GABA. Compared to the amount of Glu there is more GABA found in ammonium-grown seedlings than in nitrate-grown ones. This may indicate a higher decarboxylation of Glu in  $\text{NH}_4^+$ -grown seedlings.

Anyway, it might be possible that GABA is rapidly metabolised to provide TCA cycle intermediates for amino acids metabolism possibly via the GABA shunt (Fig. 5.2) as shown for soybean cotyledons (Tuin and Shelp 1994, 1996). The GABA shunt describes a pathway

converting glutamate to succinate. The hypothesis should be treated with great care due to limited experimental support.



**Figure 5.2** Scheme of the GABA ( $\gamma$ -aminobutyrate) shunt (left-hand side) for converting glutamate in succinate. The GABA shunt is a (theoretical) alternative pathway to the usually oxidative decarboxylation via  $\alpha$ -ketoglutarate (right hand side) (Shelp et al.1999, modified).

GDH is encoded by at least five distinct genes (TAIR). There were probes of two isoforms on the microarray. One of them was differentially expressed (Table 4.7). But the results from Northern Blot analysis did not support the microarray data. The interpretation of the behaviour of this transcript is not possible right now.

ASN is the gene coding for asparagine synthetase (AS). It is supposed that when the N/C ratio is high AS redirects the flow of N into asparagine (Asn) which acts as a shunt for N storage and long-distance transport of nitrogen (Lam et al.1994). For ASN three isoforms are described (Lam et al. 1998). All of them were represented on the microarray but only ASN1 was differentially expressed (higher in  $\text{NO}_3^-$  under HL, Table 4.7). ASN1 is tightly correlated with free Asn levels (Lam et al. 1994) and is up-regulated in the dark and under carbon starvation (Lam et al. 1998). This does not seem to be true for the results presented here in which the ASN1 gene showed up-regulation in the light in  $\text{NO}_3^-$ -grown seedlings. Because of this further experiments are needed before a clear conclusion can be drawn.

Summarising the above statements,  $\text{NH}_4^+$ -grown seedlings showed a different amino acid pattern compared to  $\text{NO}_3^-$ -grown seedlings pointing to a detoxification by scavenging free  $\text{NH}_4^+$  and to a N-storage strategy due to a high nitrogen supply in ammonium-grown seedlings. This is in parts supported by the gene expression studies. But these results should be interpreted with great care due to the occurrence of multiple isoforms of the enzymes. The

differences in amino acid patterns, especially the high amount of arginine under ammonium nutrition needs further research to fully understand the physiological implications.

## 5.2 A new aspect of growth retardation under $\text{NH}_4^+$ -nutrition

### 5.2.1 New experimental results from seedlings of *A. thaliana*

The observed reduction in  $\text{CO}_2$  fixation (Fig. 4.10) and starch (Fig. 4.9) may suggest that leaves are the site to analyse the mechanism behind the  $\text{NH}_4^+$ -toxicity. For this scenario, Guo et al. (2005) suggested a hypothesis trying to explain photosynthesis related damage in  $\text{NH}_4^+$ -grown plants. The basic idea was that the absence of N-assimilation in  $\text{NH}_4^+$ -grown plants imposes the need to use alternative electron acceptors for surplus photosynthetic electron flow. They assumed that these superfluous redox equivalents were exported to the mitochondria where they led to the production of excess toxic radicals. This hypothesis was supported by the measurement of an N-form dependent compensation point for  $\text{CO}_2$  fixation (Guo et al. (2005) and by the high activity of scavenging enzymes (Zhu et al. 2000).

This hypothesis led to two expectations:

1. Higher ROS-Production in  $\text{NH}_4^+$ -grown plants
2. Up-regulation of enzymes of the scavenging systems

None of these expectations was found to be fulfilled in the present studies.

#### 5.2.1.1. ROS production

The experiments of section 4.4.7 show that ROS production is different from what was expected according to the theory of Guo et al. (2005). There was light-induced ROS production as indicated by DCF or NBT in  $\text{NO}_3^-$ -grown seedlings (Fig. 4.18). However, the ROS production in  $\text{NH}_4^+$ -grown seedlings was a surprise. At a first glance, inspecting only ROS production under the light guide, it seemed that ROS production under  $\text{NH}_4^+$ -nutrition was even lower than in  $\text{NO}_3^-$ -grown seedlings. This statement had to be revised, when the effect of spreading was taken into account. Integrating ROS production over a wider area including the range outside the light spot led to the finding of higher ROS production in  $\text{NH}_4^+$ -grown *A. thaliana* (Figs. 4.26, 4.27). However, as discussed in more detail below, this ROS production was not of the kind as suggested by Guo et al. (2005). There are clear indications from the effects of buffer capacity and pH that this ROS production occurs mainly in the apoplast (and not in the mitochondria as postulated by Guo et al. 2005).

This statement is supported by the effects of CO<sub>2</sub>. CO<sub>2</sub> depletion in NO<sub>3</sub><sup>-</sup>-grown seedlings led to an increase of DCF fluorescence (Fig. 4.20). This is expected when an acceptor for redox equivalents is withdrawn from the photosynthetic electron transfer chain (ETC) (Guo et al. 2005). However, this effect was not observed in NH<sub>4</sub><sup>+</sup>-grown seedlings. This led to the conclusion that the acceptor problems of the photosynthetic ETC are not a primary cause of ROS production in NH<sub>4</sub><sup>+</sup>-grown seedlings.

Consequent upon this, the gene expression studies did not reveal a clear indication of up-regulation of the enzymes of ROS detoxification. This seems to be in contrast to the findings of Zhu et al. (2000) who found an increase in the activity of such enzymes. The gene encoding for the GDP-epimerase, being involved in the ascorbate biosynthesis, was up-regulated in NO<sub>3</sub><sup>-</sup>-grown seedlings (Fig. 4.44). This is surprising in the light of the findings of Bendixen et al. (2001) that NH<sub>4</sub><sup>+</sup>-grown plants had a strong demand on ascorbate. This demand was so strong that the ascorbate level in NH<sub>4</sub><sup>+</sup>-grown leaves was reduced (and could be restored by feeding ascorbate via the petiole). This behaviour of the detoxification system indicated that ROS formation does not mainly occur inside the cell of NH<sub>4</sub><sup>+</sup>-grown seedlings.

Here, the phenomena related to ROS production are not discussed in greater detail. This is done in sections 5.3.2 and 5.3.3 below. However, these findings can be taken as hints that photosynthetic ROS production is smaller in NH<sub>4</sub><sup>+</sup>-grown seedlings than in NO<sub>3</sub><sup>-</sup>-grown ones. These results are mentioned as an indication that in the young leaves of *A. thaliana* mechanisms have to be considered which are different from those suggested by Guo et al. (2005). A hint to what is different in the seedlings of *A. thaliana*, investigated in the present study, came from gene expression studies dealing with β-oxidation.

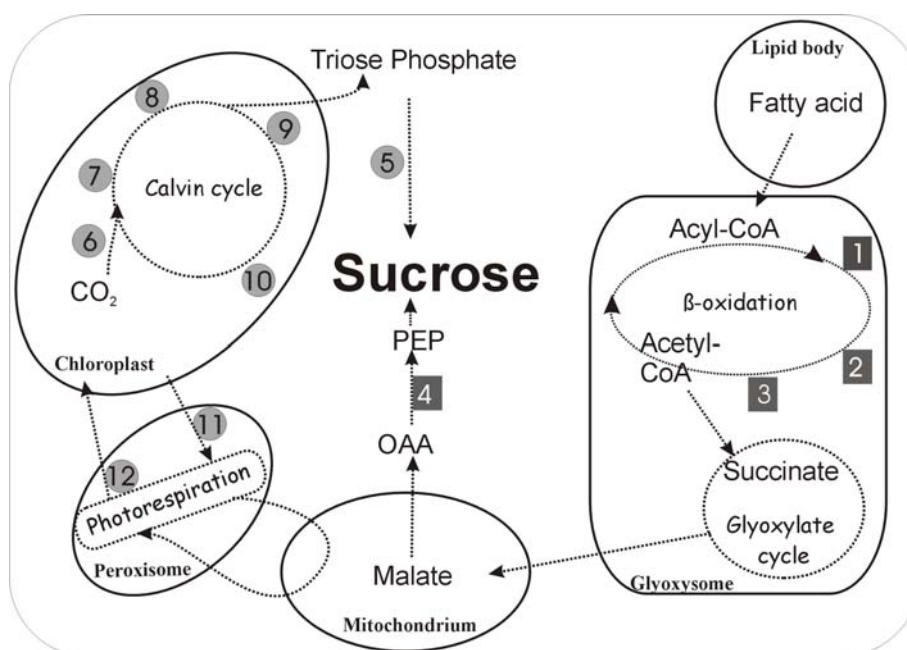
### **5.2.1.2 Expression of genes encoding for the energy supply of sucrose synthesis**

The investigated genes (Table 4.13) encode for enzymes acting in the pathways shown in Fig. 5.3. In oil seeds including *A. thaliana* (Eastmond and Graham 2001), β-oxidation is employed to utilize lipids stored in the oleosomes of the cotyledons (Rylott et al. 2001). According to the gene expression studies (Fig. 4.37, Table 4.13), this pathway is found to be more active in NH<sub>4</sub><sup>+</sup>-grown seedlings than it was in NO<sub>3</sub><sup>-</sup>-grown ones. The stronger expression of the gene encoding for phosphoenolpyruvate-carboxykinase (PEPCK, catalysing the final step in the pathway using lipid storage mobilisation for sucrose synthesis, Rylott et al. 2003) in NH<sub>4</sub><sup>+</sup>-grown seedlings indicates that the products of this pathway are used for sucrose synthesis.

The glyoxylate cycle, as a second indicator for sucrose synthesis from lipid sources, was not included in the analysis because there are reports that its involvement is not obligatory for

growth from fatty acids. Such a short-cut as known from *Saccharomyces cerevisiae* (van Roermund et al. 1995) may also be active in *A. thaliana* (Eastmond and Graham 2001). In that case, acetyl-CoA may be directly fed to the TCA cycle (van Roermund et al. 1995) or via a citrate/oxalacetate shuttle (Salon et al. 1988, Ramond et al. 1992).

In  $\text{NO}_3^-$ -grown seedlings, the metabolites for sucrose synthesis are delivered from photosynthesis as can be concluded from the enhanced expression of cytosolic fructose biphosphate aldolase (FBA cyt) and carbonic anhydrase (CA) (Fig. 4.37). The picture is less obvious for the genes of the enzymes of the Calvin cycle and of photorespiration (Fig. 4.39). Most of them are equally stimulated by light in  $\text{NH}_4^+$ -grown seedlings and in  $\text{NO}_3^-$ -grown ones. This is not a surprise since in both kinds of seedlings there is photosynthetic activity. The factor of two between photosynthetic fluxes indicated by  $\text{CO}_2$  uptake (Fig. 4.10) may be brought about by a) posttranslational regulation (Wedel et al. 1997), b) the supply of  $\text{CO}_2$  (e.g. differential expression of carbonic anhydrase, Fig. 4.37, Table 4.13) or c) the supply of ATP and NADPH from the photosynthetic ETC.



**Figure 5.3** Scheme of the putative different pathways of sucrose synthesis in  $\text{NO}_3^-$ - and  $\text{NH}_4^+$ -grown seedlings of *A. thaliana*.  $\text{NH}_4^+$ -grown seedlings mainly utilize lipids via  $\beta$ -oxidation whereas in  $\text{NO}_3^-$ -grown ones the metabolites for sucrose synthesis are delivered from photosynthesis. (1 ACX4, 2 MFP2, 3 thiolase, 4 PEPCK, 5 FBA cyt, 6 CA, 7 RuBisCo, 8 GapA, 9 FBA plast, 10 SBPase, 11 GOX, 12 AGT1)

■ Enzymes of pathways mainly used by  $\text{NH}_4^+$  grown plants

● Enzymes of pathways mainly used by  $\text{NO}_3^-$  grown plants



Nevertheless, differential expression of CA and of FBA cyt, supported by that of sedoheptulose biphosphatase (SBPase) and the enzymes of photorespiration indicate that in  $\text{NO}_3^-$ -grown seedlings photosynthesis is the major source of sucrose synthesis (Figs. 4.37, 4.39). These results from gene expression studies correspond to the physiological studies on photosynthesis and starch catabolism in Figs. 4.9-11 indicating higher photosynthetic activity in  $\text{NO}_3^-$ -grown seedlings. Especially, the higher expression of SBPase is a strong indication of higher photosynthetic activity, since Lefebvre et al. (2005) have shown that overexpression of this enzyme alone resulted in a stimulation of Calvin cycle activity. The absence of starch deposits in Fig. 4.9 is another hint that mobilisation of stored lipids rather than photosynthesis is the major source for metabolism in  $\text{NH}_4^+$ -grown seedlings.

### 5.2.2 The new hypothesis

The description of the results of gene expression in Fig. 5.3 leads immediately to the hypothesis for the different behaviour in our plants.

15-days-old plants of *A. thaliana* grown under low light are at the transition from energy supply from the oleosomes to energy supply from photosynthesis. The  $\text{NO}_3^-$ -grown seedlings have already completed this transition, the  $\text{NH}_4^+$ -grown ones are still in the process. This is indicated by the high scatter in leaf development (Fig. 4.1) and ROS production (Fig. 4.25). In summary,  $\text{NH}_4^+$ -grown seedlings still live mainly from the  $\beta$ -oxidation (right-hand side Fig. 5.3) whereas  $\text{NO}_3^-$ -grown seedlings have already switched to photosynthesis.

Consequently, it has to be assumed that there is an early adaptation to the form of N-nutrition controlling the activation of metabolic pathways. The perception of the stimulus and the involved signalling network remains to be elucidated. However, it has to occur prior to the onset of photosynthesis. The consequences are discussed in the following sections.

## 5.3 Explaining previous findings in the light of the scheme in Figure 5.3

### 5.3.1 Influence of N-form on growth

As described in the Introduction, it is a well known phenomenon that growth is retarded in  $\text{NH}_4^+$ -grown plants in contrast to those grown on a  $\text{NO}_3^-$ -nutrient. This holds also for the seedlings of *A. thaliana* used in the present studies. However, the explanation related to Fig. 5.3 has different aspects than previous hypotheses.

The hypothesis of Givan (1979) implies that  $\text{NH}_4^+$  in the roots requires high delivery of carbohydrates, and that this may be a strong drain on photosynthetic energy generation (Britto and Kronzucker 2002). This can be ruled out for the seedlings of *A. thaliana* used here because  $\text{NH}_4^+$ -grown seedlings still live from the oleosomes (as concluded from gene expression, Table 4.13) indicating that metabolic turnover seems to be lower than in  $\text{NO}_3^-$ -grown ones. This is even more convincing as it occurs under the condition that photosynthesis has not yet reached its full capacity (Fig. 4.10).

As mentioned above, Zhu et al. (2000) reported that there was a stronger load of toxic radicals in  $\text{NH}_4^+$ -grown beans (*P. vulgaris*) as compared to  $\text{NO}_3^-$ -grown ones. Guo et al. (2005) suggested that the higher level of toxic radicals in  $\text{NH}_4^+$ -grown plants was caused by superfluous redox equivalents from the photosynthetic ETC exported to the mitochondria. This export was stronger than in  $\text{NO}_3^-$ -grown plants because N-assimilation as a sink of superfluous redox equivalents was absent in  $\text{NH}_4^+$ -grown plants.

This model does not apply here because  $\text{NH}_4^+$ -grown seedlings mainly live from the oleosomes (Fig. 4.37) and photosynthesis has not yet reached its full power (Fig. 4.10). Thus, the branching of photosynthetic redox equivalents seems to be a minor problem. This excludes damage by ROS as a possible explanation for the finding here.

### 5.3.2 Different ROS sources under $\text{NH}_4^+$ -nutrition compared to $\text{NO}_3^-$ -nutrition

In the case of ROS formation, two different phenomena were observed for  $\text{NH}_4^+$ -grown seedlings. First the response to light in leaf tissue under the light-guide was smaller than that in  $\text{NO}_3^-$ -grown ones (Fig. 4.28) and ROS production was not stimulated by  $\text{CO}_2$  deficiency (Fig. 4.27). Second, there was spreading of ROS into the non-illuminated parts of the leaf, and the increase of DCF-fluorescence was dependent on buffer (pH) whereas in  $\text{NO}_3^-$ -grown seedlings no such pH dependency was observed (Figs. 4.23, 4.15).

The response of  $\text{NO}_3^-$ -grown seedlings to the light is in line with the hypothesis of Zhu et al. (2000) and Guo et al. (2005). It indicates a photosynthetic origin of ROS. In contrast, the behaviour of ROS in  $\text{NH}_4^+$ -grown seedlings cannot directly be related to redox fluxes in the chloroplasts or mitochondria, because this would not be sensitive to external pH or buffer capacity. This is not a surprise in the light of Fig. 5.3 attributing a dominant role of  $\beta$ -oxidation over photosynthesis in  $\text{NH}_4^+$ -grown seedlings.

The assumption of apoplastic ROS generation, mentioned already several times, needs some comments: The hypothesis that the source of ROS in  $\text{NH}_4^+$ -grown seedlings might be

localised in the apoplast is supported by the observed sensitivity of DCF fluorescence signal to pH changes. Sanders measured the pH of the unstirred layer in *Chara* (Lucas et al. 1983). By means of Thomas-type pH-microelectrodes (Thomas 1978) they have shown that the pH in the unstirred layer of the cell wall close to the plasmalemma can be about one pH unit below that of the bulk medium. These experiments were performed in the green alga *Chara* because geometry of the single cell allowed the stepwise approach of the electrode towards the plasmalemma. This acidification is probably caused by the activity of proton pumps (Sanders et al. 1981) which acidify the outer layer of the plasma membrane in order to drive uptake of solutes and anions by co-transport (Sanders and Hansen, 1981, Maathuis and Sanders 1992) and to convert bicarbonate to CO<sub>2</sub> for photosynthetic use (Walker et al. 1980, Miedema and Prins 1992).

Measurements of this kind are not available from intact leaves. However, the biophysical conditions in leaves are similar to those in *Chara*. Proton pumps are active to drive co-transport and to facilitate CO<sub>2</sub> uptake (Miedema and Prins 1992). A cell wall with high density of negative charges causes an enrichment of cations including protons in the medium of the layer at the plasmalemma, and impedes the exchange with the bulk solutions. Thus it is reasonable to assume that in the experiments reported here the pH in the unstirred layer in the cell wall is more acidic than the bulk medium. Assuming also a difference in pH of 1 unit would be enough to explain that DCF fluorescence is quenched if the bulk medium is at pH 6.1 (Fig. 4.12).

In the experiments above, two different concentrations of the buffer were used. At high buffer concentration (50 mM) the pH of the medium would exert increasing influence on the pH close to the plasmalemma. This becomes evident from the comparison of the effects of different buffer capacities on the quenching of DCF fluorescence at pH 7.5 in NH<sub>4</sub><sup>+</sup>-grown seedlings (Fig. 4.15). At low buffer concentration quenching of DCF fluorescence is stronger than at high concentrations (Fig. 4.27B). There is no influence in the case of NO<sub>3</sub><sup>-</sup>-grown seedlings. This indicates that there is obviously no effect of apoplastic conditions on ROS indication by DCF in NO<sub>3</sub><sup>-</sup>-grown seedlings. In NH<sub>4</sub><sup>+</sup>-grown seedlings, low pH (6.1) and low buffer concentrations (5 mM) suppress the response of DCF fluorescence found at pH 7.5 and high buffer concentrations (50 mM). This implies that the apoplastic medium plays an important role. We conclude that ROS production occurs in the apoplast. Then, low pH would quench DCF fluorescence and impede any changes in ROS production. This leads to the horizontal line in Fig. 4.15.

This assignment of ROS production to the apoplast is also supported by the finding of spreading (described in section 4.4.7.3), because the apoplast is the compartment, which connects all cells of the leaf.

Additionally, in the experiments of Fig. 4.27 performed with  $\text{NH}_4^+$ -grown seedlings, basal ROS production (before illumination) and light-induced ROS production are higher in 10 mM than in 0.1 mM  $\text{NaHCO}_3$ . This is in contrast to the effects in  $\text{NO}_3^-$ -grown seedlings shown in Fig. 4.20. According to the discussion above dealing with the role of the pH in the unstirred layer at the plasmalemma, it cannot be concluded that an effect on photosynthesis is the origin of this inverse bicarbonate dependence in  $\text{NH}_4^+$ -grown seedlings. Probably, it is the effect of the stronger buffer capacity of the solution containing 10 mM  $\text{NaHCO}_3$  and 50 mM HEPES which suppresses acidification in the unstirred layer. This would lead to the enhanced DCF-responses shown in Fig. 4.27.

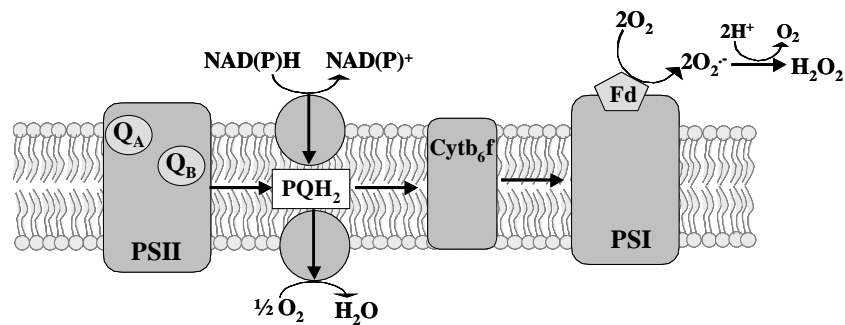
Unfortunately, a more conclusive statement does not seem to be possible at the present state of investigation. ROS production in the apoplast normally is involved in the defence strategies against pathogens (Neill et al. 2002, Jabs et al. 1997). However, at the moment we have no information of why  $\text{NH}_4^+$ -grown seedlings have installed a more sensitive system in the apoplast than  $\text{NO}_3^-$ -grown ones. A very weak argument is that the  $\text{NH}_4^+$ -grown seedlings are still in a juvenile state. Embedding germinating seeds in a cloud of ROS has been reported by Schopfer et al. (2001).

The above considerations may be related to another feature, i.e., the strong transient response of ROS production in  $\text{NH}_4^+$ -grown seedlings (Figs. 4.15C, 4.24C) prior to actinic illumination. This may be an effect of mechanical wounding caused by handling the cells. The question is of why such a strong effect is not observed in  $\text{NO}_3^-$ -grown seedlings. The answer may be related to the above suggestion that defence mechanisms using ROS production in the apoplast are more easily induced in  $\text{NH}_4^+$ -grown seedlings than in  $\text{NO}_3^-$ -grown ones.

### 5.3.3 Influence of $\text{CO}_2$ on ROS formation in $\text{NO}_3^-$ -grown seedlings

When summarizing the experimental findings which lead to the hypothesis of section 5.2.2 it was mentioned that the effect of  $\text{CO}_2$  in  $\text{NH}_4^+$ -grown plants was different from what would be expected if photosynthesis would play a dominant role in  $\text{NH}_4^+$ -grown seedlings of *A. thaliana*. In  $\text{NO}_3^-$ -grown seedlings the decrease in the light-induced ROS production after restoring normal  $\text{CO}_2$  concentration is not unexpected and is discussed here in more detail.

CO<sub>2</sub> is important for the normal functioning of photosynthesis related processes. Both, blockade by DCMU and CO<sub>2</sub> deficiency are expected to impede electron flow in the photosynthetic ETC, and thus to prevent re-oxidation of the primary quencher Q<sub>A</sub>. However, their effects on ROS production are different. The effect of DCMU in Fig. 4.22 can be compared with the findings of Fufezan et al. (2002) that in contrast to phenolic inhibitors of electron transfer from Q<sub>A</sub> to Q<sub>B</sub> DCMU decreases the production of <sup>1</sup>O<sub>2</sub> in PS II. It has to be mentioned that DCF (in contrast to DanePy, Hideg et al. 2002) is not a dye for recording <sup>1</sup>O<sub>2</sub>. However, it cannot be excluded that <sup>1</sup>O<sub>2</sub> initiates a chain of redox reactions which may lead to peroxides influencing DCF fluorescence. On the other hand, another reason for the DCMU-induced decrease of the production of peroxides may be involved: Reactions at PS I, too, can be a strong source of ROS (Cleland and Grace 1999, Tjus et al. 2001). Thus, the DCMU-induced reduction of the light-induced increase in DCF fluorescence (Fig. 4.22) may also indicate that ROS production at PS I is eliminated. This is expected as DCMU blocks electron transfer from PS II to PS I.



**Figure 5.4** Scheme of photosynthetic electron transport chain (ETC) with possible reactions of chlororespiration (oxidation of NADPH and reduction of O<sub>2</sub> to H<sub>2</sub>O by means of plastoquinone pool (PQH<sub>2</sub>)) and Mehler-reaction (left hand side at PSI). DCMU inhibits PS II. (Peltier and Cournac 2002 modified)

In the case of ROS production stimulated by CO<sub>2</sub> deficiency (which also occurs in the DCMU experiment in SM medium in Fig. 4.22), the overlay of light-induced ROS production and chlorophyll fluorescence in Fig. 4.18C suggests that it is located mainly in the chloroplasts. Unfortunately, the CO<sub>2</sub> effect on Q<sub>A</sub>/Q<sub>A</sub><sup>-</sup> redox potential is unknown. Thus, it cannot be decided how impeding the ETC flow downstream PS I influences the ROS production at PS II. It may result in a decrease of ROS at PS II similar to that caused by DCMU or an increase mediated by phenolic inhibitors (Fufezan et al. 2002). However, the most likely explanation is that CO<sub>2</sub> deficiency increases ROS production at or downstream PS I.

The related putative ROS generator is still unknown, even though some hints are obtained from the experiments above (section 4.4.6). Some of the ROS may result from increased photorespiration if O<sub>2</sub> concentration is still sufficient. The effect of degassing during the dye loading procedure may be partially compensated by O<sub>2</sub> evolution from PS II. Nevertheless photorespiration has not completely been replaced. The higher energy quenching indicates a higher energization of the thylakoid membrane (Fig. 4.21) (Schreiber and Krieger 1998, Schreiber and Bilger 1993, Hansen et al. 1993). Energization increases when strong consumers of ATP like carboxylation or oxygenation at the Rubisco are replaced by acceptors that use less ATP (Noctor and Foyer 1998).

Several candidates can be discussed as possible electron sinks in the ETC downstream PS II: Mehler reaction (Hormann et al. 1994, Makino et al. 2002), chlororespiration and other chloroplastic acceptors (Cournac et al. 2000), N-assimilation (Noctor and Foyer 1998, Guo et al. 2005), or export of redox equivalents via the malate/oxalate shuttle (Krömer 1995, Backhausen et al. 1994).

The Mehler reaction (i.e. the generation of O<sub>2</sub> radicals at PS I, Hormann et al. 1994) is a strong source of ROS. A caveat results from a comparison of photo-acoustically measured O<sub>2</sub> evolution and ETC electron flow: It was concluded that the role of the Mehler reaction is restricted to the first seconds after switching on the light in order to support a fast establishment of thylakoid energization (Schinner et al. 1998, Zhu et al. 2000). Nevertheless, the Mehler reaction is still a likely candidate when under CO<sub>2</sub> deficiency its operation exceeds the induction period. The role of other peroxidases and hydrogenases related to plastoquinone can hardly be quantified since little is known about their importance in vivo (Cournac et al. 2000). N-assimilation is a sink of excess redox equivalents (Noctor and Foyer 1998), but is not known to be a source of ROS. The absence of an increase of ROS production in the presence of SHAM (Fig. 4.22) indicates that export from the chloroplasts and burning of redox equivalents in the mitochondria as found in other studies (Raghavendra et al. 1994, Maxwell et al. 1999, Affourtit et al. 2001) seems to be of minor importance (Fig. 4.22).

Whatever the source of ROS, induced by CO<sub>2</sub> deficiency, is the above investigations show that CO<sub>2</sub> supply has to be provided when ROS production is investigated in infiltrated leaves of NO<sub>3</sub><sup>-</sup>-grown plants.

### 5.3.4 ROS detoxification and scavenging systems

As mentioned above the absence of significant differential expression of scavenging enzymes was taken as evidence that the hypothesis of Zhu et al. (2000) does not apply.

In this project, additional approaches analyzing the antioxidant capacity of the plants in relation to N-form have been implemented. Physiological studies revealed a lower zeaxanthin content in ammonium-grown seedlings (Fig. 4.29). This was in line with the findings of Zhu et al. (2000) and Bendixen et al. (2001). Surprisingly, the investigations of catalase (CAT) activity (section 4.8.8.3) and the transport rate of substrates into the vacuole (BCECF, section 4.8.8.2) showed no significant differences between the two N-forms. The results were in line with the gene expressions studies. The genes encoding for DHAR, GST (three isoforms), GPX, and CAT2 were up-regulated in the light in both N-forms. Only one gene encoding for a peroxidase did not show regulation in  $\text{NH}_4^+$  under HL (Table 4.7).

In relation to N-form dependent differentiations in gene expression there are just two GSTs and a peroxidase showing higher expression values in  $\text{NH}_4^+$ -grown seedlings. It has to be stated that there are multiple isoforms of these enzymes, especially GST. The genome of *A. thaliana* contains 48 GST genes divided in 5 classes (Dixon et al. 2002). The microarray results stated above are not approved by another method and the spotted PCR products were not sequenced yet, except for GST (At2g29450), DHAR (At1g75270) and CAT2 (At4g35090). Because of this, the interpretation of the results has to be done with caution, especially, concerning the N-form dependent differences. Nevertheless, the results dealing with excess light indicate that both types of plants had to cope with radicals due to high light and in turn regulate their scavenging systems. The slightly higher ratios in  $\text{NO}_3^-$ -grown seedlings are not surprising since the photosynthetic rate in these plants is twice as high as in ammonium grown ones (Fig. 4.10).

Genes encoding for other proteins have not been subject to further analysis but it was found that there were some genes encoding for HSP as well as genes encoding for ABC-transporters up-regulated under HL without significant dependence on the N-form (A.4). The ABC-transporters located in the membrane of the vacuole may be responsible for fast transport of toxic elements into the vacuole (Theodoulou 2000). However, there was no sign of their involvement in an N-form dependent detoxification strategy. This was supported by the uptake studies using BCECF (section 4.8.8.2).

There is still the discrepancy that zeaxanthin is found to be reduced in  $\text{NH}_4^+$ -grown seedlings, but that there is no prominent difference in gene expression of the detoxification

enzymes. Only a reduced expression of the GDP-epimerase gene in  $\text{NH}_4^+$ -grown seedlings was observed, which may influence zeaxanthin formation via ascorbate deficiency. Nevertheless, this field needs further research, which also has to be aware of the transient occurrence of detoxification enzymes (Zhu et al. 2000).

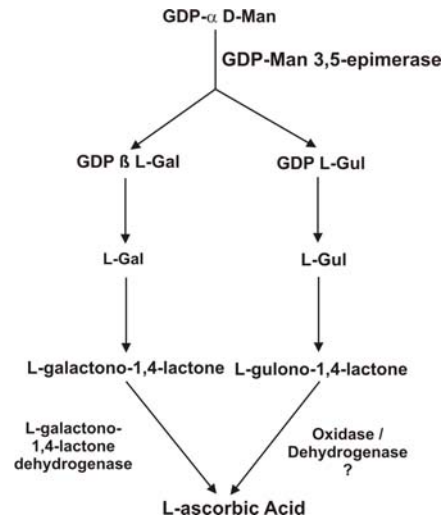
### 5.3.5 GDP-Epimerase

GDP-mannose 3,5,-epimerase is supposed to be a key regulatory enzyme of the *de novo* biosynthesis of ascorbic acid (Wolucka et al. 2001, Valpuesta and Botella 2004). It is up-regulated in  $\text{NO}_3^-$ -grown seedlings under HL conditions as revealed by microarray and Northern Blot analysis (Fig. 4.44, Table 4.14).

Ascorbic acid has important antioxidant and metabolic functions in plants. It may represent one of the major soluble carbohydrates and is involved in important physiological processes like e.g. development, cell wall biosynthesis and stress response (Wolucka and Montagu 2003). Its biosynthetic pathway remained unknown for a long time. In 1998, Wheeler et al. proposed a pathway involving GDP-mannose. They suggested the conversion of GDP-mannose via GDP-L-galactose and L-galactose to L-galactono-1,4-lactone, which is the direct precursor for L-ascorbic acid (Fig. 5.5). Other researchers approved the hypothesis of GDP-mannose as precursor for ascorbic acid synthesis (Conklin et al. 1999, Wolucka et al. 2001). In addition, a second *de novo* pathway involving GDP-mannose was discovered (Wolucka and Montagu 2003). In this pathway, GDP-L-gulose is formed instead of conversion to GDP-L-galactose. It is suggested that GDP-gulose is channelled directly into the ascorbic acid synthesis pathway whereas GDP-galactose can also be used for biosynthesis of glycoconjugates like cell wall polysaccharides (Wolucka and Montagu 2003). The pathway using galactose as a precursor is cytosolic, except for the last step, which is located on the inner mitochondrial membrane (Smirnoff 2000). The pathway involving gulose is also thought to take place in the cytosol, but especially the last step involving an organelle-specific dehydrogenase is suggested to take place at different locations leading to an *in situ* synthesis of ascorbic acid with no need of intracellular transport (Wolucka and Montagu 2003).

Regulatory enzymes in these pathways (Fig. 5.5) seem to be GDP-mannose phosphorylase (forming GDP-mannose from d-mannose-1-phosphate), GDP-mannose 3,5,-epimerase, (converting GDP-mannose into GDP-gal or GDP-gul) and galactono-1,4-lactone dehydrogenase responsible for the reaction of galactono-1,4-lactone to ascorbic acid.





**Figure 5.5** Pathways of L-ascorbic acid biosynthesis via GDP-galactose (right hand side) or via GDP-gulose (left hand side). (Wolucka and Montagu 2003 modified)

Here the focus lies on the epimerase since the genes encoding for the other enzymes, important for the *de novo* synthesis of ascorbic acid, are unfortunately not included on the microarray or did not show differential expression. Anyway, the epimerase seems to be one of the most interesting enzymes regulating this pathway. It is stimulated by NAD(P) but inhibited by the reduced form NAD(P)H and by ascorbic acid. The main functions of epimerase are catalysation of the first step in the ascorbic acid biosynthesis and its feedback inhibition, sensing of the redox state of the cell and playing a role in cell wall / glycoprotein biosynthesis (Wolucka and Montagu 2003).

In the experiments presented GDP-epimerase is up-regulated in  $\text{NO}_3^-$ -grown seedlings under HL conditions (Fig. 4.44), which sheds a new light on old findings of Bendixen et al. (2001). They found lower contents of ascorbate in  $\text{NH}_4^+$ -grown leaves of *P. vulgaris*. This lower ascorbate level was also indicated by the results from the determination of zeaxanthin (a carotenoid of the xanthophyll cycle protecting photosystems under HL conditions). As its conversion from violaxanthin needs ascorbate, the lower level of zeaxanthin in  $\text{NH}_4^+$ -grown plants under HL conditions was understood as an indication of ascorbate deficiency. Feeding of ascorbate via the petiole increased the zeaxanthin level in  $\text{NH}_4^+$ -grown plants.

Bendixen et al. (2001) explained this finding by the higher load of toxic radicals in  $\text{NH}_4^+$ -grown plants (as concluded from the results of Zhu et al. 2000), which decreased the ascorbate pool. The findings here may lead to a quite different view, namely that not

consumption is increased in  $\text{NH}_4^+$ -grown seedlings, but production is enhanced in  $\text{NO}_3^-$ -grown seedlings.

Nevertheless, these two different models do not necessarily contradict each other. In the studies of Bendixen et al. (2001) grown-up plants of *P. vulgaris* were used, whereas in the studies here, the  $\text{NH}_4^+$ -grown plants of *A. thaliana* were still at the border between nutrition from the oleosomes and from photosynthesis. Thus, ROS production linked to photosynthesis may be weaker in  $\text{NH}_4^+$ -grown leaves. This would lead to different conditions as in grown-up *P. vulgaris*. A stimulation of the epimerase by higher need of ascorbate would not occur in young  $\text{NH}_4^+$ -grown plants since light-induced ROS production is still moderate (section 4.4.7). In  $\text{NO}_3^-$ -grown seedlings, light-induced ROS production is higher and leads to the need of increased expression of GDP-epimerase.

## 5.4 Excluding possible sources of error

The discussion above demonstrates that the experimental results of our studies on *A. thaliana* can be explained in the frame work of the model shown in Fig. 5.3. Nevertheless, the above conclusions could only be obtained by coming close to limits of experimental approaches. Because of this, the validity of the results is discussed in the forthcoming paragraphs.

### 5.4.1 Effect of pH in external medium on growth

Even though the above considerations seem to clearly indicate that N-form is the major cause of the changes in the pathways of Fig. 5.3 it has to be excluded that secondary effects and not primarily the N-form is the cause of the observed differences.

One serious argument is an effect on N-form on the pH in the vicinity of the roots. In principal, this might have become a problem as "solution" in the agar plate is stagnant, and buffer capacity may become exhausted in the long run. The yellow colour around roots of *S. oleracea* and around fungal spores in Fig. 4.4 clearly showed that this problem does exist. Fortunately, transport activity in the tiny roots of *A. thaliana* is so small that a pH gradient near the roots could not be detected (Figs. 4.2, 4.3). Because of this, pH differences can be excluded as a putative cause for the observed differences in growth behaviour between  $\text{NH}_4^+$ - and  $\text{NO}_3^-$ -grown seedlings of *A. thaliana*.

### 5.4.2 Use of dyes to localise sites of ROS formation - assets and drawbacks

As mentioned at the beginning of the chapter on the ROS experiments (section 4.4.1), the use of dyes, fluorescent or non-fluorescent, is a common method to track different kinds of ROS in the cell and to localise sites of ROS formation. Nevertheless, the validity of the result can suffer from a variety of obstacles. This holds true especially for DCF (Esposti et al. 1998, Ohasi et al. 2001, Rota et al. 1999, Tarpey et al. 2004).

The feature that DCF is not a highly specific ROS indicator (i.e. that many different agents like  $\text{H}_2\text{O}_2$ , peroxides, peroxy products and peroxy radicals change fluorescence, Rota et al. 1999) is not a major problem, as long as we are only interested in the overall production of reactive oxygen species. This may also include indirect effects of singlet oxygen, (Bilski et al. 2002) superoxide anion, and free hydroxyl radical (LeBel et al. 1992, but see Myhre et al. 2003) even though these agents do not primarily react with DCF. However, within the time scale of the recordings (s to min) the redox chains in the cells would rapidly transform these species into those which are sensed by DCF.

The arguments against the usage of DCF are further weakened by the experimental approach of our investigations: The main argument for the reliability of the results presented is the comparison of leaves, which differed only with respect to one treatment. The issue of the application of the dye was not to determine precisely the absolute rate of  $\text{H}_2\text{O}_2$  formation. The physiological conclusions were based on the relative differences induced by the change of a few parameters like N-form or pH. Remaining doubts on the applicability of DCF were refuted by the comparison with another dye: The measurements with NBT in Fig. 4.18 gave the same results as those with DCF. NBT is a chromogenic probe used to determine superoxide ( $\text{O}_2^-$ ) production. The discussion about NBT does not seem to be as controversial as for DCF (Freyer et al. 2002, Maly et al. 1989).

Two other influences on the results have to be considered, photoreaction of the dye (Afzal et al. 2003) and quenching mechanisms by, for example, redox equivalents (Batandier et al. 2002). In the case of photo-oxidation Afzal et al. (2003) found that photo-oxidation increases with the concentration of DCF. But this does not seem to account for the experiments done here since in control experiments it was observed that photo-oxidation of the dye due to actinic light does not play a role (Fig. 4.13). Nevertheless, even if there would be any photo-oxidation the method of subtracting background would diminish its influence on the final results.

More serious is the argument based on quenching of DCF by reducing equivalents. There are indications that NADH may act as a quencher of DCF fluorescence (Batandier et al. 2002). However, the related experiments are not well described and need further investigations. This argument was also considered by Hammes et al. (2005). In those investigations, we found that under conditions of inhibition by SHAM light induced a decrease of DCF-fluorescence. However, in that case the response to light was much faster than the slow decay of fluorescence observed after the primary light-induced increase in e.g. Figs. 4.22, 4.24. The fast response in Hammes et al. (2005) corresponds to the expectation that delivery of NAD(P)H from the chloroplasts would be fast. Because of the time scale, the involvement of a putative direct effect of NADH on DCF fluorescence in the slow decay of fluorescence in Figs. 4.22, 4.24 can be excluded. The time constant of this decay is in the order of the time constant of BCECF uptake (section 4.8.8.2) used for monitoring putative uptake of dye into the vacuole. However, a definite identification of the underlying mechanism is not yet possible.

Despite all contradictory findings the dye remains an attractive probe as an overall indicator of oxidative stress. The reliability of the DCF results gets strong support by the application of a second dye, i.e., NBT.

### 5.4.3 Gene expression studies

Even though the gene expression results and the physiological data seemed to support each other there were drawbacks concerning reliability of gene expression data, which have to be addressed. The theoretical background for the data analysis of gene expression studies is described in section 4.5.1. As stated above, the major concern was (and always is) to gain the most reliable data set.

Therefore, the experimental design was carefully chosen. Here, the “loop” design (Fig. 4.30) appeared to be quite useful. The benefit of the loop is its inherent control. The “loop amplification” (i.e. the product of the expression values corrected for the correct direction) has to be “1”, as mentioned in the results section (4.5.1). Calculation of this loop amplification for the genes in Table 4.7 showed that about 80 % of the data were in the range of 30 % deviation from “1” and 45 % were in the range of 10 % deviation (Table 4.8). A deviation of 30 % seemed to be acceptable taking all factors into account e.g. pipetting, labelling differences, hybridisation inhomogeneities and especially biological variability.

The reliability of the loop design as indicated by the loop amplification was supported by the results of Northern blot analysis. The Northern blot analysis for the genes showing a very good "loop amplification" value of about 1 revealed a very good correspondence to the microarray data (Nia1 and CA) (Table 4.7, Figs. 4.35, 4.37). The lower the "loop amplification" value the worse was the correspondence between Northern and microarray values.

Also the number of replicates (biological and technical) were found to be sufficient. In the example shown in Table 4.10, the homogeneity of the three technical replicates was extraordinary good. Unfortunately this did not hold for all technical replicates. Anyway, the three technical replicates appeared to be very helpful to gain knowledge about the inhomogeneity of the microarray hybridisation. The geometric average calculated from the technical replicates resulted in more reliable data than having only one spot to analyse.

The same was true for biological replicates. They appeared to be quite useful and essential to account for any variance. As seen in Table 4.10 outliers can occur. In the case of Nia2, there was just one replicate in one of the conditions of the loop which showed an abnormal value. Since in all other conditions the related third replicate had values similar to the other ones this single one could be treated as an outlier. If only two biological replicates were hybridised the identification of the outlier would have been much more complicated. Another reason to use at least three replicates is shown in Table 4.12 for Nia1. In three out of four conditions the third replicate failed to produce a signal. Since there are two more data sets showing almost equal regulations the data are still useful. Having only a second dataset would have led to difficulties in interpreting the data. Nevertheless, if material and money are not limiting, it seems to be useful to have more than three replicates for better reliability.

Looking at Table 4.10 another important topic comes into focus, the normalisation. From the raw and control values it became quite clear that the signal intensities varied a lot between the biological replicates but the normalized values did not. This indicated that the normalization is absolutely necessary to produce comparable data sets.

The 8k microarray gave a good idea of the N-form dependent regulation of some important metabolic pathways. They are discussed above together with the physiological data in more detail. One big disadvantage was however that the chip covers only one fourth of the whole genome of *A. thaliana* and does not contain all genes encoding for the enzymes of interest and not all isoforms for the enzymes investigated. Some of the missing isoforms or genes encoding for interesting enzymes were investigated by Northern blot analysis to fill the gap and to prove the hypothesis (Figs. 4.36, 4.37). Another drawback was the error rate of

annotations for the spots. 10 % of the sequenced products did not correspond to the annotations (Table 4.4). This indicated that sequencing of at least the key genes for the hypothesis is recommended. Overall there was an error rate of almost 40 % taking into account also the non corresponding Northern blots (Table 4.5). This seemed to be a high loss of data. However, the synopsis of the errors increased the reliability of those yielding corresponding behaviour from microarray and Northern blot. This provided a solid basis for building up the hypotheses.

## 6 General conclusions and Outlook

Summarising the outcome of the work presented, the question arises of whether the investigations of N-form dependent differences on very young plants and the use of gene expression studies can shed some new light on the underlying mechanism of ammonium toxicity or not. The answer is yes even though the underlying mechanism remains in the dark.

The results stress the importance to consider multiple causes for the phenomena of ammonia toxicity. Several hypotheses assign an important role to photosynthesis as an origin of the problems related to  $\text{NH}_4^+$  as the sole nitrogen source. These hypotheses are not invalidated by the present studies, but they obviously do not apply to the seedlings of *A. thaliana* used here, since the delayed onset of photosynthesis is a consequence of the (still unknown) signalling pathway induced by  $\text{NH}_4^+$ -nutrition.

In the case of the hypothesis of Zhu et al. (2000) superfluous redox equivalents for the photosynthetic electron transfer chain play the crucial role as they are assumed to generate an extra load of radicals in  $\text{NH}_4^+$ -grown plants. The toxicity of the radicals and the resulting metabolic costs for scavenging systems and repair mechanisms are a serious obstacle for  $\text{NH}_4^+$ -grown plants. This hypothesis is based on the same ideas as those searching the origin of degenerative diseases in the mitochondrial ROS production (Beal 2004). In the field of plants, the problem of high metabolic costs is known from herbicide-resistant plants, which decay under high light, because the metabolic cost for repairing the D1 protein of PS II becomes unpayable (Sundby et al. 1993).

Also the hypothesis of uncoupling of photosynthesis by  $\text{NH}_4^+$  as postulated by Magalhaes and Huber (1989) does not apply here, because photosynthesis has not yet replaced nutrition from the oleosomes and thus uncoupling would not hurt. Besides, Bendixen et al. (2001) have shown that uncoupling of the thylakoid membrane does not occur even in grown-up *Phaseolus vulgaris*, because energy quenching of chlorophyll fluorescence is not eliminated in  $\text{NH}_4^+$ -grown plants. Energy quenching would be prevented in a uncoupled thylakoid membrane (Horton and Ruban 1992, 1993).

Furthermore, our findings disprove the hypothesis of Givan (1979) for the seedlings of *A. thaliana*. Givan (1979) and others (e.g. Schortemeyer et al. 1997, Hodge et al. 1997) assumed that the higher demand of photosyntheates for detoxification of  $\text{NH}_4^+$  in the roots is the reason for  $\text{NH}_4^+$ -related growth retardation.

The findings here are not in contradiction to those hypotheses, which are not related to photosynthesis. Salsac et al. (1987) suggested an impaired osmoregulation in  $\text{NH}_4^+$ -grown plants as a cause of growth retardation. Another putative explanation is disturbance of pH regulation as caused by export of  $\text{H}^+$  during  $\text{NH}_4^+$  uptake. This hypothesis was dismissed by measurement of intracellular pH by dyes or NMR (Bligny et al. 1997, Kosegarten et al. 1997, Wilson et al. 1998, McQueen and Bailey 1991).

The investigations of the present work revealed phenomenological aspects of  $\text{NH}_4^+$ -toxicity in young plants. They could demonstrate relationships between physiological findings such as reduced photosynthetic activity, different kind of ROS production and gene expression. This resulted in a fairly consistent picture of  $\text{NH}_4^+$ -grown seedlings, which are at the edge of switching from oleosome-based nutrition to photosynthetic supply. This was also indicated by the high scatter in the developmental state (Fig. 4.1) and in ROS production (Fig. 4.25).

However, describing the relationships between different phenomena related to N-form dependent nutrition does not answer the question of how the signal is perceived. It is not even clear whether the signal is “presence of  $\text{NH}_4^+$ ” or “absence of  $\text{NO}_3^-$ “. It is quite obvious that some effects like increased  $\text{Cl}^-$  contents in  $\text{NH}_4^+$ -grown plants (juvenile or grown-up) are just a consequence of the absence of the anion  $\text{NO}_3^-$  which has to be replaced by some other anion for charge balance. Also the hypothesis of toxic photosynthetic radicals (Zhu et al. 2000, Guo et al. 2005) argues with the absence of  $\text{NO}_3^-$ -assimilation in the leaves as electron sink rather than toxicity of  $\text{NH}_4^+$ . And likewise, in the hypothesis of hormonal signalling (Rahayu et al. 2005, Walch-Liu et al. 2000) the absence of  $\text{NO}_3^-$  seems to be more important than the presence of  $\text{NH}_4^+$ .

Even more difficult is the answer to the question, which effects are caused by the putative toxicity of  $\text{NH}_4^+$ . Other scientists have considered the following mechanisms: a) disturbance of cytosolic pH by  $\text{NH}_4^+$ -uptake (Kosegarten et al. 1997, McQueen and Bailey 1991), b) enrichment of free  $\text{NH}_4^+$  in the cytosol (Givan 1979, Magelhaes and Huber 1989) and c) impaired water uptake efficiency and lower contents of cations and organic acids resulting in a higher osmotic potential (Gerendás et al. 1997). However, all of these findings are in controversial discussion and the relevance for the growth retardation of the seedlings of *A. thaliana* used here is not yet clear.

Further studies are needed to unravel the mechanistic background of the findings reported here and can be conducted along the following lines: Firstly, it should be investigated whether the differences in gene expression and physiology are related solely to



the different developmental states in  $\text{NO}_3^-$ - and  $\text{NH}_4^+$ -grown *A. thaliana*. The alternative scenarios may be as follows: A. Nutrition causes a signal which determines the velocity of development. At the same developmental state, both kinds of nutrition result in the same phenomenology. B. N-form induces phenomena which are independent of the developmental state but occur in addition to the influence on development.

In order to distinguish between these two scenarios, plants of different nutrition, but same developmental state (as judged from leaf development) should be compared, i.e., the experiments reported here should be repeated with these kinds of plants.

The outcome of the afore mentioned experiments is probably that there is an N-form dependent influence in parallel to that of developmental state. This is expected because grown-up *P. vulgaris* exhibits many effects which were similar to those discussed in section 5.1.

Of course it would be worthwhile to have a time series which shows at which stage of development the phenomena revealed by our experiments become prominent. Furthermore, also roots should be investigated in order to find out, which effects originate in the leaves themselves and which ones are "imported" from the roots.

As can easily be imagined, the required amount of time for measuring such a time series for all effects on gene expression and phenomenology reported here would exceed the capacity of one laboratory. Thus, approaches have to be considered, which enable on-line monitoring. Suitable parameters may be found in leaf development, chlorophyll-fluorescence and ROS development. They may provide a guideline for the selection of a few crucial steps where gene expressions studies should be done.

There are microarray studies which deal with global and organ-specific gene expression during development (Schmid et al. 2005, Ma et al. 2005). However, they do not consider the influence of N-form. Nevertheless, these studies may be helpful to optimise the investigation of the influence of N-form on development.

For monitoring ROS production, new facilities are opened by a new promising tool for *in vivo* studies making use of transgenic plants expressing a GFP-ROS sensor dedicated to individual organelles (developed by C. Plieth). This system might allow real-time monitoring of ROS development in the growing plants due to the self-reporting GFP. The possibility of real-time monitoring of ROS development provides a tool to examine the time-point of the switch from ROS production in the apoplast to ROS formation in photosynthesis related organelles.

Even more important would be the determination of the loci of ROS production. The assignment of ROS production to the inside of the cell in  $\text{NO}_3^-$ -grown plants and in the apoplast of  $\text{NH}_4^+$ -grown plants was based on (hopefully conclusive) physiological effects. However, direct evidence by a targeted ROS-GFP would not only confirm these findings, but also give more details about the role of chloroplasts, peroxisomes, mitochondria and apoplast.

Additional important investigations would deal with the experimental protocol. It is necessary to study the short-term response to ammonium nutrition. In long-term studies, plants have initiated compensatory mechanisms which might hide the original effect of the imposed treatment. After a certain time of exposure to an agent, the transcriptome is supposed to be adapted to the situation, and changes between different conditions may become hardly observable. Thus, the short-term responses to a change of N-form in the medium might yield a better chance to reveal changes in metabolic pathways used under different N-nutrition.

Furthermore, the concentration of the applied N-form should be varied. Ammonium is thought to have growth-stimulating effects in some plant species if used in minor concentrations (Gerendás and Sattelmacher 1990). In the present studies, the N-concentration was very high. This was important since the underlying mechanisms of ammonium toxicity were in the focus of the investigations. Nevertheless, the comparison of gene expression and physiological behaviour of plants grown at high and low ammonium concentrations may shed some new light on the phenomena of growth retardation occurring at high  $\text{NH}_4^+$  concentrations.

All these studies still do not directly address the fundamental question: where does the perception of the signal “no  $\text{NO}_3^-$ ” or “horrible  $\text{NH}_4^+$  ante portas” occur? Answering this question requires the concentration on genes involved in signal transduction pathways. Most of them were probably not included on the cDNA microarray used here. This microarray included only 25 % of the *Arabidopsis* genome. A better chance to find such genes is given by microarrays covering the whole genome like the oligo-arrays of the Affymetrix system.

However, it is not obvious that such a signalling pathway may be revealed by gene expression studies. In addition, it may become necessary to investigate also the phosphorylation status of signalling cascades. Studying gene expression by means of microarrays can be used as a fishing net to gain new ideas in which direction to go for further research. But the transcriptional level is only one part of cellular signalling networks. They consist of long chains with lots of regulatory steps involved until the protein, important for the physiological status of the plant, is produced and active. To understand the physiological relevance of proteins, investigations on the proteome are important, e.g. Western blotting

(qualitative), ELISA (quantitative) and 2D gel-electrophoresis in combination with MALDI-TOF. The list of methods to be used shows that the present work is only the beginning of a very interesting and promising research area. Taking the proteome and the metabolome into account will lead to a deeper understanding of the processes induced by different N-forms.



## Summary

15-days old plants of *Arabidopsis thaliana* were used to study the effects of  $\text{NO}_3^-$ - and  $\text{NH}_4^+$ -nutrition on growth, physiology and gene expression. The experimental conditions were different from what was normally applied. Light intensity was low ( $40 \mu\text{mol m}^{-2}\text{s}^{-1}$ ), and the plants were grown on the selected N-form from the very beginning. The investigations were done on an early developmental stage. One reason to use seedlings was to look for N-form dependent changes in metabolism, which were initiated without the often anticipated involvement of photosynthesis.  $\text{NO}_3^-$ -grown seedlings had already started to expand their primary leaves, whereas development of  $\text{NH}_4^+$ -grown seedlings showed high scatter. Most of the seedlings had not yet begun to develop primary leaves, a few had reached the same state as the  $\text{NO}_3^-$ -grown ones.

Despite the young age of the *A. thaliana* plants, the  $\text{NH}_4^+$ -grown seedlings showed N-form dependent differences known from previous studies with respect to anion analysis, replacement of  $\text{NO}_3^-$  by  $\text{Cl}^-$ , and amount of free amino acids.

Nevertheless, there were significant differences to grown-up plants. The  $\text{NH}_4^+$ -grown seedlings were still in the progress of changing their energy supply from the oleosomes to photosynthesis. This was concluded from physiological measurements:  $\text{CO}_2$  fixation per chlorophyll was half as much as for  $\text{NO}_3^-$ -grown seedlings. There were no starch deposits in the chloroplasts, and ROS development seemed to be apoplastic in contrast to ROS production inside the cells of  $\text{NO}_3^-$ -grown leaves.

Gene expression studies provided strong support for these findings. They were done in cooperation with Eva-Mari Aro's group at the University of Turku, Finland, using a cDNA microarray, which comprised about 6500 genes, one quarter of the *Arabidopsis* genome. For experimental strategy a "loop design" was chosen. That way the N-form dependent as well as light-induced changes in gene expression could be compared. The analysis of the differentially expressed genes was hypothesis-driven, i.e., not a hierarchy of high differential expression values but the importance for the identification of metabolic pathways was the guide line of a refined analysis. For the verification of the microarray results, Northern blot analysis was applied.

In  $\text{NH}_4^+$ -grown seedlings, the genes encoding for enzymes of  $\beta$ -oxidation and for phosphoenolpyruvate carboxykinase were up-regulated. In  $\text{NO}_3^-$ -grown seedlings, up-regulation of sedoheptulose biphosphatase and cytosolic fructose biphosphate aldolase was

found. These results led to the hypothesis that the  $\text{NH}_4^+$ -grown seedlings still used the reserves in the oleosomes via  $\beta$ -oxidation, whereas  $\text{NO}_3^-$ -grown seedlings had already switched to photosynthesis.

This finding explains the results of the present study. The high scatter in leaf development and ROS formation found in  $\text{NH}_4^+$ -grown seedlings had its origin in the transition from supply by the oleosomes to supply by photosynthesis. This transition may be more or less promoted in individual plants.  $\text{NO}_3^-$ -grown seedlings had finished this transition and were in a more homogeneous state.

ROS production as measured by DCF fluorescence was very different in  $\text{NH}_4^+$ - and  $\text{NO}_3^-$ -grown seedlings. Whereas light-induced ROS in  $\text{NO}_3^-$ -grown seedlings was found only under the light guide providing the actinic light, in  $\text{NH}_4^+$ -grown seedlings a systemic response was found. There, light-induced ROS production showed enormous scatter, strong patchiness and was not restricted to the illuminated part of the leaf, but spread also to non-illuminated areas. In contrast to  $\text{NO}_3^-$ -grown seedlings, ROS production was not stimulated by  $\text{CO}_2$  deficiency. Furthermore, the response to handling (wounding) was by far stronger than in  $\text{NO}_3^-$ -grown seedlings. The sensitivity of DCF fluorescence to pH and buffer capacity in  $\text{NH}_4^+$ -grown seedlings was taken as evidence that ROS production took place in the apoplast. This would also be in line with the effect of spreading.

In contrast to earlier investigations on grown-up *Phaseolus vulgaris* showing higher activity of scavenging enzymes, there was no indication of higher expression of genes encoding for scavenging enzymes in  $\text{NH}_4^+$ -grown seedlings of *A. thaliana*. Furthermore, GDP-epimerase involved in the synthesis of ascorbate was found to be up-regulated in  $\text{NO}_3^-$ -grown seedlings. All these findings are in line with the lower ROS production inside  $\text{NH}_4^+$ -grown cells as indicated by DCF fluorescence.

The occurrence of the different developmental states depending on N-form led to the following conclusions: The origin of growth retardation has to be an N-dependent signal, which is generated in an early state of development. It cannot result from any effect of N-nutrition on photosynthesis like too strong withdrawal of photosynthates or high cost of detoxification of photosynthetic radicals, because the onset of growth retardation seems to be prior to the usage of photosynthesis. The perception of the stimulus and the involved signalling network remains to be elucidated.

## Zusammenfassung

In der vorliegenden Arbeit wurde der Effekt von  $\text{NO}_3^-$  oder  $\text{NH}_4^+$ , als einziger Stickstoffquelle, auf das Wachstum, die Physiologie und die Genexpression an 15-Tage alten *Arabidopsis thaliana* Pflanzen untersucht. In Unterschied zu anderen Versuchsbedingungen wurden die Pflanzen bei niedrigen Lichtintensitäten ( $40 \mu\text{mol m}^{-2} \text{s}^{-1}$ ) direkt auf der jeweiligen N-Quelle angezogen und die Versuche wurden in einem frühen Entwicklungsstadium durchgeführt. Ein Grund für diese Anzuchtbedingungen war die Suche nach Stoffwechselwegen in Abhängigkeit von der Stickstoffform, die nicht durch mit der Photosynthese verbundene Prozesse bedingt waren. Die  $\text{NO}_3^-$ -ernährten Pflanzen hatten begonnen, Primärblätter zu bilden, während bei den  $\text{NH}_4^+$ -Pflanzen kein einheitliches Bild in der Blattentwicklung zu sehen war. Die meisten  $\text{NH}_4^+$ -Pflanzen hatten nur Keimblätter ausgebildet oder erste Ansätze der Primärblätter waren sichtbar. Nur wenige waren auf dem gleichen Entwicklungsstand wie die  $\text{NO}_3^-$ -Pflanzen.

Trotz des frühen Entwicklungsstadiums ergab sich für die  $\text{NH}_4^+$ -ernährten Pflanzen bei der Analyse der Anionen - Ersatz von  $\text{NO}_3^-$  durch Chlorid - und beim Anteil an freien Aminosäuren ein Bild, das dem bekannten von erwachsenen Pflanzen entsprach.

Dennoch wurden gravierende Unterschiede zu erwachsenen Pflanzen sichtbar. Die  $\text{NH}_4^+$ -Pflanzen befanden sich noch in dem Prozess der Umstellung von der Energieversorgung aus den Oleosomen zur Energieversorgung aus der Photosynthese. Folgende physiologische Ergebnisse führten zu diesem Schluss: Die  $\text{CO}_2$ -Fixierung pro Chlorophyll war nur halb so groß wie in  $\text{NO}_3^-$ -ernährten Pflanzen, und es waren keine Stärkekörner in den Chloroplasten sichtbar. Zusätzlich konnte die Bildung von reaktiven Sauerstoffspezies (ROS) eher dem Apoplasten zugeordnet werden, während die ROS-Erzeugung in  $\text{NO}_3^-$ -ernährten Pflanzen eher im Zellinneren aufzutreten schien.

Genexpressionsstudien unterstützten diese Aussagen. Die Genexpressionsstudien wurden in Kooperation mit Prof. E.-M. Aro an der Universität Turku, Finnland mit einem ca. 6500 Gene (1/4 des *A. thaliana* Genoms) umfassenden cDNA-Microarray durchgeführt. Als experimentelle Strategie wurde das "Loop-Design" gewählt. Auf diese Weise konnte sowohl N-form-abhängige als auch licht-abhängige differentielle Genexpression untersucht werden. Die Datenauswertung wurde Hypothese-getrieben durchgeführt, d.h. es wurde nicht nach den größten Unterschieden in der Genexpression gesucht, sondern im Vordergrund stand die

Suche nach Hinweisen auf regulierte Stoffwechselwege. Die wichtigsten differentiell exprimierten Gene wurden per Northern Blot Analyse überprüft.

In  $\text{NH}_4^+$ -ernährten Pflanzen waren die Gene, die für die Enzyme der  $\beta$ -Oxidation und die Phosphoenolpyruvat-Carboxykinase kodieren, hochreguliert. In  $\text{NO}_3^-$ -ernährten Pflanzen war eine Induktion der Gene für die Sedoheptulose-Bisphosphatase (ein Schlüsselenzym im Calvin-Zyklus) und die cytosolische Fructose-Bisphosphat-Aldolase zu finden. Diese Ergebnisse führten zu der oben genannten Hypothese, dass die  $\text{NH}_4^+$ -ernährten Pflanzen immer noch ihre Energiereserven aus den Oleosomen via  $\beta$ -Oxidation nutzten während die  $\text{NO}_3^-$ -ernährten Pflanzen schon den Wechsel der Energieversorgung zur Photosynthese vollzogen hatten.

Im Licht dieser Hypothese lassen sich nun die weiteren Ergebnisse erklären. Das heterogene Wachstum und die hohe Streuung der ROS-Entwicklung der  $\text{NH}_4^+$ -ernährten Pflanzen zeigt, dass der Umschaltprozess von der Energieversorgung aus den Oleosomen zur Photosynthese in den individuellen Pflanzen zum Zeitpunkt der Untersuchung unterschiedlich weit vorangetrieben war. Die  $\text{NO}_3^-$ -ernährten Pflanzen hatten dieses Umschalten einheitlich beendet.

Die ROS-Entwicklung in den Pflanzen war, zusätzlich zu der hohen Streuung in  $\text{NH}_4^+$ -ernährten Pflanzen, sehr unterschiedlich zwischen den beiden Ernährungsformen. In  $\text{NO}_3^-$ -ernährten Pflanzen war die ROS-Entwicklung licht-induziert und hauptsächlich auf das Gebiet direkt unter der Lichtquelle beschränkt. Die licht-induzierte ROS-Entwicklung zeigte in  $\text{NH}_4^+$ -ernährten Pflanzen eine starke Streuung und eine ungleichmäßige, systemische Ausbreitung, die nicht auf das Gebiet direkt unter dem Lichtleiter beschränkt war, sondern sich über das ganze Blatt zu erstrecken schien. Im Gegensatz zu  $\text{NO}_3^-$ -ernährten Pflanzen wurde die ROS-Bildung durch  $\text{CO}_2$ -Mangel nicht verstärkt. Allerdings war die Antwort auf Verwundung, z.B. beim Infiltrierungsprozess, sehr viel stärker. Außerdem wies der Einfluss von pH und Pufferkapazität auf die DCF-Fluoreszenz auf eine ROS-Quelle außerhalb der Zelle, also im Apoplasten, hin. Dies wurde auch durch den Effekt der starken Ausbreitung unterstützt wurde.

In früheren Versuchen der Arbeitsgruppe an *Phaseolus vulgaris* wurde unter Ammoniumernährung eine hohe Aktivität der Entgiftungsenzyme festgestellt. Dies traf für die hier benutzten *A. thaliana* nicht zu. Besonders gegensätzlich erschien die Induktion der GDP-Epimerase in  $\text{NO}_3^-$ -ernährten Pflanzen, die in der Ascorbatbiosynthese eine wichtige Rolle spielt. Alle diese Ergebnisse weisen auf eine geringere ROS-Entwicklung in den Zellen der Keimblätter von 15 Tage alten  $\text{NH}_4^+$ -ernährten Pflanzen hin.



Das Auftreten der unterschiedlichen Entwicklungsstadien in Abhängigkeit von der Stickstoffquelle führte zu folgenden Schlüssen: Es wurde offensichtlich, dass der Ursprung der Wachstumsreduzierung ein stickstoffabhängiges Signal sein muss, welches schon in einem frühen Stadium der Entwicklung auch unter Schwachlichtbedingungen auftritt. Dieses kann damit nicht von postulierten stickstoffinduzierten Effekten auf die Photosynthese, wie z.B. erhöhter Transport von Photosyntheseprodukten in die Wurzel oder hoher Energieaufwand für die Entgiftung von Photosynthese-induzierten Radikalen, ausgehen. Denn die Wachstumsreduzierung tritt auf, bevor die Photosynthese vollständig genutzt wird. Diese Ergebnisse bringen einen neuen Schwerpunkt in die Erforschung der N-form abhängigen Stoffwechselveränderungen, nämlich die Identifikation des Perzeptionsmechanismus sowie des Netzwerkes der Signalweiterleitung als Alternative zu den Modellen, die von der Beteiligung der Photosynthese ausgehen.



## Appendix

### A.1 Solutions

#### A.1.1 General solutions

##### 1x PBS

2.7 mM KCl  
1 mM KH<sub>2</sub>PO<sub>4</sub>  
10 mM NaH<sub>2</sub>PO<sub>4</sub>  
137 mM NaCl  
pH 7.1 with KOH

##### 1x SSC

150 mM NaCl  
15 mM Na-citrate  
pH 7.0

##### 10x blue loading buffer

20 % glycerol  
50 mM Tris pH 7.5  
10 mM EDTA  
0.25 % bromphenol blue  
0.25 % xylene cyanol  
in aqua dest

##### 10x TAE

400 mM Tris acetate  
10 mM EDTA  
pH 8.3

##### 50x Denhardt`s

1 % (w/v) Ficoll 400  
1 % (w/v) Polyvinylpyrrolidon K30  
1 % (w/v) BSA

##### DCF-DA

5 mM in EtOH

##### DCMU

10 mM in EtOH

##### TE

10 mM Tris-HCl pH 7.5  
1 mM EDTA pH 8.0

##### Tris-HCL

1M Tris base  
pH 7.5 with HCL

SHAM

40 mM SHAM in 5% v/v 1M NaOH  
 2.5 mM MES  
 Use 1:20 diluted (2mM)

SM

1 mM KCl  
 1 mM CaCl<sub>2</sub>  
 1 mM MgCl<sub>2</sub>

0.1M phosphate buffer

100 mM K<sub>2</sub>HPO<sub>4</sub>  
 100 mM KH<sub>2</sub>PO<sub>4</sub>  
 mix until pH 7.4

**A.1.2 Solutions for Northern blot experiments**sodium hydroxide

0,1 M in aqua dest.

10x MOPS-buffer

200 mM MOPS  
 50 mM Natriumacetate  
 1 mM EDTA  
 pH 7 with 10 M NaOH  
 autoclave

loading buffer (156 µl)

100 µl deionised formamide (100% v/v)  
 33.2 µl formaldehyde (37 % v/v)  
 15.6 µl 10x MOPS  
 5.2 µl H<sub>2</sub>O  
 2 µl ethidiumbromide (1% w/v)

20x SSC

300 mM Na<sub>2</sub>Citrat·2H<sub>2</sub>O  
 3 M NaCl  
 pH =7 with 10 M HCl  
 autoclave

30x SSC (100 ml):

450 mM Na<sub>2</sub>Citrat·2H<sub>2</sub>O  
 4.5 M NaCl  
 pH = 7 with 1 M HCl  
 autoclave

Natriumphosphate

1 M in aqua dest.  
 pH = 7 with 1 M HCl

N-Lauroylsarcosin-solution

10 % in aqua dest

sterile filtration through 0,45 µm Filter

Blocking-reagent-solution

10 % in P1-buffer

autoclave

High-SDS-buffer

50 % formamide (v/v)

5x SSC

50 mM Natriumphosphat

2 % Blocking-Reagent-solution

0.1 % N-Lauroylsarcosin-Lösung

243 mM SDS

store at -20 °C and preheat to 65 °C before use

Prehybridisationsolution

High-SDS-buffer

Hybridisationsolution

High-SDS-buffer

20 ng probe/ml

preheat to 100°C for 10min before first use

before each use afterwards denature solution 10 min at 68°C and cool on ice quickly

P1-buffer

100 mM Maleic acid

150 mM NaCl

200 mM NaOH

pH = 7 with 1 M HCl

autoclave

P2-buffer without antibody

use autoclaved flask

1 % blocking-reagent-solution

in P1-buffer

store at -20°C; reusable

P2-buffer with antibody

use autoclaved flask

1 % blocking-reagent-solution

1:10000 Anti-Dioxygenine-AP-Fab-Fragment-solution

P1-buffer

P3-buffer

100 mM Tris

100 mM NaCl

autoclave

## A.2 Primer sequences

Primer were obtained from MWG Biotech, Ebersberg, Germany

Name	Primer (forward /reverse)	Length [bp]	Tm [°C]	sequence
SP6	5'-CATTTAGGTGACACTATAG-3'		50.2	
T7	5'-TAATACGACTCACTATAGGG-3'		53.2	
AtACT2/8	5'-GGTGATGGTGTGTCT-3' 5'-ACTGAGCACAATGTTAC-3'	435	47.8 47.9	CDS
At1g75270 DHAR	5'-AATCGAAGAAAGATCGATGG-3' 5'-AGGAGGAGTCTTGAGTAGAAGG-3'	300	60.6 59.5	Sequencing data
At5g18170 GDH	5'-CTTCAAGTTAGCTGCTAGGC-3' 5'-AGCTTGCTAGGATCACAACC-3'	308	58.5 60.8	EST
At3g26650 GapA	5'-TCAACAACCTCTCTGTGAGTAACC-3' 5'-GATCGCTCTCCGTGTACC-3'	300	58.9 58.2	Sequencing data
At3g04790 Rpi	5'-TCTTCTCACCTTACGCTACG-3' 5'-AACAAGAGGAATCCCTAACG-3'	318	59.6 59.6	EST
At1g32060 PRK	5'-TCTACTTGACATTAGCAACG-3' 5'-TGAACCTTCATCGAACAGG-3'	284	59.4 61.3	Sequencing data
At5g38420 RuBisCo2b	5'-GGCTTCCTCTATGCTCTCC-3' 5'-CACTTGTTGTCGGAGTAAGG-3'	281	60.5 59.8	Sequencing data
At1g80300 AATP1	5'-GCCAAGTACATTCTTGTTCCG-3' 5'-ATGAAGCTCTCTCCATTTC-3'	305	55.3 55.3	EST
At4g16760 (on tube At3g14420) ACX 1	5'-CAGGATTGAAGTCTCTCACC-3' 5'-GCTTCCAGTACAACATCAGG-3'	475	58.8 59.7	EST
At3g55800 SBPase	5'-AATACACACTGCGATACACC-3' 5'-CATTCTTGAGTCTTGATGTTCC-3'	303	57.5 60.1	Sequencing data
At5g38410 RuBisCo3b	5'-GATTCCTTGTTGACTTCG-3' 5'-TGAAATGAGCAGAGATGAGC-3'	458	59.7 60.7	EST
At1g68010 HPR	5'-GATGAAAAAGGAAGCAATCC-3' 5'-CTAAGGCCTTTGAGTTGACG-3'	356	53.2 57.3	EST
At2g13360 AGT1	5'-TATAGACGGTCCGGAGATTG-3' 5'-GAAAAGAGAAAACATGAGAGTTG-3'	444	57.3 55.9	EST
At4g37930 SHM 1	5'-TGAAGCTGTTGATGAGAAGG-3' 5'-AGGAGATCCAGGACAAAGG-3'	500	60.6 60.6	EST
At3g14420 GOX	5'-AATGCTACGTGATGAGTTCCG-3' 5'-GGCCTTAAGAAAGAAGTAGCC-3'	311	55.3 57.9	EST

Appendix

At2g29490 GST 2	5'-ATTTTGATGAGGCTGTATGC- <sup>3</sup> 5'-CTCAAGGGTGATCAATTCG- <sup>3</sup>	464	53.2 54.5	EST
At4g38970 FBA plast	5'-TCTCTCAAAGAAACCAAAGG- <sup>3</sup> 5'-TCTCTAGCCCTATCGAATCC- <sup>3</sup>	494	58.5 59.8	EST
At5g50950-N2 fumarase	5'-TCTTGGTGAACCTTCTCTGC- <sup>3</sup> 5'-TTCTTTGTGAGCTCTTTTGG- <sup>3</sup>	379	59.6 59.6	CDS
At3g51840 ACX 4	5'-ACTCCAGCCTCTACATTTCC- <sup>3</sup> 5'-ACTTCTCCTTCTGTGCTTCT- <sup>3</sup>	369	59.7 57.2	CDS
At3g21720 ICL	5'-TGAGCAGAGAAGAGAGGACA- <sup>3</sup> 5'-CAGAAGCGAGGACAAACTC- <sup>3</sup>	400	60.5 60.1	CDS
At2g33150 PED 1	5'-GGCATTGATAGAGAAGACGA- <sup>3</sup> 5'-TTACCAGCAGCAGTAGCA- <sup>3</sup>	447	59.4 59.8	CDS
At3g06860 MFP 2	5'-CTGGTTGGATTTGGTGTG- <sup>3</sup> 5'-TGATTCCCTCCTCTGTAAGGT- <sup>3</sup>	393	59.9 57.7	CDS
At5g03860 MS	5'-CAGAGACGGTGATTGGAG- <sup>3</sup> 5'-CCATTTTGGGGAGATAGAAG- <sup>3</sup>	442	59.3 59.9	CDS
At4g28220 Ndb 1	5'-GAAGAGTTAGAAGGCGTGGT- <sup>3</sup> 5'-AACCCAGTCTCCAGGTAGTT- <sup>3</sup>	398	59.9 59.1	CDS
At1g77760 NR1	5'- CGGTTATGGCTCTCGTCTTC - <sup>3</sup> 5'- CTCGTTCCCTTCTCCTCGCT - <sup>3</sup>	164	51.4 46.9	CDS
At1g37130 NR2	5'-AGGCTTTTTGACGACTTAACG- <sup>3</sup> 5'-TCCGGTTTACCAAATTATCCA- <sup>3</sup>	407	55.9 54	EST
At2g29450 GST	5'-TATTGCTTGCCCAACCTCTC- <sup>3</sup> 5'-AAAGCCCTTTGCTTCTTGCT- <sup>3</sup>	402	57.3 55.3	EST
At4g37870 PepCK	5'-GAGAACACACGTGCTGCCTA- <sup>3</sup> 5'-CTTCAAGAGACTGCCCGAAT- <sup>3</sup>	428	59.4 57.3	EST
At1g14150 PsbQ	5'-ATGAGCTCCTCACCACCAC- <sup>3</sup> 5'-TAATCATTCCGGCGACTCTC- <sup>3</sup>	434	59.4 57.3	EST
At5g28840 epimerase	5'-GGAGCATAACATACAAGGA- <sup>3</sup> 5'-TCTGGATAAAACCCATACCA- <sup>3</sup>	300	57.5 59.2	CDS

### A.3 List of differentially expressed genes encoding for enzymes

Columns 4-6 show average values of three biological replicates. LL, HL denote low light and high light treatments, respectively.

Systematic name	Gene accession	$\text{NH}_4^+ / \text{NO}_3^-$ LL	$\text{NH}_4^+ / \text{NO}_3^-$ HL	$\text{NO}_3^- : \text{HL} /$ LL	$\text{NH}_4^+ : \text{HL} /$ LL
701501444	At1g73480 hydrolase	1.02	1.51	2.68	3.45
701502411	At3g57520 glycosyl hydrolase family 36	1.22	0.39	5.34	1.23
701499216	At1g62660 glycosyl hydrolase family 32	1.33	1.17	2.36	1.35
701503118	At2g31750 glycosyltransferase family	1.34	1.09	2.56	1.73
701681638	At4g27820 glycosyl hydrolase family 1 beta- glucosidase	1.21	1.11	2.01	1.49
701494050	At5g64570 glycosyl hydrolase family 3	1.06	0.89	1.90	1.34
701501945	At1g68560 glycosyl hydrolase family 31	0.64	0.77	0.42	0.55
701500448	At2g38180 GDSL- motif lipase/hydrolase	0.91	1.14	0.59	0.84
701553896	At3g18080 glycosyl hydrolase family 1	0.63	0.83	0.48	0.70
701557689	At1g02640 glycosyl hydrolase family 3	0.94	0.58	1.18	0.85
701502945	At3g13750 glycosyl hydrolase family 35	0.40	0.28	1.44	0.84
701497206	At5g49360 glycosyl hydrolase family 3	1.09	0.58	1.50	0.73

Systematic name	Gene accession	$\text{NH}_4^+ / \text{NO}_3^-$ LL	$\text{NH}_4^+ / \text{NO}_3^-$ HL	$\text{NO}_3^- : \text{HL} /$ LL	$\text{NH}_4^+ : \text{HL} /$ LL
701501596	At3g23530 cyclopropane synthase	0.99	0.72	1.94	1.42
701502568	At3g05840 shaggy-related protein kinase gamma	1.01	0.94	1.62	1.52
701500648	At1g28600 lipase	1.39	1.33	1.90	1.44
701499207	At3g02720 protease-related similar to Intracellular	0.81	0.66	1.65	1.29



Appendix

	Protease				
701497322	At5g17380 2-hydroxyphytanoyl-CoA lyase-related protein	1.53	0.81	2.52	1.23
701931650	At5g22300 Nitrilase 4	0.85	0.59	4.16	1.28
701500635	At2g17120 delta-8 sphingolipid desaturase	0.99	0.73	1.82	1.34
701500656	At4g20860 FAD-linked oxidoreductase family	1.16	0.86	3.08	1.75
701672081	At4g34920 expressed protein phospholipase C	0.93	1.07	1.61	1.77
701673124	At1g06430 FtsH protease	0.86	0.79	1.60	1.37
701546633	At3g22890 ATP sulfurylase	0.87	0.74	1.93	1.63
701665720	At1g544505 protein phosphatase 2A 72 kDa regulatory subunit	1.45	1.37	2.06	2.20
701667156	At1g76680 12-oxophytodienoate reductase	2.24	1.15	8.20	2.89
701498404	At5g43450 2-oxoglutarate-dependent dioxygenase	1.23	1.02	2.21	1.94
701553802	At4g20830 FAD-linked oxidoreductase family	1.54	0.99	3.82	2.25
701500478	At5g02800 protein kinase family	0.86	1.23	0.58	0.78
701497017	At1g25230 calcineurin-like phosphoesterase family	0.92	0.79	0.60	0.56
701500465	At5g27450 mevalonate kinase	0.93	1.25	1.52	1.95
701666116	At1g09130 ATP-dependent Clp protease proteolytic subunit	1.12	1.06	1.39	1.62
701546136	At4g30210 NADPH-ferrihemoprotein reductase	1.14	0.91	2.12	1.92
701931423	At5g22650 histone deacetylase	1.23	1.95	1.12	1.25
701558296	At1g73990 SppA protease IV (SppA)	1.57	1.08	1.83	1.27

701558322	At5g51070 ATP-dependent Clp protease ATP-binding subunit (ClpD),	2.01	1.01	1.61	1.04
701516734	At5g51070 ATP-dependent Clp protease ATP-binding subunit	1.58	1.05	1.54	0.97
701495032	At1g58080 ATP phosphoribosyl transferase	0.55	0.70	0.97	1.20
701557118	At2g29340 short-chain dehydrogenase/reductase family	1.23	1.03	1.91	1.67
701501603	At1g48600 phosphoethanolamine N-methyltransferase	0.37	0.29	0.97	1.07

Systematic name	Gene accession	$\text{NH}_4^+ / \text{NO}_3^-$ LL	$\text{NH}_4^+ / \text{NO}_3^-$ HL	$\text{NO}_3^- : \text{HL} /$ LL	$\text{NH}_4^+ : \text{HL} /$ LL
701548909	At4g34050 caffeoyl-CoA 3-O-methyltransferase	1.33	1.31	2.08	2.32
701493334	At1g15950 cinnamoyl-CoA reductase	0.88	0.88	1.70	1.69
701496993	At4g30470 cinnamoyl-CoA reductase	1.02	2.41	1.50	2.02
701498658	At1g21130 O-methyltransferase 1	0.52	0.41	1.53	1.11
701500017	At1g21100 O-methyltransferase 1	0.75	0.57	1.59	1.12
701495940	At1g21110 O-methyltransferase 1	0.71	0.52	1.31	1.05

Systematic name	Gene accession	$\text{NH}_4^+ / \text{NO}_3^-$ LL	$\text{NH}_4^+ / \text{NO}_3^-$ HL	$\text{NO}_3^- : \text{HL} /$ LL	$\text{NH}_4^+ : \text{HL} /$ LL
701547323	At4g39980 2-dehydro-3-deoxyphosphoheptonate aldolase	0.91	0.82	1.68	1.19
701674073	At4g10120 sucrose-phosphate synthase	1.01	0.55	3.06	1.62
701498532	At3g16850 polygalacturonase	0.75	0.89	0.58	0.82
701932327	At4g26080 protein phosphatase ABI1	1.60	1.87	1.56	2.22

Appendix

701500484	At4g11260 phosphatase	0.84	0.59	0.88	0.74
701495390	At4g37980 mannitol dehydrogenase	0.57	0.44	1.14	1.06

Systematic name	Gene accession	$\text{NH}_4^+ / \text{NO}_3^-$ LL	$\text{NH}_4^+ / \text{NO}_3^-$ HL	$\text{NO}_3^- : \text{HL} /$ LL	$\text{NH}_4^+ : \text{HL} /$ LL
701956654	At4g27440 protochlorophyllid e reductase B	0.92	1.34	0.26	0.44
701496082	At4g27440 protochlorophyllid e reductase B	1.00	1.24	0.29	0.46
701498367	At4g30270 xyloglucan endotransglycosyl ase	8.55	1.79	3.39	0.80
701495136	At2g06850 xyloglucan endotransglycosyl ase	1.30	1.04	0.60	0.56
701558475	At1g14890 pectinesterase family	1.89	1.74	1.11	0.96
701495964	At5g57560 xyloglucan endotransglycosyl ase	2.96	1.22	1.34	0.53

## A.4 List of differentially expressed genes encoding for other proteins

Columns 4-6 show average values of three biological replicates. LL, HL denote low light and high light treatments, respectively.

Systematic name	Gene accession	$\text{NH}_4^+ / \text{NO}_3^-$ LL	$\text{NH}_4^+ / \text{NO}_3^-$ HL	$\text{NO}_3^- : \text{HL} /$ LL	$\text{NH}_4^+ : \text{HL} /$ LL
701557640	At5g56000 heat shock protein 81.4	<b>1.74</b>	<b>1.85</b>	<b>4.14</b>	<b>3.78</b>
701500113	At5g56010 heat shock protein	<b>1.67</b>	<b>1.88</b>	<b>5.33</b>	<b>4.15</b>
701558289	At3g51910 heat shock transcription factor family	1.06	1.21	<b>1.77</b>	1.35
701956591	At5g52640 heat shock protein 81-1	0.98	1.10	<b>2.14</b>	<b>2.03</b>
701498339	At3g12580 heat shock protein hsp70	1.52	1.59	<b>3.95</b>	<b>4.11</b>
701956533	At5g52310 low-temperature-induced protein 78	1.23	1.92	<b>2.97</b>	<b>2.62</b>
701495414	At5g52310 low-temperature-induced protein 78	1.45	<b>2.87</b>	<b>2.52</b>	<b>3.85</b>
701496580	At5g52640 heat shock protein 81-1	1.19	1.07	<b>2.59</b>	<b>2.06</b>
701549143	At1g79930 putative heat-shock protein	1.42	1.24	<b>2.03</b>	<b>2.08</b>
701956440	At3g23990 chaperonin (CPN60/HSP60)	<b>1.97</b>	<b>1.65</b>	<b>1.64</b>	1.55

Systematic name	Gene accession	$\text{NH}_4^+ / \text{NO}_3^-$ LL	$\text{NH}_4^+ / \text{NO}_3^-$ HL	$\text{NO}_3^- : \text{HL} /$ LL	$\text{NH}_4^+ : \text{HL} /$ LL
701500185	At1g04270 40S ribosomal protein S15	<b>1.67</b>	<b>1.86</b>	1.20	1.17
701502936	At1g59359 40S ribosomal protein S2	<b>1.52</b>	<b>2.01</b>	1.00	1.24
701495375	At1g57860 60S ribosomal protein L21	<b>1.55</b>	<b>1.71</b>	1.10	1.29

Appendix

701558128	At1g04480 60S ribosomal protein L23	<b>1.57</b>	<b>1.91</b>	1.17	1.33
701495062	At4g31700 40S ribosomal protein S6	<b>1.84</b>	<b>2.10</b>	1.11	1.18
701495058	At4g15000 60S ribosomal protein L27	<b>1.47</b>	<b>1.83</b>	1.10	1.35
701501551	At3g53870 40S ribosomal protein S3	<b>1.55</b>	<b>1.84</b>	1.13	1.42
701501452	At1g26880 60S ribosomal protein L34	1.29	<b>1.64</b>	0.95	1.22
701557921	At2g37270 40S ribosomal protein S5	1.44	<b>1.99</b>	1.10	1.18
701515308	At5g02450 60S ribosomal protein L36	<b>1.62</b>	<b>1.82</b>	1.09	1.21
701498480	At3g49910 60S ribosomal protein L26	1.36	<b>1.72</b>	1.05	1.11
701493452	At5g65220 ribosomal protein L29p family	<b>0.61</b>	<b>0.58</b>	<b>0.56</b>	<b>0.61</b>
701551951	At2g39460 60S ribosomal protein L23A	<b>1.79</b>	1.37	1.12	1.17
701674815	At1g09760 U2 small nuclear ribonucleoprotein A	<b>4.01</b>	1.37	<b>1.89</b>	<b>0.67</b>

Systematic name	Gene accession	$\text{NH}_4^+ / \text{NO}_3^-$ LL	$\text{NH}_4^+ / \text{NO}_3^-$ HL	$\text{NO}_3^- : \text{HL} /$ LL	$\text{NH}_4^+ : \text{HL} /$ LL
701514737	At4g27040 SNF8 like protein	0.99	1.04	<b>1.78</b>	1.39
701501446	At3g18290 zinc finger protein	1.27	1.13	<b>1.62</b>	1.25
701500288	At1g51700 Dof zinc finger protein	0.99	0.90	<b>2.17</b>	<b>1.80</b>
701558002	At2g18160 bZIP family transcription factor	1.21	0.94	<b>1.95</b>	<b>1.54</b>
701500056	At2g27580 zinc finger protein - related	1.41	1.21	<b>2.00</b>	<b>1.62</b>
701495069	At2g46830 MYB- related transcription factor (CCA1)	1.16	0.90	<b>2.17</b>	1.41
701503033	At1g68520 CONSTANS B-box zinc finger family	0.78	1.03	<b>0.32</b>	<b>0.40</b>
701499558	At2g25900 CCCH- type zinc finger protein -related	0.75	<b>0.60</b>	<b>0.63</b>	<b>0.57</b>
701548835	At5g08330 TCP	0.87	0.93	<b>0.65</b>	0.82

	family transcription factor				
701667258	At3g19910 C3HC4-type zinc finger protein family	1.15	1.07	<b>0.51</b>	<b>0.59</b>
701498338	At5g52510 scarecrow-like transcription factor 8 (SCL8)	1.09	1.29	1.22	<b>1.60</b>
701930805	At2g46270 G-box binding bZIP transcription factor	1.10	<b>1.65</b>	<b>1.65</b>	<b>2.34</b>
701498648	At1g63840 RING-H2 finger protein	1.24	1.46	<b>2.34</b>	<b>1.86</b>
701672661	At5g15850 Zinc finger protein CONSTANS-LIKE 1 (COL1)	1.37	1.09	1.41	<b>1.67</b>
701502975	At1g78600 CONSTANS B-box zinc finger family protein	0.73	<b>0.48</b>	1.25	1.05
701495358	At4g09460 myb family transcription factor	0.68	<b>0.40</b>	0.69	0.84
701501438	At1g06040 salt-tolerance protein	1.05	1.01	<b>2.38</b>	<b>2.22</b>

Systematic name	Gene accession	$\text{NH}_4^+ / \text{NO}_3^-$ / LL	$\text{NH}_4^+ / \text{NO}_3^-$ / HL	$\text{NO}_3^- : \text{HL} / \text{LL}$	$\text{NH}_4^+ : \text{HL} / \text{LL}$
701503269	At3g14650 cytochrome P450	1.11	0.90	<b>2.23</b>	1.29
701497314	At3g14660 cytochrome P450	1.37	0.95	<b>2.62</b>	<b>1.68</b>
701558580	At3g14690 cytochrome P450	1.30	0.93	<b>2.55</b>	<b>1.95</b>
701547489	At2g46650 cytochrome b5	1.23	1.24	<b>1.89</b>	<b>1.70</b>
701674596	At3g61880 cytochrome P450	0.81	0.84	<b>0.66</b>	0.90
701669957	At3g14690 cytochrome P450	1.20	1.19	<b>2.19</b>	<b>1.88</b>
701552072	At4g12320 cytochrome P450	0.88	1.05	<b>1.75</b>	<b>1.95</b>
701495327	At2g34500. cytochrome P450	<b>0.65</b>	1.10	0.72	<b>0.59</b>

Systematic name	Gene accession	$\text{NH}_4^+ / \text{NO}_3^-$ / LL	$\text{NH}_4^+ / \text{NO}_3^-$ / HL	$\text{NO}_3^- : \text{HL} / \text{LL}$	$\text{NH}_4^+ : \text{HL} / \text{LL}$
701501654	At1g72900 disease resistance protein (TIR-NBS class)	<b>1.91</b>	<b>1.53</b>	<b>2.76</b>	<b>2.12</b>
701502434	At5g05410 DRE binding protein (DREB2A)	1.29	1.44	<b>2.68</b>	<b>2.75</b>
701500615	At1g08570 thioredoxin family	0.83	<b>0.66</b>	<b>2.12</b>	<b>1.92</b>

Appendix

701551724	At2g38230 SOR1	1.27	0.97	<b>3.06</b>	<b>1.71</b>
701496877	At1g72930 disease resistance protein (TIR class)	0.95	<b>0.67</b>	<b>2.37</b>	<b>1.73</b>
701555815	At1g30360 ERD4 protein	<b>0.49</b>	<b>0.53</b>	0.84	0.87
701497022	At5g18600 glutaredoxin protein family	0.70	<b>0.43</b>	0.93	0.96
701545713	At3g12610 DNA-damage- repair/toleration protein	<b>0.59</b>	1.00	0.72	0.91
701932325	At5g15960 stress-induced protein KIN1	<b>0.37</b>	0.89	1.07	<b>2.84</b>
701503223	At4g02380 late embryogenesis abundant protein family	1.09	0.78	<b>5.79</b>	<b>2.35</b>
701668715	At5g63790 No apical meristem (NAM) protein family	<b>2.49</b>	1.10	<b>3.24</b>	<b>2.95</b>
701668489	At1g01720 No apical meristem (NAM) protein family	<b>1.72</b>	1.09	<b>2.68</b>	<b>1.86</b>
701931117	At5g36910 thionin (THI2.2)	0.74	<b>0.31</b>	<b>4.57</b>	<b>1.98</b>
701497349	At2g40000 nematode- resistance protein - related	1.35	<b>0.66</b>	<b>3.00</b>	<b>1.54</b>

Systematic name	Gene accession	$\text{NH}_4^+ / \text{NO}_3^-$ LL	$\text{NH}_4^+ / \text{NO}_3^-$ HL	$\text{NO}_3^- : \text{HL} /$ LL	$\text{NH}_4^+ : \text{HL} /$ LL
701514381	At4g17530 ras- related small GTP- binding protein RAB1c	<b>1.62</b>	1.17	<b>2.46</b>	<b>1.50</b>
701500447	At5g46250 RNA recognition motif (RRM)	1.10	1.31	<b>1.93</b>	<b>1.99</b>
701500731	At3g61060 F-box protein (lectin- related)	0.94	<b>0.55</b>	<b>2.25</b>	1.21
701499801	At1g09340 RNA- binding protein	1.06	0.99	<b>1.79</b>	1.42
701499859	At1g09340 RNA- binding protein	0.92	0.76	<b>1.88</b>	1.41
701498615	At1g09340 RNA- binding protein - related	0.89	0.84	<b>1.87</b>	1.37
701956526	At1g22740 Ras- related GTP- binding protein (Rab7)	<b>0.62</b>	1.57	<b>0.57</b>	0.70

701493455	At1g01300 chloroplast nucleoid DNA binding protein -related	0.88	1.00	<b>0.58</b>	0.78
701493420	At5g20010 GTP- binding nuclear protein (RAN-1)	<b>1.88</b>	<b>1.95</b>	0.99	1.10
701497326	At1g11650 RNA binding protein 45 (RBP45)	<b>1.98</b>	1.49	1.43	1.08
701558431	At1g09140 arginine/serine-rich splicing factor, atSRp30 SF2/ASF splicing modulator Srp30	1.20	1.77	1.31	<b>1.86</b>
701495694	At4g30960 CBL- interacting protein kinase 6	1.45	<b>1.85</b>	1.08	1.20
701931136	At5g03470 B' regulatory subunit of PP2A (AtB'alpha)	<b>0.42</b>	1.46	0.82	1.17
701496931	At4g11420 initiation factor 3a (translation initiation)	1.25	<b>1.73</b>	1.05	1.00

Systematic name	Gene accession	$\text{NH}_4^+ / \text{NO}_3^-$ LL	$\text{NH}_4^+ / \text{NO}_3^-$ HL	$\text{NO}_3^- : \text{HL} /$ LL	$\text{NH}_4^+ : \text{HL} /$ LL
701499954	At4g17340 major intrinsic protein (MIP) family	1.08	0.96	<b>3.07</b>	<b>1.86</b>
701676647	At1g64500 peptide transporter -related	1.05	0.70	<b>3.84</b>	<b>2.05</b>
701553466	At4g31390 ABC transporter -related	1.16	1.06	<b>1.97</b>	<b>1.79</b>
701498685	At2g34660 glutathione S- conjugate ABC transporter (AtMRP2)	<b>1.60</b>	1.16	<b>2.91</b>	<b>1.96</b>
701493691	At2g22500 mitochondrial carrier protein family	1.08	0.73	<b>1.99</b>	<b>1.72</b>
701502814	At1g52190 peptide transporter -related	0.68	0.82	<b>0.61</b>	0.78
701931818	At2g38170 calcium exchanger (CAX1)	0.76	0.82	<b>0.54</b>	0.77
701497330	At1g72180 leucine- rich repeat transmembrane protein kinase	0.97	1.05	<b>0.60</b>	<b>0.60</b>
701495078	At5g55230 microtubule associated protein (MAP65/ASE1) family	0.79	1.21	<b>0.53</b>	0.77



Appendix

701956677	At2g38540 nonspecific lipid transfer protein 1 (LTP 1)	1.13	<b>1.82</b>	1.09	<b>1.68</b>
701496876	At2g45960 plasma membrane intrinsic protein 1B	0.78	0.86	<b>1.50</b>	<b>1.69</b>
701670768	At4g36670 mannitol transporter	0.57	0.85	<b>0.67</b>	<b>0.42</b>
701500275	At1g12110 putative NPK1-related protein kinase 2	<b>2.36</b>	<b>1.81</b>	0.88	0.73
701496871	At1g01620 plasma membrane intrinsic protein 1c	<b>1.68</b>	<b>2.14</b>	1.00	1.27
701932108	At1g12110 putative NPK1-related protein kinase 2	<b>2.21</b>	<b>2.32</b>	1.09	0.85
701499133	At1g59870 ABC transporter family protein	0.96	<b>0.58</b>	<b>1.65</b>	1.06
701664994	At5g40890 CLC-a chloride channel protein	<b>0.58</b>	1.06	0.87	1.36
701546333	At4g23400 major intrinsic protein (MIP) family	<b>0.47</b>	0.95	0.74	0.88
701956506	At3g50970 dehydrin (Xero2)	1.15	<b>1.86</b>	<b>2.85</b>	<b>2.22</b>
701498356	At5g54670 kinesin-like protein C (katC)Protontransport	<b>3.62</b>	1.35	<b>2.11</b>	0.72
701498966	At4g36640 sec14 cytosolic factor family (phosphoglyceride transfer protein family)	0.94	1.17	<b>1.93</b>	1.38
701495160	At3g08530 clathrin heavy chain	0.80	0.86	<b>0.55</b>	0.78
701494908	At4g12360 protease inhibitor/seed storage/lipid transfer protein (LTP) family	<b>0.61</b>	<b>0.55</b>	<b>0.29</b>	<b>0.30</b>
701549552	At5g49740 ferric reductase-like transmembrane component family	<b>0.58</b>	0.79	<b>1.75</b>	<b>1.53</b>
701498472	At5g20230 plastocyanin-like domain	<b>3.45</b>	0.84	<b>3.73</b>	1.04
701517025	At1g76100 plastocyanin identical to plastocyanin	0.74	0.99	<b>0.63</b>	0.75
701495057	At2g26560 patatin	1.29	<b>0.57</b>	<b>2.91</b>	1.17
701494944	At2g37170 plasma membrane intrinsic protein 2B	<b>0.68</b>	0.95	1.37	<b>2.02</b>

Systematic name	Gene accession	$\text{NH}_4^+ / \text{NO}_3^-$ LL	$\text{NH}_4^+ / \text{NO}_3^-$ HL	$\text{NO}_3^- : \text{HL} /$ LL	$\text{NH}_4^+ : \text{HL} /$ LL
701495230	At3g04730 auxin-responsive protein IAA16	1.33	1.15	<b>1.73</b>	1.47
701494074	At1g76520 auxin efflux carrier protein family	<b>2.28</b>	1.33	<b>2.38</b>	1.33
701495725	At2g33830 auxin-regulated protein	1.03	0.79	<b>0.57</b>	<b>0.51</b>
701557993	At5g61590 ethylene responsive element binding factor	0.78	0.84	0.77	<b>0.62</b>
701553336	At2g21210 auxin-induced	<b>0.30</b>	0.79	0.73	1.01
701493846	At5g22060 DnaJ protein	1.14	1.06	<b>2.53</b>	<b>1.68</b>
701545457	At5g42020 luminal binding protein 2 precursor (BiP-2)	1.41	1.35	<b>1.79</b>	<b>1.96</b>
701557850	At4g02890 polyubiquitin (UBQ14)	<b>1.80</b>	1.36	<b>2.03</b>	1.37
701495453	At5g49480 sodium-inducible calcium-binding protein	1.25	1.06	<b>9.97</b>	<b>5.38</b>

Systematic name	Gene accession	$\text{NH}_4^+ / \text{NO}_3^-$ LL	$\text{NH}_4^+ / \text{NO}_3^-$ HL	$\text{NO}_3^- : \text{HL} /$ LL	$\text{NH}_4^+ : \text{HL} /$ LL
701499107	At5g09440 expressed protein phi-1	1.50	0.72	<b>2.77</b>	<b>1.64</b>
701498680	At1g01470 expressed protein	<b>2.13</b>	1.88	<b>3.37</b>	<b>2.86</b>
701498659	At1g08630 expressed protein	<b>2.41</b>	1.35	<b>2.73</b>	1.08
701495734	At5g61820 expressed protein MtN19	<b>3.05</b>	<b>1.74</b>	<b>7.97</b>	<b>3.47</b>
701503142	At5g25270 expressed protein Scythe protein	1.60	0.99	<b>3.76</b>	<b>2.04</b>
701496763	At4g08950 phi-1 phosphate- induced protein	<b>4.57</b>	1.26	1.52	<b>0.40</b>
701501741	At1g35140 phosphate-induced (phi-1) protein	<b>2.43</b>	0.89	1.21	<b>0.61</b>
701498676	At5g64260 phi-1-related protein	<b>3.74</b>	<b>1.92</b>	0.98	<b>0.57</b>
701551684	At3g63160 expressed protein	0.68	0.96	<b>0.58</b>	0.70

Appendix

701667383	At3g48360 expressed protein MEL-26	0.09	<b>0.66</b>	<b>0.42</b>	0.95
701498536	At5g46730 glycine-rich protein	0.86	1.29	<b>0.45</b>	<b>0.62</b>
701555689	At5g65660 proline-rich protein	0.79	0.98	<b>0.59</b>	0.68
701500086	At5g02380 metallothionein 2b	<b>1.85</b>	<b>1.62</b>	1.37	1.19
701549284	At3g09390 metallothionein	<b>2.17</b>	1.03	1.36	1.20
701550916	At5g48540 33 kDa secretory protein	0.81	0.67	<b>1.86</b>	1.20
701551236	At5g64620 invertase/pectin methylesterase inhibitor	1.12	1.27	0.94	<b>0.57</b>
701495939	At5g44020 vegetative storage protein	1.17	0.90	<b>0.57</b>	<b>0.48</b>
701667793	At2g32240 myosin heavy chain	0.98	0.92	<b>2.93</b>	<b>2.53</b>
701495006	At5g08120 myosin heavy chain- related protein	0.85	0.90	<b>0.65</b>	0.84
701498459	At3g15356 lectin -related	0.87	<b>0.26</b>	<b>6.52</b>	<b>1.80</b>
701546851	At1g55960 membrane related protein CP5	0.99	1.20	<b>2.60</b>	<b>1.73</b>
701558042	At3g52470 harpin-induced protein 1 family (HIN1)	<b>0.64</b>	<b>0.60</b>	<b>1.84</b>	1.39
701499092	At3g11660 harpin-induced protein 1 family (HIN1)	0.99	0.83	<b>1.76</b>	1.36

Systematic name	Gene accession	$\text{NH}_4^+ / \text{NO}_3^-$ LL	$\text{NH}_4^+ / \text{NO}_3^-$ HL	$\text{NO}_3^- : \text{HL} /$ LL	$\text{NH}_4^+ : \text{HL} /$ LL
701547044	At1g74940 senescence- associated protein - related	0.80	1.22	<b>0.53</b>	<b>0.58</b>
701502110	At5g46700 senescence- associated protein	1.47	<b>2.00</b>	0.72	1.18
701496169	At1g74670 GAST1-related protein	<b>0.49</b>	<b>0.56</b>	<b>0.31</b>	<b>0.45</b>
701502422	At1g74560 SET protein, phosphatase 2A inhibitor	1.49	<b>1.81</b>	1.00	1.10
701932081	At2g28950 expansin	1.40	1.00	0.75	<b>0.47</b>

## A.5 Kits, chemicals and enzymes

### A.5.1 Kits

Epoxy embedding medium kit	Fluka, Buchs, Switzerland
RNeasy Plant Mini Kit	Qiagen, Hilden Germany
QIAquick PCR Purification Kit	Qiagen, Hilden, Germany
DYEnamic ET Dye Terminator Cyclor sequencing kit	GE Healthcare, Freiburg, Germany

### A.5.2 Chemicals

Acetone	Roth, Karlsruhe, Germany
Agarose	Serva, Heidelberg, Germany
BCECF	Invitrogen, Karlsruhe, Germany
Blocking-Reagent-solution	Roche, Mannheim, Germany
Bromocresol purple	Fluka, Buchs, Switzerland
Cacodylic acid	Fluka, Buchs, Switzerland
CDP Star	Roche, Mannheim, Germany
Chloroform	Roth, Karlsruhe, Germany
Cy3-dUTP/Cy5-dUTP (1 mM)	GE Healthcare, Freiburg, Germany
DCF-DA	Sigma-Aldrich, Munich, Germany
10x DIG-dNTP-Label-Mix	Roche, Mannheim, Germany
DMSO	Fluka, Buchs, Switzerland
dNTP mix	Promega, Mannheim, Germany
DTT	Invitrogen, Karlsruhe, Germany
EDTA	Roth, Karlsruhe, Germany
Ethanol	Walter Kiel, Germany
Ethidiumbromide	Sigma, Taufkirchen, Germany
5 x First Strand Reaction Buffer	Invitrogen, Karlsruhe, Germany
Formaldehyde	Roth, Karlsruhe, Germany
deion. Formamide	Roth, Karlsruhe, Germany
Glycerin	AppliChem, Darmstadt, Germany
H <sub>2</sub> O <sub>2</sub>	Merck Darmstadt, Germany
HCl	Merck Darmstadt, Germany
HEPES	Sigma, Taufkirchen, Germany
Maleic acid	Roth, Karlsruhe, Germany
MES	Sigma, Steinkirchen, Germany
MOPS	Roth, Karlsruhe, Germany
Nitroblue tetrazolium	Biomol, Hamburg, Germany
N-Lauroylsarcosin-Lösung	Sigma, Steinkirchen, Germany
Plant agar	Sigma, Steinkirchen, Germany
PCR mastermix	Promega, Mannheim, Germany
Salicylhydroxamic acid,	Aldrich, Steinheim, Germany
SDS	Roth, Karlsruhe, Germany
Sodium acetate	Roth, Karlsruhe, Germany
Sodium citrate	Merck Darmstadt, Germany
Sodium hydroxyl pellets	Merck Darmstadt, Germany
Sodium hypochlorite	Walter, Kiel, Germany
TBE Tris-Borat-EDTA-Puffer	Merck Darmstadt, Germany

Trichloroacetic acid	Roth, Karlsruhe, Germany
Tris base	Merck Darmstadt, Germany
Tween	Roth, Karlsruhe, Germany
Ca(NO <sub>3</sub> ) <sub>2</sub>	Merck Darmstadt, Germany
CaCl <sub>2</sub>	Merck Darmstadt, Germany
CuSO <sub>4</sub>	Merck Darmstadt, Germany
Fe-Na-EDTA	Merck Darmstadt, Germany
H <sub>3</sub> BO <sub>3</sub>	Merck Darmstadt, Germany
KCl	Sigma Taufkirchen, Germany
KH <sub>2</sub> PO <sub>4</sub>	Merck Darmstadt, Germany
K <sub>2</sub> SO <sub>4</sub>	Merck Darmstadt, Germany
MgCl <sub>2</sub>	Merck Darmstadt, Germany
MgSO <sub>4</sub>	Merck Darmstadt, Germany
MnSO <sub>4</sub>	Merck Darmstadt, Germany
NaCl	Merck Darmstadt, Germany
NaH <sub>2</sub> PO <sub>4</sub>	Merck Darmstadt, Germany
NaHCO <sub>3</sub>	Merck Darmstadt, Germany
(NH <sub>4</sub> ) <sub>6</sub> Mo <sub>7</sub> O <sub>24</sub>	Merck Darmstadt, Germany
(NH <sub>4</sub> ) <sub>2</sub> SO <sub>4</sub>	Merck Darmstadt, Germany
ZnSO <sub>4</sub>	Merck Darmstadt, Germany

### A.5.3 Enzymes

Catalase from bovine liver	Sigma, Steinkirchen, Germany
DNase	Qiagen, Hilden Germany
Omniscript	Qiagen, Hilden Germany
Superscript II (200 U/μl)	Invitrogen, Karlsruhe, Germany
RNase inhibitor (30 U/μl)	Invitrogen, Karlsruhe, Germany
PolyA, 10 mg/ml	Roche, Mannheim, Germany
yeast tRNA, 10 mg/ml	Roche, Mannheim, Germany
1kb marker	Promega, Mannheim, Germany
HindIII digested λ phage DNA	Promega, Mannheim, Germany



## References

- ABRC (Arabidopsis Biological Resource Center) (2004) Handling *Arabidopsis* plants and seeds. <http://www.biosci.ohio-state.edu/~plantbio/Facilities/abrc/handling.htm>
- Affourtit C, Krab K, Moore AL (2001) Control of plant mitochondrial respiration. *Biochim. Biophys. Acta* 1504: 58-69
- Afzal M, Matsugo S, Sasai M, Xu B, Aoyoma K, Takeuchi T (2003) Method to overcome photoreaction, a serious drawback to the use of dichlorofluorescein in evaluation of reactive oxygen. *Biochem. Biophys. Res. Commun.* 304: 619-24
- Andrews M (1986) The partitioning of nitrate assimilation between root and shoot of higher plants. *Plant Cell Environ.* 9: 511-519
- Backhausen JE, Kitzmann C, Scheibe R (1994) Competition between electron acceptors in photosynthesis: Regulation of the malate valve during CO<sub>2</sub> assimilation, nitrite reduction. *Photosynth. Res.* 42: 75-86
- Bass DA, Parce JW, Dechatelet LR, Szejda P, Seeds MC Thomas M (1983) Flow Cytometric Studies of oxidative Product Formation by Neutrophils: A Graded Response to Membrane Stimulation. *J. Immunol.* 130: 1910–1917.
- Batandier C, Fontaine E, Kériel C, Leverve XM (2002) Determination of mitochondrial reactive oxygen species: methodological aspects. *J. Cell. Mol. Med.* 6: 175–187.
- Beal MF (2004) Mitochondrial dysfunction and oxidative damage in Alzheimer's and Parkinson's diseases and coenzyme Q10 as a potential treatment. *J. Bioenerg. Biomembr.* 36: 381-386
- Bendixen R, Gerendás J, Schinner K, Sattelmacher B, Hansen UP (2001) Difference in zeaxanthin formation in nitrate-, NH<sub>4</sub><sup>+</sup>-grown *Phaseolus vulgaris*. *Physiol. Plantarum* 111: 255-261
- Bennet WF, Pesek J, Hanway JJ (1964) Effect of nitrate and ammonium on growth of corn in nutrient sand culture. *Agron. J.* 56: 342-345
- Bestwick CS, Bennett MH, Mansfield JW (1995) Mutant of *Pseudomonas syringae* pv *phaseolicola* Induces Cell Wall Alterations but Not Membrane Damage Leading to the Hypersensitive Reaction in Lettuce. *Plant Physiol.* 108: 503–516.
- Beyer WF, Fridovich I (1987) Assaying for superoxide dismutase activity: some large consequences of minor changes in conditions. *Anal. Biochem.* 161: 559-566

- Bialczyk J, Lechowski Z, Dziga D (2004) Composition of the xylem sap of tomato seedlings cultivated on media with  $\text{HCO}_3^-$  and nitrogen source as  $\text{NO}_3^-$  or  $\text{NH}_4^+$ . *Plant Soil* 263: 265-272
- Bilger W, Björkman O (1990) Role of xanthophyll cycle in photoprotection elucidated by measurements of light-induced absorbance changes, fluorescence and photosynthesis in leaves of *Hedera canariensis*. *Photosynth. Res.* 25: 173-186
- Bilski P, Belanger AG, Chignell CF (2002) Photosensitized oxidation of 2,7-dihlorofluorescein: singlet oxygen does not contribute to the formation of fluorescent oxidation product 2,7-dihlorofluorescein. *Free Radic. Biol. Med.* 33: 938-946
- Bligny R, Gout E, Kaiser W, Heber U, Walker D, Douce R (1997) pH regulation in acid-stressed leaves of pea plants grown in the presence of nitrate or ammonium salts: Studies involving  $^{31}\text{P}$ -NMR spectroscopy and chlorophyll fluorescence. *Biochim. Biophys. Acta* 1320: 142–152
- Bloom AJ, Sukrapanna SS, Warner RL (1992) Root respiration associated with ammonium and nitrate absorption and assimilation by barley. *Plant Physiol.* 99: 1294-1301
- Brewster JL, Beason KB, Eckdahl TT, Evans IM (2004) The microarray revolution. *Biochem. Mol. Biol. Edu.* 32: 217-227
- Britto DT, Kronzucker HJ (2002)  $\text{NH}_4^+$  toxicity in higher plants: a critical review. *Plant Physiol.* 159: 567-584
- Buchanan BB, Gruissem W, Jones RL (2000) *Biochemistry and Molecular Biology of plants*. American Society of Plant Physiologists, Rockville, Maryland.
- Casolo V, Braidot E, Chiandussi E, Macri F and Vianello A (2000) The role of mild uncoupling and non-coupled respiration in the regulation of hydrogen peroxide generation by plant mitochondria. *FEBS Lett.* 474: 53-57
- Cheng CL, Acedo GN, Dewdney J, Goodman HM, Conkling MA (1991) Differential expression of the two *Arabidopsis* nitrate reductase genes. *Plant Physiol.* 96: 275-279
- Chen ZH, Walker RP, Técsi LI, Lea PJ, Leegood RC (2004) Phosphoenolpyruvate carboxykinase in cucumber plants is increased by both ammonium and acidification, and is present in the phloem. *Planta* 219: 48-58
- Cleland RE, Grace SC (1999) Voltammetric detection of superoxide production by photosystem II. *FEBS Lett.* 457: 348-352
- Conklin PL, Norris SR, Wheeler GL, Williams EH, Smirnoff N, Last RL (1999) Genetic evidence for the role of GDP-mannose in plant ascorbic acid (vitamin c) biosynthesis. *Proc. Natl. Acad. Sci.* 96: 4198-4203



## References

---

- Cournac L, Josse E-M, Joet T, Rumeau D, Redding K, Kuntz M, Peltier G (2000) Flexibility in photosynthetic electron transport: a newly identified chloroplast oxidase involved in chlororespiration. *Phil. Trans. R. Soc. B* 355: 1447-1454
- Crawford NM, Smith M, Bellissimo D, Davis RW (1988) Sequence and nitrate regulation of the *Arabidopsis thaliana* mRNA encoding nitrate reductase, a metalloflavoprotein with three functional domains. *Proc. Natl. Acad. Sci.* 85: 5006-5010
- Crawford NM (1995) Nitrate: nutrient and signal for plant growth. *Plant Cell* 7: 859–868
- Crawford NM, Glass ADM (1998) Molecular and physiological aspects of nitrate uptake in plants. *Trends Plant Sci* 3: 389-395
- Crawford NM, Forde BG (2002) Molecular and developmental biology of inorganic nitrogen nutrition. *The Arabidopsis Book*, eds. C.R. Somerville and E.M. Meyerowitz, American Society of Plant Biologists, Rockville, MD, doi:10.1199/tab.0011 <http://www.aspb.org/publications/arabidopsis/>
- Davis BH (1976) Carotenoids. In: Goodwin TW (ed) *Chemistry and biochemistry of plant pigments*, vol II. Academic, New York, pp 38-165
- Del Rio LA, Pastori GM, Palma JM, Sandalio LM, Sevilla F, Corpas FJ, Jimenez A, Lopez - Huertas E, Hernandez JA (1998) The activated oxygen role of peroxisomes in senescence. *Plant Physiol.* 116: 1195-1200
- Demming B, Winter K (1988) Characterisation of three components of non-photochemical quenching and their response to photoinhibition. *Aust. J. Plant Physiol.* 15: 163-177
- Deng Y, Kohlwein SD, Manella CA (2002) Fasting induces cyanide-resistant respiration and oxidative stress in the amoeba *Chaos carolinensis*: implications for the cubic structural transition in mitochondria. *Protoplasma* 219: 160-167
- Dixon DP, Laphorn A, Edwards R (2002) Plant glutathione transferases. *Genome Biol.* 3: 3004.1-3004.10
- Dörr I (1997) How *Striga* Parasitizes its Host: a TEM and SEM Study. *Ann. Bot.* 79: 463-472
- Drághici S (2003) *Data analysis tools for DNA microarrays*. Chapman & Hall / CRC, Boca Raton
- Eastmond PJ, Graham IA (2001) Re-examining the role of the glyoxylate cycle in oilseeds. *Trends Plant Sci* 6: 72-77
- Eastmond PJ, Hooks M, Graham IA (2000) The *Arabidopsis* acyl-CoA oxidase gene family. *Biochem. Soc. Trans.* 28: 755-557
- Errebhi M, Wilcox GE (1990) Tomato growth, nutrient uptake pattern as influenced by nitrogen form ratio. *J. Plant Nutr.* 13: 1031–1043

- Esposti MD, Mc Lennan H (1998) Mitochondria and cells produce reactive oxygen species in virtual anaerobiosis: relevance to ceramide-induced apoptosis. *FEBS Lett.* 430: 338-342
- Faure JD, Vincentz M, Kronenberger J, Caboche M (1991) Coregulated expression of nitrate and nitrite reductases. *Plant J.* 1: 107-113
- Flohe MJ, Otting F (1984) Superoxide dismutase assays. *Methods Enzymol.* 105: 93-104
- Forde BG, Clarkson DT (1999) Nitrate and ammonium nutrition of plants: physiological and molecular perspective. *Adv. Bot. Res.* 30: 1-9.
- Francis D, Sorrell DA (2001) The interface between the cell cycle and plant growth regulators: a mini review. *Plant Growth Regul.* 33: 1-12
- Freyer MJ, Oxborough K, Mullineaus PM, Baker NR (2002) Imaging of photo-oxidative stress responses in leaves. *J. Exp. Bot.* 53: 1249-1254
- Fufezan C, Rutherford AW, Krieger-Liskay A (2002) Singlet oxygen production in herbicide-treated photosystem II. *FEBS Lett.* 532: 407-410
- Genty B, Briantais JM, Baker NR (1989) The relationship between the quantum yield of photosynthetic electron transport and quenching of chlorophyll fluorescence. *Biochim. Biophys. Acta* 990: 87-92
- Gerendás J, Ratcliff RG, Sattelmacher B (1990)  $^{31}\text{P}$  nuclear magnetic resonance evidence for differences in intracellular pH in the roots of maize seedlings grown on nitrate or ammonium. *Plant Physiol.* 137: 125-128
- Gerendás J (1992) Einfluß von Form und Konzentration des Stickstoffangebots auf Wachstum und Physiologie junger Maispflanzen (*Zea mays* L.). PhD thesis University Kiel, Schriftenreihe Nr.20, Institute of Plant Nutrition and Soil Science
- Gerendás J, Ratcliff RG, Sattelmacher B (1993) Relationship between intracellular pH and N metabolism in maize (*Zea mays* L.) roots. *Plant Soil* 155/156: 167-170
- Gerendás J, Sattelmacher B (1995) Einfluß des Ammoniumangebotes auf Wachstum, Mineralstoff- und Polyamingehalt junger Maispflanzen. *Z Pflanzenern. Bodenk.* 158: 299-305
- Gerendás J, Zhu Z, Bendixen R, Ratcliffe RG, Sattelmacher B (1997) Physiological, biochemical processes related to ammonium toxicity in higher plants. *Z. Pflanzenern. Bodenk.* 160: 239-251
- Gerendás J, Ratcliffe RG (2000) Intracellular pH regulation in maize root tips exposed to ammonium at high external pH. *J. Exp. Bot.* 51:207-219
- Givan CV (1979) Metabolic detoxification of ammonia in tissues of higher plants. *Phytochem.* 18: 375-382

- Guerrero MG, Vega JM, Losada M (1981) The assimilatory nitrate reducing system and its regulation. *Annu. Rev. Plant Biol.* 32: 169-204
- Guo S. (2002) The effects of N form (ammonium *versus* nitrate) on growth, photosynthesis and water uptake of *Phaseolus vulgaris* L. plants. PhD thesis Kiel
- Guo S, Schinner K, Sattelmacher B., Hansen UP (2005) Different Apparent CO<sub>2</sub> Compensation Points in Nitrate-and Ammonium-grown *Phaseolus Vulgaris* L. and its relationship to non-photorespiratory CO<sub>2</sub> evolution. *Physiol. Plantarum* 123: 288-301
- Hammes E (2005) Biophysikalische Untersuchungen zur Wirkung des Pilzbefalls im Weizen auf die Prozesse der Photosynthese und ihre Eignung für die Befallserfassung vom fahrenden Traktor. PhD thesis Kiel
- Hammes E, Hoffmann A, Plieth C, Hansen UP (2005) Light-induced decrease in DCF-fluorescence of leaves of wheat in the presence of SHAM. *Protoplasma* in press
- Hansen U-P, Moldaenke C, Tabrizi H, Ramm D (1993) The effect of transthylakoid proton uptake on cytosolic pH and the imbalance of ATP and NAPDH/H<sup>+</sup> production as measured by CO<sub>2</sub>- and light-induced depolarisation of the plasmalemma. *Plant Cell Physiol.* 34: 681-695
- Heldt HW (1999) Pflanzenbiochemie. Spektrum Akademischer Verlag, Heidelberg
- Hideg É, Barta C, Kálai T, Vass I, Hideg K, Asada K (2002) Detection of singlet oxygen and superoxide with fluorescent sensors in leaves under stress by photoinhibition or UV radiation. *Plant Cell Physiol.* 43: 1154-1164
- Hinderhofer K, Zentgraf U (2001) Identification of a transcription factor specifically expressed at the onset of leaf senescence. *Planta* 213: 469-473
- Hodge A, Paterson E, Thornton B, Millard P, Killham K (1997) Effects of photon flux density on carbon partitioning and rhizosphere carbon flow of *Lolium perenne*. *J. Exp. Bot.* 48: 1797-1805.
- Hoffmann A, Hammes E, Plieth C, Desel C, Sattelmacher B, Hansen UP (2005) Effect of CO<sub>2</sub> supply on ROS formation in *Arabidopsis thaliana*. *Protoplasma* in press
- Hormann H, Neubauer C, Schreiber U (1994) An active Mehler-peroxidase reaction sequence can prevent cyclic PS I electron transport in the presence of dioxygen in intact spinach chloroplasts. *Photosynth. Res.* 41: 429-437
- Horton P, Ruban AV, Rees D, Pascal AA, Noctor G, Young AJ (1991) Control of the light-harvesting function of chloroplast membranes by aggregation of the LHC II chlorophyll-protein complex. *FEBS Lett.* 292: 1-4
- Horton P, Ruban AV (1992) Regulation of photosystem II. *Photosynth. Res.* 34: 375-385

- Horton P, Ruban AV (1993)  $\Delta$ pH-dependent quenching of the  $F_0$  level of chlorophyll fluorescence in spinach leaves. *Biochim. Biophys. Acta* 1142: 203-206
- Hückelhoven R, Fodor J, Trujillo M, Kogel K-H (2000) Barley *Mla* and *Rar* mutants compromised in the hypersensitive cell death response against *Blumeria graminis* f.sp. *hordei* are modified in their ability to accumulate reactive oxygen intermediates at sites of fungal invasion. *Planta* 212: 16-24
- Hütter LA (1994) *Wasser und Wasseruntersuchung*. 6.Auflage, Verlag Salle und Sauerländer
- Ivanova M, Rost TL (1998) Cytokinins and the plant cell cycle: problems and pitfalls of proving their function. In: Bryant JA, Chiatante D, eds. *Plant cell proliferation and its regulation in growth and development*. New York: John Wiley & Sons, 45–57.
- Ishiyama K, Inoue E, Watanabe-Takahashi A, Obara M, Yamaya T, Takahashi H (2004) Kinetic properties and ammonium-dependent regulation of cytosolic isoenzymes of glutamine synthetase in *Arabidopsis*. *J. Biol. Chem.* 279: 16598-16605
- Jabs T, Tschöpe M, Colling C, Hahlbrock K, Scheel D (1997) Elicitor-stimulated ion fluxes and  $O_2^-$  from the oxidative burst are essential components in triggering defense gene activation and phytoalexin synthesis in parsley. *Proc. Natl. Acad. Sci.* 94: 4800-4805
- Jakob T, Goss R, Wilhelm C (1999) Activation of Diadinoxanthin de-epoxidase due to a chlororespiratory proton gradient in the dark in the diatom *Phaeodactylum tricornutum*. *Plant Biol.* 1: 76-82
- Kimura M, Yamamoto YY, Seki M, Sakurai T, Sato M, Abe T, Yoshida S, Manabe K, Shinozaki K, Matsui M (2003) Identification of *Arabidopsis* genes regulated by high light stress using cDNA microarray. *Photochem. Photobiol.* 77: 226-233
- Koch KE (1997) Molecular crosstalk and the regulation of C- and N-responsive genes. In *A molecular approach to primary metabolism in higher plants*. CH Foyer and WP Quick, eds (London: Taylor and Francis), pp.105-124
- Kosegarten H, Crolig F, Wieneke J, Wilson G, Hoffmann B (1997) Differential ammonia-elicited changes of cytosolic pH in root hair cells of rice and maize as monitored by 2',7'-bis-(2-carboxyethyl)-5 (and -6)-carboxyfluorescein-fluorescence ratio. *Plant Physiol.* 113: 451-461
- Krause GH, Verrotte C, Briantais JM (1982) Photoinduced quenching of chlorophyll fluorescence in intact chloroplasts and algae. *Biochim. Biophys. Acta* 679: 116–124
- Krömer S (1995) Respiration during photosynthesis. *Annu. Rev. Plant Physiol. Plant Mol. Biol.* 46: 45-70

## References

---

- Kuiper D (1988) Growth responses of *Plantago major* L. ssp. *pleiosperma* (Pilger) to changes in mineral supply. *Plant Physiol.* 87: 555-557
- Lam HM, Peng SSY, Coruzzi GM (1994) Metabolic regulation of the gene encoding glutamine-dependent asparagine synthetase in *Arabidopsis thaliana*. *Plant Physiol.* 106: 1347-1357
- Lam HM, Hsieh MH, Coruzzi G (1998) Reciprocal regulation of distinct asparagine synthetase genes by light and metabolites in *Arabidopsis thaliana*. *Plant J.* 16: 345-353
- Lancien M, Martin M, Hsieh MH, Leustek T, Goodman H, Coruzzi GM (2002) *Arabidopsis* *glt1-T* mutant defines a role for NADH-GOGAT in the non-photorespiratory ammonium assimilatory pathway. *Plant J.* 29: 347-358
- LeBel CP, Ischiropoulos H, Bondy SC (1992) Evaluation of the probe 2,7-dihlorofluorescein as an indicator of reactive oxygen species formation and oxidative stress. *Chem.Res.Toxicol.* 5: 227-231
- Lee MT, Kuo FC, Whitmore GA, Sklar J (2000) Importance of replication in microarray gene expression studies: Statistical methods and evidence from repetitive cDNA hybridisations. *Proc. Natl. Acad. Sci.* 97: 9834-9839
- Lefebvre S, Lawson T, Fryer M, Zakhleniuk OV, Lloyd JC, Raines CA (2005) increased sedoheptulose-1,7-bisphosphatase activity in transgenic tobacco plants stimulates photosynthesis and growth from an early stage in development. *Plant Physiol.* 138: 451-460
- LeLeu O, Vuylsteker C (2004) Unusual regulatory nitrate reductase activity in cotyledons of *Brassica napus* seedlings: enhancement of nitrate reductase activity by ammonium supply. *J. Exp. Bot.* 55: 815-823
- Lucas WJ, Keifer DW, Sanders D (1983) Bicarbonate transport in *Chara corallina*: evidence for cotransport of  $\text{HCO}_3^-$  with  $\text{H}^+$ . *J. Membr. Biol.* 73: 263-274
- Ma L, Sun N, Liu X, Jiao Y, Zhao H, Deng XW (2005) Organ-specific expression of *Arabidopsis* genome during development. *Plant Physiol.* 138: 80-91
- Maathuis FJM, Sanders D (1992) Plant membrane transport. *Curr. Opin. Cell Biol.* 4: 661-669
- MacKintosh C, Meek SEM (2001) Regulation of NR activity by reversible phosphorylation, 14-3-3 proteins and proteolysis. *Cell. Mol. Life Sci.* 58:205-214
- Magalhaes JR, Huber DM (1989) Ammonium assimilation in different plant species as affected by nitrogen form and pH control in solution culture. *Fert. Res.* 21: 1-6
- Makino A, Miyake C, Yokota A (2002) Physiological functions of the water-water cycle (Mehler reaction), the cyclic electron flow around PS I in rice leaves. *Plant Cell Physiol.* 43: 1017-1026

- Maly FE, Nakamura M, Gauchat JF, Urwyler A, Walker G, Dahinden CA, Cross AR, Jones OTC, Weck AL (1989) Superoxide-dependent nitroblue tetrazolium reduction and expression of cytochrom b<sub>245</sub> components by human tonsillar lymphocytes and B cell lines. *J. Immunol.* 142: 1260-1267
- Marschner H. 1995. Mineral nutrition of higher plants. London, Academic Press.
- Maxwell DP, McIntosh L, Wang Y (1999) The alternative oxidase lowers mitochondrial reactive oxygen production in plant cells. *Proc. Natl. Acad. Sci.* 96: 8271-8276
- McQueen A, Bailey JE (1991) Growth inhibition of hybridoma cells by ammonium ion: Correlation with effects on intracellular pH. *Bioproc. Eng.* 6: 49-61
- Merkel D (1973) Der Einfluß des NO<sub>3</sub> : NH<sub>4</sub>-Verhältnisses in der Nährlösung auf Ertrag und Gehalte an organischen und anorganischen Ionen von Tomatenpflanzen. *Z. Pflanzener. Bodenk.* 134: 236-246
- Miedema, H, Prins, HBA (1992) Coupling of proton fluxes in the polar leaves of *Potamogeton lucens* L. *J. Exp. Bot.* 43: 907-914
- Moore S, Spackman DH, Stein WH (1958) Chromatography of amino acids on sulfonated polystyrene resins. *Anal. Chem.* 30: 1185-1190
- Müller HJ, Röder T (2004) *Der Experimentator: Microarrays.* Elsevier Spektrum akademischer Verlag, München
- Myhre O, Andersen JM, Aarnes H, Fonnum F (2003) Evaluation of the probes 2,7-dichlorofluorescein diacetate, luminol, and lucigenin as indicators of reactive species formation. *Biochem. Pharmacol.* 65: 1575-1582
- Neill SJ, Desikan R, Clarke A, Hurst RD, Hancock JT (2002) Hydrogen peroxide and nitric oxide as signalling molecules in plants. *J. Exp. Bot.* 53: 1237-1247
- Noctor G, Foyer CH (1998) A re-evaluation of the ATP: NADPH budget during C<sub>3</sub> photosynthesis: a contribution from nitrate assimilation, its associated respiratory activity? *J. Exp. Bot.* 49: 1895-1908
- Ohasi T, Mizutani A, Murakami A, Kojo S, Ishii T, Taketani S (2002) Rapid oxidation of dichlorofluorescein with heme and hemoproteins: formation of the fluorescein is independent of the generation of reactive oxygen species. *FEBS Lett.* 511: 21-27
- Orendi G, Zimmermann P, Baar C; Zentgraf U (2001) Loss of stress-induced expression of catalase3 during leaf senescence in *Arabidopsis thaliana* is restricted to oxidative stress. *Plant Sci.* 161: 301-314

- Padmasree K, Raghavendra AS (1999) Importance of oxidative electron transport over oxidative phosphorylation in optimizing photosynthesis in mesophyll protoplasts of pea (*Pisum sativum* L). *Physiol. Plantarum* 105: 546-553
- Peltier G, Cournac L (2002) Chlororespiration. *Annu. Rev. Plant Biol.* 53: 523-550
- Pfündel E, Bilger W (1994) Regulation and possible function of the violaxanthin cycle. *Photosynth Res* 42: 89-109
- Plieth C, Sattelmacher B, Hansen UP (1997) Cytoplasmic  $\text{Ca}^{2+}$ - $\text{H}^{+}$ -exchange buffers in green algae. *Protoplasma* 198: 107-124
- Plieth C, Hansen UP (1996) Methodological aspects of pressure loading of fura-2 into characean cells. *J. Exp. Bot.* 47: 1601-1612
- Porra RJ, Thompson WA, Kriedmann PE (1989) Determination of accurate extinction coefficients and simultaneous equations for assaying chlorophylls a and b extracted with four different solvents: Verification of the concentrations of chlorophyll standards by atomic absorption spectroscopy. *Biochem. Biophys. Acta* 975: 384-394
- Raab TK, Terry N (1994) Nitrogen source regulation of growth and photosynthesis in *Beta vulgaris* L. *Plant Physiol.* 105: 1159-1166
- Raghavendra AS, Padmasree K, Saradadevi K (1994) Interdependence of photosynthesis, respiration in plant cells: Interactions between chloroplasts, mitochondria. *Plant Sci.* 97: 1-14
- Rahayu YS, Walch-Liu P, Neumann G, Römheld V, von Wiren N, Bangerth F (2005) Root-derived cytokinins as long-distance signals for  $\text{NO}_3^-$ -induced stimulation of leaf growth. *J. Exp. Bot* 56: 1143-1152
- Ramond P, Spiteri A, Dieuaide M, Gerhardt B, Pradet A (1992) Peroxisomal  $\beta$ -oxidation of fatty acids and citrate formation by particulate fraction from early germinating sunflower seeds. *Plant Physiol. Biochem.* 30: 153- 161
- Raven JA (1986) Biochemical disposal of excess  $\text{H}^+$  in growing plants? *New Phytol.* 104: 175-206
- Römheld, V, Muller, C, Marschner, H (1984) Localization and Capacity of Proton Pumps in Roots of Intact Sunflower Plants. *Plant Physiol.* 76: 603-606
- Rossel JB, Wilson IW, Pogson BJ (2002) Global changes in gene expression in response to high light in *Arabidopsis*. *Plant Physiol.* 130: 1109-1120
- Rota C, Fann YC, Mason RP (1999) Phenoxyl free radicals formation during the oxidation of the fluorescent dye 2',7'-dichlorofluorescein by horseradish peroxidase. *J. Biol. Chem.* 274: 28161-28168

- Rylott EL, Hooks MA, Graham IA (2001) Co-ordinate regulation of genes involved in storage lipid mobilization in *Arabidopsis thaliana*. *Biochem. Soc. Trans.* 29: 283–287
- Rylott EL, Gilday AD, Graham IA (2003) The gluconeogenic enzyme phosphoenolpyruvate carboxykinase in *Arabidopsis* is essential for seedling establishment. *Plant Physiol.* 131: 1834-1842
- Salon C, Raymond P, and Pradet A (1988) Quantification of carbon fluxes the tricarboxylic acid in early germination lettuce embryos. *J. Biol. Chem.* 263: 12278-12287
- Salsac L, Chaillou S, Morot-Gaudry JF, Lesaint C und Jolivet E (1987) Nitrate and ammonium nutrition in plants *Plant Physiol. Biochem.* 25: 805-812
- Sanders D, Hansen UP (1981) Mechanism of Cl<sup>-</sup> Transport at the plasma membrane of *Chara corallina*. II. Transinhibition and the determination of H<sup>+</sup>/Cl<sup>-</sup> binding order from a reaction kinetic model. *J. Membr. Biol.* 58: 139-153
- Sanders D, Hansen UP, Slayman CL (1981) Role of the plasma membrane pump in pH regulation in non-animal cells. *Proc. Natl. Acad. Sci.* 78: 5903-5907
- Scheible WR, Morcuende R, Czechowski T, Fritz C, Osuna D, Palacios-Rojas N, Schindelasch D, Thimm O, Udvardi MK, Stitt M (2004) Genome-wide reprogramming of primary and secondary metabolism, protein synthesis, cellular growth processes, and the regulatory infrastructure of *Arabidopsis* in response to nitrogen. *Plant Physiol.* 136: 2483-2499
- Schinner K, Tabrizi H, Hansen UP (1998) Indication for the Mehler reaction obtained from comparing photoacoustic, fluorescence-clamp measurements. In: *Photosynthesis: Mechanisms, Effects*. Vol. III. G.Garab ed. Kluwer Academic Publishers Dordrecht, Boston, London pp. 1759-1762
- Schinner K (2001) Signalanalyse und Austauschvorgänge zwischen Photosynthese und Respiration in Hinblick auf die stickstoffabhängige Lichtstressresistenz. PhD thesis Universität Kiel
- Schinner K, Sattelmacher B, Hansen UP (2001) Inhibitor-dependent stimulation of photosynthetic electron transport by far-red light in NO<sub>3</sub><sup>-</sup>- and NH<sub>4</sub><sup>+</sup>-grown plants of *Phaseolus vulgaris* L. In: *Plant Nutrition. Food Security and Sustainability of agroecosystems through basic and applied research*. W. J.Horst et al., eds. Kluwer Academic Publishers. Dordrecht, Boston, London., pp. 102-103
- Schmid M, Davison TS, Henz SR, Pape UJ, Demar M, Vingron M, Schölkopf B, Weigel D, Lohmann JU (2005) A gene expression map of *Arabidopsis thaliana* development. *Nat. Genet.* 37: 501-506



- Schopfer P, Plachy C, Frahry G (2001) Release of reactive oxygen intermediates (superoxide radicals, hydrogen peroxide, hydroxyl radicals) and peroxidase in germinating radish (*Raphanus sativus* L.) seeds controlled by light, gibberellin and abscisic acid. *Plant Physiol.* 125: 1591-1602
- Schortemeyer M, Stamp P, Feil B (1997) Ammonium tolerance and carbohydrate status in maize cultivars. *Ann. Bot.* 79: 25–30
- Schreiber U, Schliwa U, Bilger W (1986) Continuous recording of photochemical and non-photochemical chlorophyll fluorescence quenching with a new type of modulation fluorometer. *Photosynth. Res.* 10: 51-62.
- Schreiber U, Bilger W (1993) III. Progress in chlorophyll fluorescence research: Major developments during the past years in retrospect. *Prog. Bot.* 54: 151-173
- Schreiber U, Krieger A (1998) Two fundamentally different types of variable chlorophyll fluorescence in vivo. *FEBS Lett.* 397: 131-135
- Schroeter B, Green TGA, Kappen L, Seppelt RD (1994) Carbon dioxide exchange at subzero temperatures. Field measurements on *Umbilicaria aprina* in Antarctica. *Crypt. Bot.* 4: 233-241
- Schuchhardt J, Beule D, Malik A; Wolski E, Eickhoff H, Lehrach H, Herzel H (2000) Normalization strategies for cDNA microarrays. *Nucleic Acids Res.* 28: e47
- Shelp BJ, Bown AW, McLean MD (1999) Metabolism and functions of gamma-aminobutyric acid. *Trends Plant Sci* 4: 446-452
- Sherameti I, Sopory SK, Trebicka A, Pfannschmidt T, Oelmüller R (2002) Photosynthetic electron transport determines nitrate reductase gene expression and activity in higher plants. *J. Biol. Chem.* 277: 46594-46600
- Simon R, Radmacher D, Dobbin K (2002) Design of studies using DNA microarrays. *Genet. Epidemiol.* 23: 21-36
- Sluse FE, Jarmuszkievicz W (1998) Alternative oxidase in the branched mitochondrial respiratory network: an overview on structure, function, regulation, and role. *Braz. J. Med. Biol. Res.* 31: 733-747
- Smirnoff N (2000) Ascorbic acid: metabolism and functions of a multifacette molecule. *Curr. Opin. Plant Biol.* 3: 229-235
- Somerville SR, Ogren WL (1980) Inhibition of photosynthesis in *Arabidopsis* mutants lacking leaf glutamate synthase activity. *Nature* 286: 257-259
- Stitt M (1999) Nitrate regulation of metabolism and growth. *Curr. Op. Plant Biol.* 2: 178–186

- Stitt M, Müller C, Matt P, Gibon Y, Carillo P, Morcuende R, Scheible WR, Krapp A (2002) Steps towards an integrated view of nitrogen metabolism. *J. Exp. Bot.* 53: 959-970
- Streeter JG (1979) Allantoin and allantoic acid in tissues and stem exudates from field-grown soybean plants. *Plant Physiol.* 63: 478-480
- Sundby C, Chow WS, Anderson JM (1993) Effects on photosystem II, photoinhibition, and plant performance of the spontaneous mutation of serine-264 in the photosystem II reaction center D1 protein in triazine-resistant *Brassica napus* L. *Plant Physiol.* 103: 105-113
- Takei K, Takahashi T, Sugiyama T, Yamaya T, Sakakibara H (2002) Multiple routes communicating nitrogen availability from roots to shoots: a signal transduction pathway mediated by cytokinin. *J. Exp. Bot.* 53: 971-977
- Tarpey MM, Wink DA, Grisham MB (2004) Methods for detection of reactive metabolites of oxygen and nitrogen: in vitro and in vivo considerations. *Am. J. Physiol. Regul. Integr. Comp. Physiol.* 286: R431-R444
- Taiz L, Zeiger E (2000) *Physiology der Pflanzen*. Spektrum Akademischer Verlag, Heidelberg
- The Arabidopsis Genome Initiative (2000) Analysis of the genome sequence of the flowering plant *Arabidopsis thaliana*. *Nature* 408: 796-815
- Theodoulou FL (2000) Plant ABC transporters. *Biochim. Biophys. Acta* 1465: 79-103
- Thomas RC (1978) Ion-sensitive intracellular microelectrodes: How to make and use them. Academic Press, London, pp. 32-44
- Tjus SE, Scheller HV, Andersson B, Möller BL (2001) Active oxygen produced during selective excitation of photosystem I is damaging not only to photosystem I, but also to photosystem II. *Plant Physiol.* 125: 2007-2015
- Tocquin P, Corbesier L, Havelange A, Pieltain A, Kurtem E, Bernier G, Périelleux C (2003) A novel high efficiency, low maintenance, hydroponic system for synchronous growth and flowering of *Arabidopsis thaliana*. *BCM Plant biology* 3: article 2 pp1-10
- Trayner ID, Rayner AP, Freeman GE, Farzaneh F (1995) Quantitative multiwell myeloid differentiation assay using dichlorodihydrofluorescein diacetate (H<sub>2</sub>DCF-DA) or dihydrorhodamine 123 (H<sub>2</sub>R123). *J. Immunol. Methods* 186: 275-284
- Tuin LG, Shelp BJ (1994) *In situ* <sup>14</sup>C glutamate metabolism by developing soybean cotyledons. I. Metabolic routes. *Plant Physiol.* 143: 1-7
- Tuin LG, Shelp BJ (1996) *In situ* <sup>14</sup>C glutamate metabolism by developing soybean cotyledons. II. The importance of glutamate decarboxylation. *Plant Physiol.* 147: 714-720

## References

---

- Turano FJ, Fang TK (1998) Characterization of two glutamate decarboxylase cDNA clones from *Arabidopsis*. *Plant Physiol.* 117: 1411-1421
- Valpuesta V, Botella MA (2004) Biosynthesis of L-ascorbic acid in plants: new pathways for an old antioxidant. *Trends Plant Sci.* 9: 573-577
- van Roermund CW, Elgersma Y, Singh N, Wanders RJ, Tabak HF (1995) The membrane of peroxisomes in *Saccharomyces cerevisiae* is impermeable to NAD(H) and acetyl-CoA under *in vivo* conditions. *EMBO J.* 14: 3480-3486
- Vanselow KH, Kolbowski J, Hansen UP (1989) Further evidence for the relationship between light-induced changes of plasmalemma transport and transthylakoid proton uptake. *J Exp. Bot.* 40: 239-245
- Vanselow KH (1993) The effect of N-nutrients on the acceptor pool of PS I and thylakoid energization as measured by chlorophyll fluorescence of *Dunaliella salina*. *J. Exp. Bot.* 44: 1331-1340
- Vessey JK, Raper CD Jr, Henry LT (1990) Effect of ammonium sulfate, ammonium chloride and root-zone acidity on inorganic ion content of tobacco. *J. Plant Nutr.* 13: 827-842
- von Caemmerer S, Farquhar GD (1981) Some relationships between the biochemistry of photosynthesis and the gas exchange of leaves. *Planta* 153: 376-387
- Walch-Liu P, Neumann G, Bangerth F, Engels C (2000) Rapid effect of nitrogen form on leaf morphogenesis in tobacco. *J. Exp. Bot.* 51: 227-237
- Walker NA, Smith FA, Cathers IR (1980) Bicarbonate assimilation by fresh-water charophytes and higher plants: I. Membrane transport of bicarbonate ions is not proven. *J. Membr. Biol.* 57: 51-58
- Wang R, Guegler K, LaBrie ST, Crawford NM (2000). Genomic analysis of a nutrient response in *Arabidopsis* reveals diverse expression patterns and novel metabolic and potential regulatory genes induced by nitrate. *Plant Cell* 12: 1491–1509
- Wang R, Okamoto M, Xing X, Crawford NM (2003) Microarray analysis of the nitrate response in *Arabidopsis* roots and shoots reveals over 1,000 rapidly responding genes and new linkages to glucose, trehalose-6-phosphate, iron and sulfate metabolism. *Plant Physiol.* 132: 556-567
- Wang R, Tischner R, Gutiérrez RA, Hoffman M, Xing X, Chen M, Coruzzi G, Crawford NM (2004) Genomic analysis of the nitrate response using a nitrate reductase-null mutant of *Arabidopsis*. *Plant Physiol.* 136: 2512-2522
- Wedel N, Soll J, Paap BK (1997) CP12 provides a new mode of light regulation of Calvin cycle activity in higher plants. *Proc. Natl. Acad. Sci.* 94: 10479-10484

- Wheeler GL, Jones MA, Smirnoff N (1998) The biosynthetic pathway of vitamin c in higher plants. *Nature* 393: 365-369
- Wilkinson JQ, Crawford NM (1991) Identification of the *Arabidopsis* CHL3 gene as the nitrate reductase structural gene NIA2. *Plant Cell* 3: 461-471
- Wilson GH, Grolig F, Kosegarten H (1998) Differential pH restoration after ammonia-elicited vacuolar alkalisation in rice and maize root hairs as measured by fluorescence ratio. *Planta* 206: 154–161
- Wolucka BA, Persiau G, van Doorselaere J, Davey MW, Demol H, Vandekerckhove J, van Montagu M, Zabeau M, Boerjan W (2001) Partial purification of GDP-mannose 3,5-epimerase of *Arabidopsis thaliana*, a key enzyme in plant vitamin c pathway. *Proc. Natl. Acad. Sci.* 98: 14843-14848
- Wolucka BA, Van Montagu M (2003) GDP-mannose 3,5-epimerase forms GDP-L-gulose, a putative intermediate for the de novo biosynthesis of vitamin c in plants. *J. Biol. Chem.* 278: 47483-47490
- Zhang H, Jennings A, Barlow PW, Forde BG (1999) Dual pathway for regulation of root branching by nitrate. *Proc. Natl. Acad. Sci.* 96: 6529–6534
- Zhu Z, Gerendas J, Bendixen R, Schinner K, Tabrizi H, Sattelmacher B, Hansen UP (2000) Different tolerance to light stress in  $\text{NO}_3^-$ ,  $\text{NH}_4^+$ -grown *Phaseolus vulgaris* L. *Plant Biol.* 2: 558-570
- Zhuo D, Okamoto M, Vidmar JJ, Glass AD (1999) Regulation of a putative high-affinity nitrate transporter (Nrt2;1At) in roots of *Arabidopsis thaliana*. *Plant J.* 17: 563-568

## **Danksagung**

An erster Stelle steht der Dank an Prof. U.P. Hansen für die Bereitstellung des Themas, die gute Betreuung und die vielen hilfreichen Diskussionen.

Danken möchte ich auch Prof. B. Sattelmacher für die Bereitstellung des Themas und für sehr konstruktive Ratschläge.

PD R. Siebert danke ich für die Empfehlung an Prof. Hansen und sein mir entgegengebrachtes Vertrauen über die zurückliegenden 6 Jahre.

Desweiteren danke ich Prof. K. Krupinska und Prof. K. Schwarz, ohne die es das GRK 820-Natürliche Antioxidantien- nicht gegeben hätte. Vielen Dank für die Bereitstellung des Stipendiums durch die DFG und die vielen hilfreichen Seminare, Vorlesungen, Gastwissenschaftlervorträge und Tagungen. An dieser Stelle auch ein herzlicher Dank an alle Teilnehmer des GRK 820 für die gute Zusammenarbeit und die vielen netten Stunden beim Stammtisch.

Special thanks I would like to give to Prof. E.-M. Aro for the possibility to use their cDNA microarray and the warm welcome in Turku. Very special thanks to Mirva and Arto for all their help.

Ein besonderer Dank geht an Christine Desel für die sehr gute Zusammenarbeit und die vielen hilfreichen Diskussionen.

Christoph Plieth möchte ich herzlich danken für sein immer offenes Ohr, die vielen guten Ideen und die schnelle Umsetzung neuer experimenteller Aufbauten.

Jon Falk möchte ich besonders danken für die hilfreichen Anmerkungen zu meiner Arbeit und seinen unglaublichen Wissensschatz, der mir stundenlanges Suchen im Internet erspart hat.

Sabine Milde danke ich von Herzen für die gute Zusammenarbeit, die arbeitsreiche, tolle Zeit in Turku und die Unterstützung in allen Fragen des Lebens.

Meiner Arbeitsgruppe danke ich für viele nette Tee und Kaffeerunden, die mir besonders den Anfang erleichtert haben. Vielen Dank an Toby, Steffi, Hendrik. Ein besonderer Dank geht auch an Anja für die große Unterstützung bei den Northern Blots, an Enno für die Hilfe die den PAM-Messungen und an Christin für ihre Ausdauer beim Pflanzen ernten.

Der AG Prof. Bilger sei herzlich gedankt für viele kleine Hilfestellungen. Edith und Karna sei besonders gedankt für die Hilfe bei der HPLC. Hartmut Kaiser danke ich für die Hilfe bei der Gasflussmessung und viele hilfreiche Gespräche.

Der AG Prof. Sattelmacher danke ich für die Unterstützung vor allem in den letzten Wochen. Vielen, vielen Dank Bijan, Joska, Bärbel und Steffi für alle eure Mühen.

Kerstin, Matthias und Indra gebührt mein herzlicher Dank für das geduldige Korrekturlesen meiner Arbeit. Was hätte ich ohne Euch gemacht!

Boris möchte ich danken für seine stete Bereitschaft sich meine kleinen und großen Sorgen anzuhören und mir den Rücken zu stärken.

Und dann sind da noch die vielen, vielen anderen Menschen, die mich bis hierher begleitet und mir geholfen haben. Danke an alle, die ich hier nicht mehr namentlich aufführen kann.

Zum Schluss ein ganz besonderer Dank an meine Eltern und Geschwister für ihre Unterstützung, speziell an meine Mutter für die gute Idee mich zwischendurch nach Sylt zu schicken. Herzlich danken möchte ich meinem Bruder für die vielen kleinen Nettigkeiten in den letzten Monaten.

# Lebenslauf

Name: Anne Friederike Hoffmann  
Geburtsdatum: 02.01.1978  
Geburtsort: Hamburg  
Staatsangehörigkeit: deutsch

## Ausbildung

1984 - 1988                    Grundschule Woellmerstrasse Hamburg-Harburg

1988 - 1997                    Gymnasium Sophie-Barat-Schule Hamburg  
Abschluss: Abitur

Feb. 1998 - Aug. 2002        Studium der Biotechnologie  
University of Applied Sciences Gießen-Friedberg

    Feb. - Mai 2000            Auslandssemester an der University of Greenwich, UK

    April - Aug. 2001         Berufspraktisches Semester  
    St. Jude Children's Research Hospital, Memphis, TN, USA

    Feb. - Juli 2002          Diplomarbeit  
    Evotec OAI AG, Hamburg

    Aug. 2002                 Abschluss: Diplom  
    University of Applied Sciences Gießen-Friedberg  
    Dipl.-Ing. (FH) Biotechnologie

Nov. 2002                    Beginn der experimentellen Arbeit zur Dissertation  
    Betreuung: Prof. U.P. Hansen  
    Zentrum für Biochemie und Molekularbiologie  
    Christian-Albrechts-Universität zu Kiel





## **Erklärung**

Hiermit erkläre ich, dass die vorliegende Arbeit - abgesehen von der Beratung durch meine akademischen Lehrer - nach Inhalt und Form meine Arbeit ist. Es wurden nur die angegebenen Quellen und Hilfsmittel benutzt. Diese Arbeit wurde bis jetzt weder ganz noch teilweise einer anderen Stelle im Rahmen eines Prüfungsverfahrens vorgelegt. Ferner erkläre ich, dass ich noch keine früheren Promotionsversuche unternommen habe.

Kiel,